

VOLUME 77

APRIL 26, 1973 .

NUMBER 9

JPCHAx

THE JOURNAL OF
PHYSICAL
CHEMISTRY

PUBLISHED BIWEEKLY BY THE AMERICAN CHEMICAL SOCIETY

THE JOURNAL OF PHYSICAL CHEMISTRY

BRYCE CRAWFORD, Jr., *Editor*

STEPHEN PRAGER, *Associate Editor*

ROBERT W. CARR, Jr., **FREDERIC A. VAN-CATLEDGE**, *Assistant Editors*

EDITORIAL BOARD: A. O. ALLEN (1970-1974), C. A. ANGELL (1973-1977), J. R. BOLTON (1971-1975), F. S. DAINTON (1972-1976), M. FIXMAN (1970-1974), H. S. FRANK (1970-1974), R. R. HENTZ (1972-1976), J. R. HUIZENGA (1969-1973), W. J. KAUZMANN (1969-1973), R. L. KAY (1972-1976), W. R. KRIGBAUM (1969-1973), W. J. MOORE (1969-1973), R. M. NOYES (1973-1977), J. A. POPLE (1971-1975), B. S. RABINOVITCH (1971-1975), H. REISS (1970-1974), S. A. RICE (1969-1975), F. S. ROWLAND (1973-1977), R. L. SCOTT (1973-1977); W. A. ZISMAN (1972-1976)

AMERICAN CHEMICAL SOCIETY, 1155 Sixteenth St., N.W., Washington, D. C. 20036

Books and Journals Division

JOHN K CRUM *Director*

RUTH REYNARD *Assistant to the Director*

CHARLES R. BERTSCH *Head, Editorial Processing Department*

D. H. MICHAEL BOWEN *Head, Journals Department*

BACIL GUILLEY *Head, Graphics and Production Department*

SELDON W. TERRANT *Head, Research and Development Department*

©Copyright, 1973, by the American Chemical Society. Published biweekly by the American Chemical Society at 20th and Northampton Sts., Easton, Pa. 18042. Second-class postage paid at Washington, D. C., and at additional mailing offices.

All manuscripts should be sent to *The Journal of Physical Chemistry*, Department of Chemistry, University of Minnesota, Minneapolis, Minn. 55455.

Additions and Corrections are published once yearly in the final issue. See Volume 76, Number 26 for the proper form.

Extensive or unusual alterations in an article after it has been set in type are made at the author's expense, and it is understood that by requesting such alterations the author agrees to defray the cost thereof.

The American Chemical Society and the Editor of *The Journal of Physical Chemistry* assume no responsibility for the statements and opinions advanced by contributors.

Correspondence regarding accepted copy, proofs, and reprints should be directed to Editorial Processing Department, American Chemical Society, 20th and Northampton Sts., Easton, Pa. 18042. Head: CHARLES R. BERTSCH. Assistant Editor: EDWARD A. BORGER. Editorial Assistant: JOSEPH E. YURVATI.

Advertising Office: Centcom, Ltd., 142 East Avenue, Norwalk, Conn. 06851.

Business and Subscription Information

Remittances and orders for subscriptions and for single copies,

notices of changes of address and new professional connections, and claims for missing numbers should be sent to the Subscription Service Department, American Chemical Society, 1155 Sixteenth St., N.W., Washington, D. C. 20036. Allow 4 weeks for change of address. Please include an old address label with the notification.

Claims for missing numbers will not be allowed (1) if received more than sixty days from date of issue, (2) if loss was due to failure of notice of change of address to be received before the date specified in the preceding paragraph, or (3) if the reason for the claim is "missing from files."

Subscription rates (1973): members of the American Chemical Society, \$20.00 for 1 year; to nonmembers, \$60.00 for 1 year. Those interested in becoming members should write to the Admissions Department, American Chemical Society, 1155 Sixteenth St., N.W., Washington, D. C. 20036. Postage to Canada and countries in the Pan-American Union, \$5.00; all other countries, \$6.00. Single copies for current year: \$3.00. Rates for back issues from Volume 56 to date are available from the Special Issues Sales Department, 1155 Sixteenth St., N.W., Washington, D. C. 20036.

This publication and the other ACS periodical publications are now available on microfilm. For information write to MICROFILM, Special Issues Sales Department, 1155 Sixteenth St., N.W., Washington, D. C. 20036.

THE JOURNAL OF
PHYSICAL CHEMISTRY

Volume 77, Number 9 April 26, 1973

JPCHAx 77(9) 1083-1192 (1973)

- Chemical Reactions of Carbon Atoms and Molecules from Laser-Induced Vaporization of Graphite and Tantalum Carbide
Richard T. Meyer,* Arthur W. Lynch, and James M. Freese 1083
- Rapid Gas-Phase Reactions. The Reaction of Ammonia and the Methylamines with Boron Trifluoride. III. Pressure Dependence of Rate Constant
Sol Glicker 1093
- Reactions of HO₂ with Carbon Monoxide and Nitric Oxide and of O(¹D) with Water
R. Simonaitis and Julian Heicklen* 1096
- An Electron Spin Resonance Study of the Radicals Produced by the γ -Irradiation of Xanthene
G. Orlandi,* G. Poggi, F. Barigelletti, and A. Breccia 1102
- Concentration and Temperature Dependence of the Quantum Yield and Lifetime of the Lowest Triplet State of Benzene in the Liquid Phase
Robert R. Hentz* and Ronald M. Thibault 1105
- Behavior of CO₃⁻ Radicals Generated in the Flash Photolysis of Carbonatoamine Complexes of Cobalt(III) in Aqueous Solution
Schoen-nan Chen, Virgil W. Cope, and Morton Z. Hoffman* 1111
- Reaction of OH and O⁻ Radicals with Aromatic Carboxylate Anions in Aqueous Solution
M. Simic, Morton Z. Hoffman,* and M. Ebert 1117
- Infrared Kinetic Study of Reactions of Alcohols on the Surface of Alumina
William Hertl* and Angela Maria Cuenca 1120
- Absorption and Flash Photolysis Kinetic Spectroscopy Studies on Difluoro-, Chlorodifluoro-, Dichlorofluoro-, and Tetrafluorophosphine
Edward G. Skolnik, Robert J. Salesi, Charles R. Russ, and P. L. Goodfriend* 1126
- Disulfide Vibrational Spectra in the Sulfur-Sulfur and Carbon-Sulfur Stretching Region
Ernest J. Bastian, Jr., and R. Bruce Martin* 1129
- Nuclear Spin-Lattice Relaxation in Long Chain Viscous Hydrocarbons
J. D. Cutnell,* R. M. Schisla, and W. C. Hamann 1134
- Thermodynamics of the Helix-Coil Transition of Polypeptides in Binary Solvent Systems
F. E. Karasz* and G. E. Gajnos 1139
- Crystal Structure of Methylenediphosphonic Acid
D. DeLaMatter, J. J. McCullough, and C. Calvo* 1146
- A Far-Infrared Study of the Association of Benzoic Acid with Substituted Ammonium Halides in Benzene
R. A. Work, III, and R. L. McDonald* 1148
- Photolysis of Nitrogen Dioxide to Produce Transient O, NO₃, and N₂O₅
Alan B. Harker and H. S. Johnston* 1153
- Torsional Frequencies and Conformational Equilibria of Ortho-Substituted Phenols
Gerald L. Carlson* and William G. Fateley 1157
- A Study of Methyl Methacrylate in γ -Irradiated Organic Glasses at 77 K
Tomas Gillbro,* Hitoshi Yamaoka, and Seizo Okamura 1163

ห้องสมุด กรมวิทยาศาสตร์
* ๑๑ ๖๕๑๖

Pulse Radiolytic Investigations of the Catalyzed Disproportionation of Peroxy Radicals. Aqueous Cupric Ions	Joseph Rabani,* Dina Klug-Roth, and J. Lilie	1169
Electron Scavenging and Product Formation in the γ -Radiolysis of Nitrous Oxide-Liquid Xenon Solutions	Stefan J. Rząd* and George Bakale	1176
Reaction of Atomic Oxygen with Hydrogen Bromide	G. A. Takacs and G. P. Glass*	1182
Radiation Chemical Studies of the Oxidation and Reduction of Nitrofurans. Oxidative Denitration by OH Radicals	C. L. Greenstock, I. Dunlop, and P. Neta*	1187

COMMUNICATIONS TO THE EDITOR

Comparison of Micellar Effects on Singlet Excited States of Anthracene and Perylene	Larry K. Patterson* and Eric Vieil	1191
--	---	------

AUTHOR INDEX

Bakale, G., 1176	Freese, J. M., 1083	Karasz, F. E., 1139	Rabani, J., 1169
Barigelletti, F., 1102	Gajnos, G. E., 1139	Klug-Roth, D., 1169	Russ, C. R., 1126
Bastian, E. J., Jr., 1129	Gillbro, T., 1163	Lilie, J., 1169	Rząd, S. J., 1176
Breccia, A., 1102	Glass, G. P., 1182	Lynch, A. W., 1083	Salesi, R. J., 1126
Calvo, C., 1146	Glicker, S., 1093	Martin, R. B., 1129	Schisla, R. M., 1134
Carlson, G. L., 1157	Goodfriend, P. L., 1126	McCullough, J. J., 1146	Simic, M., 1117
Chen, S., 1111	Greenstock, C. L., 1187	McDonald, R. L., 1148	Simonaitis, R., 1096
Cope, V. W., 1111	Hammann, W. C., 1134	Meyer, R. T., 1083	Skolnik, E. G., 1126
Cuenca, A. M., 1120	Harker, A., 1153	Neta, P., 1187	Takacs, G. A., 1182
Cutnell, J. D., 1134	Heicklen, J., 1096	Okamura, S., 1163	Thibault, R. M., 1105
DeLaMatter, D., 1146	Hentz, R. R., 1105	Orlandi, G., 1102	Vieil, E., 1191
Dunlop, I., 1187	Hertl, W., 1120	Patterson, L. K., 1191	Work, R. A., III, 1148
Ebert, M., 1117	Hoffman, M. Z., 1111, 1117	Poggi, G., 1102	Yamaoka, H., 1163
Fateley, W. G., 1157	Johnston, H. S., 1153		

In papers with more than one author the name of the author to whom inquiries about the paper should be addressed is marked with an asterisk in the by-line.

THE JOURNAL OF PHYSICAL CHEMISTRY

Registered in U. S. Patent Office © Copyright, 1978, by the American Chemical Society

VOLUME 77, NUMBER 9 APRIL 26, 1973

Chemical Reactions of Carbon Atoms and Molecules from Laser-Induced Vaporization of Graphite and Tantalum Carbide¹

Richard T. Meyer,* Arthur W. Lynch, and James M. Freese

High Temperature Sciences Division 5324, Sandia Laboratories, Albuquerque, New Mexico 87115 (Received September 22, 1972)

Publication costs assisted by Sandia Laboratories

The vapor composition above graphite and above tantalum carbide together with the chemical reactions of C_1 , C_2 , and C_3 have been studied by the techniques of pulsed laser heating, time-resolved mass spectrometry, and gas-phase titrations. The relative abundances for the vaporized species C_1 , C_2 , and C_3 were 1.0:1.4:17 for graphite and 1.0:0.059:2.2 for tantalum carbide. The different relative abundances of vaporized C_n species from graphite and from tantalum carbide were selected to provide an identification of some of the specific gas-phase reactions with O_2 , H_2 , and CH_4 . The C_n species reacted quantitatively with O_2 in the gas phase to form CO and CO_2 ; CO_2 was the product of the reactions of C_2 and/or C_3 . C_2H_2 was the major product of C_n reactions with H_2 and accounted for 85–90% of the mass loss from graphite. CH_4 , C_4H_2 , and mass 78 were minor products. A low-pressure plateau at ~ 0.5 Torr in the H_2 titration curve was attributed to the completion of the reaction of C_2 via a two-step mechanism: (i) $C_2 + H_2 \rightarrow C_2H + H$; (ii) $C_2H + H_2 \rightarrow C_2H_2 + H$. C_3 reacted with H_2 at pressures from ~ 0.5 to 10 Torr to form the major quantity of C_2H_2 , but the mechanism was not elucidated. The overall reaction probability of laser-vaporized carbon species (predominately C_3) was approximately 17 times greater with O_2 than with H_2 . The reaction of C_n species with CH_4 was complicated by the pyrolysis of the CH_4 on the laser-heated substrate; C_2H_2 and H_2 were the principal products of both the vapor-phase reactions and the pyrolysis. The techniques and results evolved in this study provide a foundation for evolving the elementary reactions of carbon atoms and molecules and for determining the vapor compositions of graphites and carbides at very high temperatures.

1. Introduction

The high-temperature chemistry of carbon has profound impact on numerous areas of modern technology. In recent years, studies of the chemical reactions of gaseous carbon atoms and molecules have emerged as a result of the development of techniques for producing and detecting these highly reactive species. The reactions of C_1 have been explored extensively by Wolfgang and coworkers,^{1–10} Wolf,^{11–14} Skell,^{15–22} and Braun.²³ A few results on reactions of C_2 and C_3 have been reported by Skell,^{17,20} Namba,^{24–26} and Verdieck.^{27,28}

The vapor composition for graphites has been explored with equal vigor over the past 10–15 years. The equilibrium vapor pressures of C_1 through C_5 determined by Drowart, *et al.*, are the standards of today, but are recognized as being somewhat limiting because the experimental measurements did not exceed 2700 K.²⁹ In 1968, Palmer and Shelef reviewed all of the existing data and pro-

posed “best approximations” of the partial pressures and the heats of sublimation.³⁰ More recently, vapor pressure measurements extended to as high as 3200 K have been

- (1) This work was supported by the US Atomic Energy Commission.
- (2) (a) For the most current summary of Wolfgang's studies and a complete list of pertinent publications, see R. F. Peterson, Jr., and R. Wolfgang, *Advan. High Temperature Chem.*, **4**, 43 (1971); (b) J. Dubrin, C. MacKay, M. L. Pandow, and R. Wolfgang, *J. Inorg. Nucl. Chem.*, **26**, 2113 (1964).
- (3) C. MacKay and R. Wolfgang, *Science*, **148**, 899 (1965).
- (4) M. Marshall, C. MacKay, and R. Wolfgang, *J. Amer. Chem. Soc.*, **86**, 4741 (1964).
- (5) R. Wolfgang, *Progr. React. Kinet.*, **3**, 99 (1965).
- (6) J. Dubrin, C. MacKay, and R. Wolfgang, *J. Amer. Chem. Soc.*, **86**, 4747 (1964).
- (7) J. E. Nicholas, C. MacKay, and R. Wolfgang, *J. Amer. Chem. Soc.*, **87**, 3008 (1965).
- (8) J. Nicholas, C. MacKay, and R. Wolfgang, *J. Amer. Chem. Soc.*, **88**, 1065 (1966).
- (9) J. Nicholas, C. MacKay, and R. Wolfgang, *J. Amer. Chem. Soc.*, **88**, 1610 (1966).
- (10) C. MacKay, J. Nicholas, and R. Wolfgang, *J. Amer. Chem. Soc.*, **89**, 5758 (1967).

reported by Zavitsanos and Carlson,³¹ Milne, *et al.*,³² and Wachi and Gilmartin.³³ A number of investigators have used pulsed laser heating to achieve still higher temperatures (~4000 K) and to determine the vapor composition under nonequilibrium vaporization conditions.³⁴⁻³⁶

In this paper we report parallel studies of (a) the chemical reactions of the laser-vaporized carbon species with selected reactant gases, O₂, H₂, and CH₄, and (b) the vapor compositions above laser-heated graphites and above tantalum carbide. The carbide was used in the chemical titration procedures in order to change the carbon vapor compositions and final product distribution and to provide an identification of the carbon vapor species produced at the very high temperatures associated with laser heating. Time-resolved mass spectrometry was applied to the vapor composition analyses, which showed that the relative abundances of the C_n species above graphite and tantalum carbide were significantly different. This observation facilitated the evolution of the chemical titration procedures and insight on the elementary chemical reactions of the C_n species with the titrating gases. In the Discussion section, first the relative abundances of the carbon vapor species determined from the mass spectrometric analyses are shown to be applicable to the laser conditions utilized for the titration experiments. Then, the titration data are evaluated to demonstrate that the reaction products were formed in homogeneous gas-phase reactions and that the amounts formed correlated quantitatively with the amount of vaporized carbon. Finally, chemical mechanisms, which offer consistency with the vapor compositions and titration data, are discussed for the reactions of C₁, C₂, and C₃ with O₂ and H₂.

2. Experimental Methods

2.1 Gas Titration Procedures. The gas titration experiments were carried out in a 1-l. glass reaction vessel which contained the graphite or tantalum carbide sample, the titration gas, a quartz window for the laser beam, and a gas sampling valve. The sample was irradiated with a Korad K-1 laser, which utilized a Nd³⁺ glass rod (1.27-cm diameter) capable of both a normal-mode pulse of 70 J, 800- μ sec duration, and a Q-switched pulse of 3 J, 25-nsec duration. The laser beam was focused by a 250-mm lens to a spot approximately 0.5-mm diameter on the sample surface. In order to obtain a measurable weight loss in the Q-switched mode experiments, the samples were subjected to four irradiations of 2.5-3.0 J per irradiation for each titration experiment. Single irradiations of 50 J were sufficient for the normal-mode experiments. The laser samples consisted of Poco AXF-QB graphite (1.85 g/cc, 500 ppm ash), Pyroid pyrolytic graphite (2.2 g/cc, 10 ppm ash), and Alfa Inorganics tantalum carbide (TaC, 13 g/cc, 99.8% purity). The Pyroid samples were aligned with the *c* face perpendicular to the laser beam. All the titration samples were polished, outgassed in a vacuum oven at 1800 K for 3 hr, and then weighed in air on a microbalance (Mettler Automatic Model M5S/A) to an accuracy of $\pm 1 \mu$ g.

After insertion into the reaction vessel, each sample was again evacuated to approximately 5×10^{-6} Torr. It was observed that laser heating of the samples induced further outgassing; therefore, mass spectrometric determinations of the laser outgassing into the evacuated reaction vessel were always made prior to the titration experiments in order to correct for this contribution to the total amount

of products. Addition of the titration gas to the evacuated vessel was measured with a MKS Baratron pressure indicator to an accuracy of 1% or better.

The titration and calibration gases consisted of oxygen (Linde Ultra High Purity), hydrogen (Matheson Extra Dry, 99.9%), methane (Matheson Chemically Pure, 99.0%), helium (Matheson High Purity, 99.995%), carbon monoxide (Matheson Chemically Pure, 99.5%), carbon dioxide (Matheson Bone Dry, 99.8%), and acetylene (J. T. Baker Purified, 99.6%).

The gaseous reaction products were expanded into a known volume to measure the total pressure and were then admitted into the ion source of a time-of-flight mass spectrometer (Bendix Model 3015.). Measured ion intensities of each gaseous component were converted to absolute numbers of molecules by timely calibrations of the gas inlet and spectrometer system. Background peak intensities (from impurities in the pure reactant gas and from the mass spectrometer) were measured and subtracted from the product peak intensities to determine the absolute amount of reaction product. The measured weight loss of the sample (expressed as atoms of carbon for the graphite samples) was then compared to the total amount of gaseous products produced.

Calibration of the mass spectrometer was performed by filling the reaction vessel and inlet system with a pure product gas (C₂H₂, CO, CO₂, etc.) or mixtures of gases. The ion intensities and gas pressures were monitored over a pressure range typical of the partial pressures of the product gases.

2.2 Time-Resolved Mass Spectrometry. The abundances of carbon species, vaporizing from graphite and tantalum carbide samples during pulsed laser heating, were measured in a Bendix Model 14-101 time-of-flight mass spec-

- (11) A. P. Wolf, *Advan. Phys. Org. Chem.*, **2**, 202 (1964).
- (12) G. Stocklin and A. P. Wolf, *J. Amer. Chem. Soc.*, **85**, 229 (1963).
- (13) F. Cacace and A. P. Wolf, *J. Amer. Chem. Soc.*, **87**, 5301 (1965).
- (14) H. J. Ache and A. P. Wolf, *J. Amer. Chem. Soc.*, **88**, 888 (1966).
- (15) P. S. Skell and R. R. Engel, *J. Amer. Chem. Soc.*, **87**, 1135 (1965).
- (16) P. S. Skell and R. R. Engel, *J. Amer. Chem. Soc.*, **87**, 1135 (1965).
- (17) P. S. Skell, L. D. Wescott, Jr., J. P. Golstein, and R. R. Engel, *J. Amer. Chem. Soc.*, **87**, 2829 (1965).
- (18) R. R. Engel and P. S. Skell, *J. Amer. Chem. Soc.*, **87**, 4663 (1965).
- (19) P. S. Skell and R. R. Engel, *J. Amer. Chem. Soc.*, **88**, 3749 (1966).
- (20) P. S. Skell and R. F. Harris, *J. Amer. Chem. Soc.*, **88**, 5933 (1966).
- (21) P. S. Skell and R. R. Engel, *J. Amer. Chem. Soc.*, **88**, 4883 (1966).
- (22) P. S. Skell and R. R. Engel, *J. Amer. Chem. Soc.*, **89**, 2912 (1967).
- (23) W. Braun, A. M. Bass, D. D. Davis, and J. D. Simmons, *Proc. Roy. Soc., Ser. A*, **312**, 417 (1969).
- (24) K. Taki, P. H. Kim, and S. Namba, *Bull. Chem. Soc. Jap.*, **42**, 823 (1969).
- (25) K. Taki, P. H. Kim, and S. Namba, *Bull. Chem. Soc. Jap.*, **42**, 2377 (1969).
- (26) K. Taki, P. H. Kim, and S. Namba, *Sci. Pap. Inst. Phys. Chem. Res., Tokyo*, **63**, 41 (1969).
- (27) J. F. Verdick, *Nucl. Appl.*, **6**, 474 (1969).
- (28) J. F. Verdick and A. W. Mau, *Chem. Commun.*, 226 (1969).
- (29) J. Drowart, R. P. Burns, G. DeMaria, and M. G. Inghram, *J. Chem. Phys.*, **31**, 1131 (1959).
- (30) H. B. Palmer and M. Shelef in "Chemistry and Physics of Carbon," Vol. 4, P. L. Walker, Jr., Ed., Marcel Dekker, New York, N. Y., 1968, pp 85-136.
- (31) P. D. Zavitsanos and G. C. Carlson, Sandia Corporation Contract Report No. SC-CR-70-6126, Sandia Laboratories, Albuquerque, N. Mex., Aug 1972.
- (32) T. A. Milne, J. E. Beachey, and F. T. Greene, Midwest Research Institute Technical Management Report No. 2, (1 Sept-30 Nov 1971), Kansas City, Mo., Dec 23, 1971.
- (33) F. M. Wachi and D. E. Gilmartin, *High Temp Sci.*, **4**, 423 (1972).
- (34) J. Berkowitz and W. A. Chupka, *J. Chem. Phys.*, **40**, 2735 (1964).
- (35) P. D. Zavitsanos, General Electric Space Sciences Laboratory Report No. R67SD11, Mar 1967.
- (36) K. A. Lincoln in "High Temperature Technology," Butterworths, London, 1969 pp 323-332.

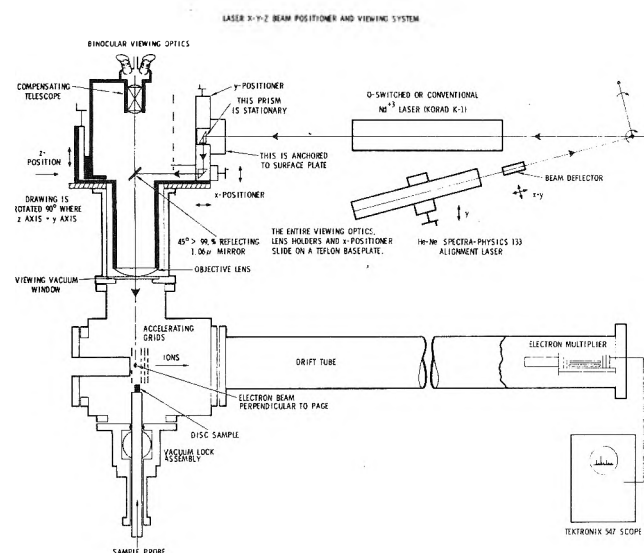


Figure 1. Diagram of apparatus for time-resolved mass spectrometric studies of laser-induced vaporization; principal components are Bendix Model 14-101 time-of-flight mass spectrometer, Korad K1Q neodymium laser, and microscope for focusing of laser beam.

trometer by time-resolved recording techniques.^{37,38} The Pyroid graphite sample was placed 5 cm below the ionizing electron beam of the ion source. An electron beam energy of 18.6 eV prevented major fragmentations of C_n species that occur above 20 eV. The laser beam, attenuated to an intensity of 0.1 J for the Q-switched mode to prevent saturation of the ion source and electron multiplier, was focused with an optical microscope through the ion source onto the sample to a spot size of 0.5-mm diameter. The microscope was patterned after an optical system developed by Vastola, Pirone, and Knox.^{39,40} A partial schematic of the laser, mass spectrometer, and microscope optics is shown in Figure 1.

The TaC sample was placed below a baffle containing a 11.4×0.8 mm rectangular slit at a distance of 25 cm from the electron beam. The laser beam was directed through a side window in the baffle housing and focused onto the sample with an external lens. The baffle was required in order to allow only a fraction of the vapor to enter the ionization space and to prevent saturation of the spectrometer. For the TaC, the laser was operated in the normal mode at an incident energy of 18 J.

Carbon vapor ion intensities were monitored by a synchronized z-axis gating method for quantitative measurements and by a three-dimensional intensity-modulated raster display for qualitative results.³⁸ Both methods employ photographic recording of an oscilloscope trace.

Conversion of ion intensities integrated over the duration of vaporization, Π^+ , to relative vapor-phase abundances, $A(C_n)$, were made by⁴¹

$$\frac{A(C_n)}{A(C_1)} = \frac{\Pi^+(C_n)}{\Pi^+(C_1)} \left(\frac{\sigma(C_1)}{\sigma(C_n)} \right) \left(\frac{\Delta E(C_1)}{\Delta E(C_n)} \right) \left(\frac{\gamma(C_1)}{\gamma(C_n)} \right) \quad (1)$$

The conversion factors include maximum ionization cross sections, σ , relative ionization cross sections, ΔE , and the electron multiplier yields, γ . The values were those recommended by Meyer and Lynch⁴² and are tabulated in Table I.

Equation I was also used to calculate relative partial pressures, $P(C_n)/P(C_1)$, at the peak surface temperature created by the laser heating. This ratio was obtained by

TABLE I: Factors for Conversion of Ion Intensities to Relative Abundances or Partial Pressures for Carbon Vapor Studies

Conversion factor ^a	Carbon vapor species		
	C_1	C_2	C_3
Relative maximum ionization cross sections	1.00	1.50	1.84
Relative ionization cross sections at 18.6 eV	1.00	0.90	0.82
Relative electron multiplier yields	1.00	0.71	0.58
Langmuir vaporization coefficients	0.24	0.50	0.023

^a See text for references.

substituting the peak ion intensities recorded immediately after the laser pulse, I^+ , for the integrated ion intensities, Π^+ . Two additional modifications to eq I were required for a comparison of the calculated partial pressure ratios with the literature. First, the ratio of electron multiplier yields was set equal to unity for all species in order to be consistent with the evaluations of partial pressure data as reported in the literature (ref 29–31, 43, and 44). Second, the vaporization conditions for the mass spectrometric analyses were more nearly free evaporation (Langmuir vaporization) in nature than equilibrium (Knudsen cell type); hence, Langmuir vaporization coefficients, α , were applied to obtain relative “equilibrium” partial pressures

$$P_{eq} = \alpha P \quad (II)$$

The absolute values of the Langmuir coefficients used were those obtained by Zavitsanos⁴³ (see Table I).

3. Results

3.1 Survey of Laser-Induced Chemical Reaction Products. Identification of specific gaseous products from the reaction of laser-vaporized carbon species with O_2 , H_2 , and CH_4 was performed using the gas titration procedures described above. Outgassed Poco graphite samples were heated with Q-switched laser energy of 2.5–3.0 J, focused to about 1200 J/cm^2 . Initial pressures of the reactant gases were about 0.2 Torr.

The observed products were CO and CO_2 from the O_2 reaction, C_2H_2 , a small amount of C_4H_2 , and a trace amount of mass 78 (possibly a C_6H_6 compound) from the H_2 reaction, and C_2H_2 , and a small amount of C_4H_2 from the CH_4 reaction. The products of laser vaporization in He and under vacuum were $CO + H_2$ and $CO_2 + CO + H_2 + C_2H_2$, respectively; the absolute amounts of products were always significantly less in He and under vacuum than the amounts produced with the reactive gases. For example, the amount of C_2H_2 produced from H_2 was 3.8×10^{17} molecules compared to 4×10^{16} molecules out-

- (37) R. T. Meyer, *J. Sci. Instrum.*, **44**, 422 (1967).
 (38) R. T. Meyer in “Time-of-Flight Mass Spectrometry,” D. Price and J. E. Williams, Ed., Pergamon Press, Oxford, 1969, pp 61–87.
 (39) F. J. Vastola, A. J. Pirone, and B. E. Knox, Paper presented at 14th Annual Conference on Mass Spectrometry and Allied Topics, Dallas, Tex., May 1966.
 (40) F. J. Vastola and A. J. Pirone, *Advan. Mass Spectrom.*, **4**, 107 (1968).
 (41) R. T. Grimley in “The Characterization of High Temperature Vapors,” J. L. Margrave, Ed., Wiley, New York, N. Y., 1967, pp 195–243.
 (42) R. T. Meyer and A. W. Lynch, *High Temp. Sci.*, **5**, (1973).
 (43) P. D. Zavitsanos, General Electric Company Report No. R66SD31, May 1966; also in “Dynamic Mass Spectrometry,” Heyden & Son, Ltd., 1970, p 1.
 (44) “JANAF Thermochemical Tables,” *Nat. Stand. Ref. Data Ser., Nat. Bur. Stand., (U.S.)*, **37** (1971).

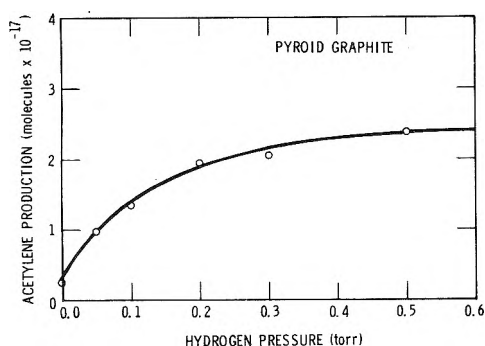


Figure 2. Titration curve for the production of C_2H_2 from the reaction of carbon species, which were laser vaporized from Pyroid graphite, with H_2 as a function of H_2 pressure: Q-switched laser, 2.5–3.0 J focused per irradiation, four irradiations per experiment.

gassed in the vacuum experiment. Likewise, $CO + CO_2$ totaling 9.7×10^{17} molecules were produced from the O_2 reaction, but only 2.5×10^{16} molecules of CO_2 were outgassed. In each of these experiments, the equivalent of approximately 4×10^{18} atoms of carbon was lost from the Poco graphite sample.

Graphite samples which were not outgassed prior to laser vaporization yielded larger quantities and a larger variety of desorbed molecules. The latter included CO , CO_2 , H_2 , CH_4 , C_2H_2 , C_2H_4 , C_4H_2 , and some C_3 compounds.

3.2 Product Analysis Using Titration Techniques. The formation of the principal products was followed as a function of reactant gas pressure for both Poco and Pyroid graphites. The data curves for Pyroid graphite are shown in Figures 2 and 3; similar titration curves were obtained from the Poco graphite. The laser parameters were the same as cited in section 3.1.

The formation of C_2H_2 from H_2 , shown in Figure 2, increased with increasing pressure of H_2 and achieved an apparent plateau at about 0.5 Torr of H_2 with the production of about 2.4×10^{17} molecules. The actual number of carbon atoms vaporized was determined from weight loss measurements. Mass loss from the Pyroid graphite was very reproducible, the average value for the six experiments (each consisting of four laser irradiations of the sample) being $1.16 (\pm 0.12) \times 10^{18}$ atoms of carbon. Thus, the number of molecules of C_2H_2 generated was less than the number of carbon atoms vaporized.

Figure 3 shows that the onsets of the plateaus for CO and for CO_2 production were different, occurring at approximately 0.1 Torr for CO and 0.4 Torr for CO_2 . O_2 consumption leveled off between 0.3 and 0.5 Torr. The ratio of CO to CO_2 reached a constant value of 2.5 above 0.2 Torr. The maximum number of molecules of $CO + CO_2$ produced was 1.45×10^{18} at 0.5 Torr. If the amount of $CO + CO_2$ produced in the vacuum experiment (0.38×10^{18} molecules) is subtracted, the net increase in $CO + CO_2$ (1.05×10^{18} molecules) corresponds very closely with the average number of carbon atoms vaporized ($1.18 (\pm 0.08) \times 10^{18}$ atoms) for the six experiments.

3.3 Vapor Products and Mass Loss. Titration experiments were conducted as a function of incident laser energy in order to determine the correlation between the mass of carbon vaporized and the number of molecules of gaseous titration products. The results are given in Table II for the vaporization of Pyroid graphite with the Q-switched laser operated from 2.0 to 3.0 J (1000–1500

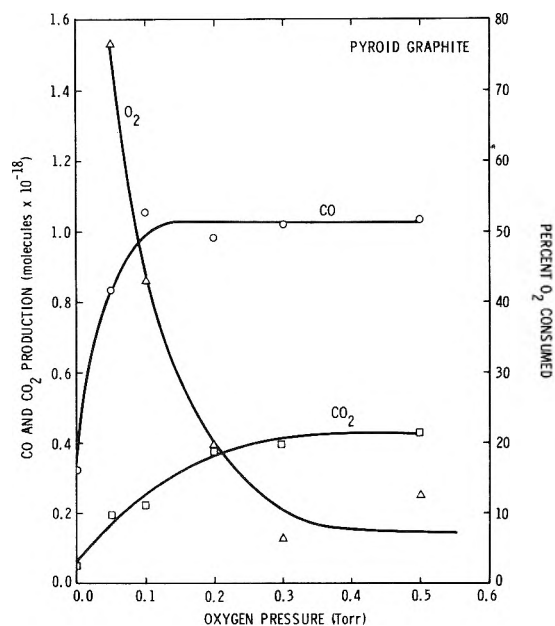


Figure 3. Titration curves for the production of CO and CO_2 and for the per cent consumption of O_2 from the reaction of carbon species, which were laser vaporized from Pyroid graphite, with O_2 as a function of O_2 pressure: Q-switched laser, 2.5–3.0 J focused per irradiation, four irradiations per experiment.

TABLE II: Gas Titrations and Mass Losses for Laser-Vaporized Pyroid Graphite as a Function of Laser Energy^a

Incident laser energy, J/irradiation	Carbon mass loss, atoms $\times 10^{-17}$	CO , molecules $\times 10^{-17}$	CO_2 , molecules $\times 10^{-17}$	Total $CO + CO_2$, molecules $\times 10^{-17}$
Reaction with Oxygen (0.2 Torr)				
3.0	8.0	6.7	2.0	8.7
2.5	6.0	4.0	1.7	5.7
2.0	3.5	2.0	1.0	3.0
Reaction with Hydrogen (0.2 Torr)				
3.0	8.0		4.3	
2.0	2.5		2.2	
Reaction with Methane (0.2 Torr)				
3.0	7.0	12.5	2.7	~ 1.2
2.0	2.0	6.3	1.6	~ 0.6

^a Q-switched laser, four focused irradiations per experiment.

J/cm² focused). The titrations were separately performed with O_2 , H_2 , and CH_4 , each at 0.2 Torr.

Table II shows that the measured mass loss systematically decreased with decreasing laser energy. This indicated that the total quantity of vaporized carbon species could be varied.

The titrations with O_2 provided the interesting result that the amounts of CO , CO_2 , and $CO + CO_2$ produced were proportional to the laser energy and to the amount of carbon vaporized. In fact the $CO + CO_2$ sum quantita-

TABLE III: Gas Titrations of Carbon Vapor Species from Laser-Vaporized Tantalum Carbide^a

Gaseous products ^b	Titrating conditions (gases at 0.2 Torr)		
	Vacuum	H ₂	O ₂
C ₂ H ₂		6.5 × 10 ¹⁵	
CO	2.4 × 10 ¹⁶		3.2 × 10 ¹⁷
CO ₂			5.1 × 10 ¹⁶
Total	2.4 × 10 ¹⁶	6.5 × 10 ¹⁵	3.7 × 10 ¹⁷
Mass loss, ^c μg	139	100	71

^a Normal mode laser, 50 J focused, one irradiation per experiment.
^b Products are in units of molecules. ^c 100 μg ≡ 3.1 × 10¹⁷ molecules of TaC.

tively agrees with the number of carbon atoms vaporized in each of the three experiments.

The titrations with H₂ and CH₄ also showed a correlation between incident laser energy, mass loss, and number of product molecules. The production of C₂H₂ molecules from the H₂ reaction, however, was only about 7% of the number of carbon atoms vaporized. This is in agreement with the two H₂ titrations previously described, in which it was found that the amount of C₂H₂ produced from H₂ was substantially less than the total of CO + CO₂ produced from O₂.

The reaction with CH₄ actually yielded a larger quantity of C₂H₂, H₂, and C₄H₂ than could be ascribed to the vaporization of carbon species. This result was due to pyrolysis of the CH₄ gas on the sample; hence, reactions with CH₄ were not investigated further.

3.4 Titrations of Laser-Vaporized Tantalum Carbide. In order to achieve a different initial distribution of vaporized C_n species, TaC was chosen, since some information indicated that C₁ should be the predominant vapor species.⁴⁵ The results of gas titrations with O₂, H₂, and CH₄ at 0.2 Torr are shown in Table III. The TaC was vaporized with the laser operating in the normal mode at 50 J of focused energy; the higher energy was needed due to the higher reflectivity of TaC.

A quantitative correlation of molecules produced with mass loss cannot be made with TaC because it does not vaporize congruently; however, comparisons of the relative amounts of various products are informative. It was found first that the ratio of CO to CO₂ was about 6:1, which is higher by a factor of 2–2.5 than the ratios measured at an O₂ pressure of 0.2 Torr in the titrations of laser-vaporized graphites. Second, for a given mass loss the ratio of CO + CO₂ from the O₂ reaction to the C₂H₂ from the H₂ reaction was about 80:1, whereas the ratios for the graphite experiments varied but averaged about 10:1.

3.5 Higher Pressure Hydrogen Titrations. Experiments with Pyroid graphite in which D₂ was substituted for H₂ as the titrating gas revealed that ten times more D₂ than H₂ was required to produce approximately an equivalent quantity of C₂D₂ as C₂H₂. Essentially no C₂D₂ was produced in titration experiments with D₂ at a gas pressure of 0.3 Torr. It was only when the D₂ pressure was increased to 5.0 Torr that a significant quantity of C₂D₂ was detected. This result correlates with the known isotope effect on the rate constants for D₂ and H₂ reactions. That is, the heavier mass D₂ reacts more slowly than does H₂.^{46,47} Therefore, the conclusion applied to our results was that at 0.3 Torr of D₂, the reaction probability was too low for reaction to occur before the vaporized C_n

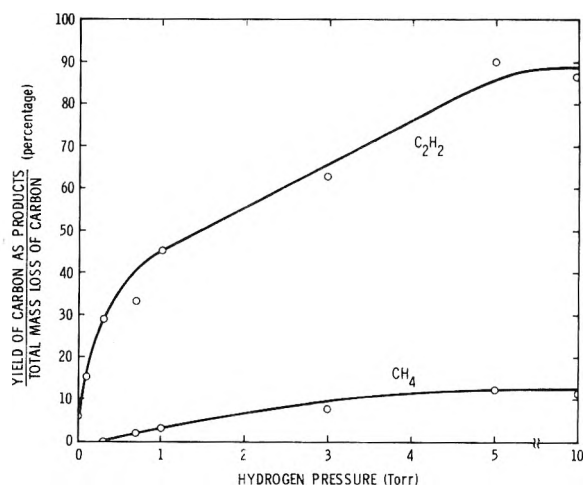


Figure 4. Titration curves for the yields of C₂H₂ and CH₄ from the reaction of carbon species, which were laser vaporized from Pyroid graphite, with H₂ at gas pressures up to 10 Torr. Yields are expressed in terms of the per cent of total carbon mass loss from the graphite sample: Q-switched laser, 2.5–3.0 J focused per irradiation, four irradiations per experiment.

species were trapped out on the walls of the 1-l. reaction vessel. This conclusion suggested that the C₂H₂ plateau at 0.5 Torr in the H₂ titration (Figure 2) also corresponded to the termination of the reaction due to diffusion of the C_n species to the walls.

Hence, titration experiments were performed with H₂ for the range from 0.1 to 10 Torr. The data are shown in Figure 4, where the yield of carbon in each product is expressed in terms of the per cent of the total carbon mass loss from the Pyroid graphite target. The most important feature is that the C₂H₂ yield does not level off at a constant value at 0.5 Torr of H₂, but the yield curve does undergo a change in slope. The C₂H₂ yield reaches its maximum value at 5 Torr for there is no further increase in yield at 10 Torr of H₂. The low-pressure change in slope occurs at about 30% carbon mass loss, the number which is obtained by extrapolating the high-pressure portion of the curve down to zero pressure and subtracting out the outgassed contribution at zero pressure. The high-pressure plateau occurs between 85 and 90% carbon mass loss.

A new feature of these H₂ titrations is the production of CH₄. A measurable amount was obtained for the experiments at or above about 0.5 Torr of H₂. The CH₄ yield then increased up to 5 Torr, at which point it leveled off at a value corresponding to about 12% of the carbon mass loss. C₄H₂ was also detected at the higher pressures, but the quantity remained very small and apparently independent of the total pressure. A very small amount of mass 78 was detected starting at 0.7 Torr of H₂ and appeared to increase slightly as the pressure was increased. The molecular structure of mass 78 has not been identified.

The results indicate that essentially complete titration of the vaporized C_n species can also be accomplished with H₂ if sufficient H₂ or a sufficient gas pressure is maintained to prevent diffusion of the C_n species or successor radicals to the walls.

(45) C. H. Williams, Sandia Laboratories, private communication.

(46) S. Glasstone, K. J. Laidler, and H. Eyring, "The Theory of Rate Processes," McGraw-Hill, New York, N. Y., 1941, pp 228–236.

(47) L. Melander, "Isotope Effects on Reaction Rates" Ronald Press, New York, N. Y., 1969.

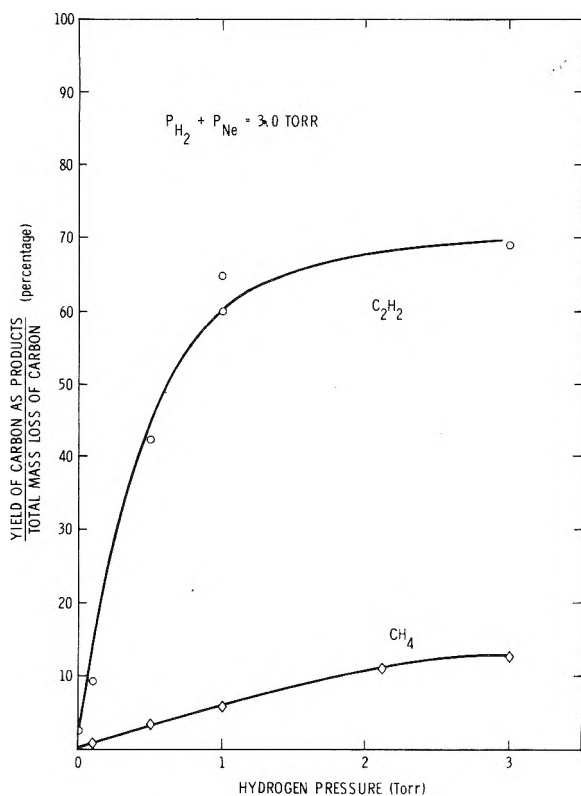


Figure 5. Titration curves for the yields of C_2H_2 and CH_4 from the reaction of carbon species, which were laser vaporized from Pyroid graphite, with H_2 in a $H_2 + Ne$ mixture with total pressure constant at 3 Torr. Yields are expressed in terms of the per cent of total carbon mass loss from the graphite sample: Q-switched laser, 2.5–3.0 Joules focused per irradiation, four irradiations per experiment.

In order to further test the role of diffusion on C_2H_2 production, a series of experiments with hydrogen–neon mixtures at a constant total pressure of 3 Torr was performed. The results are plotted in Figure 5 as a function of the partial pressure of H_2 . The neon did increase the C_2H_2 and CH_4 yields over that obtained in pure H_2 . For example, at 0.5 Torr of H_2 , the C_2H_2 yield was 40–45% of the carbon mass loss in the presence of 2.5 Torr of neon, but was only 30–35% in pure H_2 ; at 1.0 Torr of H_2 , the C_2H_2 yield was 60–65% in the neon experiment and only 40–45% in the pure H_2 experiment. However, at 0.3 Torr of H_2 , the yields with and without neon present were both 25–30%. At the 3-Torr point which was pure H_2 , the C_2H_2 yield was 69% and was in good agreement with the 65% value obtained in Figure 4. Thus, the yields above the low-pressure plateau at 0.5 Torr of H_2 were increased by the presence of an inert gas which reduced diffusion to the walls, while the yields below the low-pressure plateau were affected in only a small way.

3.6 Tests for Surface Reactions. The possible occurrence of surface reactions on the graphite was tested in two ways. The first was whether the mass loss was greater in the presence of added gases than under vacuum. The data collected for Figures 2 and 3 clearly show that the mass loss was the same for the experiments with the Pyroid graphite whether or not the heated surface was exposed to hydrogen, oxygen, or vacuum. The second test was whether the CO_2 was produced from the oxidation of CO adsorbed on a surface. A tantalum sample was laser heated in the presence of a mixture of CO and O_2 prepared to

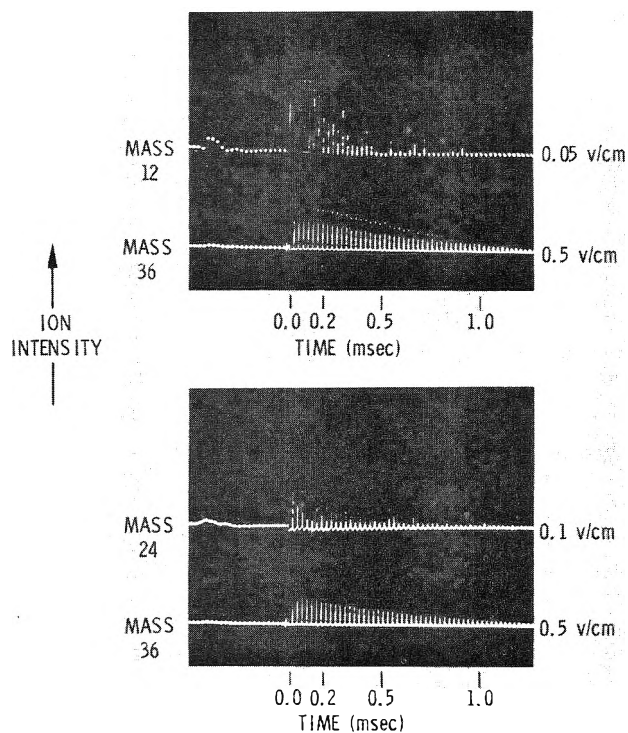


Figure 6. Polaroid film records of time-resolved mass spectra (18.6 eV) of C_1 , C_2 , and C_3 vapor species from laser-heated Pyroid graphite. Relative abundances of species are proportional to ion intensities integrated over the duration of vaporization: Q-switched laser, 0.1 J focused, one irradiation.

simulate a typical titration product environment ($p(CO) = 0.003$ Torr, $p(O_2) = 0.2$ Torr). No CO_2 was produced.

3.7 Vapor Compositions Determined by Time-Resolved Mass Spectrometry. The vapor compositions for laser-heated Pyroid graphite and TaC were measured directly by time-resolved mass spectrometry in order to identify the vapor species that reacted to form the various products in the titration experiments. The major vapor species released from graphite were C_1 (mass 12), C_2 (mass 24), C_3 (mass 36), H_2 (mass 2), CO (mass 28), C_2H_2 (mass 26), C_4H_2 (mass 50), and C_6H_2 (mass 74). Small amounts of C_4 (mass 48), C_5 (mass 60), and C_7 (mass 84) were also recorded immediately after the laser pulse in some experiments. Various quantities of other hydrocarbon impurities were released and were faintly detectable over the entire mass range after 0.5 msec. Of the C_n species, C_3 was by far the most abundant. On occasion, small amounts of thermal ions C_n^+ were seen immediately after the laser pulse, but they never persisted beyond 20 μsec .

The TaC vapor composition consisted principally of C_1 (mass 12), C_3 (mass 36), C_2H_2 (mass 26), and CO (mass 28). Only a small amount of C_2 (mass 24) was detected. Very small amounts of C_1^+ and Ta^+ , vaporized as ionic species, were also observed.

The relative ion intensities of C_1 , C_2 , and C_3 were recorded for several identical laser vaporization experiments using the z -axis gating technique for a comparison of C_3 and C_1 and then for C_3 and C_2 . Typical oscillographic records are shown in Figure 6 for graphite and in Figure 7 for TaC. The total quantity of each C_n species vaporized was measured by integrating the area under the curve traced out by the maximum peak heights of the spectrometer signals for each mass. The averages of these integrated ion intensities are summarized in Table IV.

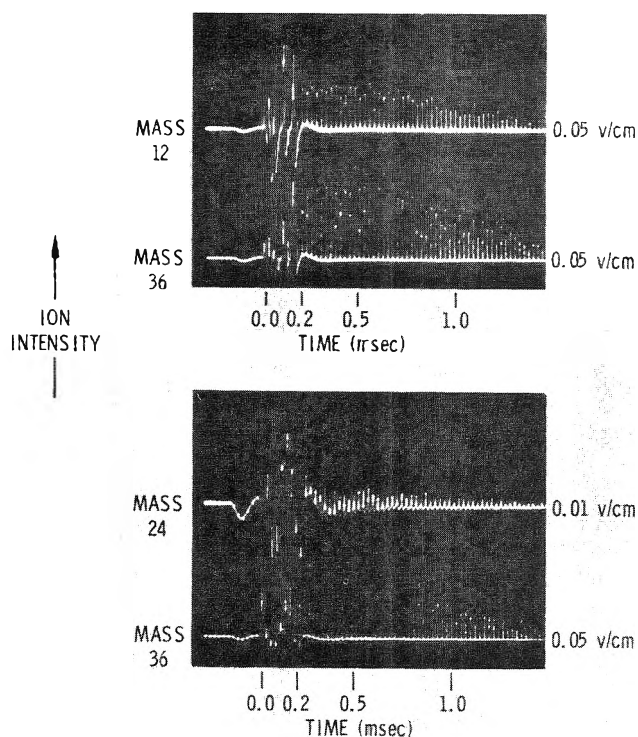


Figure 7. Polaroid film records of time-resolved mass spectra (18.6 eV) of C_1 , C_2 , and C_3 vapor species from laser-heated TaC. Relative abundances of species are proportional to ion intensities integrated over the duration of vaporization: normal-mode laser, 18 J focused, one irradiation.

Relative vapor-phase abundances, A , of the C_n species were obtained from the integrated ion intensities II^+ by applying eq I. As used in the present context, the relative vapor-phase abundances are not relative partial pressures since the integrated ion intensities are measured over an interval of time during which the temperature of the vaporizing surface is decreasing. The abundances are a measure of the total amount of each C_n species vaporized, which is precisely the quantity needed for comparison with the gas titration results.

Significant differences in the vapor compositions for graphite and for TaC were observed. The relative abundances of C_1 , C_2 , and C_3 for graphite were 1.0:1.4:17, and for TaC were 1.0:0.059:2.2 (see Table IV). The relative abundances were not observed to change much as the incident laser energy was varied, although increasing the laser energy did cause an increase in the absolute amounts of all species. The $A(C_3)/A(C_1)$ and $A(C_2)/A(C_1)$ ratios were both lower for TaC than for graphite. As previously mentioned, C_2 was barely detectable from TaC and, therefore, probably can be excluded from consideration in the titration experiments. The data expressed as weight fractions are also listed in Table IV.

While the emphasis so far has been on calculating the relative abundances of the C_n species, the relative partial pressures will be used later in order to estimate the maximum surface temperature achieved with the laser heating. The relative partial pressures at the maximum temperature may also be obtained from the time-resolved ion intensity data records. The ion intensities used for this calculation are the peak values recorded shortly after the laser pulse; for example, in Figure 6 the ion intensities achieved a maximum value at 80 μ sec and then decayed in amplitude for the next 1000 μ sec. For Pyroid graphite the relative peak ion intensities, averaged from several ex-

TABLE IV: Relative Abundances and Partial Pressures of Carbon Vapor Species as Computed from Time-Resolved Mass Spectrometry Ion Intensities and Various Conversion Factors

Parameters	Carbon vapor species		
	C_1	C_2	C_3
Pyroid graphite integrated ion intensities	1.0	1.3	18
Pyroid graphite relative abundances	1.0	1.4	17
Pyroid graphite weight fractions	0.018	0.049	0.93
Tantalum carbide integrated ion intensities	1.0	0.056	1.9
Tantalum carbide relative abundances	1.0	0.059	2.2
Tantalum carbide weight fractions	0.13	0.015	0.86
Pyroid graphite peak ion intensities	1.0	0.9	5.1
Pyroid graphite relative partial pressures	1.0	0.32	35
JANAF relative partial pressures for graphite at 4500 K	1.0	1.9	13
Palmer and Shelef relative partial pressures for graphite at 4500 K	1.0	2.1	36

periments, were 1.0:9.0:5.1 for $C_1:C_2:C_3$. These values were converted to relative partial pressures by use of eq 1 and 2 and yielded average pressure ratios of 1.0:0.32:35.

4. Discussion

4.1 Effect of Laser Energy. The mass spectrometric determinations of the relative abundances of the C_n species may be applied to the chemical titration experiments even though different incident laser energies were employed. This is a consequence of the surface temperature having achieved a maximum value independent of laser energy at incident energies equal to or lower than those used in the mass spectrometry experiments. Meyer, *et al.*, have compiled vapor composition data for a number of pulsed laser investigations of graphite vaporization and have shown that the measured relative partial pressures of the C_n species are essentially the same for incident laser energies ranging from 50 to 8000 J/cm^2 .⁴⁸ The surface temperatures estimated by the original investigators all fall within the 4000- to 4500-K range.^{34-36,49,50}

The relative partial pressures measured at maximum temperature in the present experiments were 1.0:0.32:35 for $C_1:C_2:C_3$. Comparison of the $C_3:C_1$ ratio with the Palmer and Shelef³⁰ evaluation of carbon vapor-pressure data indicates an effective vaporization temperature of 4500 K, while comparison with Drowart's²⁹ original data, which have been extrapolated in the "JANAF Thermochemical Tables,"⁴⁴ indicates a temperature in excess of 4500 K.

The titration data of Table II for graphite show that the mass loss, CO production, and CO_2 production all were roughly proportional to the incident laser energy (2.0-3.0 J or 1000-1500 J/cm^2). These results imply that a change in laser energy at the applied levels changed primarily the bulk amount of material heated rather than the temperature of the material; in other words, a larger volume of the sample was heated to vaporization temper-

(48) R. T. Meyer, A. W. Lynch, and J. M. Freese, paper presented at 20th Annual Conference on Mass Spectrometry and Allied Topics, Dallas, Tex., June 1972.

(49) K. A. Lincoln, private communication.

(50) J. A. Howe, *J. Chem. Phys.*, **39**, 1362 (1963).

ature but the effective vaporization temperature remained about the same. Since the incident laser energy for these experiments fell within the range of values cited by Meyer, *et al.*, in their comparison of laser experiments,⁴⁸ it appears that a temperature of 4000–4500 K was achieved.

When the above evidence is combined with the fact that the relative abundances of C₁, C₂, and C₃ do not change very much with temperature,³⁰ we conclude that the vapor composition measured by time-resolved mass spectrometry was approximately the same as that produced in the titration experiments.

4.2 Evaluation of Chemical Titrations. The most convincing evidence for the gas-phase titration of the vaporized carbon species is the excellent quantitative agreement between the measured mass loss from the Pyroid graphite samples and the total amount of CO and CO₂ formed. The data have been presented in Table II and in Figure 3. These data show that all of the vaporized species, regardless of the C_n distribution, end up as two stable gaseous products. The fact that the mass loss was constant from experiment to experiment and was not reduced for the oxygen-free vacuum experiments substantiates that the mass loss was not a result of O₂ reacting at the hot surface and converting solid carbon to gaseous CO and CO₂.

The reproducibility of the oxygen titration data and the existence of a plateau in the titration curves supports the conclusion that chemical titration of the laser-vaporized carbon species occurred. The general shape of the plots of CO and CO₂ vs. O₂ partial pressure has been reproduced in a number of experiments using both Poco and Pyroid graphites. All of the plots display plateaus indicating a completion of chemical reaction above a certain minimum oxygen partial pressure. In addition, the total amount of product formed at completion of reaction was directly proportional both to the number of laser shots and to the laser energy per shot (see Table II), *i.e.*, to the total mass vaporized. The experiments using Pyroid graphite were quantitatively reproducible to ±10% over extended periods of time (days and months) between experiments.

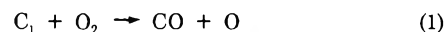
The low-pressure (<0.5 Torr) titration data for pure hydrogen also exhibited acetylene yields which were fairly reproducible. Extension of the hydrogen titration experiments to higher pressures (Figures 4 and 5) yielded amounts of C₂H₂ which accounted for 85–90% of the total vaporized carbon. The total amount of gaseous products, C₂H₂ + CH₄ + C₄H₂, accounted for at least 95% of the vaporized carbon. Therefore, like the oxygen titration results, gas-phase chemical titration of C_n with H₂ does occur. Higher H₂ pressures than O₂ pressures are required to overcome the apparently lower reaction probabilities of C_n with H₂.

Evidence has been presented by Clarke and Fox,^{51,52} Baddour and Blanchett,⁵³ and Wood and Wise⁵⁴ which further shows that homogeneous gas-phase reactions dominate over surface reactions when temperatures exceeding 3000 K are achieved in the carbon plus O₂, H₂, or CH₄ systems.

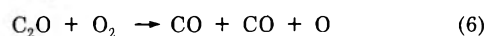
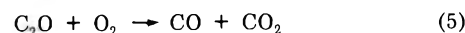
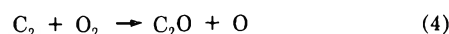
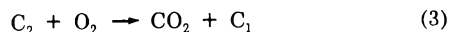
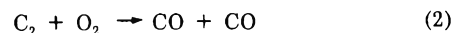
4.3 Chemical Mechanisms. 4.31 Reactions with Oxygen. An objective of this research was to find specific chemical reactions for the selective titration of individual C_n species. Titration of the vaporized carbon species, which were shown by the mass spectrometry results to be principally C₁, C₂, and C₃, with O₂ produced two products, CO

and CO₂. The ratio of CO:CO₂ was observed to be approximately 2.5:1 for graphite vaporization and 6:1 for TaC vaporization.

Wolfgang showed that C₁ reacts with O₂, according to the reaction^{1,3}

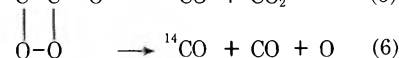
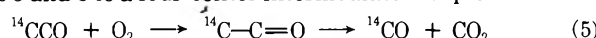


No CO₂ is formed. The present results indicate, therefore, that CO₂ must be a product of C₂ and/or C₃ reacting with oxygen. Possible mechanisms for C₂ reactions are

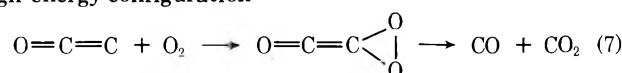


Reactions 2 and 3 followed by reaction 1 could readily account for a CO:CO₂ ratio greater than unity if C₂ were the only carbon vapor species and if all three reactions were equally probable. C₂O is known to react with O₂ to produce CO and CO₂ and is regarded as a carbon-atom donor equivalent to hydrocarbon fragment molecules,⁵⁵ therefore, reactions 4–6 must also be considered.

In their studies of the C₂O + O₂ reaction, Williamson and Bayes recorded an 8:1 ratio for CO:CO₂.⁵⁶ Peterson and Wolfgang, using end-labeled ¹⁴CCO, attributed reactions 5 and 6 to a four-center intermediate complex⁵⁵

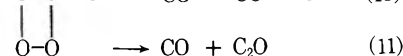
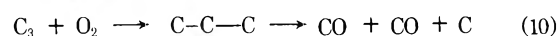
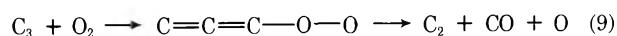
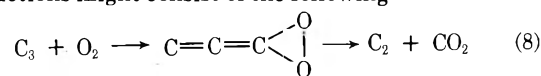


They concluded that reaction 7 would not be a significant source of CO₂ since it requires an intermediate with a high-energy configuration



Reaction 3 would require a similar high-energy complex and is, therefore, much less probable than reactions 2 and 4; hence, reaction 5 is regarded as the pathway to CO₂ formation from C₂.

A large number of reactions of C₃ with O₂ can be written which will generate both CO and CO₂ as products. Initial reactions might consist of the following



Reaction 8 has been proposed by Zavitsanos and Brewer as a source of the electronically excited C₂ molecules responsible for the Swan bands that have been observed in the oxidation of gaseous carbon.⁵⁷ However, reaction 8 re-

(51) J. T. Clarke and B. R. Fox, *J. Chem. Phys.*, **46**, 827 (1967).

(52) J. T. Clarke and B. R. Fox, *J. Chem. Phys.*, **51**, 3231 (1969).

(53) R. F. Baddour and J. L. Blanchett, *Ind. Eng. Chem., Process Des. Develop.*, **3**, 258 (1964).

(54) B. J. Wood and H. Wise, *J. Phys. Chem.*, **73**, 1348 (1969).

(55) R. F. Peterson, Jr., and R. L. Wolfgang, *Chem. Commun.*, 1201 (1968).

(56) D. G. Williamson and K. D. Bayes, *J. Amer. Chem. Soc.*, **89**, 3390 (1967).

(57) P. D. Zavitsanos and L. E. Brewer, *J. Chem. Phys.*, **47**, 3093 (1967).

TABLE V: Comparison of the Mole Fractions of the Carbon Vapor Species with the CO₂ Product Mole Fractions for the Experiments with Pyroid Graphite and Tantalum Carbide

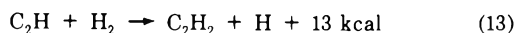
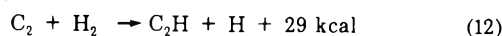
Mole fractions	Pyroid graphite	Tantalum carbide
Time-Resolved Mass Spectrometry Data		
C ₁ /(C ₁ + C ₂ + C ₃)	0.052	0.31
C ₂ /(C ₁ + C ₂ + C ₃)	0.072	0.018
C ₃ /(C ₁ + C ₂ + C ₃)	0.88	0.68
Gas-Phase Titration Data		
CO ₂ /(CO + CO ₂)	0.29	0.14

quires an intermediate complex involving a high-energy configuration similar to reaction 7 whereas reaction 9 does not. Reactions 10 and 11 are patterned after Wolfgang's model for C₂O reactions 5 and 6.⁵⁵

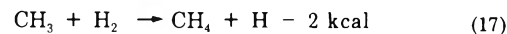
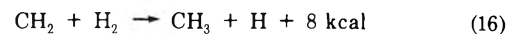
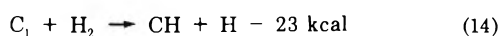
CO₂ is not directly generated in reactions 9 or 11, but subsequent reactions of C₂ or C₂O with O₂ could yield CO₂. If reactions 3–11 all occur, then the production of CO₂ cannot be ascribed specifically to one or the other, C₂ or C₃; however, if reaction 4 has a very low probability relative to the others, the CO₂ might be uniquely identified with C₃ reaction 11 followed by reaction 5. In any case, C₂O appears to be the precursor to CO₂ formation from the reaction of C₂ or C₃ with O₂.

Assuming the above set of reactions, the production of CO is common to all three carbon vapor species. The increase in the CO:CO₂ ratio for TaC vaporization compared to graphite vaporization then carries implications regarding the relative abundances of the vapor species and possibly regarding the relative importance of the CO and CO₂ producing reactions. The CO:CO₂ ratio increase for TaC was accompanied by changes in the ratios of the C_n species, as derived from the mass spectrometry results. A comparison of the mole fractions of vapor species with the mole fractions of product molecules is given in Table V. The mole fractions of C₂ are too low to account for the complete formation of CO₂. The mole fractions of C₃ do exceed the mole fractions of CO₂, which is consistent with a set of reactions, e.g., eq 9–11, in which pathways to multiple products exist. Furthermore, the mole fraction of CO₂ decreased by a factor of 2.0 from graphite to TaC and the mole fraction of C₃ decreased by a factor of 1.3, whereas the mole fraction of C₂ decreased by a factor of 4.0. Therefore, it appears that C₃ is the principal source of the CO₂ formation.

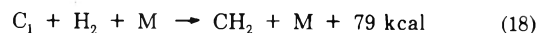
4.32 Reactions with Hydrogen. The objective of the hydrogen titration experiments was to test whether the formation of acetylene could be attributed principally to the reaction of C₂ via the mechanism suggested by Namba, *et al.*,^{24–26} and by Verdieck, *et al.*^{27,28}



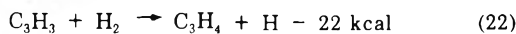
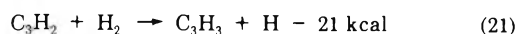
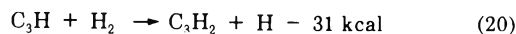
If C₁ and C₃ reacted to form other products and if C₂ reacted to form only C₂H₂, then a measurement of the C₂H₂ formed would provide a direct measurement of the vapor abundance of C₂. Wolfgang, *et al.*, showed that C₁ reacted with H₂ to form methyne, methylene, and methyl radicals with methane as the principal final product;^{8,10} *i.e.*



Wolfgang, *et al.*, and Braun, *et al.*, both reported that higher gas pressures were required before a methylene radical could be formed by direct combination^{8,10,23}



Reactions of C₃ with H₂ have not been studied previously. The premise of the present study was that C₃ would probably abstract hydrogen atoms in a manner analogous to the C₁ and C₂ reactions shown above;⁵⁸ *i.e.*



It was presumed that C₃ reactions would yield products other than C₂H₂; therefore, C₂H₂ would remain a unique product of C₂ with H₂.

The low-pressure ($p(\text{H}_2) < 0.5$ Torr) titrations of laser-vaporized graphite and tantalum carbide repeatedly showed C₂H₂ as the principal final product, although small amounts of C₄H₂ were occasionally detected (C₄H₂ ≤ 0.1C₂H₂). No methane was observed. The absolute amount of C₂H₂ at the apparent low-pressure plateau of the titration curves for graphite typically accounted for 10–30% by weight of the vaporized carbon. For TaC, the C₂H₂ equalled only 2% of the total amount of CO + CO₂ formed in the oxygen titrations. These results suggested that the C₂H₂ formed at low pressure was indeed attributable to a single C_n species.

Extension of the H₂ titration experiments to higher pressures of H₂ and to higher total pressures using H₂–Ne mixtures did reveal that the low-pressure plateau was not a final state in C₂H₂ formation.

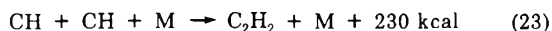
These results are consistent with a model in which the effective reaction time is limited by diffusion of the reacting species to the vessel walls. An increase in the total pressure of hydrogen or the addition of a heavier inert gas (neon) increases the number of gas-phase collisions and the residence time of the vaporized carbon species in the gas phase. Therefore, condensation and reaction termination of the carbon species on the walls is reduced and the probability of gas-phase reaction is increased. (This model for termination of the reaction was supported by an auxiliary experiment in which the carbon target was placed closer to the wall of the Pyrex vessel; at 3 Torr of pure H₂, the amount C₂H₂ formed was 60% less than the amount formed with the target at its normal position.)

Application of the diffusion-controlled reaction concept to the present results means that the onsets of the final plateaus in the C₂H₂ yields for the H₂ titrations all correspond to approximately the same reaction time in the gas phase. The reaction systems are essentially pseudo-first order in the gas phase due to the excess of H₂ over vaporized carbon species. Therefore, the apparent low-pressure plateau in the C₂H₂ yield at ~0.5 Torr of H₂ is a consequence of a change in the reaction mechanism. That is,

(58) The heats of formation used for various polyacetylene molecules and hydrocarbon radicals were those estimated by R. E. Duff and S. H. Bauer, Los Alamos Scientific Laboratory Report No. LA-2556, Sept 1961; *J. Chem. Phys.*, **36**, 1754 (1962).

one reaction between a C_n species and H_2 dominates the C_2H_2 yield below and another reaction dominates above the low-pressure plateau. The plateau corresponds to the completion of the reaction between H_2 and that C_n species which has the highest net reaction probability for C_2H_2 formation. In terms of maximum collision frequency and minimization of reaction steps, the dominant low-pressure reactions should be reactions 12 and 13 with C_2 as the precursor to C_2H_2 formation.

Formation of C_2H_2 from the combination of CH radicals

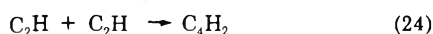


is not likely to be competitive with reaction 13 because a third body is needed to stabilize the product molecule and two CH radicals are required per C_2H_2 formed.

While a mechanism to account for the low-pressure plateau in C_2H_2 formation has been prescribed, a mechanism to account for the high H_2 pressure phase of C_2H_2 formation cannot be readily defined. Since the mass spectrometry data show that C_3 is the most abundant vapor species, the high-pressure phase of C_2H_2 formation must be associated with C_3 .

As previously noted, CH_4 becomes a significant product only at higher pressures. Its formation at high pressure is attributed to the stabilization of CH_2 complexes via reaction 18, followed by reactions 16 and 17. The multistep mechanism, reactions 14–17, is less likely to occur because of the low reaction probability expected for reaction 14 if ground-state $C(^3P)$ atoms are the predominant C_1 vapor species.²³

The formation of the small amount of C_4H_2 is attributed to the combination of C_2H radicals



This reaction is probably independent of total pressure because of the multiple number of degrees of freedom available for relaxation of the reaction exothermicity to internal energy.

Comparison of the H_2 titration results with the O_2 titration results allows some general conclusions regarding reaction probability. One Torr of gas in the 1-l. reaction vessel at room temperature corresponds to 3.2×10^{19} molecules, which is greater than 25 times the maximum number of carbon species vaporized in these laser experiments. Hence, sufficient gas molecules existed for complete reaction. Complete titration of the carbon species occurred at about 0.3 Torr of O_2 , whereas approximately 5 Torr of H_2 was required. Therefore, we conclude that the average probability for reaction of C_n species with hydrogen is 17 times lower than for reaction with oxygen.

5. Conclusions

This study of the vapor composition and chemical reactions of the carbon species produced by laser-induced vaporization of graphite and tantalum carbide has provided a number of new and interesting results for the broad field of carbon research.

The original objective of devising a technique for the selective titration of the various carbon vapor species has been accomplished in part. The gaseous products CO and CO_2 do quantitatively account for all the carbon vaporized in a low-pressure O_2 environment. This O_2 titration

procedure allows a determination of the relative amounts of mass loss as vapor and particulate matter, which has been demonstrated in another paper.⁵⁹ Conceivably it might be applied as a measure of the total vapor pressure of graphite at very high temperatures near the triple point.

The detection of CO_2 as a product of a gas-phase reaction of C_2 and/or C_3 suggest the goal of elucidating the reaction mechanism and introduces CO_2 as an important chemical entity for the thermochemical theories of reentry ablation chemistry.

Titration of carbon vapor species with H_2 is less well defined at this time. It does appear that the abundance of C_2 in carbon vapor may be approximately determined from the amount of C_2H_2 formed at the "low-pressure plateau" in the H_2 pressure dependence. The C_2 mechanism for C_2H_2 formation, namely, $C_2 + H_2 \rightarrow C_2H + H$ followed by $C_2H + H_2 \rightarrow C_2H_2 + H$, is supported by this study. The probability of reaction of C_3 with H_2 is lower than that of C_2 , but C_2H_2 is also the principal product. The mechanism of the C_3 reaction has not yet been determined but its eventual identification should provide additional insight into the chemistry of carbon formation from gases.⁶⁰

Other products of the reaction of carbon vapor species with H_2 at higher pressures are CH_4 , C_4H_2 , and mass 78. The sum of these plus C_2H_2 , which alone accounts for 85–90% of the laser-vaporized mass loss, again provides nearly 100% agreement with the measured mass loss and a possible method for the complete titration of vaporized carbon species. The formation of CH_4 appears to be pressure dependent and is believed to involve CH_2 as a precursor via the reaction $C_1 + H_2 + M \rightarrow CH_2 + M$.

Methane is readily pyrolyzed by the laser heating of a graphite or metal substrate and yields C_2H_2 and H_2 as gaseous products. Reaction of carbon vapor with CH_4 also occurs; C_2H_2 and H_2 are again the principal products.

The reaction probability of laser-vaporized carbon is approximately 17 times greater with O_2 than with H_2 . Since C_3 was the predominant vapor species, this number principally reflects the relative rates of the C_3 reactions.

The mass spectrometric analyses on laser heated TaC showed C_2 and C_3 as well as C_1 in the vapor phase. The relative abundances of the C_n species from the carbide were not equivalent to those from graphite. These results permitted the use of TaC in the gas-phase titration experiments as a source of C_n species having a distribution different from that of graphite in order to identify the chemical reactions of the C_n species. Other carbides are expected to be found which will have vapor-phase carbon compositions that may reflect the molecular structure of the solid phase and which can be used as selected sources of the carbon vapor species. If this proves correct, then the proper carbides may be used to elucidate further the chemical reactions of carbon atoms and molecules and to calibrate mass spectrometers for absolute partial pressure measurements of the carbon vapor species.^{33,61}

(59) R. T. Meyer and A. W. Lynch, *High Temp. Sci.*, **4**, 283 (1972).

(60) H. B. Palmer and C. F. Cullis in "Chemistry and Physics of Carbon," Vol. 1, P. L. Walker, Jr., Ed., Marcel Dekker, New York, N. Y., 1965 pp 266–325.

(61) F. M. Wachi and D. E. Gilmartin, *Carbon*, **8**, 141 (1970).

Rapid Gas-Phase Reactions. The Reaction of Ammonia and the Methylamines with Boron Trifluoride. III. Pressure Dependence of Rate Constant

Sol Glicker

Astrochemistry Branch, Laboratory for Extraterrestrial Physics, NASA/Goddard Space Flight Center, Greenbelt, Maryland 20771
(Received November 11, 1972)

Publication costs assisted by NASA

A steady-state flow apparatus, shown earlier to be suitable for the study of rapid gas reactions, has been used to determine the pressure dependence of the relative quasi-bimolecular rate constants for the reactant pairs ammonia (AM)-trimethylamine (TMA) and dimethylamine (DMA)-trimethylamine in reaction with boron trifluoride. The pressure dependence of the former was determined in the range 0.03–75 Torr and that of the latter in the range 0.02–720 Torr. In the low-pressure region, the relative limiting rate constants are $k_{am}:k_m:k_d:k_t = 1.0:2.2:19:40$ (with an experimental error of about 10%). The estimated relative limiting high-pressure constants, based on extrapolation of the data, are $k_{m^\infty}:k_{d^\infty}:k_{t^\infty} = 4:2:1$. Values of the absolute limiting high-pressure rate constants, when the relative rate data are combined with those of Kistiakowsky and coworkers, for MMA, DMA, and TMA, are 2×10^{13} , 1×10^{13} , and 5×10^{12} cm³/mol sec, respectively. Half-pressure estimates for MMA, DMA, and TMA have been obtained, namely 70, 4, and 1.5 Torr, respectively. The values for monomethylamine (MMA) included here have been taken from previous work. These data indicate a family of amines in which a loose activated complex is probable, along with the rapid exchange of energy among the internal degrees of freedom.

Introduction

There has been a continuing flow of experimental data available for the testing of the quasi-unimolecular reaction rate theory. Of particular interest has been the chemical activation method developed by Rabinovitch and coworkers,¹ which has provided extensive data in support of the RRKM theory assumption that all internal degrees of freedom may be taken as active in intramolecular energy transfer. This work has been based primarily on reactants in which a rigid activated complex is assumed, the behavior of which has been determined over a relatively wide range of pressure. Confidence in the theory has reached the point where attempts can now be made for its use in elucidating a mechanism. Dorer, Brown, Do, and Ress² have applied the theory to distinguish between stepwise and concerted simultaneous rupture of C–N bonds in the N₂ elimination step during photolysis of 3-vinyl-1-pyrazoline. They conclude, based on RRKM calculations, that a concerted bond rupture is more probable. Bauer³ has discussed similar cases where such an analysis might be profitably employed.

An equally important reactant series is one which involves a loose activated complex. To this end Kistiakowsky and coworkers,⁴ using a variant of the Polanyi diffusion flame technique, have studied the rapid association reaction between ammonia and the methylamines with boron trifluoride at low pressure. The absolute quasi-bimolecular rate constants obtained were then supplemented by a low-pressure relative rate study by Daen and Marcus,⁵ and subsequently extended to higher pressures by Glicker and Marcus.⁶ Another relative rate study by Bauer and coworkers⁷ has been reported.

The present work involves the determination of the pressure dependence of the relative quasi-bimolecular rate constants k_{am}/k_t and k_d/k_t , where subscripts, am, d, and

t refer to AM, DMA, and TMA, respectively. Ammonia and the methylamines represent a reaction series in which the number of degrees of freedom are systematically varied while the energy of the bond being formed (or broken) remains approximately equal. Information concerning the nature of the activated complex and the effective number of internal degrees of freedom can be obtained from the high-pressure limiting value and the pressure dependence of the rate constant.

Experimental Section

The experimental details and apparatus have been described in parts I and II.^{5,6} Briefly, the method consists of a flow system (at room temperature) in which a mixture of two amines compete for less than stoichiometric quantity of BF₃, where all the reactants are diluted with ethane. Additional gases used here are Research grade AM, DMA, and ethane obtained from the Matheson Co. which were purified by repeated low-temperature distillation between –78° (Dry Ice–acetone slush) and –195°. The maximum impurities were 0.3 mol % of other amines as determined by mass spectrometry.

In those experiments (at higher pressures) cited in the discussion of pumping selectivity, the procedure included

- (1) (a) B. S. Rabinovitch and D. W. Setser, *Advan. Photochem.*, **3**, 1 (1964); (b) L. D. Spicer and B. S. Rabinovitch, *Annu. Rev. Phys. Chem.*, **21**, 349 (1970).
- (2) F. H. Dorer, E. Brown, J. Do, and R. Ress, *J. Amer. Chem. Soc.*, **75**, 1640 (1971).
- (3) S. H. Bauer, *J. Amer. Chem. Soc.*, **91**, 3688 (1969).
- (4) (a) D. Garvin and G. B. Kistiakowsky, *J. Chem. Phys.*, **20**, 105 (1952); (b) G. B. Kistiakowsky and R. Williams, *ibid.*, **23**, 334 (1955); (c) D. Garvin, V. P. Guinn, and G. R. Kistiakowsky, *Discuss. Faraday Soc.*, **17**, 32 (1954).
- (5) Part I: J. Daen and R. A. Marcus, *J. Chem. Phys.*, **26**, 162 (1957).
- (6) Part II: S. Glicker and R. A. Marcus, *J. Amer. Chem. Soc.*, **91**, 7607 (1969).
- (7) S. H. Bauer, I. V. Martinez, D. Price, and W. D. Jones, *Advan. Chem. Ser.*, **No. 42**, 35 (1964).

the collection and analysis of excess amines remaining in the reaction vessel at the termination of reaction, in addition to the usual analysis of the gases accumulated in the collection trap. The relative rate constants for nonsteady-state experiments were calculated using the ratio of amines remaining in the reaction vessel at the end of an experiment, since the collection trap sample contained unusually small quantities of amines and their ratio differed appreciably from the reaction vessel amine ratio.

All analyses were made with a Perkin-Elmer Model 421 double-beam infrared spectrophotometer. Calibrations, using Beer's law, were obtained for the gases AM, DMA, and TMA, and also for their boron trifluoride adducts in acetonitrile solution. The quantity of adduct formed was typically 10^{-4} mol. The experimental error in all these analyses was approximately 1.8%. The stability of the adducts in acetone and acetonitrile solutions was determined by infrared analysis. There were no spectral changes over a period of 3 hr, which was much longer than the time required for an analysis.

Results

The relative quasi-bimolecular rate constants were calculated from eq 1, where R_{amb}/R_{tb} and R_{am}/R_t are, respectively, the ratio of the formation of products and the ratio of excess amines for the AM-TMA system. A similar equation can be written for the DMA-TMA reactant pair. Two assumptions were made in the derivation of eq 1 (see

$$k_{am}/k_t = (R_{amb}/R_{tb})/(R_{am}/R_t) \quad (1)$$

ref 5 and 6 for details), namely an absence of local concentration depletion for either amine and a negligible pumping selectivity for the amines. The latter is defined here as the ratio of amine pumping speeds to the ratio of amine pressures in the reactor. Tables I and II contain the relative rate constants (plotted in Figure 1) as a function of pressure for the AM-TMA and DMA-TMA reactant pairs.

Included in Figure 1 for the DMA-TMA system at 650 Torr is the average of five nonsteady-state experiments, *i.e.*, the last five tabulated in Table II. The steady state refers to the equality of the amine ratio in the reactor and in the collection volume, and similarly for the amine/ethane ratio. Equation 1 may hold in the nonsteady-state case if the amine concentrations remain uniform in the reaction zone and if the conversions are small enough that the ratio of ambient pressures is constant in time. Also appearing in Figure 1 is a plot of the MMA-TMA data from part II.⁶

It was possible to do a material balance measurement for the last two experiments in Table I and the last and tenth experiment in Table II, where the rate of product formation was not a small difference between two large numbers. A balance was obtained (indicating a 1:1 stoichiometry) between the known amine flow rate into the reactor and the sum of the products and excess amines to within an experimental error of 3%. At flow rates required to maintain a steady-state above 75 and 120 Torr for AM-TMA and DMA-TMA, respectively, appreciable amounts of solid product appeared beyond the reactor exit traps.

A direct determination of the pumping selectivity was obtained for the last two experiments in Table I and 11-15 in Table II. The selectivity ratio was equal to unity in all these cases within an experimental error of 1.5%. Similarly, the selectivity of ethane compared with each amine

TABLE I: Experimental Data for the Reaction of AM and TMA with BF_3

$p,^a$ Torr	k_{am}/k_t	R_{am}	R_t	R_{amb}	R_{tb}	R_e^b	R_e^c
0.030	0.027	1.79	0.59	0.016	0.186	0.90	2.47
0.15	0.025	4.02	1.51	0.023	0.352	4.11	7.10
1.4	0.038	47.1	6.19	1.89	6.53	82	214
31	0.14	16.3	11.2	0.91	4.33	157	498
75	0.23	35.4	31.0	1.10	4.20	459	1940

^a p is the total reaction pressure. R is the rate of flow of the indicated gas in Torr/min into a known volume of 54.2 cm³. The subscripts am, t, amb, tb, and e refer to AM, TMA, AM adduct, TMA adduct, and ethane, respectively. ^b Flow through amine nozzle. ^c Flow through boron trifluoride nozzle. The sum $R_{am} + R_{amb}$ gives the flow rate of AM into the reaction vessel, and similarly for TMA. All experiments appearing in this and earlier work were performed at room temperature.

was also equal to unity. These equalities did not hold in the nonsteady-state experiments cited above. For a discussion of the selectivity problem below 1 Torr see ref 5 and 6, where it is shown that a relatively small deviation from unity is indicated, particularly at high ethane dilution.

The possibility of exchange reactions has been examined elsewhere.⁵ A mixture of one methylamine adduct was placed in contact with a second gaseous methylamine for 15 min. No base displacement was observed within the experimental error for all three methylamines. In addition, Bauer and coworkers⁷ report an absence of base displacement for at least 0.5 hr in their AM-TMA and DMA-TMA relative rate studies.

Discussion

In order to avoid local depletion of the total amine concentration, Heller's⁸ criterion was applied; namely, at values of v/D greater than 12 cm⁻¹ whirl formation in the reactor produced a decrease in the depletion of alkyl halide in his sodium diffusion-flame study (v = linear velocity of gas emerging from the nozzle and D = diffusion constant of emerging gas were calculated as described in ref 4a). At values of the ratio between 5 and 12 cm⁻¹ a spherical reaction zone was maintained with a maximum depletion of 10%. Kistiakowsky and coworkers⁴ have reported a higher limit (16 cm⁻¹) in the amine- BF_3 system.

In a competitive rate study strict adherence to the (v/D) upper limit restriction is not required. Whirl formation could result in a more rapid mixing of the reactants. Those experiments above 0.15 Torr in Table I and above 0.28 Torr in Table II were performed at values much greater than the upper limit; *e.g.*, at 120 Torr the ratio is equal to 10⁵ cm⁻¹. The latter is the lower limit involving a calculation⁶ of v determined from the Poiseuille equation. The first experiment in Table I and the first and second in Table II were obtained under flow conditions where the lower limit of the ratio was not maintained, namely 2 cm⁻¹, 2 and 3 cm⁻¹, respectively. However, visual examination of the internal surfaces of the nozzles produced no evidence of solid product formation. In addition, an approximate determination of the expected quantity of products formed agreed with that collected so that no large loss was likely.

Variation of the conversion ratio by seven-fold in the high-pressure experiments at 110 and 120 Torr (Table II)

(8) W. Heller, *Trans. Faraday Soc.*, **33**, 1566 (1937).

TABLE II: Experimental Data for the Reaction of DMA and TMA with BF_3

$\rho, ^a \text{ Torr}$	k_d/k_t	R_d	R_t	R_{db}	R_{tb}	R_e^b	R_e^c
0.020	0.47	0.76	0.65	0.126	0.232	3.89	10.5
0.036	0.47	0.57	0.43	0.154	0.246	2.99	7.24
0.050	0.49	1.07	0.91	0.151	0.26	3.31	11.9
0.070	0.51	4.50	2.22	0.321	0.310	6.06	9.71
0.10	0.49	0.37	0.25	0.170	0.234	1.47	6.11
0.15	0.53	0.77	0.58	0.119	0.168	3.95	12.2
0.28	0.66	4.21	3.90	0.183	0.259	13.8	30.1
0.52	0.67	8.73	7.60	0.768	0.997	94.8	84.0
2.4	1.0	4.85	4.47	0.597	0.535	15.8	48.9
5.8	1.1	3.65	3.39	1.72	1.49	18.2	44.9
18.0	1.4	14.9	12.9	0.996	0.638	40.7	320
18.5	1.4	11.9	11.6	0.713	0.506	40.5	271
40.0	1.8	13.2	13.0	0.984	0.554	249	475
110	1.9	18.3	31.6	0.977	0.912	581	2490
120	2.0	11.1	21.1	5.09	4.86	500	2510
605	(1.7) ^d	8.16	8.44	0.60	0.36	130	95
608	(1.5) ^d	5.46	5.74	1.17	0.82	125	100
680	(1.1) ^d	11.9	11.4	1.36	1.17	394	419
680	(2.2) ^d	7.23	10.5	0.97	0.65	315	319
720	(2.8) ^d	9.66	17.7	0.83	0.54	367	299

^a See footnote a in Table I. ^b Flow through amine nozzle. ^c Flow through boron trifluoride nozzle. ^d Nonsteady conditions (they appear in Figure 1 at 650 Torr as an average of the five experiments)

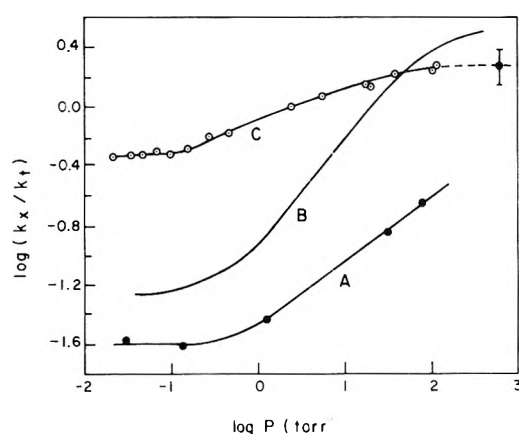


Figure 1. Plots of k_x/k_t vs. pressure. Curves A, B, and C represent k_{am}/k_t (Table I), k_m/k_t (part II), and k_d/k_t (Table II), respectively. The point at 650 Torr on curve C represents the average of five nonsteady-state experiments (Table II).

produced no measurable effect on the relative rate constants. Similarly, in Table I the last two experiments involved a 2.5-fold variation with no change in the relative rate constant. These results along with application of the Heller criteria suggest a limited local depletion effect if any. Additional support is obtained from the higher pressure data where the relative rate constants are appreciably greater than unity; since depletion would produce relative rates approaching unity.

The pressure dependence of the relative rate constants for the family of amines plotted in Figure 1 clearly shows quasi-bimolecular behavior, *i.e.*, the reverse of quasi-unimolecular decomposition. The relative limiting high-pressure rate constants obtained from these plots are $k_m^\infty:k_d^\infty:k_t^\infty = 4:2:1$. From earlier work,⁶ the minimum values of the high-pressure limiting value of k_m^∞ and k_t^∞ were estimated at 2×10^{13} and 5×10^{12} cc/(mole sec), respectively. Curve C suggests a value of 2 for k_d^∞/k_t^∞ ; therefore $k_d^\infty = 2(5 \times 10^{12}) \text{ cm}^3/(\text{mol}$

sec). The latter may be estimated by a second procedure involving one point from Kistiakowsky and Williams,⁴ namely $k_d = 2 \times 10^{12} \text{ cm}^3/(\text{mol sec})$ at 0.1 Torr in the more accurate range of their work. Again taking a value of 2 for the limiting high-pressure ratio, curve C indicates a decrease of 2/0.5 at 0.1 Torr. Assuming a large difference in the half-pressures of DMA and TMA (*i.e.*, pressure at which k^∞ drops to $k^\infty/2$), a minimum value of $k_d^\infty = (2/0.5) 2 \times 10^{12} \text{ cm}^3/(\text{mol sec})$ is obtained in good agreement with the result calculated above. The large values of the k_d^∞ 's, approaching the kinetic theory value of $10^{14} \text{ cm}^3/(\text{mol sec})$, are indicative of a loose activated complex, *i.e.*, a low energy barrier for rotation.

The relative limiting low-pressure values of the rate constants are $k_{am}:k_m:k_d:k_t = 1.0:2.2:19:40$, as indicated in Figure 1. Daen and Marcus⁵ and Kistiakowsky⁴ and coworkers give values for the DMA-TMA system (at 0.1 Torr) of 0.42 and 0.60, respectively. Kistiakowsky and coworkers also report a value of 0.018 (at 0.1 Torr) for the AM-TMA system. Considering the experimental precision, reasonably good agreement is obtained. Bauer⁷ and coworkers report $k_d/k_t = 1.1(\pm 20\%)$ in the pressure range 0.65–42.5 Torr, whereas the present work shows an increase in the ratio from 0.7 to 1.6. The relative rate constant maintaining a value near unity, 1.1 in this case, over a relatively large pressure range may be due to local depletion.

The half-pressures of the methylamines can be estimated from curves A, B, and C, since they appear to be well separated. Noting the pressure at which the limiting high-pressure value of k_x/k_t falls to one half its value (curve B and C), and following a similar procedure at low pressures for TMA, the MMA, DMA, and TMA half-pressures are 1.5, 4, and 70 Torr, respectively. These results show a direct relationship between the number of degrees of freedom and the lifetime of the active molecule, since the half-pressure is a measure of the decomposition of the active molecule by re-accumulation of energy in the newly formed bond relative to collisional deactivation.

Reactions of HO₂ with Carbon Monoxide and Nitric Oxide and of O(¹D) with Water

R. Simonaitis and Julian Heicklen*

Department of Chemistry and Ionosphere Research Laboratory, The Pennsylvania State University, University Park, Pennsylvania 16802 (Received November 8, 1972)

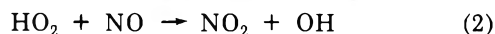
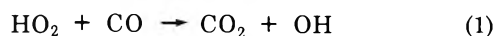
Publication costs assisted by the National Science Foundation

HO₂ radicals were generated by the photolysis of N₂O at 2139 Å in the presence of excess H₂O or H₂ and smaller amounts of CO and O₂. The O(¹D) atoms produced from the photolysis of N₂O react with H₂O to give HO radicals or H₂ to give HO + H. With H₂O, two HO radicals are produced for each O(¹D) removed at low pressures (*i.e.*, ~ 20 Torr of H₂O), but the HO yield drops as the pressure is raised. This drop is attributed to the insertion reaction O(¹D) + H₂O + M → H₂O₂ + M. This reaction removes 20 ± 10% of the O(¹D) atoms at ~650 Torr of H₂O (at 200°). The HO radicals generated can react with either CO or H₂ to produce H atoms which then add to O₂ to produce HO₂. In the absence of NO, the HO₂ radicals could react by two routes: HO₂ + CO → HO + CO₂ (1) and 2HO₂ → H₂O₂ + O₂ (11). Reaction 1 is so slow, even at 200°, that only an upper limiting value of 1.9 × 10⁻¹² (cm³/sec)^{1/2} could be found for k₁/k₁₁^{1/2}. When combined with the value of k₁₁ = 6 × 10⁻¹² cm³/sec, this ratio gives k₁ < 5 × 10⁻¹⁸ cm³/sec at both 100 and 200°. With NO present, NO₂ is produced in a long chain process *via* HO₂ + NO → HO + NO₂ (2). In this case reaction 2 is so rapid at 25° that only a lower limiting value of 0.6 × 10⁻⁷ (cm³/sec)^{1/2} could be found for k₂/k₁₁^{1/2}. Thus k₂ > 1.5 × 10⁻¹³ cm³/sec at 25°.

Introduction

The hydroperoxyl radical is an important intermediate in atmospheric and combustion chemistry. However, up to the present time the reactions of this radical have not been extensively studied. This is due, no doubt, to the fact that a good method for generating this radical in systems free from complications has not been available.

Two reactions of the hydroperoxyl radical which are of particular interest are with CO and NO

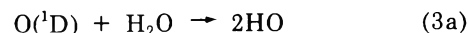


The reaction with CO has already been studied by several investigators, but k₂ has not yet, as far as we know, been reported in the literature. Baldwin, *et al.*,¹ studied the chain decomposition of H₂O₂ in the presence of CO at temperatures >440°. They obtained an approximate Arrhenius expression for the rate constant of reaction 1, k₁ = 10⁻¹⁰ exp(-23000/RT) cm³/sec. At room temperature k₁ extrapolates to ~10⁻²⁶ cm³/sec. On the other hand Westenberg and deHaas² studied reaction 1 in the H-O₂-CO system and found reaction 1 to be very fast at room temperature with k₁ ~10⁻¹² cm³/sec. Consequently, a serious discrepancy exists between these two studies. If the latter value of k₁ is correct, reaction 1 plays an important role in the chemistry of the terrestrial atmosphere, whereas if the former value is correct then reaction 1 is completely unimportant as far as the earth's atmosphere is concerned.

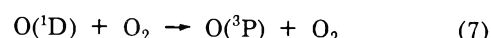
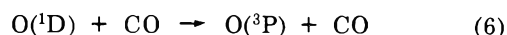
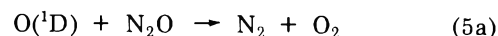
Since our manuscript was written two other values have been reported for k₁. Volman and Gorse,³ on the basis of one experiment, reported that k₁ is much slower than the rate coefficient for the HO + CO reaction. Davis, *et al.*,⁴ have reported a study similar to the one reported here and found k₁ < 10⁻²⁰ cm³/sec at 300°K.

In this paper we report a study of reactions 1 and 2 in a static system. Also we reexamine the reaction of O(¹D) with H₂O. The HO₂ radicals were generated by the pho-

tolysis of N₂O at 2139 Å in the presence of excess H₂O or H₂ and smaller amounts of CO and O₂. The O(¹D) atoms produced from the photolysis of N₂O react with H₂O or with H₂ to give OH radicals in the case of H₂O or OH radicals and H atoms in the case of H₂. In a previous report from this laboratory,⁵ reaction 3a was shown to be the dominant, if not exclusive, fate of the reaction between O(¹D) and H₂O. This reaction is further examined in the present paper. Reaction 4 has been shown to be the exclusive fate of the O(¹D)-H₂ interaction.⁶



The O(¹D) atom might be removed by reaction with the other gases added in substantial amounts, *i.e.*, N₂O, CO, or O₂. These are reactions which we wish to minimize. The relative rate coefficients for the pertinent reactions are listed in Table I. The experiments were so designed that reactions 5-7 were unimportant compared to reactions 3a or 4. Reactions 6 and 7 have been neglected, but the somewhat larger, but still small, correction due to reaction 5 has been included in our analysis.



The only fate of HO radicals in the absence of H₂ is to react with CO to give H atoms *via*

(1) R. R. Baldwin, R. W. Walker, and S. J. Webster, *Combust. Flame*, **15**, 167 (1970).

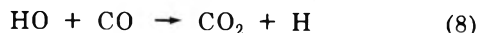
(2) A. A. Westenberg and N. deHaas, *J. Phys. Chem.*, **76**, 1586 (1972).

(3) D. H. Volman and R. A. Gorse, *J. Phys. Chem.*, **76**, 3301 (1972).

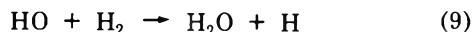
(4) D. D. Davis, W. A. Payne, and L. J. Stief, *Science*, **179**, 280 (1973).

(5) R. Simonaitis and J. Heicklen, *Int. J. Chem. Kinet.*, in press.

(6) G. Paraskevopoulos and R. J. Cvetanović, *J. Amer. Chem. Soc.*, **91**, 7572 (1969).



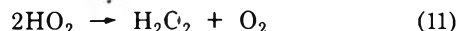
In the presence of H_2 , the HO radicals also react with H_2



Thus in the presence of either excess H_2O or H_2 and a smaller amount of CO, the net result is the production of H atoms. The resulting H atoms react exclusively with O_2 to give HO_2 radicals



The resulting HO_2 radicals may be removed by reactions 1 or 2, or they may disproportionate



The measurement of the quantum yield of CO_2 , $\Phi\{\text{CO}_2\}$, in the absence of NO permits the determination of $k_1/k_{11}^{1/2}$, and the measurement of the quantum yield of NO_2 , $\Phi\{\text{NO}_2\}$, in the presence of NO permits the determination of $k_2/k_{11}^{1/2}$. Since reactions 1 and 2 are chain-regenerating reactions, even low values of their rate coefficients should be accessible to measurement.

TABLE I: Relative Rate of $\text{O}(^1\text{D})$ Reactions

Ratio	Value	Ref
k_3/k_5	2.1	5
k_4/k_5	2.0	6
k_{5a}/k_5	0.41	7
k_6/k_5	0.36	a
k_7/k_5	0.59	6

^a P. M. Scott and R. J. Cvetanović, *J. Chem. Phys.*, **54**, 1440 (1971).

Experimental Section

NO Absent. A conventional high-vacuum line utilizing Teflon stopcocks with Viton "O" rings was used. The reaction vessel was a cylindrical quartz cell 10 cm long and 5 cm in diameter. The cell was enclosed in a wire-wound aluminum block furnace, the temperature of which was controlled to $\pm 1^\circ$ by a Ccle-Parmer Proportio null regulator Series 1300.

The N_2O and CO used were Matheson CP grade. The N_2O was purified by passage over ascarite and degassed at -196° . Gas chromatographic analysis indicated no detectable impurities. In particular CO_2 and N_2 were absent. The CO was purified by passage over glass beads and several traps at -196° , degassing at -196° , and distillation from liquid argon. The CO thus purified was free of CO_2 but contained 540 ppm of N_2 . The N_2 yield in any photolysis experiment was appropriately corrected for this background N_2 . Small amounts of tap water were degassed at -96° prior to use in order to remove dissolved air and CO_2 . Air Products research grade O_2 was purified by passage over traps at -196° . The only remaining detectable impurity was 7 ppm of N_2 . This amount of N_2 was entirely negligible.

All gas pressures including H_2O below its room temperature vapor pressure were measured with either a McCleoud gauge or a Hg manometer. The high H_2O pressures were not measured directly, but calculated assuming the perfect gas law. Our procedure was to introduce H_2O below its room temperature vapor pressure into the line, measure its pressure on the Hg manometer, and condense it into the reaction vessel. The stopcock to the insulated reaction vessel was closed and the temperature raised to

100 or 200° . From the known volume ratios the H_2O pressure was calculated.

Irradiation was from a Phillips Zn resonance lamp Type 93106E. The effective radiation was at 2139 Å. After irradiation the gases noncondensable at -196° were collected with a Toepler pump and analyzed for N_2 by gas chromatography using a 10-ft long by 0.25-in. diameter column packed with 5A molecular sieves. A second fraction volatile at -96° was removed and analyzed for CO_2 using a 24-ft long by 0.25-in. column packed with Porapak Q operating at 25° .

At 100° a very small amount of CO_2 (~ 0.03 mTorr/min) was produced in the dark. At 200° the dark reaction was somewhat larger (~ 0.15 mTorr/min). The correction for the dark reaction was small, usually less than a few per cent.

NO Present. For this system a conventional greaseless high-vacuum line was also employed, but Hg was rigorously excluded. The reaction vessel was also a cylindrical quartz cell 10 cm long and 5 cm in diameter.

The N_2O , CO, and O_2 were purified as described for the HO_2 -CO system. The H_2 , Matheson (CP grade), was purified by passage over traps at -196° . The pressure of all gases in this system was measured with an alphasatron gauge.

Irradiation was from a Zn lamp similar to that described for the HO_2 -CO system. The NO concentration was maintained at ≤ 120 mTorr, so that the 2139-Å radiation was absorbed only by the N_2O .

The NO_2 was analyzed photometrically using a simple dual-beam photometer. Light from a tungsten lamp was split in two beams. One of these passed through the reaction vessel and was focused on an RCA 935 photodiode, the other beam was focused on a second RCA 935 photodiode without passing through the vessel. The diodes were part of a simple electrical circuit which allowed the difference of the two signals to be measured. The minimum NO_2 pressure that could be measured in this way was ~ 15 mTorr.

Actinometry was performed by the photolysis of N_2O at 2139 Å at the same pressure as used in an actual run. For this system $\Phi\{\text{N}_2\}$ is accurately known to be 1.41.⁷ Thus a determination of the nitrogen produced allows the absorbed light intensity, I_a , to be determined. After irradiation an aliquot of the N_2 was analyzed by gas chromatography as described for the HO_2 -CO system.

$\text{O}(^1\text{D}) + \text{H}_2\text{O}$

Results. First experiments were performed in the absence of O_2 and NO in order to measure the importance of reaction 5a compared to other possible reactions of $\text{O}(^1\text{D})$ with H_2O . Mixtures of N_2O and CO were irradiated at 2139 Å in the presence of excess H_2O . The HO radicals produced in the $\text{O}(^1\text{D}) + \text{H}_2\text{O}$ interaction are scavenged by CO to give CO_2 . The resulting CO_2 is a measure of the HO production efficiency. These experiments are similar to those already reported in our earlier study of the $\text{O}(^1\text{D})$ - H_2O system,⁵ but have been extended to higher pressures and temperatures. The results are presented in Table II.

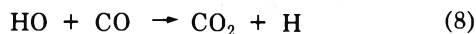
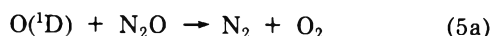
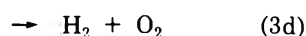
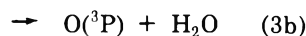
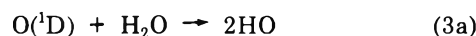
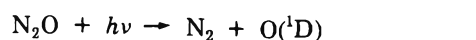
Measurements were made at 25 and 100° with two runs at 200° . At room temperature all the runs were at about the same conditions ($[\text{N}_2\text{O}] \sim 3$ Torr, $[\text{H}_2\text{O}] \sim 18$ Torr,

(7) R. Simonaitis, R. I. Greenberg, and J. Heicklen, *Int. J. Chem. Kinet.*, **4**, 497 (1972).

and $[\text{CO}] \sim 5$ Torr) due to constraints placed by the H_2O vapor pressure and the requirements that $[\text{N}_2\text{O}] \ll [\text{H}_2\text{O}]$ and $[\text{CO}] \ll [\text{H}_2\text{O}]$. The average ratio of $R\{\text{CO}_2\}/R\{\text{N}_2\}$ is 1.63 in close agreement with the earlier measurements.⁵ At 100° the pressure of each component as well as the total pressure was varied by a factor of almost 20. Except for minor variations, most of which may be accounted for by some quenching of $\text{O}(^1\text{D})$ by N_2O and CO (see Discussion), $R\{\text{CO}_2\}/R\{\text{N}_2\}$ is independent of the $[\text{N}_2\text{O}]/[\text{CO}]$, $[\text{H}_2\text{O}]/[\text{CO}]$, and $[\text{N}_2\text{O}]/[\text{H}_2\text{O}]$ ratios and is almost independent of the total pressure. The results are also independent of the absorbed light intensity and of the per cent conversion. However, $R\{\text{CO}_2\}/R\{\text{N}_2\}$ is always lower at 100° than at 25°. We have found earlier that if the CO is not carefully purified, irradiation of $\text{CO-N}_2\text{O}$ mixtures result in high quantum yields of CO_2 and N_2 formation.⁸ To ensure that this impurity-initiated reaction does not play a role we have made careful comparison of the rate of N_2 production in the absence and presence of CO . To be certain that the light intensity did not change from run to run the experiments were performed in two identical vessels simultaneously, one containing mixtures of $\text{N}_2\text{O-H}_2\text{O-CO}$ and the other containing mixtures of $\text{N}_2\text{O-H}_2\text{O}$ and small amounts of C_3H_6 to scavenge the OH radicals. The values of I_a for the two cells were obtained by irradiating N_2O at the same pressure in both cells. The rate of N_2 production, $R\{\text{N}_2\}$, was identical with either CO or C_3H_6 present.

Two runs were done at 200° and a total pressure of H_2O of about 650 Torr. The results at 200° are similar to those at 100°.

Discussion. The reaction scheme is



where reaction 6 has been neglected because it is unimportant. Even when it does occur some CO_2 is formed by the interaction of $\text{O}(^3\text{P})$ and CO , so that its inhibiting effect on CO_2 production is further minimized. The H atoms recombine either homogeneously or heterogeneously.

An upper limit on reactions 3b and 3d of 4 and 0.4%, respectively, has been found at 100° by determination of $\text{O}(^3\text{P})$ and H_2 production.⁵ Reaction 3c has not been determined directly, but its importance relative to reaction 3a was estimated to be <5% at 25°.⁵

From the above scheme, the following kinetic expression may be obtained

$$\Phi\{\text{CO}_2\} \equiv \alpha R\{\text{CO}_2\}/R\{\text{N}_2\} = 2k_{3a}/k_3 \quad (I)$$

where

$$\alpha \equiv 1 + (k_5 + k_{5a})[\text{N}_2\text{O}]/k_3[\text{H}_2\text{O}]$$

If $\Phi\{\text{CO}_2\}$ is equal to 2 then k_{3a}/k_3 is unity, and reaction 3a is the exclusive reaction of $\text{O}(^1\text{D})$ with H_2O . A value of

TABLE II: Photolysis of N_2O at 2139 Å in the Presence of H_2O and CO

$[\text{N}_2\text{O}]$, Torr	$[\text{H}_2\text{O}]$, Torr	$[\text{CO}]$, Torr	Irradiation time, min	$R\{\text{N}_2\}$, ^a μ/min	$R\{\text{CO}_2\}$, ^a μ/min	$R\{\text{CO}_2\}/R\{\text{N}_2\}$	$\Phi\{\text{CO}_2\}$
25°C							
3.00	17.5	5.0	393	0.51	0.77	1.53	1.71
3.05	16.5	7.0	945	0.27	0.46	1.71	1.92
2.90	17.1	4.5	762	0.33	0.52	1.59	1.78
2.70	19.3	6.0	455	0.37	0.63	1.71	1.87
100°C							
40.0	273	47.0	45	5.20	7.45	1.42	1.54
35.0	280	19.5	56	5.00	7.25	1.43	1.54
39.0	266	41.0	35	5.00	6.93	1.40	1.53
18.0	266	10.0	795	0.40	0.59	1.48	1.54
10.3	280	54.0	185	2.14	3.08	1.44	1.47
10.2	280	9.00	113	2.45	3.40	1.38	1.41
10.0	280	9.00	60	1.84	2.62	1.48	1.45
9.00	280	40.0	90	1.60	2.37	1.48	1.51
7.40	273	16.5	950	0.26	3.95	1.51	1.53
2.95	21.0	1.10	780	0.43	0.63	1.51	1.66
2.65	19.9	5.50	1140	0.30	0.455	1.51	1.85
2.65	19.9	5.00	1140	0.36	0.61	1.69	1.84
200°C							
48.0	610	44	30	13.2	1.86	1.41	1.49
10.0	640	8.0	20	3.79	4.91	1.32	1.34

^a Pressures for products are given at 25°.

2.0 ± 0.1 was obtained earlier at 25° and low H_2O pressures.⁵ In the same study the competition of CO and C_3H_6 for OH was also studied at high H_2O pressures and higher temperatures. The value of $\Phi\{\text{CO}_2\}$ deduced from this data was also ~ 2 , but with considerably greater uncertainty.

The values of $\Phi\{\text{CO}_2\}$ for different experimental conditions are presented in Table II. Examination of the data shows that at 100 and 200°, $\Phi\{\text{CO}_2\}$ is significantly less than at 25°, but is otherwise independent of all other variables, except total pressure. $\Phi\{\text{CO}_2\}$ for the runs at 100° and a total pressure of about 300 Torr is somewhat less than for the runs at 100° and a total pressure of about 20–30 Torr. The average value of $\Phi\{\text{CO}_2\}$ at 100° is 1.5 ± 0.07 and at 25° it is 1.82 ± 0.07 . The value of 1.82 at 25° is consistent with our earlier findings, but the values at 100 and 200° are significantly lower and are outside the experimental error. The value of $\Phi\{\text{CO}_2\}$ obtained in the C_3H_6 experiments, mentioned above, was ~ 2.0 , but the uncertainty was sufficiently large so that the present results are not inconsistent with the earlier measurements. The fact that $\Phi\{\text{CO}_2\}$ at low total pressure is slightly less than 2 may be accounted for by contribution of reaction 3b, and/or by some quenching of $\text{O}(^1\text{D})$ by CO which was not taken into account. For the low-pressure runs at 25 and 100° it can be estimated that about 10% of the $\text{O}(^1\text{D})$ are quenched by CO , consequently the above considerations raise $\Phi\{\text{CO}_2\}$, within experimental error, to a value of 2.0 ± 0.05 .

At 100 and 200°, experiments could be done at higher pressures. It is at these higher pressures that $\Phi\{\text{CO}_2\}$ is significantly below 2.0 to be meaningful. Presumably this is due to reaction 3c, which should increase with impor-

(8) R. Simonaitis and J. Heicklen, *J. Chem. Phys.*, **56**, 2004 (1972).

TABLE III: Photolysis of N₂O at 2139 Å in the Presence of H₂O, CO, and O₂

[CO], Torr	[H ₂ O], Torr	[N ₂ O], Torr	[O ₂], Torr	Irradiation time, min	R{N ₂ }, ^a μ/min	R{CO ₂ }, ^a μ/min	R{CO ₂ }/R{N ₂ }	Φ' ₀ {CO ₂ }
100°C								
66	290	48	46	46	6.10	12.5	1.93	2.14
60	126	19	21	60	3.43	5.85	1.70	1.87
56	126	20	21.5	60	3.40	6.58	1.94	2.13
58	320	8.0	42	144	1.18	3.75	3.10	3.14
57	240	52.0	45	45	7.32	18.1	2.47	2.83
59	280	52.0	43	175	0.692	1.74	2.52	2.84
54	280	55.0	46	23	7.40	19.1	2.61	2.95
52	270	50.0	40	210	0.114	0.285	2.50	2.81
50	270	51.0	43	300	0.533	1.66	3.13	3.52
12.0	300	51.5	40	30	0.735	1.41	1.93	2.15
9.0	270	49.0	43	32	8.60	22.0	2.53	2.84
49.5	126	19.0	18.5	55	2.16	4.95	2.20	2.42
200°C								
108	630	48	46	46	7.80	20.0	2.58	2.70
99	600	46.5	42	31	7.55	20.0	3.03	3.19
59	635	60.0	50	45	5.80	16.9	2.92	3.10
50	635	55	50	46	6.30	19.6	3.10	3.19
47	142	15	15	133	2.40	9.25	3.84	4.08
10	570	48	40	12	8.70	22.4	2.58	2.71
8.5	620	47	48	32	6.65	12.8	1.93	2.03
60	635	50	42.5	45	8.00	22.4	2.80	2.94

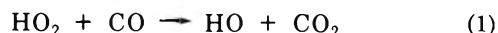
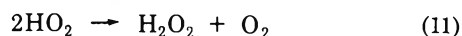
^a Pressure for products are given at 25°

tance as the pressure is raised. With about 650 Torr of H₂O vapor (at 200°), reaction 3c apparently accounts for 20 ± 10% of the removal of O(¹D) by H₂O. However, we have not analyzed for H₂O₂, so that this conclusion is not established unambiguously.

HO₂ + CO

Results. The previous experiments were repeated with O₂ present at 100 and 200°. At each temperature the CO pressure as well as the [N₂O]/[CO] and [H₂O]/[CO] ratio was varied over a substantial range. The light intensity was varied at 100° by about a factor of 10. The results are presented in Table III. It can be seen that R{CO₂}/R{N₂} is higher in the presence of O₂ than in its absence (Table II). There is no clear trend in the data with either the CO pressure, total pressure, temperature, or absorbed intensity.

Discussion. In the presence of O₂, three additional reactions are introduced into the reaction scheme



If H adds to CO, it will be oxidized to produce HO₂ + CO, so that this reaction need not be considered separately. Under our experimental conditions, other radical-radical reactions are unimportant.

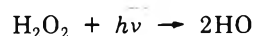
The rate coefficient for reaction 11 has been determined to be 6 × 10⁻¹² cm³/sec.^{9,10} Thus even at our lowest intensities the HO₂ radical lifetime does not exceed 2 sec. Usually, it is much less. Therefore wall removal of HO₂ cannot be as important as reaction 11, even if HO₂ is removed at every collision with the wall. A detailed calculation using the method of Jackson and Armstrong¹¹ shows that wall removal cannot account for more than 20% of the HO₂ loss under any conditions.

The mechanism leads to the prediction that

$$\Phi'\{\text{CO}_2\} - \Phi_0'\{\text{CO}_2\} = k_1[\text{CO}] (2\alpha\Phi_0'\{\text{CO}_2\}/k_{11}R\{\text{N}_2\})^{1/2} \quad (\text{II})$$

where Φ₀'{CO₂} is Φ'₀{CO₂} in the absence of O₂, but for otherwise comparable conditions, *i.e.*, the same [N₂O]/[H₂O] ratio. From the data in Table III, it can be seen that the functional form of eq II is not followed. Thus there must be an additional source of CO₂. However from the data in Tables II and III an upper limit to k₁/k₁₁^{1/2} can be computed to be 1.9 × 10⁻¹² (cm³/sec)^{1/2}. When combined with the value of k₁₁ = 6 × 10⁻¹² cm³/sec, this ratio gives k₁ < 5 × 10⁻¹⁸ cm³/sec at both 100 and 200°. This value is consistent with the results of Baldwin, *et al.*,¹ which when extrapolated to 200° gives k₁ ~ 10⁻²⁰ cm³/sec, but is much lower than the measurement of Westenber and deHaas² who obtained ~10⁻¹² cm³/sec at room temperature.

In addition to the reaction steps discussed above, some role may be played by the photolysis of H₂O₂ as it accumulates



At the end of a run, the H₂O₂ pressure is about 0.1–1% of that of N₂O. However, the extinction coefficients at 2139 Å are 0.09¹² and 7.35¹³ atm⁻¹ cm⁻¹, respectively, for N₂O and H₂O₂. The photolysis of H₂O₂ regenerates HO radicals and thus enhances CO₂ production. This could account for all or part of the increase in Φ'₀{CO₂} observed in the presence of O₂. The upper limiting value for k₁ would then be even lower than 5 × 10⁻¹⁸ cm³/sec.

- (9) T. T. Paukert and H. S. Johnston, *J. Chem. Phys.*, **56**, 2824 (1972).
 (10) C. J. Hochenadel, J. A. Ghormley, and P. J. Ogren, *J. Chem. Phys.*, **56**, 4426 (1972).
 (11) D. P. Jackson and D. A. Armstrong, *J. Phys. Chem.*, **75**, 2883 (1971).
 (12) M. Zeilikoff, K. Watanabe, and I. C. Y. Inn, *J. Chem. Phys.*, **21**, 1643 (1943).
 (13) D. H. Volman, *Advan. Photochem.*, **1**, 43 (1963).

TABLE IV: Photolysis of N₂O at 2139 Å and 25° in the Presence of H₂, O₂, NO, and CO^a

[CO], Torr	Irradiation time, sec	[NO ₂], mTorr ^c	[NO ₂], mTorr ^d	[CO], Torr	Irradiation time, sec	[NO ₂], mTorr ^c	[NO ₂], mTorr ^d
$I_a = 1.4 \times 10^{12}$ quanta/cc sec, [NO] = 30 mTorr				$I_a = 1.9 \times 10^{11}$ quanta/cc sec, [NO] = 30 mTorr			
0	5	7.5	6.0	0	30	9.2	8.2
55	5	20.6	18.6	0	150	25.5	24
110	5	21	19.0	0	150	26.0	25
110	5	17	15.0	55	30	17	17
$I_a = 1.4 \times 10^{12}$ quanta/cc sec, [NO] = 60 mTorr				110	30	18	17
0	10	12	7	110	30	19	18
0	10	12	8	$I_a = 1.9 \times 10^{11}$ quanta/cc sec, [NO] = 60 mTorr			
55	10	27	22	0	150	22.7	18
110	5	25	21	0	300	40	35
110	10	37	32	0	600	56	51
110	10	33	30	0	1800	50	45
110	10	37	33	55	60	29	24
110	10	35	31	110	60	42	36
110	10	36	32	110	30	25	21
110	10	33	29	110	15	15	10
110	10	33	29	110	120	45	40
110	20	49	42	110	300	57	53
110	30	37	32	110	600	55	51
110	40	56	52	110	60	36	31
110	70	55	50	110 ^b	60	28	27
$I_a = 1.4 \times 10^{12}$ quanta/cc sec, [NO] = 120 mTorr				110 ^b	60	24	23
110	5	26	13	$I_a = 1.9 \times 10^{11}$ quanta/cc sec, [NO] = 120 mTorr			
110	10	36	23	0	300	45	25
110	10	33	20	0	330	45	25
110	20	47	37	0	600	59	39
110	35	68	55	0	1800	95	75
110	70	110	97	110	60	44	24
110	120	109	96	110	180	71	51
110	375	95	95	110	360	107	87
110	1200	39	39	110	600	108	88
				110	1800	84	64

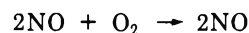
^a [H₂] = 760 Torr, [O₂] = 50 Torr, [N₂O] = 47 Torr. ^b [O₂] = 14 Torr. ^c Observed. ^d Corrected for dark reaction.

HO₂ + NO

Results. The results for the photolysis of N₂O at 2139 Å and 25° in the presence of H₂, O₂, CO, and NO are presented in Table IV and in graphical form in Figures 1 and 2. Table IV and the figures give the NO₂ pressure as a function of the irradiation time for different experimental conditions.

The NO pressures used were 30, 60, and 120 mTorr. The CO pressure was either 0, 50, or 100 Torr. Most runs were done with an O₂ pressure of 50 Torr. However, a few were done at lower O₂ pressure. The N₂O pressure was always 47 Torr and the H₂ pressure was always maintained at 760 Torr. The total pressure was 970 Torr in most runs except in a few runs it was somewhat lower. The [H₂]/([O₂] + [CO] + [N₂O]) ratio was maintained as high as possible to minimize the reaction of O(¹D) with O₂, CO, and N₂O. The [N₂O]/[NO] ratio was maintained at ≥390 to ensure that radiation is absorbed only by the N₂O. An O₂ pressure of 50 Torr was employed to prevent the reaction of H atoms with NO, CO, or the NO₂ product. Experiments were done at absorbed light intensities of 1.4×10^{12} and 1.9×10^{11} quanta/cc sec.

At the pressure of NO and O₂ employed some NO₂ was produced in the well-known dark reaction



with a rate which was in good agreement with the rate predicted from the known rate constant. At 30 and 60 mTorr the dark reaction amounted to less than 10 and 20%, respectively. But at 120 mTorr the NO produced in the dark reaction was about the same as in the light reaction for the points at lower conversions. Most of the dark reaction occurred during the gas mixing period prior to irradiation. Since this period was accurately known, accurate corrections could be applied. The amount of dark reaction during the irradiation was generally negligible.

In Table IV both the corrected and observed NO₂ pressures are presented. The NO₂ pressures plotted in Figures 1 and 2 are corrected for the dark reaction and only the data for the maximum CO and O₂ pressures are plotted.

It can be seen that the NO₂ pressure at first increases with irradiation time up to a maximum value and then declines on further irradiation. Examination of Table IV shows that the maximum observed NO₂ pressure (uncorrected for the dark reaction) is very close to the initial NO pressure employed. Consequently, the stoichiometric relation

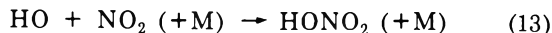
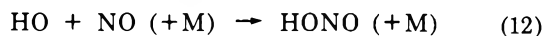
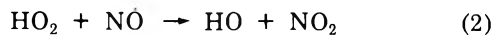
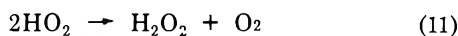
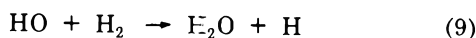
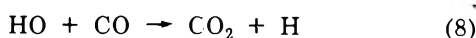
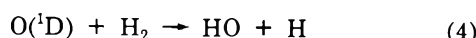
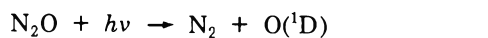
$$[\text{NO}_2] = [\text{NO}]_0 - [\text{NO}]$$

applies to a good approximation for conversions below the

maximum, where $[\text{NO}]_0$ is the initial NO concentration.

From the graphs it is obvious that initial rates, and therefore the initial quantum yields may be obtained from the data at 60 and 120 mTorr, but not at 30 mTorr due to insufficient data. The initial rates and quantum yields are given in Table V. From Table V it is clear that the initial quantum yields of NO_2 production, $\Phi_i\{\text{NO}_2\}$ are very large. $\Phi_i\{\text{NO}_2\}$ decreases by almost a factor of 2 when the NO pressure changes from 60 to 120 mTorr. From Table IV it is evident that the initial rate at 60 and 120 mTorr increases by about a factor of 3 upon the addition of 55 Torr of CO; a further increase occurs upon addition of more CO. Approximately the same effect is observed at 30 mTorr of NO as well. An increase of O_2 from 14 to 50 Torr at 60 mTorr of NO and 60-sec exposure increases the rate of oxidation slightly, but not significantly. A change in the light intensity by a factor of 7.3 did not significantly alter the initial quantum yields.

Discussion. The results may be discussed in terms of the following chain mechanism for the conversion of NO into NO_2



The reactions of $\text{O}({}^1\text{D})$ with gases other than H_2 have been ignored since they cannot be important. Under all of our conditions at least 90% of the $\text{O}({}^1\text{D})$ atoms must react with H_2 , as deduced from the relative rate coefficients in Table I.

The H atoms produced in reactions 8 and 9 will react predominantly with O_2 to give HO_2 . The possible competing reactions of H with NO or the NO_2 produced in the reaction cannot be important based on computations with the known rate coefficients for these reactions. Furthermore this was demonstrated experimentally, since a reduction in the O_2 pressure from 50 to 14 Torr had no substantial effect.

In addition to the chain-terminating step, reaction 11, it is also necessary to consider reactions 12 and 13 as termination reaction. Both are rapid, and in fact are the dominant chain-terminating reactions, as we will demonstrate.

Because $\Phi_i\{\text{NO}_2\} \gg 2$, NO_2 is produced primarily in chain-propagating reactions. Reaction 2 is the only conceivable reaction to do this, and it must account for the NO_2 production. The outlined mechanism explains the general features of the curves in Figures 1 and 2. Initially NO is rapidly oxidized to NO_2 via reaction 2 until conversion is complete. On further photolysis the NO_2 pressure declines, because now NO_2 is slowly consumed by reaction with HO and possibly HO_2 radicals.

The complete mechanism leads to a complex rate law for NO_2 formation. However, simplifications can be made if reaction 11 is either the dominant or unimportant terminating reaction. If reaction 11 is dominant, *i.e.*, reac-

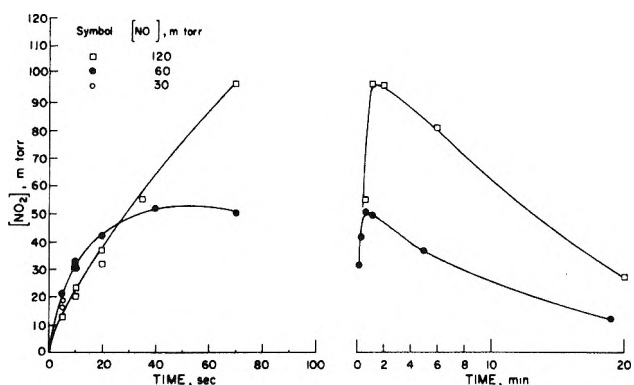


Figure 1. Plots of the corrected NO_2 pressure vs. irradiation time in the photolysis of N_2O at 2139 Å and 25° in the presence of H_2 , O_2 , NO, and CO. All data are at 110 Torr of CO and $I_a = 1.9 \times 10^{11}$ quanta/cc sec. The two sets of plots are for the same data, but have different time scales.

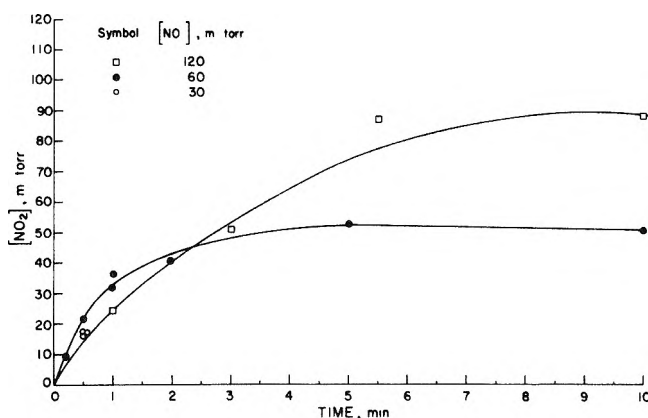


Figure 2. Plots of the corrected NO_2 pressure vs. irradiation time in the photolysis of N_2O at 2139 Å and 25° in the presence of H_2 , O_2 , NO, and CO. All data are at 110 Torr of CO and $I_a = 1.4 \times 10^{12}$ quanta/cc sec.

TABLE V: Initial Quantum Yields of NO_2 ^a

[NO], mTorr	I_a , quanta/cc sec	$\Phi_i\{\text{NO}_2\}$
60	1.4×10^{12}	100
120	1.4×10^{12}	59
60	1.9×10^{11}	119
120	1.9×10^{11}	73

^a [CO] = 110 Torr.

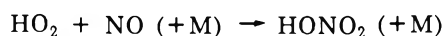
tions 12 and 13 are unimportant, then

$$\Phi_i\{\text{NO}_2\} = k_2[\text{NO}]/(I_a k_{11})^{1/2} \quad (\text{III})$$

On the other hand, if reaction 11 is unimportant compared to reactions 12 and 13, then

$$\Phi_i\{\text{NO}_2\} = 2(k_8[\text{CO}] + k_9[\text{H}_2])/(k_{12}[\text{NO}] + k_{13}[\text{NO}_2]) \quad (\text{IV})$$

Our results indicate that $\Phi_i\{\text{NO}_2\}$ varies inversely with $[\text{NO}]$, linearly with $[\text{CO}]$, and is independent of I_a . Thus eq IV applies for all of our conditions. It is interesting to note that two other possible reactions might be involved in termination



There is no prior evidence for either reaction. They cannot be the dominant chain termination reactions in our system because then the rate expression would be independent of [CO]. The dependence of our data on [CO] excludes the possibility that these reactions occur to any significant extent.

With the known values of k_8 and k_9 , and the initial rates at 60 and 120 mTorr of NO, the value of k_{12} may be computed with eq IV. The result is 5.6×10^{-12} and 6.5×10^{-12} cm³/sec at 120 and 60 mTorr, respectively. The average value is 6.0×10^{-12} cm³/sec. The values of $k_9 = 7 \times 10^{-15}$ and $k_8 = 1.35 \times 10^{-13}$ cm³/sec used in the calculation are those obtained by Stuhl and Niki.¹⁴ These values for k_8 and k_9 are in very good agreement with other determinations¹⁵ and are probably good to 20%. Recently two measurements of k_{12} have been reported. One of these is by Stuhl and Niki¹⁴ who found reaction 12 to be in the fall off region at ~ 80 Torr of He. They calculated a limiting high-pressure rate constant $k_{12^\infty} = 2 \times 10^{-12}$ cm³/sec. The other report was by Morley and Smith¹⁶ who, contrary to Stuhl and Niki, found the reaction to be entirely in the third-order region at similar pressures with $k_{12^0} = 9.4 \times 10^{-31}$ cm⁶/sec for H₂ as the third body. Using RRKM theory, Morley and Smith computed the high-pressure limiting rate constant, k_{12^∞} , to be 1.7×10^{-10} cm³/sec. With this value for k_{12^∞} and the value for k_{12^0} , it may be computed that at 1 atm of H₂, reaction 12 should still be almost entirely in the third-order regime,

with a pseudo-second-order rate constant of 2×10^{-11} cm³/sec. Thus the value of $k_{12} = 6.0 \times 10^{-12}$ cm³/sec obtained in this work at 1 atm of H₂ is midway between the values of Morley and Smith and of Stuhl and Niki.

Since reaction 11 is not important in this system, a value of $k_2/k_{11}^{1/2}$ cannot be determined. However, a lower limit can be found since $[\text{HO}_2] < (I_a/k_{11})^{1/2}$. Then

$$\Phi_i[\text{NO}_2] = k_2[\text{NO}][\text{HO}_2]/I_a < k_2[\text{NO}]/(k_{11}I_a)^{1/2}$$

Our data led to the result that $k_2/k_{11}^{1/2} > 0.6 \times 10^{-7}$ (cm³/sec)^{1/2}. With the average value of $k_{11} = 6 \times 10^{-12}$ cm³/sec found by Paukert and Johnston⁹ and Hochanadel, *et al.*,¹⁰ $k_2 > 1.5 \times 10^{-13}$ cm³/sec.

Acknowledgment. The authors wish to thank Professors Marcel Nicolet and Eduardo Lissi for useful discussions. This work was supported by the Atmosphere Sciences Section of the National Science Foundation through Grant No. GA-12385 and the National Aeronautics and Space Administration through Grant No. NGL-009-003 for which we are grateful.

- (14) F. Stuhl and H. Niki, Presented at the 10th Informal Conference on Photochemistry, Oklahoma State University, 1972.
 (15) D. L. Baulch, D. D. Drysdale, and A. C. Lloyd, "High Temperature Reaction Rate Data," No. 1 and 2, Department of Physical Chemistry, The University of Leeds, 1968.
 (16) C. Morley and I. W. M. Smith, *J. Chem. Soc., Faraday Trans. 2*, 1016 (1972).

An Electron Spin Resonance Study of the Radicals Produced by the γ -Irradiation of Xanthene

G. Orlandi,* G. Poggi, F. Barigelletti,

Laboratorio di Fotochimica e Radiazioni Alta Energia, del C.N.R., 40126 Bologna, Italy

and A. Breccia

Cattedra di Chimica Generale ed Inorganica, Università di Bologna, 40126 Bologna, Italy

(Received September 21, 1972)

Publication costs assisted by Consiglio Nazionale delle Ricerche, Laboratorio di Fotochimica e Radiazioni d'Alta Energia

Xanthene powders were γ -irradiated at 77°K and the radical species formed were investigated by esr technique. The spectra obtained are attributed to the overlapping of a singlet and a triplet. The triplet spectrum disappears upon heating to 105°K. On the basis of theoretical spin density calculations the triplet is attributed to xanthene radical ions while the singlet is tentatively assigned to xanthyl radical.

Introduction

In many γ -irradiated solid or frozen systems radical and ionic species are trapped and can be detected by esr. The purpose of this work is to clarify the nature of the radicals produced in xanthene microcrystals.

Experimental Section

Xanthene was obtained from Fluka and recrystallized from benzene.

Irradiations were performed with a Gammacell ⁶⁰Co source, with doses ranging from 0.5 to 3 Mrads. The shape of the spectra was found to be independent of the dose. The samples were irradiated at 77°K and the esr spectra were recorded at the same temperature (a) immediately after irradiation and (b) after a 15 min of annealing at 105°K. The spectrometer used was a Varian 4502 operating at a modulation frequency of 100 kHz. Second-derivative presentation, obtained by means of audio range modulation, was used throughout.

Spin density calculations were performed using a modified version of QCPE Program No. 76. Previous attempts to apply McLachlan calculations were unsuccessful due to the high apparent symmetry, in this framework, of the radicals investigated.

Results

The spectrum of xanthene as observed after irradiation at 77°K is reproduced in Figure 1a. It consists of three lines characterized by a coupling of 25 G and by a bandwidth of approximately 20 G. The intensity ratio differs from the value 1:2:1 typical of a spectrum arising from two equivalent spin 1/2 nuclei, in that the center line is too intense. We attributed the excess centerline intensity to the superimposition of a singlet line on a triplet spectrum of similar g value. This interpretation is confirmed by the annealing experiment, the result of which is illustrated by the spectrum in Figure 1b. This spectrum consists of one line only, characterized by a bandwidth slightly larger than the one observed before, centered on the field corresponding to the center line of the previous triplet. The difference between the two spectra is illustrated in Figure 1c. The intensity distribution here closely approximates the usual 1:2:1 triplet value.

Discussion

The above results can be rationalized assuming that two different radicals are formed upon irradiation at 77°K and that one of them, the one corresponding to the triplet pattern, disappears with heating.

The triplet spectrum is attributed to xanthene radical ions (cation or anion), its hyperfine structure arising from coupling with the two methylenic hydrogens. In fact they lie outside the molecular plane and can interact strongly with the electron spin and give rise to a splitting of the order of the one obtained. The aromatic hydrogens, on the other hand, are characterized by a relatively small hyperfine coupling which is not resolvable under the line width magnitudes typical of powder spectra. For the same reason, the singlet spectrum was attributed to a radical whose hydrogens all lie in the molecular plane. A prime candidate for this species is the one resulting from the removal of one of the methylenic hydrogens, *i.e.*, xanthyl radical. Theoretical spin density calculations have been carried out on the three species quoted. The method applied was the UHF π MO method of Pople and Nesbet^{1,2} as the more sophisticated CNDO methods³ do not seem to be reliable for computing spin densities of methylenic hydrogens.^{4,5} In our calculations bond lengths of 1.4, 1.5, and 1.3 Å were taken for the C-C, C-CH₂, C-O bonds, respectively. The parameters and repulsion integrals for the C atoms were those proposed by Amos and Snyder.⁶ For oxygen the parameters are ionization potential $W_O = -32.9$ eV, monocentric repulsion integral $\gamma_{OO} = 21.53$ eV, and $\beta_{CO} = -3.3$ eV, and the CO repulsion integrals were chosen in such a way as to give the same ratio γ_{CO}/γ_{CC} as obtained by use of the Mataga method.⁷ Since UHF spin densities may be incorrect due to spurious components arising mainly from quartet states, we evaluated also the projected spin densities⁶ ρ_{aa} and ρ_{asa} by an approximated projection method.⁸ In fact, correct spin densities are supposed to lie somewhere between ρ_{UHF} and ρ_{aa} and it has been suggested^{6,9} that $\rho_{av} = \frac{1}{2}(\rho_{aa} + \rho_{asa})$ gives a good estimate of spin densities.

Hyperfine splitting constants for the in-plane hydrogens were calculated with the McConnell formula using $Q = 23$

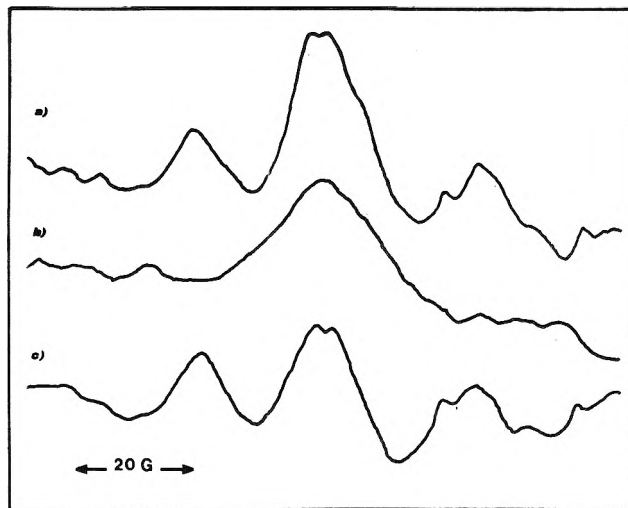


Figure 1. ESR spectra of γ -irradiated xanthene at 77°K: (a) taken immediately after irradiation; (b) after annealing at 105°K; (c) difference between the esr spectra reported in a and b. The traces were obtained by accumulation of the esr signal into a computer of average transients. The power incident on the sample was kept constant in all experiments (to a value of the order of 10 mW) and so was the leakage current.

G. For the methylenic hydrogens we applied the well-tested relationship¹⁰⁻¹²

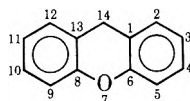
$$a_H = B\rho \cos^2 \vartheta \quad (1)$$

where ϑ is the dihedral angle between the planes C-C- p_z and C-C-H, which, for tetrahedral hybridization, is equal to 30°; B is a constant equal to 58 G; ρ is the value of the spin density on the vicinal benzene ring C atom. Since in our case there are two equivalent vicinal atoms, the effective spin density to be used in relationship 1 is $[(\rho_1)^{1/2} + (\rho_{13})^{1/2}]^2 = 4\rho_1$.¹³

The spin densities and hyperfine coupling constants obtained are represented in Table I and Table II, respectively. As expected, one sees clearly that in the xanthene radical ions the splitting due to the methylenic hydrogens dominates over the one due to in-plane hydrogens. For the negative ion we obtain a hyperfine coupling constant of 28–32 G, while for the positive ion we get results ranging from 40 to 25 G depending on which spin density we use, whether projected or unprojected. Accepting $\frac{1}{2}(\rho_{aa} + \rho_{asa})$ as the most reliable spin density, for the two radical ions essentially the same hyperfine coupling constant is obtained, *i.e.*, approximately 29 G. This value is to be

- (*) J. A. Pople and R. K. Nesbet, *J. Chem. Phys.*, **22**, 571 (1954).
- (2) A. Brickstock and J. A. Pople, *Trans. Faraday Soc.*, **381**, 901 (1954).
- (3) J. A. Pople, P. D. Santry, and G. A. Segal, *J. Chem. Phys.*, **43**, S129 (1965); J. A. Pople and G. A. Segal, *ibid.*, **44**, 3289 (1966).
- (4) J. A. Pople, D. L. Beveridge, and P. A. Dobosh, *J. Amer. Chem. Soc.*, **90**, 4201 (1968).
- (5) J. A. Pople and D. L. Beveridge, "Approximate Molecular Orbital Theory," McGraw-Hill, New York, N. Y., 1970.
- (6) A. T. Amos and L. C. Snyder, *J. Chem. Phys.*, **41**, 1773 (1964); **42**, 3670 (1965).
- (7) N. Mataga and K. Nishimoto, *Z. Phys. Chem., (Frankfurt am Main)*, **13**, 140 (1957).
- (8) G. Orlandi and G. Giacometti, *Ric. Sci.*, **39**, (1969).
- (9) K. M. Sando and J. F. Harriman, *J. Chem. Phys.*, **47**, 180 (1967).
- (10) E. W. Stone and A. H. Maki, *J. Chem. Phys.*, **37**, 1327 (1962).
- (11) C. Corvaja and G. Giacometti, *Theor. Chim. Acta*, **14**, 353 (1969); C. Corvaja, M. Brustolon, and G. Giacometti, *Z. Phys. Chem. (Frankfurt am Main)*, **66**, 279 (1970).
- (12) K. D. Sales, *Advan. Free Radical Chem.*, **3**, 139 (1969); P. B. Ayscough, "Electron Spin Resonance in Chemistry," Methuen, London, 1967.
- (13) D. H. Whiffen, *Mol. Phys.*, **6**, 223 (1963).

TABLE I: Electron Spin Densities for Xanthene Radical Cation (I), Xanthene Radical Anion (II), and Xanthyl(III)



Radical	Position	ρ_{UHF}	ρ_{aa}	ρ_{av}
I	1,13	0.232	0.14	0.16
	2,12	-0.145	-0.04	-0.07
	3,11	0.248	0.16	0.18
	4,10	-0.142	-0.05	-0.07
	5,9	0.234	0.17	0.19
	6,8	0.033	0.08	0.07
	7(O)	0.080	0.07	0.07
II	1,13	0.185	0.16	0.17
	2,12	0.123	0.11	0.12
	3,11	-0.066	-0.02	-0.03
	4,10	0.114	0.11	0.11
	5,9	0.187	0.15	0.16
	6,8	-0.041	-0.01	-0.02
	7(O)	-0.005	-0.00	-0.00
III	1,13	-0.132	-0.04	-0.06
	2,12	0.178	0.12	0.14
	3,11	-0.059	-0.00	-0.02
	4,10	0.093	0.09	0.09
	5,9	0.013	0.07	0.02
	6,8	0.108	0.08	0.08
	7(O)	0.029	0.02	0.03
14	0.569	0.42	0.45	

TABLE II: Hyperfine Splitting for Radicals I, II, and III (in Gauss)

Radical	Position	ρ_{UHF}	ρ_{aa}	ρ_{av}
I	2, 12	3.3	0.92	1.6
	3, 11	5.7	3.7	4.1
	4, 10	3.3	1.1	1.6
	5, 9	5.4	3.9	4.4
	Methylene	40.4	24.4	27.8 (23.2) ^a
II	2,12	2.8	2.5	2.8
	3,11	1.5	0.46	0.69
	4,10	2.6	2.5	2.5
	5,9	4.3	3.4	3.7
III	Methylene	32.2	27.8	29.6 (24.6) ^a
	2,12	4.1	2.8	3.2
	3,11	1.6	0.0	0.46
	4,10	2.1	2.1	2.1
	5,9	0.30	0.46	0.46
14	13.1	9.7	10.3	

^a These figures were evaluated assuming $\cos^2 \vartheta = 5/8$ as explained in ref 11.

singlet broad band, is at variance with the theoretical prediction. However, when considering that all the other splittings are relatively large and that the g tensor and hyperfine tensor anisotropies are again present, one cannot rule out the attribution of the singlet spectrum to the xanthyl radical. These effects can easily account for a broadening of the original doublet which could completely obscure the doublet structure itself. However, other radicals containing only in-plane hydrogens could be responsible for the singlet spectrum, but esr does not permit their identification since the hyperfine structure originating from the planar hydrogens is lost.

Conclusion

From the present study it appears that the products of γ -irradiation of xanthene powders are of two kinds. The species characterized by a singlet spectrum and higher thermal stability appears to result from hydrogen abstraction from the $-\text{CH}_2$ group. The triplet spectrum can belong to either of the two xanthene radical ions, positive or negative.

compared with the experimental finding of about 25 G. If we, now, accept the assumption that the CH_2 group is rapidly flipping up and down the molecular plane, the $\cos^2 \vartheta$ factor averages to $5/8$,¹¹ bringing the theoretical result closer to the experimental one.

The splittings from the in-plane hydrogens are fairly small and are wiped out by the line width typical of microcrystalline samples, which is due to g tensor anisotropy and to hyperfine splitting tensor anisotropy. For the xanthyl radical, there is considerable spin density on the C-14 atom, to which there would correspond a doublet structure in the spectrum. The experimental result, showing a

Concentration and Temperature Dependence of the Quantum Yield and Lifetime of the Lowest Triplet State of Benzene in the Liquid Phase

Robert R. Hentz* and Ronald M. Thibault

Department of Chemistry and the Radiation Laboratory,¹ University of Notre Dame, Notre Dame, Indiana 46556

(Received October 27, 1972)

Publication costs assisted by the U.S. Atomic Energy Commission

The 253.7-nm photosensitized isomerization of *trans*-2-octene has been studied in liquid benzene and its mixtures with methylcyclohexane at 295 and 195°K. Quantum yield of the benzene triplet state decreases from 0.71 for neat benzene to 0.24 for 0.05 *M* benzene at 295°K and from 0.94 for 0.56 *M* benzene to 0.85 for 0.056 *M* benzene at 195°K. Such results, with complementary fluorescence results in the literature, give temperature-independent specific rates of 8.7×10^6 and $35 \times 10^6 \text{ sec}^{-1}$ for intersystem crossing from the monomer excited singlet and excimer singlet of benzene, respectively. The specific rate of internal conversion from the monomer excited singlet of benzene decreases from $25 \times 10^6 \text{ sec}^{-1}$ at 295°K to zero at 195°K and that from the excimer singlet is zero at both temperatures. The benzene triplet lifetime at 295°K is found to decrease from 0.5 μsec in 0.05 *M* benzene solution to 6 nsec in neat benzene, corresponding to a specific rate of $1.7 \times 10^8 \text{ sec}^{-1}$ for quenching of triplet benzene by ground-state benzene (with concentration expressed as mole fraction); extrapolation to infinite dilution gives 1 μsec as the lower limit for the intrinsic lifetime of triplet benzene in the liquid phase at 295°K. Isomerization of *trans*-2-octene photosensitized by toluene and *p*-xylene also was studied. From the results at 295°K, specific rates are obtained for the decay modes of the monomer excited singlets of toluene and *p*-xylene. For the monomer excited singlet at 295°K, the specific rate of intersystem crossing increases and that of the activated internal conversion decreases in the sequence benzene, toluene, *p*-xylene.

Introduction

When the work reported in this paper was initiated, certain published results suggested a concentration dependence of the quantum yield and lifetime of the lowest triplet state of benzene in the liquid phase. Triplet quantum yields, χ , of² 0.57 and³ 0.53 had been obtained for neat benzene excited at 253.7 nm. However, Sandros⁴ had reported $\chi = 0.25$ for 0.029 *M* benzene in cyclohexane. From results of a study of the fluorescence lifetime of benzene in cyclohexane solutions, $\chi = 0.21$ was predicted for the infinitely dilute solution.⁵ A triplet lifetime, $^3\tau$, of 7 nsec had been estimated for benzene in the neat liquid.³ However, Sandros⁴ had reported $^3\tau = 2 \mu\text{sec}$ for 0.029 *M* benzene in cyclohexane, a value in good agreement with an earlier estimate of Lipsky⁶ for dilute solution but incompatible with results of Dubois and coworkers.⁷ In a study of the pulse radiolysis of benzene-cyclohexane mixtures, Thomas and Mani⁸ associated a growth in optical absorption at 320 nm with a transient species having triplet benzene as precursor and obtained half-lives of 3 and 20 nsec from the growth curves for neat and 10% benzene, respectively. Thus, the present study was undertaken to examine such apparent effects of concentration in a systematic manner.

The 253.7-nm photosensitized isomerization of *trans*-2-octene has been studied in liquid benzene and its mixtures with methylcyclohexane at 295 and 195°K. The results elucidate concentration dependence of the lifetime of the lowest triplet state of benzene and, with complementary fluorescence quantum yields⁹ and lifetimes,¹⁰ make possible a quantitative description of decay processes of the lowest excited monomer and excimer singlet states of benzene in the liquid phase. While the present work was in progress, some closely related¹⁰⁻¹² and simi-

lar¹³⁻¹⁵ studies were reported. Results of those studies are discussed in relation to the present results.

Experimental Section

Sources, quality, and purification procedures for benzene and methylcyclohexane were the same as those in the fluorescence lifetime study of Gregory and Helman.¹⁰ The *trans*-2-octene (Aldrich Reagent Grade) was deaerated, transferred on to LiAlH₄, and stirred overnight to remove water and peroxides. The olefin then was vacuum distilled four times by bulb-to-bulb transfers in which the middle fraction from each distillation was retained for the next distillation. The deaerated middle fraction of the final distillation was stored in an evacuated bulb at -25° and contained about 0.08% *cis*-2-octene and 0.05 wt % of unknown impurity. No increase in the amount of *cis* isomer was observed after storage or preparation of solutions.

- (1) The Radiation Laboratory of the University of Notre Dame is operated under contract with the U. S. Atomic Energy Commission. This is AEC Document No. COO-38-869.
- (2) R. B. Cundall and W. Tippet, *Trans. Faraday Soc.*, **66**, 350 (1970).
- (3) R. R. Hentz and L. M. Perkey, *J. Phys. Chem.*, **74**, 3047 (1970).
- (4) K. Sandros, *Acta Chem. Scand.*, **23**, 2815 (1969).
- (5) W. P. Helman, *J. Chem. Phys.*, **51**, 354 (1969).
- (6) S. Lipsky, *J. Chem. Phys.*, **38**, 2786 (1963).
- (7) J. T. Dubois and F. Wilkinson, *J. Chem. Phys.*, **38**, 2541 (1963); J. T. Dubois and F. Wilkinson, *ibid.*, **39**, 377 (1963); J. W. van Loben Sels and J. T. Dubois, *ibid.*, **45**, 1522 (1966).
- (8) J. K. Thomas and I. Mani, *J. Chem. Phys.*, **51**, 1834 (1969).
- (9) F. Hirayama and S. Lipsky, *J. Chem. Phys.*, **51**, 1939 (1969).
- (10) T. A. Gregory and W. P. Helman, *J. Chem. Phys.*, **56**, 377 (1972).
- (11) R. V. Bensasson, J. T. Richards, and J. K. Thomas, *Chem. Phys. Lett.*, **9**, 13 (1971).
- (12) R. B. Cundall and D. A. Robinson, *Chem. Phys. Lett.*, **13**, 257 (1972).
- (13) R. B. Cundall, L. C. Pereira, and D. A. Robinson, *Chem. Phys. Lett.*, **13**, 253 (1972).
- (14) R. B. Cundall and D. A. Robinson, *Chem. Phys. Lett.*, **14**, 438 (1972).
- (15) K. Sandros, *Acta Chem. Scand.*, **25**, 3651 (1971).

Toluene (Matheson Coleman and Bell, Spectroquality) was distilled twice with a Nester-Faust spinning-band column; the middle third from the first distillation was redistilled, and the middle third from the second distillation was retained. The *p*-xylene (Eastman Organic Chemicals, Red Label Grade) was recrystallized three times with rejection of about one-fifth of the starting material each time. Purity of all reagents used was checked by gas chromatography.

Solution preparation has been described.¹⁰ Solutions were deaerated either by about nine freeze-pump-thaw cycles or by a modified method described by Gregory and Helman.¹⁰ The method of deaeration had no effect on isomerization yields.

Procedures, cells, and equipment used in photolyses and actinometry at 295°K were the same as those used in previous work³ except that the cells were individually calibrated in the present work. A previously described¹⁰ dewar cell was used for photolyses at 195°K. Deaerated solution was transferred from a storage bulb with break seal *via* a vacuum manifold into the dewar cell. The filtered³ emission of an Amersil low-pressure mercury lamp was monitored by a Cintra quantum radiometer with 253.7-nm probe. With electrical and thermal regulation and a 24-hr warmup period, lamp intensity varied less than 5% during photolysis as determined by averaging sets of three actinic measurements performed before and after each set of six photolyses. Solutions were stirred rapidly during photolysis, and exposure time was determined accurately with a shutter. In all photolyses more than 99.5% of the incident light was at 253.7 nm and more than 99.9% of the light entering the cell was absorbed. Incident intensities were near 10^{18} and 10^{19} quanta $\text{cm}^{-2} \text{hr}^{-1}$ for photolyses at 295 and 195°K, respectively.

A Beckman GC-5 gas chromatograph with flame-ionization detection and two columns in series was used for determination of the *cis* and *trans* isomers of 2-octene. Separation of methylcyclohexane and the aromatics from the olefins was achieved on the first column, for which $\frac{1}{8}$ -in. columns of various lengths (0.5–5 ft) packed with 20% squalane on 80–100 mesh firebrick were used. Complete separation of the 2-octene isomers was accomplished on the second column, a $\frac{1}{8}$ -in. \times 10-ft column packed with 80–100 mesh firebrick coated with 20% by weight of a solution of 33% AgNO_3 in glycerol. In some solutions 3-methylheptane was used as an internal standard.

Measurements of fluorescence quenching were performed with calibrated quartz cells and a modified Cary Model 14 spectrophotometer. Fluorescence was measured from the cell face used for excitation by 253.7-nm light from the combination of a 735A7 Hanovia lamp with a high-intensity Bausch and Lomb monochromator. Absorption spectra were determined with a Cary Model 14-R spectrophotometer.

Results

The 253.7-nm photosensitized isomerization of *trans*-2-octene was studied in benzene and its mixtures with methylcyclohexane (MCH) and in dilute MCH solutions of toluene and *p*-xylene at 295 and 195°K. Except for determination of the photostationary isomer ratio, the amount of isomerization was usually about 3% and never exceeded 6%. Within the precision of measurement ($\sim 5\%$), no loss of total 2-octene was detectable by gas chromatography. A photostationary ratio of *cis* to *trans* isomer concentrations of unity was obtained in neat ben-

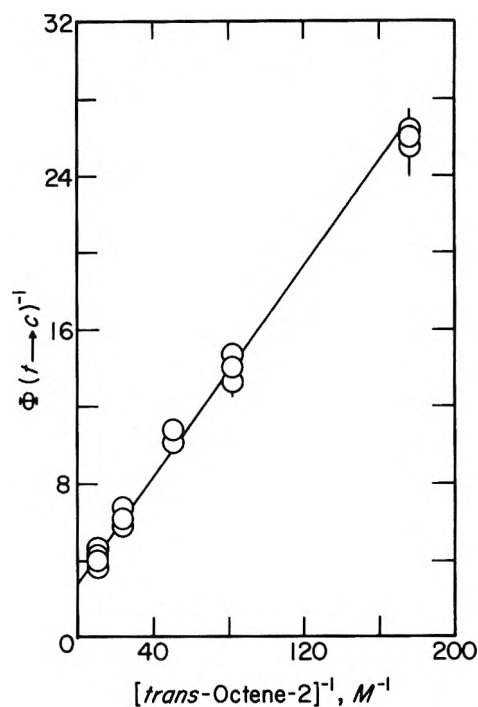


Figure 1. Concentration dependence of the corrected quantum yield for 253.7-nm photosensitized isomerization of *trans*-2-octene in neat benzene at 295°K.

zene and 0.05 *M* benzene solution at 295°K and in 0.56 *M* benzene solution at 195°K.

Quantum yields of *trans*-to-*cis* isomerization were calculated with corrections for back reaction and presence of the small initial fraction of *cis* isomer¹⁶ and (as described in the Discussion) for a small amount of quenching of benzene excited singlets at *trans*-2-octene concentrations greater than 0.02 *M*. Dependence of such "corrected" quantum yields, $\Phi(t \rightarrow c)$, on concentration of *trans*-2-octene is illustrated for neat benzene and 0.05 *M* benzene solution at 295°K in Figures 1 and 2, respectively, which show plots of $\Phi(t \rightarrow c)^{-1}$ vs. $[\text{trans-2-octene}]^{-1}$. Vertical bars represent the uncertainty (one standard deviation) in values of $\Phi(t \rightarrow c)^{-1}$; the computer-drawn line is a least-squares fit to the points with the standard deviation of each point as a weighting factor. Similarly good straight lines were obtained from such plots for each solvent composition studied at each temperature. From the slope and intercept of each such line, values were calculated (as described in the Discussion) for the quantum yield of triplet benzene, χ , and the product ${}^3\tau^3k$ of its lifetime and specific rate of triplet transfer to *trans*-2-octene. The results are presented in Table I. Corresponding results obtained in the same manner for toluene or *p*-xylene in MCH are presented in Table II.

The intensity *I* of benzene fluorescence at 282.5 nm, entirely that of the monomer excited singlet, was measured at 295°K for each benzene concentration with each concentration of *trans*-2-octene (including zero for which $I \equiv I^0$) that was used in the isomerization experiments at 295°K. For each solvent composition, the plot of I^0/I vs. concentration of *trans*-2-octene was linear. From the slopes of such plots, ${}^1k^1\tau = 1.5 M^{-1}$ was obtained (in fair agreement with previous work³) as the product of specific rate of quenching

(16) A. A. Lamola and G. S. Hammond, *J. Chem. Phys.*, **43**, 2129 (1965).

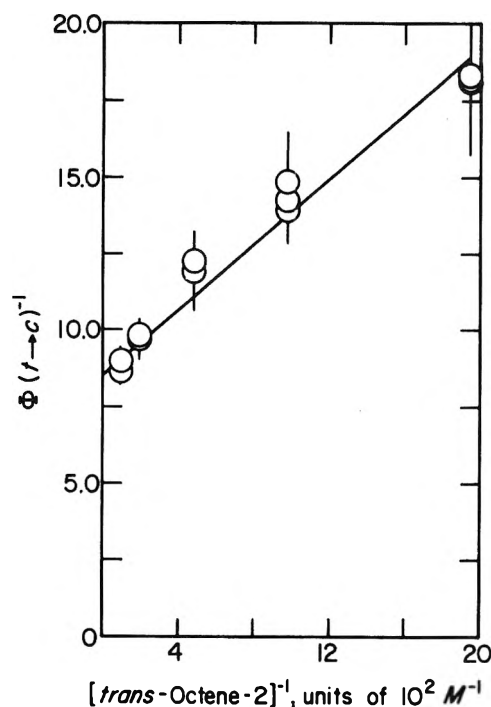


Figure 2. Concentration dependence of the corrected quantum yield for 253.7-nm photosensitized isomerization of *trans*-2-octene in 0.05 *M* benzene in methylcyclohexane at 295°K.

TABLE I: The 253.7-nm Quantum Yield, χ , of Triplet Benzene and ${}^3k^3\tau$ for Triplet Transfer from Benzene, B, to *trans*-2-Octene in Methylcyclohexane

[B], <i>M</i>	χ	${}^3k^3\tau$, <i>M</i> ⁻¹
a. 295°K		
0.05	0.236 ± 0.005 ^a	1600 ± 120 ^a
0.10	0.276 ± 0.003	1170 ± 60
0.25	0.313 ± 0.007	410 ± 30
0.50	0.385 ± 0.010	340 ± 60
2.00	0.56 ± 0.02	98 ± 9
6.00	0.69 ± 0.02	31.6 ± 1.6
11.2	0.71 ± 0.04	20.4 ± 1.6
b. 195°K		
0.056	0.851 ± 0.036	2300 ± 400
0.111	0.866 ± 0.007	820 ± 40
0.56	0.943 ± 0.036	250 ± 20

^a Standard deviation.

and lifetime of the excited singlets of benzene.¹⁷ The value of I^0/I obtained for each solution was used for calculation of the corrected quantum yield from the measured quantum yield of isomerization.

No products other than the cis isomer were detected by gas chromatography in any of the experiments. However, in experiments at 295°K with concentrations of *trans*-2-octene greater than 0.02 *M*, the absorption spectrum of a photoproduct (shown in Figure 3) was observed in benzene solutions and with reduced yield in toluene solutions but not in *p*-xylene solutions. For 0.1 *M* *trans*-2-octene in benzene at 295°K, $\sim 10^{-4}$ is estimated for the photoproduct quantum yield which increased with increase in concentration of *trans*-2-octene and with decrease in benzene concentration. The photoproduct slowly disappeared in solutions kept at room temperature. The photoproduct

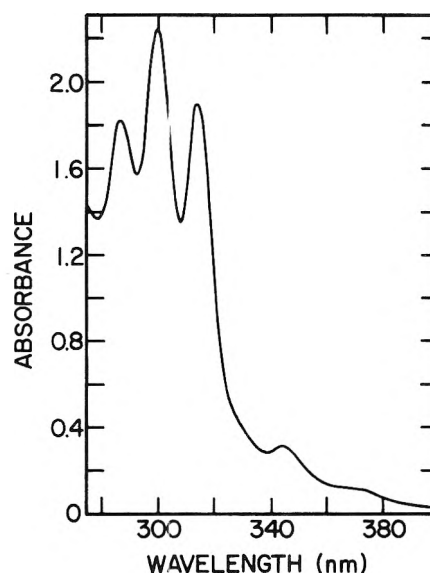


Figure 3. Absorption spectrum of the photoproduct in 253.7-nm photolysis of solutions of benzene and *trans*-2-octene in methylcyclohexane at 295°K.

TABLE II: The 253.7-nm Triplet Quantum Yield, χ , and ${}^3k^3\tau$ for Triplet Transfer to *trans*-2-Octene for the Solutes, S, Toluene and *p*-Xylene in Methylcyclohexane

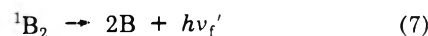
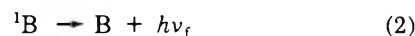
[S], <i>M</i>	<i>T</i> , °K	χ	${}^3k^3\tau$, <i>M</i> ⁻¹
a. Toluene			
0.05	295	0.419 ± 0.004 ^a	2460 ± 180 ^a
0.056	195	0.707 ± 0.024	2700 ± 900
b. <i>p</i> -Xylene			
0.05	295	0.566 ± 0.009	620 ± 40
0.056	195	0.608 ± 0.008	1300 ± 100

^a Standard deviation.

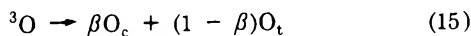
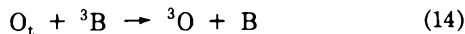
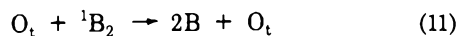
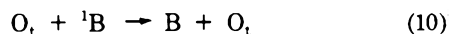
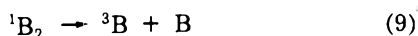
absorption spectrum was not detectable in any of the experiments at 195°K.

Discussion

The results are interpreted with the following kinetic scheme in which benzene is denoted by B and 2-octene is denoted by O with subscripts t and c for the *trans* and *cis* isomers, respectively; multiplicity of an excited state is indicated by a left superscript (its absence indicating the ground state), and the subscript 2 denotes excimer.



(17) Absence of an observable dependence of ${}^1k^1\tau$ on benzene concentration is attributable to the monomer excited singlet and excimer singlet having approximately equal decay specific rates at 295°K¹⁰ and approximately equal quenching specific rates.



The following additional symbols are introduced to simplify mathematical expressions: $k_m \equiv k_2 + k_3 + k_4$; $k_e \equiv k_7 + k_8 + k_9$; $\chi_m \equiv k_4/k_m$; $\chi_e \equiv k_9/k_e$; ${}^1k \equiv k_{10} = k_{11}$; ${}^3k \equiv k_{14}$; ${}^3\tau \equiv (k_{12} + k_{13}[\text{B}])^{-1}$; f_m and f_e denote the fractions of excited singlets of benzene that decay, in the absence of quenching, as monomer (*i.e.*, in reactions 2-4) and excimer (*i.e.*, in reactions 7-9), respectively.

Yguerabide¹⁸ has shown that reaction 1, in which ${}^1\text{B}$ corresponds to the monomer state ${}^1\text{B}_{2u}$, describes the 253.7-nm excitation of benzene in the liquid state. Studies of benzene fluorescence in the liquid state (see ref 5, 9, and 10 and the papers cited therein) have provided much information on the excimer formation and dissociation reactions 5 and 6 and decay modes of the monomer excited singlet, reactions 2-4, and excimer singlet, reactions 7-9. Quenching of the excited singlet states of benzene by *trans*-2-octene, represented by reactions 10 and 11, evidently occurs with approximately equal specific rates¹⁷ and is not expected to yield isomerization.¹⁹ In the postulated kinetic scheme, the benzene triplet is produced by intersystem crossing from both the monomer excited singlet and excimer singlet in reactions 4 and 9, respectively. Reaction 12 represents unimolecular decay of the benzene triplet, and a reaction such as 13 is required by the results as shown subsequently. Isomerization of *trans*-2-octene is assumed to occur *via* the triplet transfer in reaction 14 with decay of a certain fraction β of the 2-octene triplet to the *cis* isomer as shown in reaction 15. Assuming equality of the specific rates of triplet transfer to the *cis* and *trans* isomers of 2-octene, the observed photostationary isomer ratio of unity (independent of temperature and benzene concentration) gives $\beta = 0.50$. Such a value coincides with that obtained by Golub and Stephens²⁰ by the same method and agrees satisfactorily with $\beta = 0.48$ obtained from quantum yields of the acetone-sensitized isomerization of *trans*-2-octene.³

Gregory and Helman¹⁰ find that at 298°K

$$k_m = k_e = 3.59 \times 10^7 \text{ sec}^{-1} \ll k_6 \quad (I)$$

Consequently, $({}^1\tau)^{-1} = 3.59 \times 10^7 \text{ sec}^{-1}$ which, with the measured ${}^1k_{1\tau} = 1.5 \text{ M}^{-1}$, gives¹⁷ ${}^1k \equiv k_{10} = k_{11} = 5.4 \times 10^7 \text{ M}^{-1} \text{ sec}^{-1}$. With such a value for k_{11} and the result expressed in eq I, it follows that

$$k_{11}[\text{O}_t] \ll k_6 + k_e \quad (II)$$

for all solutions studied at 295°K. With the condition expressed in eq II, steady-state treatment of the kinetic scheme gives eq III for the measured quantum yield, Φ ,

$$\Phi = \beta(I/I^0)(\chi_e f_e + \chi_m f_m)({}^3k^3\tau[\text{O}_t]) / (1 + {}^3k^3\tau[\text{O}_t]) \quad (III)$$

of *trans*-to-*cis* isomerization. Then, rearrangement of eq III and use of $\beta = 0.5$, $\Phi(t \rightarrow c) \equiv \Phi I^0/I$, and

$$\chi \equiv f_e \chi_e + f_m \chi_m = f_e k_9/k_e + f_m k_4/k_m \quad (IV)$$

gives eq V. Thus, with values of $\Phi(t \rightarrow c)$ calculated from the measured values of Φ and I/I^0 for each solution, the

$$\Phi(t \rightarrow c)^{-1} = (0.5\chi)^{-1}(1 + 1/{}^3k^3\tau[\text{O}_t]) \quad (V)$$

straight line obtained in a plot of $\Phi(t \rightarrow c)^{-1}$ *vs.* $[\text{O}_t]^{-1}$ (such as those in Figures 1 and 2) is identified with eq V, and values are obtained for χ and ${}^3k^3\tau$ from the slope and intercept. Because of the experimental difficulty of accurate fluorescence quenching measurements at 195°K, values of χ and ${}^3k^3\tau$ were calculated by assuming negligible quenching of the excited singlets of benzene by *trans*-2-octene in all solutions studied at 195°K; from the assumption $k_{11}[\text{O}_t] \ll k_e$ it follows that eq II is satisfied and $I/I^0 = 1$ and, therefore, that eq V is applicable with $\Phi(t \rightarrow c) = \Phi$. Such an assumption is justified by the expectation that k_{11} is smaller at 195°K than at 295°K, while k_e is constant,¹⁰ and by the absence of curvature in plots of Φ^{-1} *vs.* $[\text{O}_t]^{-1}$ at the highest concentrations of *trans*-2-octene used at 195°K.

The value of χ in Table I for 0.05 *M* benzene at 295°K agrees well with values reported by Sandros^{4,15} and Cundall and coworkers^{13,14} for similar conditions. The present value of $\chi = 0.71$ for neat benzene at 295°K (*cf.* 11.2 *M* benzene in Table I) is a revision of our previous value³ owing to improvements in the techniques used. Cundall and Tippett² give $\chi = 0.57$ (though the data shown indicate $\chi = 0.59$) for neat benzene at 298°K. Such a value is obtained by assuming that triplet transfer from benzene to each of the 2-butene isomers is complete at a concentration of $\sim 0.3 \text{ M}$. However, from values obtained for ${}^3k^3\tau$ in the work of Cundall and coworkers^{2,21} (and in the present work and that of Hentz and Perkey³ for transfer to *trans*-2-octene), it appears that the fraction of benzene triplets that transfer to 0.3 *M* olefin in neat benzene is significantly less than unity. Appropriate correction of the Cundall and Tippett results² gives $\chi = 0.70$ for neat benzene.

The value of χ is clearly a function of both benzene concentration and temperature (*cf.* Table I). Such behavior can be shown to result from a difference in the specific rates of intersystem crossing, k_4 and k_9 , and temperature dependence of the specific rate of reaction 3. Rearrangement of eq IV gives

$$\chi k_e/f_e = k_4[k_e f_m/k_m f_e] + k_9 \quad (VI)$$

in the linear form

$$Y(\text{B}) = k_4[X(\text{B})] + k_9$$

Thus, the slope and intercept of a plot of eq VI for a particular temperature, such as that shown in Figure 4 for 295°K, give k_4 and k_9 , respectively, for that temperature. Values of $Y(\text{B})$ and $X(\text{B})$ for each concentration and temperature were calculated from values of χ in Table I, values of k_m and k_e (given in Table III) determined by Gregory and Helman,¹⁰ and values of f_m and f_e obtained²²

(18) J. Yguerabide, *J. Chem. Phys.*, **49**, 1018 (1968).

(19) L. M. Stephenson, D. G. Whitten, G. F. Vesley, and G. S. Hammond, *J. Amer. Chem. Soc.*, **88**, 3665 (1966).

(20) M. A. Golub and C. L. Stephens, *J. Phys. Chem.*, **70**, 3576 (1966).

(21) R. B. Cundall and W. Tippett, *Advan. Chem. Ser.*, No. **82**, 387 (1968); R. B. Cundall and P. A. Griffiths, *Trans. Faraday Soc.*, **61**, 1968 (1965).

(22) R. M. Thibault, Thesis, University of Notre Dame, 1972.

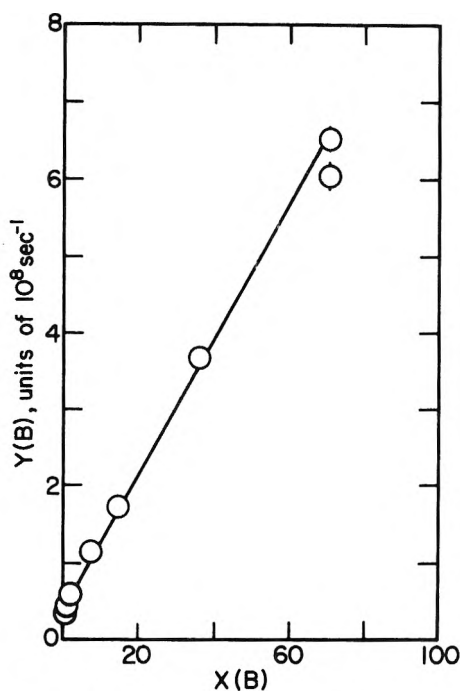


Figure 4. Plot of $Y(B) \equiv \chi k_e / t_e$ vs. $X(B) \equiv k_e f_m / k_m f_e$ for results at 295°K.

TABLE III: Specific Rates of Decay Processes of the Monomer Excited Singlet and Excimer Singlet of Benzene^a

	295°K	195°K
k_2^b	2.58 ± 0.12^c	1.56 ± 0.11^c
k_3	24.6 ± 0.9	0.0 ± 0.8
k_4	8.7 ± 0.5	8.7 ± 0.5
k_m^b	35.9 ± 0.3	10.3 ± 0.2
k_7^b	0.56 ± 0.03	0.40 ± 0.02
k_8	0.3 ± 3	0.6 ± 3
k_9	35.0 ± 2.8	35.0 ± 2.8
k_e^b	35.9 ± 0.3	36.0 ± 0.6

^a Specific rate, units of 10^6 sec^{-1} . ^b Reference 10. ^c Standard deviation.

from the benzene fluorescence quantum yields of Hirayama and Lipsky.⁹ Within the experimental error, k_4 and k_9 were found to be independent of the temperature; therefore, for each of these specific rates, the standard-deviation weighted average of values obtained at both temperatures is given in Table III for each temperature.

The results given in Table III show that the specific rate of intersystem crossing for the excimer singlet, k_9 , exceeds that for the monomer excited singlet, k_4 , by a factor of 4. Possible causes are (1) the smaller energy gap between the excimer and triplet states, by the excimer binding energy of 0.26 eV,¹⁰ (2) the near resonance between the excimer and $^3E_{1u}$ states,²³ or (3) larger coupling factors between the excimer and triplet states.²⁴ The factor of 4 difference between k_4 and k_9 causes a change in χ as relative concentrations of monomer excited singlet and excimer singlet are varied by changes in benzene concentration or temperature. From results summarized in Table III, $\chi_m \equiv k_4/k_m$ is 0.24 at 295°K and 0.84 at 195°K while $\chi_e \equiv k_9/k_e$ is 0.97 at both temperatures. The values of χ_m and χ_e correspond to χ in the limits of all monomer excited singlet and all excimer singlet, respectively.

Gregory and Helman,¹⁰ from their study of the fluorescence lifetime of benzene, obtain $k_4 = 8.4 \times 10^6 \text{ sec}^{-1}$ by assuming temperature invariance of k_4 . Such a result and assumption are in accord with results of the present work. Sandros¹⁵ also has concluded, from measurements of benzene fluorescence and sensitized biacetyl luminescence, that k_4 is independent of temperature. However, such temperature independence of k_4 can not be reconciled with an activation energy of 0.097 eV obtained for reaction 4 by Cundall and Robinson,¹⁴ nor is their¹² reported temperature dependence of k_e in accord with the results of Gregory and Helman¹⁰ (cf. Table III).

Table III includes values for k_2 and k_7 calculated by multiplication of k_m and k_e in Table III by values of k_2/k_m and k_7/k_e , respectively, obtained by Hirayama and Lipsky.⁹ Thus, with the present results for k_4 and k_9 , the values given in Table III for k_3 and k_8 are calculated from $k_m = k_2 + k_3 + k_4$ and $k_e = k_7 + k_8 + k_9$. The temperature dependence of k_3 is in accord with previous arguments^{10,15,25} that temperature dependence of the specific rate of nonradiative decay of the monomer excited singlet is attributable to an activated internal conversion. Within the experimental error, specific rates of internal conversion are zero for the excimer singlet (k_8 in Table III) and the lowest vibronic level of the monomer excited singlet (note k_3 at 195°K). Such results for k_3 and k_8 are in contrast with values for pyrene at 293°K of²⁶ $k_3 < 10^5 \text{ sec}^{-1}$ and $k_8 = 6.3 \times 10^6 \text{ sec}^{-1}$, with only k_8 being temperature dependent.²⁷ However, the behavior of intersystem-crossing specific rates for pyrene²⁶ and several other excimer-forming aromatics²⁸ is similar to that shown in Table III for benzene.

The results in Table I show that $^3k^3\tau$ is dependent on benzene concentration. With the kinetic scheme adopted, such a concentration dependence is ascribed to $^3\tau$ being given by $(k_{12} + k_{13}[B])^{-1}$. Thus

$$(^3k^3\tau)^{-1} = k_{12}/^3k + k_{13}[B]/^3k \quad (\text{VII})$$

For the solvent compositions of Table I, which range from 0.05 M to neat benzene (11.2 M), mole fraction N is the appropriate concentration unit for benzene in eq VII. The probability P that a molecule of triplet benzene will survive quenching by ground-state benzene molecules for a time t is given by eq VIII in which p is the probability that a molecule of triplet benzene will be quenched by a

$$P = (1 - pN)^{Z\nu t} \quad (\text{VIII})$$

nearest-neighbor benzene molecule during a jump period, Z is the total number of nearest-neighbor molecules, and ν is the jump frequency. For $pN \ll 1$ in eq VIII, $P = e^{-pNZ\nu t}$ and, therefore, the pseudo-first-order specific rate of reaction 13 (i.e., $k_{13}[B]$) corresponds to $pZ\nu N$ with $k_{13} = pZ\nu$ and $[B] = N$.

In Figure 5, the results in Table I for 295°K are presented in the form of a plot of $(^3k^3\tau)^{-1}$ vs. N with a straight line that is a weighted least-squares fit to the data. The line has a slope, equated to $k_{13}/^3k$, of $(4.9 \pm 0.4) \times 10^{-2}$

- (23) S. D. Colson and E. R. Bernstein, *J. Chem. Phys.*, **43**, 2661 (1965).
 (24) J. W. Rabalais, H. J. Maria, and S. P. McGlynn, *J. Chem. Phys.*, **51**, 2259 (1969).
 (25) J. W. Eastman, *J. Chem. Phys.*, **49**, 4617 (1968).
 (26) T. Medinger and F. Wilkinson, *Trans. Faraday Soc.*, **62**, 1785 (1966).
 (27) J. B. Birks, A. J. H. Alwattar, and M. D. Lumb, *Chem. Phys. Lett.*, **11**, 89 (1971).
 (28) W. Heinzelmann and H. Labhart, *Chem. Phys. Lett.*, **4**, 20 (1969).

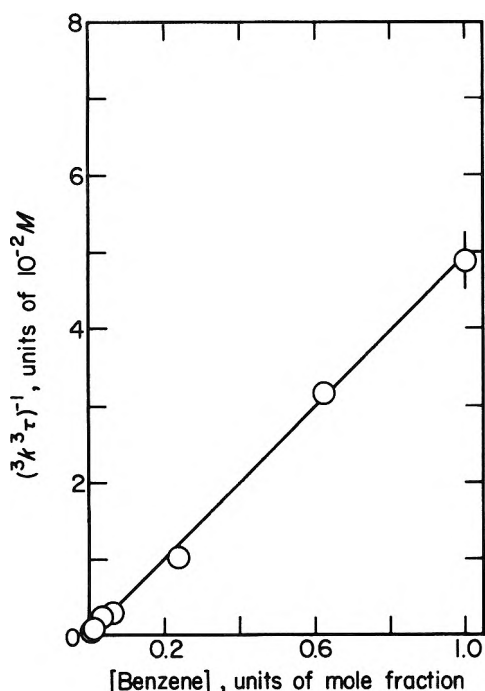


Figure 5. Plot of $(^3k^3\tau)^{-1}$ vs. mole fraction of benzene for results in Table I at 295°K.

M and (though not evident in Figure 5) a meaningful intercept, equated to $k_{12}/^3k$, of $(3.0 \pm 0.9) \times 10^{-4} M$; such results give $k_{13}/k_{12} = 1.6 \times 10^2$. That the intercept is meaningful is evident from the data in Table I for 0.05 M and neat benzene alone. For 0.05 M benzene, $(^3k^3\tau)^{-1} = 6.2 \times 10^{-4} M$ and is necessarily larger than $k_{12}/^3k$ (cf. eq VII). Thus $k_{12}/^3k$ makes no significant contribution to $(^3k^3\tau)^{-1} = 4.9 \times 10^{-2} M$ obtained for neat benzene and, therefore, $k_{13}/^3k = 4.9 \times 10^{-2} M$. Such a value multiplied by $N = 6.4 \times 10^{-3}$ for 0.05 M benzene gives $3.1 \times 10^{-4} M$ which, when subtracted from $(^3k^3\tau)^{-1} = 6.2 \times 10^{-4} M$ for 0.05 M benzene, gives $k_{12}/^3k = 3.1 \times 10^{-4} M$.

Bensasson, *et al.*,¹¹ have reported a pulse radiolysis study of the transfer of triplet excitation from benzene to anthracene in cyclohexane solutions. Lifetime of the benzene triplet was found to depend on benzene concentration, and $k_{13} = 1.8 \times 10^7 M^{-1} \text{sec}^{-1}$ was obtained from results for solutions with $[B] \leq 1.1 M$. Multiplication of such a value by the molarity of neat cyclohexane (9.25 M) gives $k_{13} = 1.7 \times 10^8 \text{sec}^{-1}$ for the mole-fraction specific rate. From $pZ\nu = k_{13} = 1.7 \times 10^8 \text{sec}^{-1}$ with estimated values of $Z = 12$ and $\nu = 2 \times 10^{10} \text{sec}^{-1}$, $p = 7 \times 10^{-4}$ is calculated. Thus, the condition $pN \ll 1$ is satisfied for all values of N . Clearly, quenching of triplet benzene by ground-state benzene is a relatively improbable process that requires many encounters. Langelaar²⁹ has observed a similar low probability of triplet self-quenching for several polyacenes in ethanol.

The value $k_{13} = 1.7 \times 10^8 \text{sec}^{-1}$ corresponds to a triplet lifetime in neat benzene of 6 nsec. With $k_{13}/k_{12} = 1.6 \times 10^2$, $^3\tau_0 = (k_{12})^{-1} = 1.0 \pm 0.4 \mu\text{sec}$ is obtained for the lifetime of triplet benzene at infinite dilution of benzene with MCH. Such a value is consistent with $^3\tau = 2 \mu\text{sec}$ (based on $^3k = 5 \times 10^9 M^{-1} \text{sec}^{-1}$ for triplet transfer to biacetyl) reported by Sandros⁴ for 0.029 M benzene in cyclohexane. Owing to the possibility of impurity quenching, $^3\tau_0 = 1.0 \pm 0.4 \mu\text{sec}$ is necessarily a lower limit to the lifetime for unimolecular decay of triplet benzene in the liquid phase at 295°K. In a previous study,³ $^3k^3\tau = 76 M^{-1}$ and $^3k^3\tau =$

TABLE IV: Specific Rates of Decay Processes of the Monomer Excited Singlets of Toluene and *p*-Xylene at 295°K^a

	k_2	k_3	k_4
Toluene	5.0 ^b	12	12.4
<i>p</i> -Xylene	13.3 ^b	1	19.0

^a Units of 10^6sec^{-1} . ^b Reference 34.

61 M^{-1} were obtained for the triplet transfers from benzene to 3,5-cycloheptadienone and *trans*-stilbene, respectively, in neat benzene. With the assumption of a diffusion-controlled $^3k = 10^{10} M^{-1} \text{sec}^{-1}$, $^3\tau \approx 7 \text{nsec}$ was estimated for neat benzene. Thus, the previous results and conclusions are in accord with $^3\tau = 6 \text{nsec}$ obtained for neat benzene from the results of Bensasson, *et al.*¹¹ Use of the latter value gives $^3k = 1.3 \times 10^{10}$ and $1.0 \times 10^{10} M^{-1} \text{sec}^{-1}$ for the triplet transfers from benzene to 3,5-cycloheptadienone and *trans*-stilbene, respectively. In the same manner, with either $k_{13}/^3k = 4.9 \times 10^{-2} M$ (from the slope of the line in Figure 5) or $^3k^3\tau = 20.4 M^{-1}$ for neat benzene (cf. Table I), $^3k = 3.4 \times 10^9 M^{-1} \text{sec}^{-1}$ is obtained for the triplet transfer to *trans*-2-octene. Specific rates about equal to that for the triplet transfer to *trans*-2-octene are obtainable from values of $^3k^3\tau$ for triplet transfer to the 2-butene isomers in neat benzene.^{2,21} Comparison of the alkene specific rates with those for 3,5-cycloheptadienone and *trans*-stilbene suggests that triplet transfer from benzene to the alkenes is not diffusion controlled (owing, perhaps, to the small difference between benzene and alkene triplet energies^{30,31}).

The results in Table I for $^3k^3\tau$ at 195°K are not adequate for determination of $k_{12}/^3k$ and $k_{13}/^3k$ with sufficient precision for detection of an effect of temperature on the ratios. However, simple comparison of values in Table I for $^3k^3\tau$ at 195 and 295°K suggests little or no effect of temperature. Thus, because small activation energies are expected in 3k (which is close to diffusion controlled) and k_{12} (perhaps³² 2.0–2.3 kcal mol⁻¹), a small activation energy is indicated for reaction 13. Consequently, the low probability of reaction 13 *per* encounter, which corresponds to a probability of reaction *per* unit time of $p\nu \approx 1.4 \times 10^7 \text{sec}^{-1}$, appears to require an appreciable negative entropy of activation.

The results in Table II for toluene and *p*-xylene are presented for comparison with the benzene results; for interpretation, the benzene kinetic scheme is adopted with B denoting toluene or *p*-xylene. With cyclohexane as solvent at 293°K, Sandros⁴ has obtained $\chi = 0.53$ for 0.03 M toluene and $\chi = 0.63$ for 0.018 M *p*-xylene from study of the sensitized luminescence of biacetyl. Such values are somewhat higher than those in Table II for comparable conditions. Because excited singlets of the aromatic sensitizers decay almost entirely from the monomer form at 295°K and 0.05 M sensitizer ($f_m \geq 0.99$ ³³), the values of χ in Table II for such conditions correspond to k_4/k_m . Thus,

- (29) J. Langelaar, unpublished results cited in J. B. Birks, "Photophysics of Aromatic Molecules," Wiley-Interscience, New York, N. Y., 1970, p 347.
 (30) W. G. Herkstroeter and G. S. Hammond, *J. Amer. Chem. Soc.*, **88**, 4769 (1966).
 (31) M. W. Schmidt and E. K. C. Lee, *J. Amer. Chem. Soc.*, **92**, 3579 (1970).
 (32) I. H. Leubner and J. E. Hodgkins, *J. Phys. Chem.*, **73**, 2545 (1969).
 (33) J. B. Birks, C. L. Braga, and M. D. Lumb, *Proc. Roy. Soc., Ser. A*, **283**, 83 (1965).

with $k_m = k_2 + k_3 + k_4$ and values given by Berlman³⁴ for k_m and k_2 , the results presented in Table IV are obtained. Comparison of results for 295°K in Tables III and IV shows that k_2 and k_4 increase and k_3 decreases with increase in the degree of benzene methylation. Such behavior of k_2 has been attributed to reduction of the symmetry and, thereby, removal of symmetry restrictions on the radiative transition.³⁴ The increase in k_4 may result from an increase in spin-orbit coupling with replacement of a hydrogen atom by a methyl group.²⁶ The decrease in k_3 is consistent with the finding by Sandros¹⁵ that k_3 of toluene has a larger activation energy than k_3 of benzene. The information necessary for calculation of specific rates from values of χ is not available for toluene and *p*-xylene at 195°K.

The small yield of photoproduct observed in the present work (*cf.* Results) increases with increase in the concentration of *trans*-2-octene and, therefore, appears to be a product of photoaddition of the olefin to the aromatic. It has been suggested that the activated internal conversion represented by reaction 3 is associated with formation of benzene isomers (benzvalene and fulvene) and photoaddition of olefins to benzene.³⁵ In accord with such a suggestion, the photoproduct yield increases with decrease in benzene concentration and changes in the same direction as k_3/k_m (*cf.* Tables III and IV) with change in temperature and in the degree of benzene methylation.

(34) I. B. Berlman, "Handbook of Fluorescence Spectra of Aromatic Molecules," 2nd ed, Academic Press, New York, N. Y., 1971, p 69.

(35) D. Bryce-Smith, *Pure Appl. Chem.*, **16**, 62 (1968).

Behavior of CO_3^- Radicals Generated in the Flash Photolysis of Carbonatoamine Complexes of Cobalt(III) in Aqueous Solution¹

Schoen-nan Chen, Virgil W. Cope,² and Morton Z. Hoffman*

Department of Chemistry, Boston University, Boston, Massachusetts 02215 (Received October 27, 1972)

The flash photolysis of $\text{Co}(\text{NH}_3)_4\text{CO}_3^+$ in aqueous solution generates the CO_3^- radical which is characterized by its absorption spectrum with λ_{max} 600 nm and its second-order decay kinetics. The radical is also generated from $\text{Co}(\text{NH}_3)_5\text{CO}_3^+$ and, to a lesser extent, from $\text{Co}(\text{en})_2\text{CO}_3^+$. By monitoring the decay of the CO_3^- absorption as a function of the concentration of added scavenger solutes, values of $k(\text{CO}_3^- + \text{S})$ have been obtained for some organic and inorganic solutes. In particular, $k(\text{CO}_3^- + \text{indole-3-propionic acid})$ was determined as a function of ionic strength and pH; at pH 7, k is independent of ionic strength while at pH 12 there is a positive dependence of $\log k$ vs. $\mu^{1/2}$. From the data it is concluded that at pH 7 the radical must exist in its acidic form, CO_3H , with a $\text{p}K_a = 9.6 \pm 0.3$. The dependence of k on pH at constant ionic strength for *N*-acetyltryptophan and β, β' -dithiodipropionic acid supports the model presented as does the lack of a pH dependence for indole.

Introduction

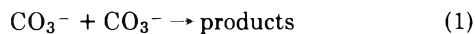
The CO_3^- radical can be generated radiolytically in aqueous solution through the interaction of OH radicals and carbonate.³⁻⁵ However, although the reaction of OH radicals with CO_3^{2-} to form CO_3^- is only moderately fast ($k = 4.2 \times 10^8 \text{ M}^{-1} \text{ sec}^{-1}$), the corresponding reaction with CO_3H^- is considerably slower ($k = 1.5 \times 10^7 \text{ M}^{-1} \text{ sec}^{-1}$).⁶ As a result, the use of the pulse radiolytic technique to observe and characterize the CO_3^- radical has been limited to studies in rather strongly alkaline solution. The spectrum of CO_3^- , with its absorption maximum at 600 nm, has been recorded at pH values at which the CO_3^{2-} concentration can be maintained near 0.1 M; the $\text{p}K$ for the equilibrium $\text{CO}_3\text{H}^- \rightleftharpoons \text{H}^+ + \text{CO}_3^{2-}$ is 10.36. The radical spectrum has also been generated in the direct flash photolysis⁷ of CO_3^{2-} at pH 12.8 and in the flash photolysis of H_2O_2 solutions⁸ containing CO_3^{2-} . In the latter case, the spectra obtained (from the photolytic decomposition of H_2O_2 to form OH radicals which then attack CO_3^{2-}) in the pH range 8-13 had identical

λ_{max} . The observation of a lack of a spectral change for CO_3^- as a function of pH was taken as evidence that the radical did not undergo acid-base equilibrium in that region; the acid-base forms of many radicals exhibit different absorption spectra.⁹ However, it must be pointed out that a change in the absorption spectrum is not a requirement for radical acid-base equilibria. For example, the

- (1) This research was supported by the National Science Foundation through Grant No. GP11213 and the College Teachers Research Program.
- (2) Participant, NSF College Teachers Research Program, Summer 1971. Permanent address: Department of Chemistry, University of Michigan, Flint College, Flint, Mich. 48503.
- (3) G. E. Adams and J. W. Boag, *Proc. Chem. Soc., London*, 112 (1964).
- (4) G. E. Adams, J. W. Boag, and B. D. Michael, *Trans. Faraday Soc.*, **61**, 1674 (1965).
- (5) G. E. Adams, J. W. Boag, and B. D. Michael, *Proc. Roy. Soc., Ser. A*, **287**, 321 (1965).
- (6) J. L. Weeks and J. Rabani, *J. Phys. Chem.*, **70**, 2100 (1966).
- (7) E. Hayon and J. J. McGarvey, *J. Phys. Chem.*, **71**, 1472 (1967).
- (8) D. Behar, G. Czapski, and I. Duchovny, *J. Phys. Chem.*, **74**, 2206 (1970).
- (9) P. Neta, M. Simic, and E. Hayon, *J. Phys. Chem.*, **73**, 4207 (1969).

spectra of the $\text{CO}_2\text{H}-\text{CO}_2^-$ ⁹ and $\text{C}_2\text{O}_4\text{H}-\text{C}_2\text{O}_4^-$ ¹⁰ pairs are virtually identical.

The second-order rate constant ($2k_1$) for the decay of CO_3^-



has been measured in the pulse and flash experiments. Hayon and McGarvey⁷ reported a value of $1.7 \times 10^7 \text{ M}^{-1} \text{ sec}^{-1}$ in the absence of O_2 for the direct flash of CO_3^{2-} at pH 12.8 in 0.1 M Na_2CO_3 . The flash in H_2O_2 ⁸ does not produce useful values for $2k_1$ inasmuch as the $\text{CO}_3^- + \text{H}_2\text{O}_2$ reaction is kinetically competitive with reaction 1. The Weeks and Rabani pulse radiolytic study⁶ showed that in the pH range 10.5–13.5, $2k_1$ had a constant value that was affected only by ionic strength; a plot of $\log 2k_1$ vs. $\mu^{1/2}/(1 + 0.4\mu^{1/2})$ was linear with a fitted slope of unity. An experiment at pH 8.4 in 1 mM HCO_3^- is reported but the result falls significantly below the line. From these ionic strength studies, a value of $2k_1 = 1.25 \times 10^7 \text{ M}^{-1} \text{ sec}^{-1}$ at zero ionic strength was calculated. The pH independence of the recombination rate constant of the radical, apart from the ionic strength effect, was also taken⁸ as evidence of the lack of radical acid-base equilibrium in the pH range studied. However, the practical lower limit of the pH range of the Weeks and Rabani study⁶ was 10.5.

We have already reported¹¹ that the flash photolysis of $\text{Co}(\text{NH}_3)_4\text{CO}_3^+$ can serve as a convenient source of CO_3^- radicals in neutral aqueous solution in which the radicals can be generated cleanly from a strongly absorbing substrate without resort to ionizing radiation and ultraviolet techniques involving weakly absorbing materials. In this paper we shall examine the behavior of CO_3^- generated by this technique with particular emphasis on the acid-base properties of the radical.¹²

Experimental Section

$\text{Co}(\text{NH}_3)_5\text{CO}_3^+$ (as the nitrate salt) was prepared according to literature procedures¹³ as was $\text{Co}(\text{NH}_3)_4\text{CO}_3^+$ (as the chloride salt).¹⁴ Conversion of the bidentate complex to the perchlorate salt was accomplished by dissolving the chloride salt in a minimum volume of water at 60°, filtering quickly, and adding the filtrate to an equal volume of 50% NaClO_4 solution (w/v). A bright purple solid was obtained after 1 hr at 0° which was filtered, washed with alcohol-ether, and air dried. Recrystallization did not change the absorption spectrum of the complex which compared very well with the literature.¹⁵ $[\text{Co}(\text{en})_2\text{CO}_3]\text{ClO}_4$ was prepared¹⁶ from $[\text{Co}(\text{en})_2\text{Cl}]\text{Cl}$ which in turn had been prepared by the procedure of Bailar.¹⁷ All solutions were prepared from triply distilled water which had been radiolyzed and photolyzed. Phosphate was used to buffer the solutions at pH 4–9.

Flash photolysis was performed using a 22-cm optical cell and procedures which have already been reported.^{18,19} For monitoring the 600-nm region, a Hamamatsu R136 PM tube was operated at about 600 V. The linearity of the detection system was checked and found to be satisfactory. A glass filter (Corning 3-72) was always in place between the analyzing lamp (Osram 150w Xe lamp) and the cell and an electric shutter restricted the exposure of the solution to the light. The solutions used were very dilute ($\sim 5 \times 10^{-5} \text{ M}$) to ensure homogeneous absorption of the photolyzing flash and the distribution of transient species in the cell. Transient absorption spectra were obtained from the optical density of the absorption mea-

sured 50 μsec after the start of the flash as a function of monitoring wavelength. Rate constants were calculated from a least-squares computer fit of the data to the appropriate rate law.

At pH <4.5, where the acid-catalyzed thermal aquation of $\text{Co}(\text{NH}_3)_4\text{CO}_3^+$ becomes rapid,²⁰ the useful life of the solution was about 5 min. In these cases, the solid salt was added to the phosphate buffer solution at the last moment and all subsequent procedures were carried out as rapidly as possible (usually within 1.5 min). Similarly in alkaline solution (pH >11), solutions were prepared directly from the salt in order to minimize base-catalyzed hydrolysis.²¹ Alternatively, in neutral or mildly alkaline solution, a fresh stock solution of 0.01 M $\text{Co}(\text{NH}_3)_4\text{CO}_3^+$ was used to prepare the solutions for flashing. The solutions for flashing were prepared in less than 1 min and the stock solution was discarded within 2 hr of preparation. For experiments involving $\text{Co}(\text{NH}_3)_5\text{CO}_3^+$, the flash solution was prepared directly from the solid and was never at pH <9.5 because of the very rapid hydrolysis of the complex.²² All solutions were discarded after one flash. Since O_2 had no effect on the kinetics of the transient species, air-saturated solutions were used directly as prepared. The ionic strength of the solution was established by the phosphate buffer, added NaClO_4 , or the KOH in alkaline solution.

Results

Irradiation of $\text{Co}(\text{NH}_3)_4\text{CO}_3^+$ at 254 nm in its intense ($\epsilon > 10^3 \text{ M}^{-1} \text{ cm}^{-1}$) ligand-to-metal charge transfer band generates Co^{2+} and $\text{Co}(\text{NH}_3)_4(\text{OH}_2)_2^{3+}$ with quantum yields in neutral solution of 0.06 and 0.1, respectively. Irradiation in the presence of 1 M 2-propanol in deaerated solution causes $\phi(\text{Co}^{2+})$ to double suggesting the presence of a radical which can oxidize the alcohol generating the strongly reducing $(\text{CH}_3)_2\text{COH}$ radical which can reattack the substrate.

Figure 1 shows the absorption spectrum of the transient species with λ_{max} 600 nm from the flash photolysis of $7.0 \times 10^{-5} \text{ M}$ $\text{Co}(\text{NH}_3)_4\text{CO}_3^+$ solution at pH 6.4 (with the optical density read 50 μsec after the start of the flash) which is identical with that of the CO_3^- radical generated by pulse radiolysis^{3-6,8} from the reaction of OH radicals with CO_3^{2-} or by the flash photolysis⁷ of CO_3^{2-} . The intensity and position of the absorption maximum was not affected by the presence of O_2 , by the pH of the solution (3–13), nor by the temperature (14–37°). The same transient absorption was also obtained from the flash photoly-

- (10) N. Getoff, F. Schwörer, V. M. Markovic, K. Sehested, and S. O. Nielsen, *J. Phys. Chem.*, **75**, 749 (1971).
- (11) V. W. Cope and M. Z. Hoffman, *Chem. Commun.*, 227 (1972).
- (12) A preliminary account of this work has already been published: S.-N. Chen and M. Z. Hoffman, *Chem. Commun.*, 991 (1972).
- (13) F. Basolo and R. K. Murmann, *Inorg. Syn.*, **4**, 171 (1953).
- (14) A. B. Lamb and E. B. Damon, *J. Amer. Chem. Soc.*, **59**, 383 (1937).
- (15) Y. Shimura and R. Tsuchida, *Bull. Chem. Soc. Jap.*, **28**, 572 (1955).
- (16) M. Linhard and G. Stirn, *Z. Anorg. Chem.*, **268**, 105 (1952).
- (17) J. C. Bailar, *Inorg. Syn.*, **2**, 222 (1946).
- (18) G. Caspari, R. G. Hughes, J. F. Endicott, and M. Z. Hoffman, *J. Amer. Chem. Soc.*, **92**, 6801 (1970).
- (19) A. F. Vaudo, E. R. Kantrowitz, M. Z. Hoffman, E. Papconstantinou, and J. F. Endicott, *J. Amer. Chem. Soc.*, **94**, 6655 (1972).
- (20) T. P. Dasgupta and G. M. Harris, *J. Amer. Chem. Soc.*, **91**, 3207 (1969).
- (21) D. J. Francis and R. B. Jordan, *J. Amer. Chem. Soc.*, **89**, 5591 (1967); **91**, 6626 (1969).
- (22) T. P. Dasgupta and G. M. Harris, *J. Amer. Chem. Soc.*, **90**, 6360 (1968).

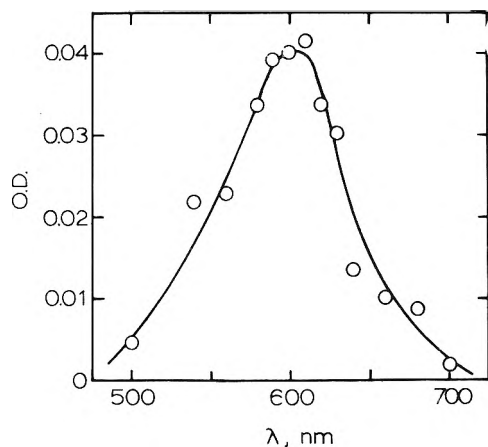


Figure 1. Spectrum of the CO_3^- radical from the flash photolysis of $7.0 \times 10^{-5} \text{ M}$ $\text{Co}(\text{NH}_3)_4\text{CO}_3^+$ at pH 6.4. Optical density read 50 μsec after the start of the flash.

sis of $\text{Co}(\text{en})_2\text{CO}_3^+$ (with a markedly reduced yield) and $\text{Co}(\text{NH}_3)_5\text{CO}_3^+$.

The absorbance of the solution at 600 nm after the decay of the transient was the same as that before the flash. A second-order plot of the decay data (Figure 2) shows linearity through approximately 60% of the decay with the rate becoming faster than expected in the final stages of the reaction. Such deviations from complete linearity are also shown for the decay of CO_3^- generated pulse radiolytically²³ at pH 10.2. It is to be noted that in more alkaline solution, the decay of CO_3^- , generated pulse radiolytically or flash photolytically, shows a more perfect second-order plot (Figure 2). This effect had been noted previously⁶ but no reason for this apparent catalytic behavior had been advanced. More recently,⁸ it was suggested that if the bimolecular recombination of CO_3^- generates H_2O_2 , then the rapid reaction of CO_3^- with H_2O_2 could produce this catalytic behavior as the H_2O_2 builds up.

Because the decay of the 600-nm absorption from $\text{Co}(\text{NH}_3)_4\text{CO}_3^+$ also gave respectable first-order plots, an independent test of the order of the initial decay was performed by measuring the half-life of the decay as a function of the initial optical density of the transient. The intensity of the flash was varied by varying the voltage of the discharge and the capacitance of the energizing condensers. In the first place, the intensity of the initial transient absorbance was proportional to the intensity of the flash ($I \propto \frac{1}{2}CV^2$) indicating that the 600-nm absorption is generated in a monophotonic process. Secondly, Figure 3 shows that $t_{1/2} \propto 1/(\text{OD})_0$ and that the decay of the transient generated from the complex is unquestionably second order. It should be mentioned that at no time was any formation of the 600-nm transient observed with the full absorption being present at the start of the observation period (50 μsec after the start of the flash). The decay of the transient was unaffected by the presence of O_2 and small ($\sim 10^{-4} \text{ M}$) concentrations of CO_3^{2-} , NO_3^- , and ClO_4^- , and by changes in temperature.

Assuming that the species that absorbs at 600 nm is the CO_3^- radical and that its second-order decay corresponds to reaction 1, then $2k_1$ can be obtained from the slope of the plots in Figure 2 taking⁷ $\epsilon_{600} 1830 \text{ M}^{-1} \text{ cm}^{-1}$. The values of $2k_1$ from $\text{Co}(\text{NH}_3)_4\text{CO}_3^+$ at pH 7 are very weakly dependent on ionic strength; at high pH values, $2k_1$ becomes dependent on ionic strength with the rate constant

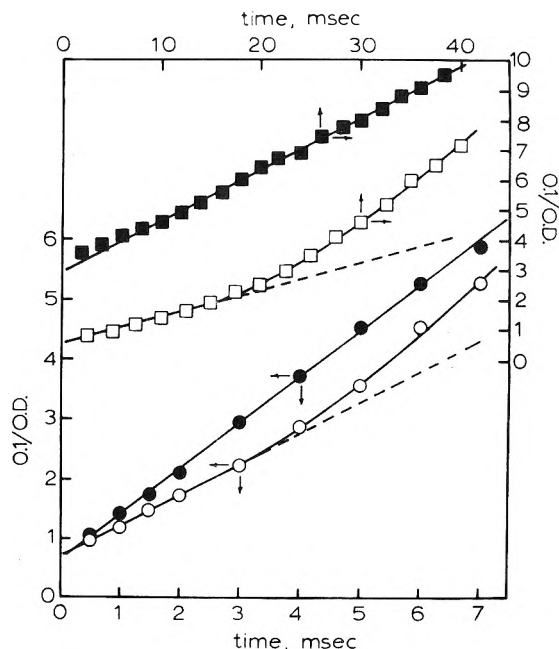


Figure 2. Second-order decay kinetics of the CO_3^- radical generated by various techniques, monitoring wavelength 600 nm: O, 0.1 M K_2CO_3 , N_2O -saturated solution, pH 10.2, pulse radiolysis, 2-cm optical cell; ●, same at pH 12.7; □, $5.0 \times 10^{-5} \text{ M}$ $\text{Co}(\text{NH}_3)_4\text{CO}_3^+$, air-saturated solution, pH 7.0, flash photolysis, 22-cm optical cell; ■, 0.1 M Na_2CO_3 , N_2 -saturated solution, pH 11.8, flash photolysis, 22-cm optical cell.

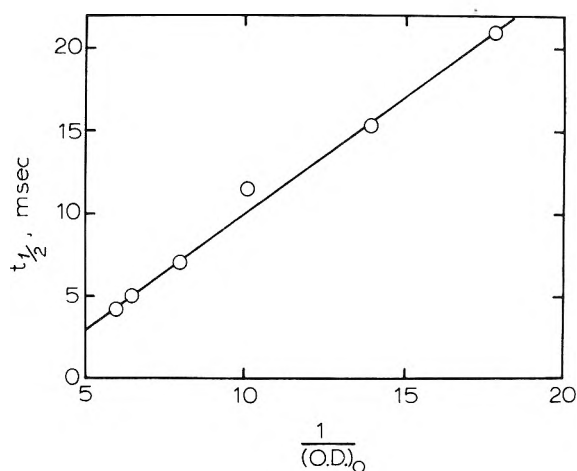


Figure 3. Dependence of $t_{1/2}$ for the decay of the CO_3^- radical on the initial radical concentration (optical density): $[\text{Co}(\text{NH}_3)_4\text{CO}_3^+] = 5.0 \times 10^{-5} \text{ M}$, pH 7.0, air-saturated solution, monitoring wavelength 600 nm, ionic strength = 0.1 M. Inasmuch as $t_{1/2} = \frac{1}{2}k[\text{CO}_3^-]_0$ for bimolecular second-order decay, taking $\epsilon_{600} 1.83 \times 10^3 \text{ M}^{-1} \text{ cm}^{-1}$ and an optical cell path length of 22 cm gives $2k = 2.8 \times 10^7 \text{ M}^{-1} \text{ sec}^{-1}$.

increasing as ionic strength is increased. As Table I shows, whereas $2k_1$ for CO_3^- generated from pulse radiolysis is virtually independent of pH (10.2–12.7) with the variation in rate attributable to the change of ionic strength, the radical from the complexes shows a marked increase in rate at pH > 10 with $2k_1$ rising to a maximum at pH 12. Even in highly alkaline solution the observed decay is second order and the spectrum and its intensity are the same as in neutral solution.

(23) The pulse radiolysis facilities at the U. S. Army Natick Laboratories were used for this experiment and the authors thank Dr. E. Hayon for the use of the instrument.

TABLE I: Decay of CO_3^- ^a

System	pH	$2k_1, M^{-1} \text{sec}^{-1}$ ^b
0.1 M K_2CO_3 ^c	10.2	1.9×10^7
	12.7	2.9×10^7
0.1 M Na_2CO_3 ^d 5×10^{-5} M $\text{Co}(\text{NH}_3)_4\text{CO}_3^+$	7.1	3.8×10^7
	7.6	4.1×10^7
	8.7	4.0×10^7
	9.5	6.1×10^7
	10.0	7.6×10^7
	10.6	2.0×10^8
	10.8	3.1×10^8
	11.0	1.1×10^9
5×10^{-5} M $\text{Co}(\text{NH}_3)_5\text{CO}_3^+$	11.6	8.0×10^8
	12.0	1.1×10^9
	12.7	1.2×10^9
	13.0	1.3×10^9
	9.5	1.1×10^8
	9.8	1.7×10^8
	10.0	1.3×10^8
	10.2	1.8×10^8
	10.5	1.9×10^8
	10.9	4.1×10^8
11.0	5.3×10^8	
11.2	7.4×10^8	
11.5	8.0×10^8	
11.9	1.4×10^9	
12.2	1.3×10^9	
12.6	1.3×10^9	
13.0	1.3×10^9	

^a Determined at 600 nm from flash photolysis in air-saturated solution unless otherwise noted; ionic strength controlled at 0.1 M with NaClO_4 .
^b Determined from the slope of a plot of $1/\text{OD}$ vs. time taking $\epsilon_{600} 1830 M^{-1} \text{cm}^{-1}$ and a cell path length of 22 cm (2 cm path length in the pulse radiolysis experiments). ^c Pulse radiolysis experiment in N_2O -saturated solution; ionic strength not controlled. ^d Ionic strength not controlled; solution deaerated with N_2 .

The value of $2k_1$ for $\text{Co}(\text{NH}_3)_4\text{CO}_3^+$ is constant below pH 7 to about pH 3 where the decay rate of the radical again increases sharply. A similar sharp increase in the decay rate was shown for CO_3^- from $\text{Co}(\text{NH}_3)_5\text{CO}_3^+$ at pH <9. Of course, under these extreme conditions, the acid-catalyzed aquation of the complexes^{20,22} is very rapid so that a flashed solution contains, in addition to at least some substrate, appreciable quantities of the aquation products. Although we were able to observe the CO_3^- radical from $\text{Co}(\text{en})_2\text{CO}_3^+$, the intensity of the absorption is too low, even under the most optimum conditions, to obtain the rate constant with any precision. However, it is apparent from the oscilloscope traces that the decay rate is of the same magnitude as for the tetraammine complex and the same effect is observed in alkaline solution.

The addition of other solutes to the solution containing $\text{Co}(\text{NH}_3)_4\text{CO}_3^+$ causes the second-order decay of the CO_3^- radical to become pseudo-first order with the observed first-order rate constant dependent upon the concentration of the scavenger. Figure 4 shows a sample of these data for methanol, 2-propanol, *tert*-butyl alcohol, and formate at pH 6.4. From the slopes of these lines $k(\text{CO}_3^- + \text{S})$ can be calculated and some selected values relevant to this study are given in Table II. We recognize, of course, that the use of high concentrations of solutes in order to scavenge for a radical species contains the danger that an adventitious impurity in the solute, although at a

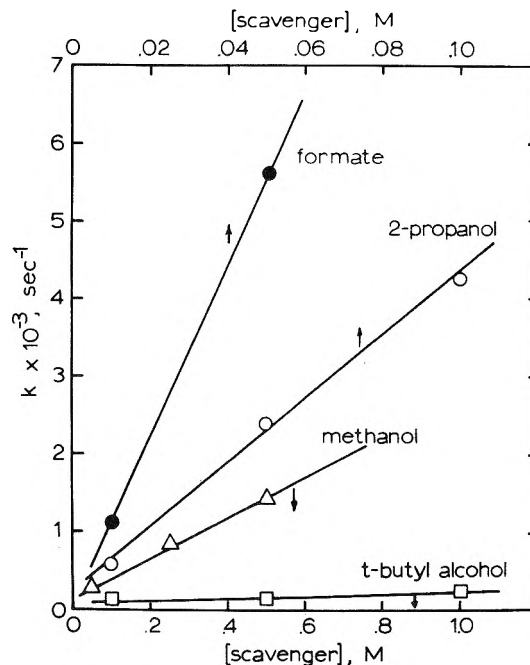


Figure 4. Pseudo-first-order rate constant for the decay of CO_3^- as a function of [scavenger]: $[\text{Co}(\text{NH}_3)_4\text{CO}_3^+] = 6.0\text{--}8.4 \times 10^{-5}$ M, pH 6.4, ionic strength = 0.026 M, air-saturated solution, monitoring wavelength 600 nm.

TABLE II: Rate Constants for the Reaction of CO_3^- Radicals with Scavenger Solutes ^a

Solute, S	pH	$k(\text{CO}_3^- + \text{S}), M^{-1} \text{sec}^{-1}$
Methanol	6.4	2.6×10^3
2-Propanol	6.4	4.0×10^4
<i>tert</i> -Butyl alcohol	6.4	1.6×10^4
Formate	6.4	1.1×10^5
$\text{Co}(\text{NH}_3)_4\text{CO}_3^+$	7.0	$< 10^6$
$\text{Co}(\text{NH}_3)_4(\text{OH}_2)_2^{3+}$	7.0	1.4×10^7
$\text{Co}(\text{NH}_3)_5\text{OH}_2^{3+}$	7.0	2.9×10^6
$\text{Co}_{\text{aq}}^{2+}$	7.0	4.4×10^6
Indole-3-propionic acid ^b	7.0	4.1×10^8
	12.0	6.8×10^8
<i>N</i> -Acetyltryptophan ^b	7.0	4.2×10^8
	11.8	6.2×10^8
Indole ^b	7.0	3.2×10^8
	12.0	3.2×10^8
β, β' -Dithiodipropionic acid ^b	6.8	1.3×10^7
	11.5	3.0×10^7

^a Ionic strength = 0.03 M unless otherwise indicated. ^b Ionic strength = 0.1 M.

low concentration, may react with the radical at relatively high rates. Therefore, any value of $k(\text{CO}_3^- + \text{S}) < 10^5 M^{-1} \text{sec}^{-1}$ should be viewed as an upper limit for that solute S.

For $\text{Co}(\text{NH}_3)_4\text{CO}_3^+$ the upper limit was determined by observing that the presence of 1.0×10^{-4} M substrate had no effect on the decay rate of the radical. In the case of the other Co(III) complexes, $\text{Co}_{\text{aq}}^{2+}$, and organic compounds, although these solutes are absorbing to varying extents, at the low concentrations involved sufficient light is absorbed by the $\text{Co}(\text{NH}_3)_4\text{CO}_3^+$ for the CO_3^- radical to be formed. The flash photolysis of these particular solutes alone did not yield any appreciable transient absorption

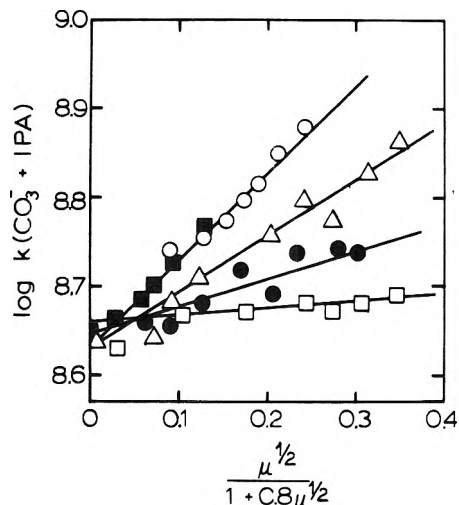


Figure 5. Dependence of $k(\text{CO}_3^- + \text{indole-3-propionic acid})$ on ionic strength (varied by NaClO_4): $[\text{Co}(\text{NH}_3)_4\text{CO}_3^{+}] = 5.0 \times 10^{-5} \text{ M}$, $[\text{IPA}] = 1.1 \times 10^{-5} \text{ M}$: \square , pH 7.0; \bullet , pH 8.3; Δ , pH 9.9; \blacksquare , pH 11.0; \circ , pH 12.0.

in the 600-nm region. Thus, although the initial intensity of the CO_3^- radical decreased as the concentration of the scavenger solute was increased, pseudo-first-order kinetics were observed and values of $k(\text{CO}_3^- + \text{S})$ could be evaluated.

Among the large numbers of compounds for which values of $k(\text{CO}_3^- + \text{S})$ have now been measured,²⁴ the highest rates are shown by indole and its derivatives such as tryptophan and indole-3-propionic acid. Because of this high rate, which means that very little scavenger need be present in order to produce pseudo-first-order kinetics, these compounds were chosen for further experiments concerning the nature of the CO_3^- radical. Indole-3-propionic acid (IPA) is commercially available from Matheson Coleman and Bell and, being a derivative of propionic acid, has a $\text{p}K_a$ value of ~ 4 . Thus, in neutral and alkaline solution, the acid would exist as the well-defined conjugate base with a charge of -1 . The pseudo-first-order rate constant for the reaction of CO_3^- with IPA was determined as a function of pH and ionic strength from which was calculated the second-order rate constant. Figure 5 shows a plot of $\log k(\text{CO}_3^- + \text{IPA})$ vs. $\mu^{1/2}/(1 + \alpha\mu^{1/2})$ at various pH values. The value of $\alpha = 0.8$ was chosen on the basis of the discussion by Weeks and Rabani⁶ and the fact that a good fit with a slope of 1.0 is obtained at high pH. It is evident from Figure 5 that at pH 7 the slope of the line is near zero and that the slope increases with increasing pH reaching the maximum of 1.0 at pH 11. Inasmuch as the charge of IPA is -1 throughout this pH range and the slope of the line is an indication of the charge type of the species involved in the reaction, it must be concluded that the radical has a zero charge at pH 7 and a -1 charge at pH 11 with a smooth transition between these values. With the ionic strength set at 0.1 M , $k(\text{CO}_3^- + \text{IPA})$ was determined as a function of pH and the results are shown in Figure 6. The "titration curve" yields a $\text{p}K_a$ value of 9.6 ± 0.3 . It must be pointed out that in all cases the rate of disappearance of CO_3^- with IPA exceeded the rate of the second-order disappearance of the radical so that complications due to the possible presence of base-hydrolysis products²¹ are of no concern.

A similar dependence of $k(\text{CO}_3^- + \text{S})$ on pH at 0.1 M ionic strength was exhibited by *N*-acetyltryptophan

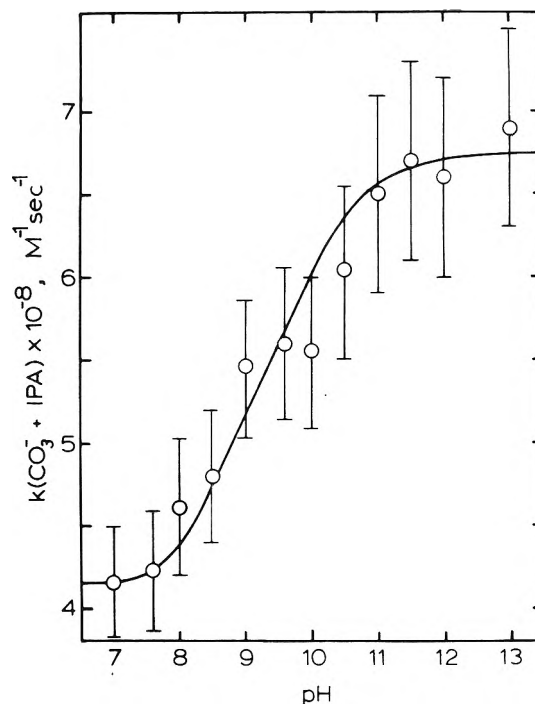


Figure 6. Dependence of $k(\text{CO}_3^- + \text{indole-3-propionic acid})$ on pH at constant ionic strength (0.1 M): $[\text{Co}(\text{NH}_3)_4\text{CO}_3^{+}] = 5.0 \times 10^{-5} \text{ M}$, $[\text{IPA}] = 1.1 \times 10^{-5} \text{ M}$. Error flags represent the uncertainty ($\pm 10\%$) in the determination of the value of k .

(Cyclo Chemicals), which exists as a -1 anion in neutral and alkaline solution, and by β, β' -dithiodipropionic acid, $(-\text{SCH}_2\text{CH}_2\text{CO}_2\text{H})_2$ (recrystallized Eastman product), which has a -2 charge. On the other hand, indole (Calbiochem), being uncharged, showed no pH dependence of k . Tryptophan and some of its other derivatives have $\text{p}K_a$ values of their own in the 9.5 region due to deprotonation of the amino group which produces a composite effect not amenable to simple interpretation. The $\text{p}K_a$ values for the radical reaction with *N*-acetyltryptophan and β, β' -dithiodipropionic acid are 9.6 ± 0.3 and 9.9 ± 0.3 , respectively.

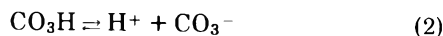
Discussion

The values of $2k_1$ reported in Table I show reasonable agreement among the various modes of generating the radical except for the complexes at pH > 10 . There are even common deviations from linearity of the second-order plots which suggest the autocatalytic decay of the radical. All the evidence is consistent with the generation of the CO_3^- radical from the carbonato complexes. It is interesting that $2k_1$ for the radical at pH 7 is only weakly dependent on ionic strength compared with the Weeks and Rabani report⁶ at pH > 10.5 . Unfortunately, the results of $2k_1$ for the complexes at pH > 10 are completely inconsistent with the other results from flash photolysis and pulse radiolysis except that a positive dependence of the rate constant on increasing ionic strength is seen at pH 12. Because the spectrum of the 600-nm absorption is independent of pH up to pH 13, we feel that the CO_3^- radical is still the absorbing species in alkaline solution. Its very rapid decay could arise from scavenging by a species present at a comparable concentration (so as to preserve second-order kinetics) which is either generated by the base hydrolysis of the substrate²¹ or through a pho-

(24) S. -N. Chen and M. Z. Hoffman, to be submitted for publication.

olytic reaction. We tested the effect of the presence of $\text{Co}(\text{NH}_3)_4(\text{OH}_2)_2^{3+}$, $\text{Co}(\text{NH}_3)_5\text{OH}_2^{3+}$, and $\text{Co}_{\text{aq}}^{2+}$ on the decay kinetics of the radical generated from the carbonate complexes at pH 12. With up to $5 \times 10^{-4} M$ of $\text{Co}(\text{NH}_3)_4(\text{OH}_2)_2^{3+}$ and $\text{Co}(\text{NH}_3)_5\text{OH}_2^{3+}$ (which are in their hydroxy form at pH 12), no effect on the decay kinetics of the radical was discerned. For $\text{Co}_{\text{aq}}^{2+}$, which precipitates at pH 12, its saturated solution did not quench the CO_3^- radical. The variation of the substrate concentration from 1 to $4 \times 10^{-5} M$ had no effect on the radical decay. It must be concluded that the rates of reaction of these ions with CO_3^- at pH 12 are $<10^7 M^{-1} \text{sec}^{-1}$ and are probably the same as at pH 7 (Table II). We therefore suggest that the rapid rate of decay of the radical at pH 12 cannot be the result of scavenging by $\text{Co}_{\text{aq}}^{2+}$, $\text{Co}(\text{NH}_3)_5\text{OH}_2^{3+}$, or $\text{Co}(\text{NH}_3)_4(\text{OH}_2)_2^{3+}$ generated in a thermal or photochemical process. However, photosubstitution of an ammine group by hydroxide on the substrate or on a thermal product, for example, could yield a species which would rapidly scavenge CO_3^- .²⁵

A further evaluation of the characteristics of the CO_3^- radical generated from the carbonate complexes can be made on the basis of the experiments performed with the indole and disulfide compounds as scavengers. From the lack of any significant ionic strength effect on $k(\text{CO}_3^- + \text{IPA})$ and $2k_1$ at pH 7, we conclude that the radical has a neutral charge at that pH and must exist in its acidic form, CO_3H . As the pH is increased and the dependence of $k(\text{CO}_3^- + \text{IPA})$ on ionic strength is observed, the radical is converted into its basic form with pK for reaction 2



equal to 9.6 ± 0.3 . Extrapolation of the data in Figure 5 to zero ionic strength shows that $k(\text{CO}_3^- + \text{IPA})$ is quite constant in the pH 7-12 range and that the variation in the rate data shown in Figure 6 is a result of the ionic strength effect. Similarly, this ionic strength effect leads to the observed variation of k upon change of pH for *N*-acetyltryptophan and $(-\text{SCH}_2\text{CH}_2\text{CO}_2\text{H})_2$ and the lack of an effect for indole. The results also show that the indole heterocyclic structure is not required for the pK_a of the radical to be observed.

Thus, we conclude that the acidic and basic forms of the radical have virtually identical spectra and similarly low reactivities (compared to diffusion-controlled rates). Inasmuch as the origin of the spectral absorption of the radical at 600 nm is not known, it is unwarranted to speculate on the reason for the lack of spectral differences between the two forms except to point out the similar be-

havior of the analogous carboxy radicals, CO_2^- and C_2O_4^- . Except for the knowledge that CO_3^- behaves as an oxidizing radical,²⁶ the mode of reaction of the radical, whether by oxidative addition, electron transfer, or H atom transfer, is largely unknown, especially for the inorganic species. The relative stability of the radical toward combination implies that there are severe constraints toward its ultimate transformation into final products.²⁷

It is consistent with the charges on the species that the pK_a of CO_3H be lower than that of CO_3H^- although the observed difference is within one pK unit. No means for predicting the pK_a of a radical on an *a priori* basis has been devised but certain trends have been experimentally observed. The best structural analogs to the CO_3^- case are the radicals derived from phosphate anions.²⁹ Thus, whereas the pK_a values of the stable PO_4H_2^- and PO_4H^- ions are 7.2 and 12.3, respectively, the PO_4H_2 and PO_4H^- radicals show pK_a values of 5.9 and 10.7, respectively, with the latter values known to $\pm 0.2 pK$ units. Here too the observed differences between the radical and its parent are about one pK unit. If the unpaired electron is largely confined to a nonbonding orbital on an oxygen atom³⁰ and protonation of the radical occurs at one of the other oxygen atoms, then it is not unreasonable for the acidity of the radical to be only slightly greater than the acidity of the parent anion. A slight weakening of the O-H bond in the radical due to the unpaired electron several atoms away is not unexpected. The same reasoning can be applied to the observations reported here on the CO_3^- radical. By comparison, the pK_a of the CO_2H radical is reported³¹ to be 3.9 ± 0.3 while the pK_a of HCO_2H , from which it is derived by abstraction of the carbon hydrogen, is 3.75. However, in CO_2H the unpaired electron is highly localized on the central carbon atom with increased 2s character.³⁰ Apparently, even with the proximity of the unpaired electron to the O-H bond, the acidic character of the species is relatively unchanged.

(25) T. P. Dasgupta and G. M. Harris, private communication.

(26) G. E. Adams, R. H. Bisby, R. B. Cundall, J. L. Redpath, and R. L. Willson, *Radiat. Res.*, **49**, 278 (1972).

(27) These final products are presumed to be CO_3^{2-} and a radical derived from the one-electron oxidation of the scavenger. It is interesting to note that the products and stoichiometry of the bimolecular decay of CO_3^- are virtually unknown with the following reactions having been proposed: $\text{CO}_3^- + \text{CO}_3^- \rightarrow$ (1) $\text{CO}_2 + \text{CO}_4^{2-}$; (2) $2\text{CO}_2 + \text{HO}_2^- + \text{OH}^-$; (3) $\text{C}_2\text{O}_6^{2-}$.²⁸

(28) I. C. Hisatsune, T. Adl, E. C. Beahm, and R. J. Kempf, *J. Phys. Chem.*, **74**, 3225 (1970).

(29) E. D. Black and E. Hayon, *J. Phys. Chem.*, **74**, 3199 (1970).

(30) P. W. Atkins and M. C. R. Symons, "The Structure of Inorganic Radicals," Elsevier, Amsterdam, 1967.

(31) A. Fojtik, G. Czapski, and A. Henglein, *J. Phys. Chem.*, **74**, 3204 (1970).

Reaction of OH and O⁻ Radicals with Aromatic Carboxylate Anions in Aqueous Solution¹

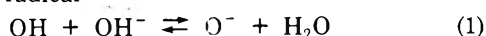
M. Simic,^{2a} Morton Z. Hoffman,*^{2b} and M. Ebert^{2c}

Radiation Biology Laboratory, University of Texas, Austin, Texas 78712, Department of Chemistry, Boston University, Boston, Massachusetts 02215, Paterson Laboratories, Christie Hospital and Holt Radium Institute, Manchester, England, and Pioneering Research Laboratory, U. S. Army Natick Laboratories, Natick, Massachusetts 01760 (Received June 16, 1972)

The reactivity of OH ($pK_a = 11.9$) and O⁻ radicals with aromatic carboxylate anions in irradiated alkaline N₂O-saturated aqueous solution has been studied using the pulse radiolysis technique. The compounds studied were the carboxylic acid derivatives of benzene, naphthalene, anthracene, and diphenyl which react with OH and O⁻ radicals by means of radical addition to the aromatic ring. The transient optical absorption spectrum of the OH adduct to a specific compound is identical with the spectrum obtained from O⁻ addition to the same compound indicating that the hydroxy group on the resultant radical is not ionized even at pH 14. From the kinetics of the formation of the transient absorption at pH 9 and 14, the rate constants for the reaction of OH and O⁻ radicals with the aromatic solutes were determined. The OH radical reacts at nearly diffusion-controlled rates ($k(\text{OH}) = 6\text{--}8 \times 10^9 \text{ M}^{-1} \text{ sec}^{-1}$) with the rate constant virtually independent of the nature of the substrate. The O⁻ radical reacts much more slowly with values of $k(\text{O}^-)$ dependent upon the charge on the substrate, the number of individual aromatic rings available, and the degree of aromaticity. The O⁻ radical is less electrophilic than is the OH radical and shows an unfavorable interaction with the π -electron system of the aromatic nucleus.

Introduction

Despite the fact that the O⁻ radical is the conjugate base of the OH radical



(with $k_1 = 1.2 \times 10^{10} \text{ M}^{-1} \text{ sec}^{-1}$, $k_{-1} = 9.2 \times 10^7 \text{ sec}^{-1}$, $pK_a = 11.85$),³⁻⁵ the chemistry of these primary species from the radiolytic decomposition of water is significantly different. In the case of simple inorganic ions, O⁻ reacts more rapidly with cations than does OH with the rate constant ratio $k(\text{O}^-)/k(\text{OH})$ increasing with the increase in the amount of positive charge on the ion.⁶ On the other hand, anions are more reactive toward OH with the relative reactivity toward OH increasing with the increase of the amount of negative charge.⁶ These observations are consistent with the differences in charge on the radicals. However, in a recent report,⁷ we showed that whereas OH radicals add rapidly to the aromatic nucleus of organic compounds and slowly undergo abstraction reactions with hydrogen atoms on aliphatic side chains, the behavior of the O⁻ radical is essentially reversed, albeit with generally diminished reactivity. When the aromatic nucleus lacks a side chain with an abstractable hydrogen atom, such as the benzoate anion, O⁻ adds to the ring producing a transient species⁸ with spectral and kinetic characteristics identical with that formed from the reaction of OH.^{8,9} The pK_a of the hydroxyl group on the resultant hydroxycyclohexadienylcarboxylate radical¹⁰ is apparently greater than 14 and the added O⁻ moiety is rapidly protonated, presumably *via* reaction with the solvent.

In this paper we wish to report the rate constants for the reaction of O⁻ with some aromatic compounds that lack aliphatic side chains and the absorption spectra of the resultant transient species as determined using the pulse radiolysis technique. The compounds used were carboxylic acid derivatives of benzene, diphenyl, naphthalene, and anthracene chosen because of their solubility in

alkaline aqueous solution and the absence of complicating effects due to substituent side chains.

Experimental Section

The compounds studied were *o*-phthalic acid (Matheson Coleman and Bell), diphenyl-4-carboxylic acid (K & K Laboratories), *o,o'*-diphenic acid (K & K), *p,p'*-diphenic acid (K & K), 1-naphthoic acid (Eastman Organic Chemicals), 2-naphthoic acid (Eastman), and 9-anthroic acid (Aldrich). All compounds were used as received except the diphenyl derivatives which were recrystallized from alcohol. Solutions were prepared in triply distilled water. At pH 9, the solutions were buffered with 1 mM sodium tetraborate; solutions at pH 14.0 were prepared from a weighed amount of Baker Analyzed KOH. All solutions were saturated with N₂O in order to convert e_{aq}^- into OH or O⁻.

Some experiments were performed at the Paterson Laboratories using the pulse radiolysis apparatus described by Keene.¹¹ Other experiments were performed at the U. S. Army Natick Laboratories using the Febetron 705 pulsed source.¹² The solutions to be examined were subjected to short (0.03–0.5 μsec) pulses of energetic electrons and the

- (1) This research was supported in part by NIH Grant No. GM-13557, AEC Contract No. AT-(40-1)-3408, and NSF Grant No. GP 11213.
- (2) (a) University of Texas; (b) Boston University; (c) Paterson Laboratories.
- (3) G. V. Buxton, *Trans. Faraday Soc.*, **65**, 2150 (1969); **66**, 1656 (1970).
- (4) J. Rabani and M. S. Matheson, *J. Phys. Chem.*, **70**, 761 (1966).
- (5) J. L. Weeks and J. Rabani, *J. Phys. Chem.*, **70**, 2100 (1966).
- (6) D. Zehavi and J. Rabani, *J. Phys. Chem.*, **75**, 1738 (1971).
- (7) P. Neta, M. Z. Hoffman, and M. Simic, *J. Phys. Chem.*, **76**, 847 (1972).
- (8) M. Simic and M. Z. Hoffman, *J. Phys. Chem.*, **76**, 1398 (1972).
- (9) R. Wander, P. Neta, and L. M. Dorfman, *J. Phys. Chem.*, **72**, 2946 (1968).
- (10) L. M. Dorfman, I. A. Taub, and R. E. Buhler, *J. Chem. Phys.*, **36**, 3051 (1962).
- (11) J. P. Keene, *J. Sci. Instrum.*, **41**, 493 (1964).
- (12) M. Simic, P. Neta, and E. Hayon, *J. Phys. Chem.*, **73**, 3794 (1969).

resulting transient absorption was detected using kinetic spectrophotometry techniques. Thus, the formation of the transient species could be monitored as a function of time and the intensity of the absorption determined as a function of wavelength. The absorbed dose per pulse was determined using KCNS dosimetry taking $\epsilon_{500} 7600 M^{-1} \text{cm}^{-1}$ for $(\text{CNS})_2^{-13}$ and $G(e_{\text{aq}}^-) = G(\text{OH}) = 2.8$.

Results and Discussion

The radiolysis of neutral and alkaline aqueous solutions generates e_{aq}^- , OH, and H with G values of approximately 2.8, 2.8, and 0.6, respectively.¹⁴ In the presence of 1 atm of N_2O , e_{aq}^- is virtually completely converted to O^- ($k(e_{\text{aq}}^- + \text{N}_2\text{O}) = 6.0 \times 10^9 M^{-1} \text{sec}^{-1}$) which is in rapid equilibrium with OH according to reaction 1. Thus, at pH 9, the predominant species is OH; at pH 14, ~99% of the radicals are in the O^- form. Under these conditions, H atoms make only a 12% contribution to the system and their effect, which is addition to the aromatic ring, can be accounted for on the basis of the known spectra of H atom adducts to aromatic systems such as benzoic acid.⁸ In highly alkaline medium H reacts with OH^- to yield e_{aq}^- which are converted to O^- upon reaction with N_2O .

Transient Absorption Spectra. Inasmuch as OH radicals react rapidly with the aromatic nucleus ($k > 10^9 M^{-1} \text{sec}^{-1}$; see following section), transient absorption spectra could be determined less than 1 μsec after the radiolysis pulse and before any appreciable decay had occurred. The reactivity of O^- radicals is considerably lower than that of OH. Therefore, at high pH, a higher concentration of organic scavenger was used in order to ensure that formation of the transient absorption occurred in a time relatively short compared to the decay time of the intermediate species. However, because of incomplete scavenging (>90%), the optical densities were normalized to the complete scavenging case. Extinction coefficients were determined by means of the KCNS dosimetry.

Similar to the results for benzoate anion^{8,9} in which addition by OH and O^- radicals generates a broad absorption spectrum with λ_{max} 330 nm and $\epsilon_{330} 3800 M^{-1} \text{cm}^{-1}$, we find here that the transient absorption spectra obtained from the reaction of OH- O^- with *o*-phthalic acid at pH 9.2 and 14 are identical with λ_{max} 330 nm and $\epsilon_{330} 3600 M^{-1} \text{cm}^{-1}$. The spectral properties of the $\cdot\text{C}_6\text{H}_4(\text{OH})(\text{CO}_2^-)_2$ radical are identical with those of the $\cdot\text{C}_6\text{H}_5(\text{OH})\text{CO}_2^-$ radical indicating that substitution of the ortho carboxylate group has little effect on the energy and oscillator strength of the transition which leads to the observed optical absorption.

With the diphenylcarboxylic acids, on the other hand, OH and O^- radical attachment can occur on either ring. For the diphenic acids, attack on either ring will give the same distribution of isomers so that the spectra shown in Figures 1A and 1C will be characteristic of the *o,o'* and *p,p'* substrate configurations. Note that both spectra show the presence of banded structure which may be indicative of the distinct absorption of the isomers. The radical from *p,p'*-diphenic acid (Figure 1C) exhibits a red-shifted band maximum with a very high ϵ value (at pH 9.7 and 14) which could arise from a strong resonance interaction between the rings involving also the para carboxylate groups. Radical addition to diphenyl-4-carboxylic acid should yield two distinct transient species with the cyclohexadienyl radical localized either on the phenyl side or the carboxylate side of the molecule. Radical attachment

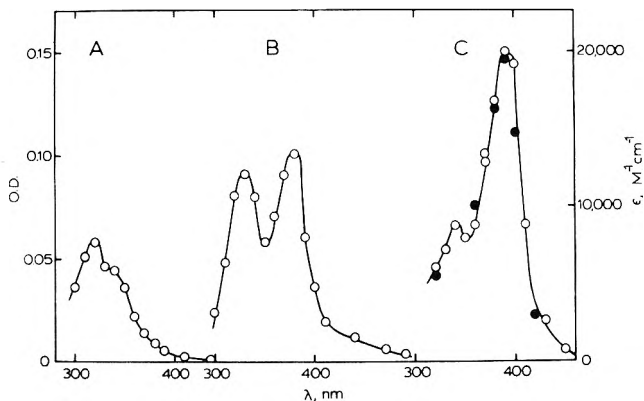
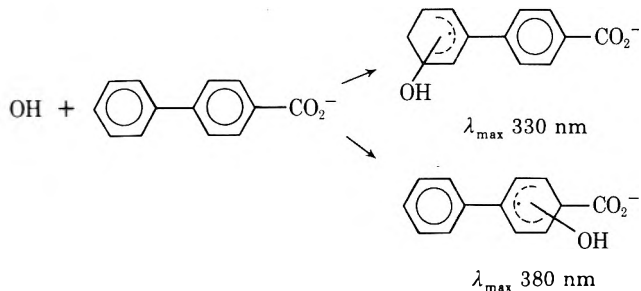


Figure 1. Transient absorption spectra obtained in N_2O -saturated aqueous solutions, 0.53 krad/pulse, 2.5-cm light path: (A) $5 \times 10^{-4} M$ *o,o'*-diphenic acid, pH 9.2; (B) $2.5 \times 10^{-4} M$ diphenyl-4-carboxylic acid, pH 9.2; (C) *p,p'*-diphenic acid, (O) $5 \times 10^{-4} M$, pH 9.7; (●) $1 \times 10^{-3} M$, pH 14.0, 1.7 krad/pulse, 2.0-cm light path, OD normalized.

on the phenyl side should resemble that for diphenyl¹⁵ while reaction on the carboxylate side should yield a spectrum similar to that of *p,p'*-diphenic acid. Figure 1B shows that this expectation is confirmed.



Addition of OH and O^- radicals to 1- and 2-naphthoic acids gives transient absorptions (Figure 2) which are not very different than that obtained from naphthalene (λ_{max} 320 nm, weak bands at ~380 nm; $\epsilon_{320} \sim 5000 M^{-1} \text{cm}^{-1}$).¹⁶ The weak band at 390 nm for 1-naphthoic acid probably reflects the presence of some particular isomer among the generated radicals; this band may also be present in 2-naphthoic acid but is hidden beneath the broad tail of the transient absorption.

The spectrum of the O^- (OH) adduct to 9-anthroic acid (Figure 3) is rather complex reflecting the large number of sites available for radical attack on the three rings, only two of which are equivalent. A similar multibanded spectrum is seen for the OH adduct to indole where the benzene and pyrrole rings are not equivalent.¹⁶

Rate Constants for OH and O^- Reaction. The kinetics of the appearance of the transient absorption spectra, monitored at the λ_{max} , were pseudo-first order from which was calculated the observed second-order rate constant, k_{obsd} . At least three traces were taken and the deviation of the individual runs from the average was less than $\pm 10\%$. At pH 9, the solute concentrations were $1 \times 10^{-4} M$; at pH 14, where the transient formation rate is slower,

(13) J. H. Baxendale, P. L. T. Bevan, and D. A. Stott, *Trans. Faraday Soc.*, **64**, 2389 (1968).

(14) See, e.g., M. Anbar in "Fundamental Processes in Radiation Chemistry," P. Ausloos, Ed., Interscience, New York, N. Y., 1968, p 651.

(15) The absorption spectrum of the OH adduct to diphenyl has never been reported, presumably because of experimental difficulties due to the extremely low solubility of the solute in aqueous solution.

(16) R. C. Armstrong and A. J. Swallow, *Radiat. Res.*, **40**, 563 (1969).

TABLE I: Rate Constants for the Reactions of OH and O⁻ in Aqueous Solutions and the Resulting Transient Optical Absorption Characteristics

Solute, S	pH 9.2 $k(\text{OH} + \text{S}),$ $M^{-1} \text{sec}^{-1}{}^a$	$k_{\text{obsd}}, M^{-1} \text{sec}^{-1}{}^a$	$k(\text{O}^- + \text{S}),$ $M^{-1} \text{sec}^{-1}{}^d$	Estimated error limits, %	Transient absorption from OH/O ⁻ + S	
					$\lambda_{\text{max}}, \text{nm}$	$\epsilon, M^{-1} \text{cm}^{-1}$
Benzoic acid	6.0×10^{9b}	$8.5 \times 10^{7c,d}$	$3.8 \times 10^{7c,d}$	± 50	330 ^{b,d}	3,800 ^{b,d}
Phthalic acid	5.9×10^9	6.5×10^7	$\leq 1.8 \times 10^7$		330	3,600
Diphenyl-4-carboxylic acid	6.8×10^9	1.2×10^8	7.0×10^7	± 30	330	13,000
<i>o,o'</i> -Diphenic acid	7.0×10^9	8.4×10^7	$\leq 2.9 \times 10^7$		380	14,000
<i>p,p'</i> -Diphenic acid	8.3×10^9	9.3×10^7	$\leq 2.8 \times 10^7$		320	8,300
1-Naphthoic acid	7.9×10^9	1.8×10^8	1.2×10^8	± 30	390	20,000
2-Naphthoic acid	7.6×10^9	1.9×10^8	1.3×10^8	± 30	330	6,000
9-Anthroic acid	8.0×10^9	5.4×10^8	4.8×10^8	± 20	340	2,400
					<280	>13,500
					325	15,500
					340	14,200
					370	7,000

^a $\pm 10\%$. ^b From ref 9. ^c From ref 7. ^d From ref 8.

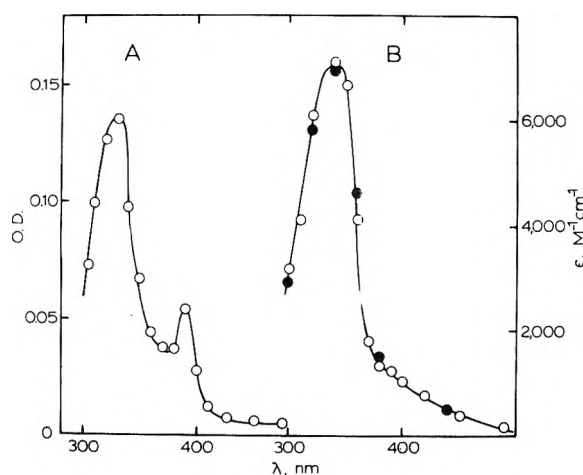


Figure 2. Transient absorption spectra obtained in N₂O-saturated aqueous solutions, 1.6 krads/pulse, 2.5-cm light path: (A) $2.5 \times 10^{-4} M$ 1-naphthoic acid, pH 10.5; (B) 2-naphthoic acid, (O) $5 \times 10^{-4} M$, pH 10.5; (●) $1 \times 10^{-3} M$, pH 14.0, 1.7 krads/pulse, 2.0-cm light path. OD normalized.

solute concentration of $1 \times 10^{-3} M$ were used. Good pseudo-first-order plots were obtained through at least three half-lives of the transient formation and a correction was applied for any small (<5%) decay of the absorption during the formation period. In strongly alkaline solution equilibrium 1 will be achieved before reaction of OH or O⁻ with the solute occurs. The observed rate constant, k_{obsd} , will be composed of two kinetic components inasmuch as both the OH and O⁻ radicals contribute to the formation of the same transient

$$k_{\text{obsd}} = k(\text{OH} + \text{S}) \times \frac{[\text{H}^+]}{[\text{H}^+] + K(\text{OH})} + k(\text{O}^- + \text{S}) \left(1 - \frac{[\text{H}^+]}{[\text{H}^+] + K(\text{OH})}\right)$$

where $K(\text{OH}) = 1.26 \times 10^{-12}$. Even at pH 14 (1 M KOH), where less than 1% of the reactive radicals are in the protonated form, the reaction of OH with the solute is a significant contribution toward the value of k_{obsd} . Table I gives the rate constant data obtained in this study as well as a summary of the spectral data presented earlier in the figures. Values of $k(\text{O}^- + \text{S})$ within 20% of those given in

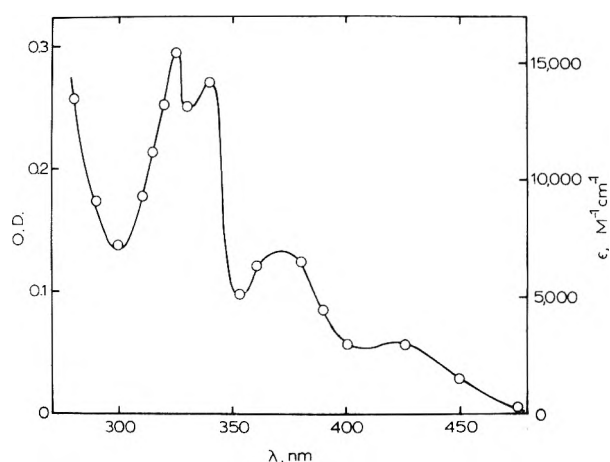


Figure 3. Transient absorption spectra obtained in N₂O-saturated aqueous solution containing $5 \times 10^{-4} M$ 9-anthroic acid, pH 14.0, 1.5 krads/pulse, 2.0-cm light path. ϵ values corrected for depletion of substrate by the pulse.

Table I were obtained at 0.5 and 1.3 M KOH. The effect of lowering the KOH concentration could not be studied since under those conditions the extent of the correction for the contribution of OH radicals becomes so great as to place the $k(\text{O}^- + \text{S})$ value in doubt.

An examination of the rate constant data in Table I reveals certain general trends. The values of $k(\text{OH} + \text{S})$ for all the compounds studied are uniformly high, near the diffusion-controlled limit, and do not show any obvious dependence on the size or number of aromatic rings or the charge on the solute. Attack by the OH radical and its addition to the aromatic ring system is clearly a process with few energetic or electronic restrictions and occurs on almost every encounter. On the other hand, the formation of the observed transient from O⁻ attack is considerably slower and depends upon the charge on the solute and the number and type of aromatic rings. Thus, $k(\text{OH} + \text{S})/k(\text{O}^- + \text{S}) \geq 160$ for singly charged benzoate and ≥ 330 for doubly charged *o*-phthalate. When comparison is made with this ratio for benzene (66),¹⁷ it becomes clear that $k(\text{O}^- + \text{S})$ depends upon the charge of S in a straightforward way with the rate constant diminishing as the num-

ber of negative charges on S increase. When an additional aromatic ring is available for O⁻ attack, as in the case of diphenyl-4-carboxylic acid, the rate is approximately twice that of benzoic acid ($k(\text{OH} + \text{S})/k(\text{O}^- + \text{S}) \geq 98$). However, with the diphenic acids which provide two aromatic rings and a doubly negative anion, the rate is established by both effects. The ortho or para nature of the diphenic acids does not have any apparent effect on the O⁻ rate.

The most interesting trend in the $k(\text{O}^- + \text{S})$ values is exhibited by the singly charged anions of benzoic, naphthoic, and anthroic acids for which the rate of the reaction increases by over a factor of 10 in going from the simplest molecule to the most complex. If the rate of addition of O⁻ to the aromatic ring were governed simply by the number of sites available for bonding, then one would expect the values of $k(\text{O}^- + \text{S})$ to be in the ratio of 6:10:14, which they are not. Furthermore, one would expect that some sites on the aromatic nucleus (for example, the bridgehead carbon atoms) would be sterically unaccessible for O⁻ addition rendering the predicted range of rate constants even smaller. Rather, the value of $k(\text{O}^- + \text{S})$ for these compounds appears to be related to the extent of delocalization of the aromatic π -electron system for which benzene < naphthalene < anthracene. Apparently, the rate of free-radical addition to aromatic hydrocarbons is governed somewhat by the energy required to isolate a single π electron at a carbon atom to form a " σ complex."¹⁸ It is unfortunate that the solubility of these aromatic hydrocarbons (even as the carboxylate deriva-

tive) is so low in aqueous solution which precludes a further test of this somewhat crude model. Mechanistically, it is not yet clear whether the O⁻ (or OH) radical adds directly to a specific site or first forms a molecular complex with the aromatic π system which rapidly undergoes reorganization to give the various isomers.

The O⁻ radical is clearly a weaker electrophilic reagent than is OH in its addition reactions with the aromatic ring as shown by its less than diffusion-controlled reaction rates. It is difficult to assess the reasons for the difference between this acid-base pair but it should be noted that a similar behavior has been observed for NH₃⁺-NH₂ radicals. Specifically, NH₃⁺ adds to benzene to give an intermediate observable by the pulse radiolysis technique; NH₂ does not give a detectable transient.¹⁹ The lowest-lying molecular orbital available for bonding in OH is virtually identical with the corresponding orbital in O⁻ thereby ruling out considerations on symmetry and energy grounds. At the present time we can only observe that the charge distribution and polarizability differences in the radicals may account for the observations reported here.

Acknowledgment. We thank Dr. E. Hayon of the U. S. Army Natick Laboratories for the use of the pulse radiolysis apparatus and his interest in this work.

- (17) G. Hughes and H. A. Makada, *Trans. Faraday Soc.*, **64**, 3276 (1968).
 (18) J. N. Murrell, S. F. A. Kettle, and J. M. Tedder, "Valence Theory," 2nd ed. Wiley, New York, N. Y., 1970.
 (19) M. Simic and E. Hayon, *J. Amer. Chem. Soc.*, **93**, 5982 (1971).

Infrared Kinetic Study of Reactions of Alcohols on the Surface of Alumina

William Hertl*¹ and Angela Maria Cuenca

Departamento de Quimica, Facultad de Ciencias, Universidad de los Andes, Mérida, Venezuela (Received December 6, 1972)

Methanol, ethanol, propanol, and butanol adsorb on alumina as stable alkoxy groups. Above 150° in the presence of alcohol vapor or air these alkoxy groups are converted to carboxyl groups. A kinetic analysis of this reaction using infrared spectroscopy showed that the surface reaction is pseudo-zero order. The presence of a Lewis acid site (Al⁺) is necessary in order that the gaseous alcohol or oxygen may adsorb and produce an oxygen-containing species. This species is mobile on the surface and reacts with the bonded alkoxy groups to produce a bonded carboxyl group. Poisoning of the Lewis acid sites with pyridine strongly inhibits the reaction. Based upon the data a reaction mechanism is proposed.

Introduction

The catalytic dehydroxylation of alcohols over alumina has been studied for many years.^{2a} Generally, lower temperatures produce ethers and higher temperatures produce alkenes, although methanol produces ethers, C₂H₄, C₂H₆, etc. at higher temperatures. The general pattern for these catalytic reactions is the removal of a hydroxyl group and of a proton.

There have been several infrared spectroscopic studies of alcohol adsorption on alumina, commencing with Ba-

bushkin and Uvarov^{2b} who found that, at low temperatures, ethanol produced surface -OH, -CH₂CH₂, and ethoxy groups. Greenler³ carried out a detailed study of methanol and ethanol adsorption on alumina, which included the use of ¹³C and deuterated compounds for iden-

- (1) Present address: Technical Staffs Division, Corning Glass Works, Corning, N. Y. 14830.
 (2) (a) M. E. Winfield in "Catalysis," Vol. VII, P. H. Emmett, Ed., Reinhold, New York, N. Y., 1960, p 93 ff; (b) A. A. Babushkin and A. V. Uvarov, *Dokl. Akad. Nauk SSSR*, **110**, 581 (1956).
 (3) R. G. Greenler, *J. Chem. Phys.*, **37**, 2094 (1962).

tifying the various bands which appeared. Three surface entities were found, *viz.*, (1) physically adsorbed alcohol removable by evacuation at 35°, (2) adsorbed alkoxy groups, and (3) surface formate ions (from methanol) or acetate ions (from ethanol) when the alumina was heated to 170° in the presence of alcohol vapor. These carboxyl groups are stable to >400°. All subsequent work has confirmed his observations and band identifications. Greenler suggested that the alcohol reacts with an Al atom to produce alkoxy groups with the elimination of one hydrogen, and with an oxide atom to produce carboxyl groups with the elimination of three hydrogens. In reviewing this work, both Little⁴ and Hair⁵ considered the reaction between the alcohol and a surface hydroxyl group as more likely to form alkoxy groups.

Kagel⁶ studied C₁ through C₄ normal alcohols, and concluded that the weakly adsorbed alcohols were H bonded to the surface. The chemisorbed alkoxy groups were formed by adsorption of alcohol on oxygen atoms to form alkoxy and hydroxyl groups. He proposed that the chemisorbed alkoxide reacts with an adjacent Al-OH group to form a bridged carboxylate.

Deo and Dalla Lana, in a study of 1-propanol⁷ and secondary alcohol⁸ adsorption on alumina, surmised that the alkoxy forms by adsorbing alcohol on Al³⁺ which then splits off H⁺, and that the carboxylate forms by reaction of an alkoxy with an adjacent OH group. On the basis of NaOH doped alumina, they concluded that the high-frequency OH groups (~3785 cm⁻¹) are the principal cause of dehydration of the alkoxy group, and that by removing these groups a reaction involving Al³⁺ ions becomes dominant.

Although the experimental observations between these different workers are generally in agreement, the mechanisms proposed for both the alkoxide and the carboxylate formation are rather divergent. Most of the experiments involved heating the alumina in alcohol vapor and recording the spectra at room temperature. All the mechanistic conclusions were drawn on the basis of these spectra and gas analyses. This study describes a kinetic evaluation of the formation of surface carboxylates using methanol, ethanol, propanol, and butanol. A study of this type yields much more information about the course of the reactions than does observation of only initial and final states. In so far as the experiments carried out here overlapped those reported above, they are in broad agreement. In this study, all spectra were recorded at reaction temperature, and reaction curves were obtained for the formation of carboxyl groups on the surface. The reactions were carried out at various temperatures, using various pressures of alcohol vapor or air. Experiments were also carried out in which the alumina surface was treated with pyridine.

Experimental Section

The details of measuring surface kinetics have been previously described.⁹ Briefly, a self-supporting disk of alumina was mounted in a cylindrical furnace cell placed in a Perkin-Elmer Model 621 infrared spectrophotometer. The furnace cell had water-cooled end plates fitted with Irtan-2 windows, and was connected to a conventional vacuum rack. Gas or vapor at any desired pressure was admitted to the cell for a given time and then evacuated. Spectra were taken at each step of the process. By measuring the intensities of the absorption bands at various times one can construct a reaction curve. Since the cell was frequently evacuated, the gas-phase concentration

was essentially constant during the course of any given experiment. All spectra were recorded at reaction temperature.

The Alon C alumina disks were prepared by pressing approximately 50 mg in a 1-in. die at 24,000 psi between two sheets of tissue paper moistened with acetone. This "sandwich" was heated at 900° in air for 1 hr and transferred to the reaction cell. The cell with the alumina disk was then heated to 400° *in vacuo* for 15 min, after which the temperature was lowered to the desired reaction temperature and the reaction carried out.

Analytical grade reagents were used throughout.

Results

In Figure 1 are given some typical spectra in the region 1700-1300 cm⁻¹ taken during the course of a kinetic experiment. The bands in the vicinity of 1460 and 1560 cm⁻¹ are due to the symmetric and asymmetric OCO group vibrations of the surface carboxylate. The precise frequencies, as well as the relative band intensities, for each alcohol are given in Table I. With the exception of methanol, the two observed carbonyl bands have integrated intensities which differ by no more than about 15%. With methanol, the symmetric band is only about 1/3 as intense as the asymmetric band. The intensities of these C=O bands during the course of an experiment were used to construct the kinetic reaction curves. Some typical reaction curves are given in Figure 2.

These C=O bands increased in intensity only in the presence of gaseous alcohol or added air. No changes were observed in these intensities when the sample was allowed to stand *in vacuo* at reaction temperature for periods up to several hours. Plots of the lower frequency C=O band against the higher frequency C=O band were linear for any given alcohol, demonstrating that both bands arise from the same functional group. Bands at 2800-3000 cm⁻¹ and near 1385 cm⁻¹, due to C-H stretching and bending vibrations, appeared initially. These C-H bands rapidly reached their final intensity. Thereafter they remain nearly constant during the course of a reaction (*cf.* Figures 1 and 3). During this initial period the hydroxyl group bands at 3600-3760 cm⁻¹ disappeared (Figure 3) and the OH group bands between 3460 and 3560 cm⁻¹ increased in intensity. During the course of the reaction there is a small increase in the region 3600-3100 cm⁻¹. When the alcohol reacted with the surface at a lower temperature (150°) bands also appeared near 1070, 1100, and 1150 cm⁻¹. Greenler³ observed bands in this vicinity and assigned them to a surface alkoxide group.

Thus, the first reaction is that between the alcohol and some of the surface hydroxyl groups to produce surface alkoxy groups. In the presence of gaseous alcohol these alkoxy groups are then oxidized to carboxyl groups.

Figure 2 shows that the reaction curves for the formation of carboxylate, using ethanol, propanol, and butanol, are linear throughout except for an initial fast reaction. With methanol, the reaction curves showed a sharp break, but the two portions were linear. In these experiments the

(4) L. H. Little, "Infrared Spectra of Adsorbed Species," Academic Press, London, 1966, p 178.

(5) M. L. Hair, "Infrared Spectroscopy in Surface Chemistry," Marcel Dekker, New York, N. Y., 1967, p 157.

(6) R. O. Kagel, *J. Phys. Chem.*, **71**, 844 (1967).

(7) A. V. Deo and I. G. Dalla Lana, *J. Phys. Chem.*, **73**, 716 (1969).

(8) A. V. Deo, T. T. Chuang, and I. G. Dalla Lana, *J. Phys. Chem.*, **75**, 234 (1971).

(9) W. Hertl, *J. Phys. Chem.*, **72**, 1248 (1968).

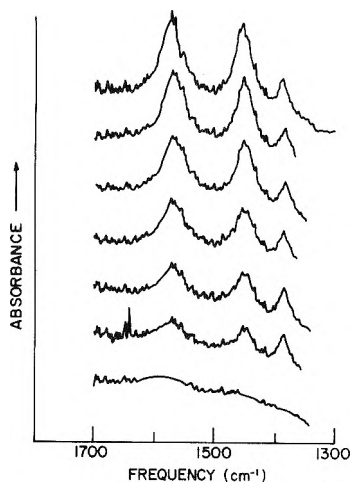


Figure 1. Spectra of alumina at various times showing growth of carboxylate bands due to reaction of 10 Torr of ethanol at 275°. The initial spectrum is at the bottom; the top spectrum is after 84 min of reaction.

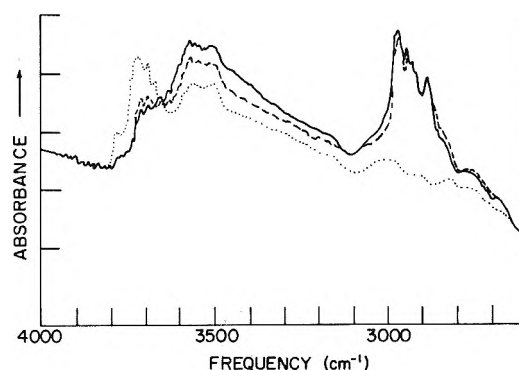


Figure 3. Spectra of alumina at 275°: ····· initially; - - - - after 30 sec of reaction with propanol; ——— after 145 min of reaction with propanol.

TABLE II: Gas-Phase Products from Reaction of Alcohols on Alumina^a

Reactant	Products
Methanol	Mixture of ether and alkanes
Ethanol	Ethylene
Propanol	Propylene

^a The alumina was heated at 400° *in vacuo* prior to the reaction with the alcohol.

In order to determine the gas-phase products, some alumina was placed on the floor of the furnace at 250°. Alcohol vapor was added for a time sufficient to ensure that the initial bonding reaction to form the alkoxide was complete. Fresh alcohol vapor was then added and allowed to stand for 45 min. Spectra were taken at various times. Initially, unreacted alcohol was observed and at later times only the products listed in Table II were found.

The rate of carboxylate formation at various alcohol pressures was measured by carrying out the reaction at a fixed datum pressure and measuring the rate; then, using a different pressure, the rate was again measured. Thus all the rates for a given alcohol are referred to a datum pressure. This method of normalization is necessary due to slight differences in thickness between different alumina disks. In Figure 4 are given the measured pressure dependencies of the reaction rates. These curves should reflect the shape of the adsorption isotherm of the alcohol which reacts with the bonded species, and appear to be type I isotherms.

The initial fast reaction which appears as an intercept on the kinetic plots accounts for about 10% or less of the total reaction and is completed within several minutes, compared to hundreds of minutes for the complete reaction. This fast reaction takes place during the time when the CH bands are building up to their final intensity and the OH bands above 3600 cm⁻¹ are disappearing. By carrying out the reaction at 150° one can readily follow this initial process. At this low temperature one observes a small growth in the C=O band at 1560 cm⁻¹ and a large growth in the C=O band at 1462 cm⁻¹ during the time when the CH bands at 1380 cm⁻¹ are building up to their final intensity, after which there is no further change. On raising the temperature to 250° with evacuation about 75% of the large C=O band and the 1380-cm⁻¹ CH band disappear, leaving small C=O bands at 1560 and 1462 cm⁻¹ and the CH band at 1380 cm⁻¹. Thus, this initial fast oxidation reaction is sufficiently rapid to be

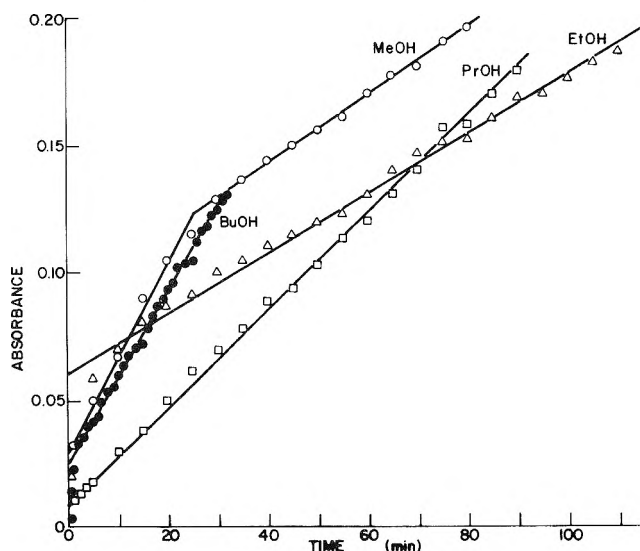


Figure 2. Kinetic plots obtained at 250° for: O, 20 Torr of methanol; Δ, 20 Torr of ethanol; □, 10 Torr of propanol; ●, 5 Torr of butanol.

TABLE I: Observed Frequencies (in cm⁻¹) and Intensities of Carboxyl Bands Produced by Reaction of Alcohols on Alumina

Alcohol	Asymmetric OCO	Symmetric OCO	CH bending	Intensity symmetric OCO / intensity asymmetric OCO
Methanol	1587	1378	1390	33%
Ethanol	1572	1455	1388	89%
Propanol	1564	1444	1384	85%
Butanol	1556	1469	1380	110%
	1555	1455		
	1567	1463		

alcohol vapor was evacuated at short intervals and fresh vapor added, so that the gas-phase composition was essentially constant during an experiment. Under these conditions the reaction curves describe a pseudo-zero-order process.

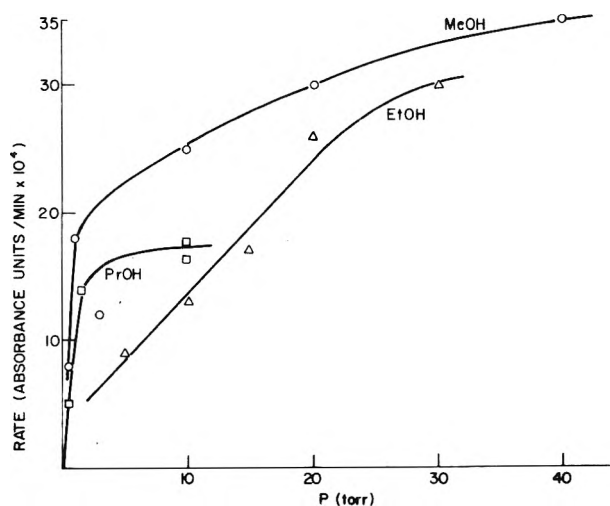


Figure 4. Plots of carboxylate reaction rate at 250° against pressure of alcohol vapor. The rate at a fixed reference pressure was determined for each disk. A different pressure was then used. All the rates are normalized with respect to the reference pressure. Reference pressures used were methanol, 20 Torr; ethanol, 20 Torr; and propanol, 10 Torr.

observable even at 150°. The experiment is somewhat obscured due to the oxidation of loosely bound alcohol, which desorbs on raising the temperature. This loosely bound alcohol would not be present at the usual reaction temperatures. These intensity changes are not due to the temperature dependence of the infrared absorption bands themselves. Over this temperature range the peak intensities normally decreased about 25%, whereas the large C=O band as well as the CH bands decreased about 75% on raising the temperature.

The temperature dependencies were also measured. The reaction rate variation with temperature will depend on at least two factors: the true activation energy of the oxidation reaction and the concentration of the intermediate adsorbed oxidant. In these experiments it is not possible to isolate the two steps. Although this experimental activation energy has no fundamental significance it is a convenient way to describe an experimental temperature dependence. The results obtained were (in kcal/mol) butanol 16, propanol 16, ethanol 17, and methanol (first linear part of reaction) 21.

The kinetic behavior of the methanol is quantitatively somewhat different. The kinetic curves show the rapid initial formation of C=O bands in parallel with the build-up of the CH bands in the 2800–3000 cm^{-1} region for the first few minutes of reaction, as with the other alcohols. After this initial fast reaction the curve for C=O formation is linear for about 50% of the reaction. After this point the reaction curve is also linear, with a slope indicating a reaction rate only about half as fast as during the first half of the reaction. There are also small increases in the CH bands at 2800–3000 and 1390 cm^{-1} . The gaseous reaction products obtained with methanol are also different from those obtained with the other alcohols.

When the partially reacted alumina is heated to 400° *in vacuo* the C=O bands are stable in frequency and intensity, but the CH band intensities decrease. This is probably due to desorption of the bonded alkoxy groups. On heating the alumina at 400° in air, after substantial reaction with methanol, no changes occur in the intensities or frequencies of the C=O bands and the CH band at 1390 cm^{-1} decreases only slightly. The CH bands near 2900

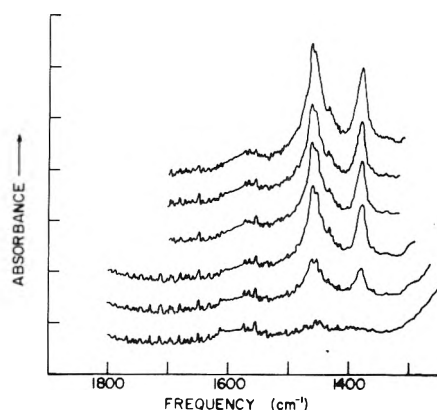


Figure 5. Spectra of alumina at various times showing the initial fast reaction at 150° using 5 Torr of butanol. The initial spectrum is at the bottom; the top spectrum was taken after 90 sec of reaction. No further changes were observed at this temperature.

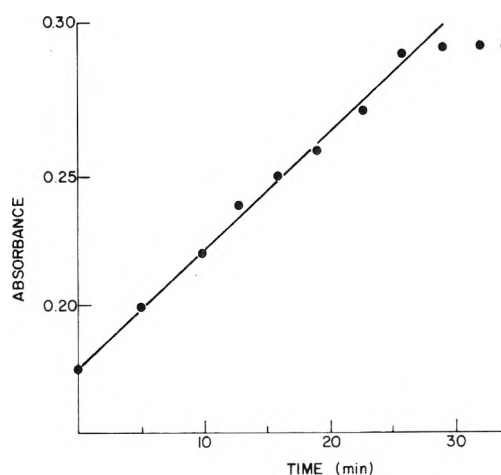


Figure 6. Kinetic plot of growth of carboxyl bands obtained at 275° using 50 Torr of air. Prior to making this plot, the alumina was exposed to 30 Torr of methanol at 150° for 5 min.

cm^{-1} are almost completely removed (15% remaining). The OH band at 3720 cm^{-1} reappears and the OH band near 3500 cm^{-1} is removed.

In Figure 6 is given a reaction curve taken under the following conditions. Methanol was added to the cell at 275° for 5 min until the intensities of the observed CH bands were essentially constant, indicating that the alkoxy bonding reaction was complete. Air (50 Torr) was introduced into the cell for a given period of time and then evacuated. This was repeated in exactly the same manner as in a kinetic experiment with alcohol vapor. The reaction curve is linear throughout. The frequencies of the C=O bands were identical with those observed when methanol vapor was used for the oxidation reaction. The same experiment was repeated with propoxy groups bonded to the surface and then oxidized with air. A linear reaction curve was also obtained, as when propanol vapor was used, but an additional C=O band was observed at 1580 cm^{-1} , as well as the bands at 1560, 1470, and 1445 cm^{-1} . This new C=O band appears near the C=O band observed with methanol (1587 cm^{-1}). It seems likely that the hydrocarbon side chain had been partially oxidized, thus giving rise to this formate C=O band, as well as the propionate C=O bands observed with propanol vapor oxidation.

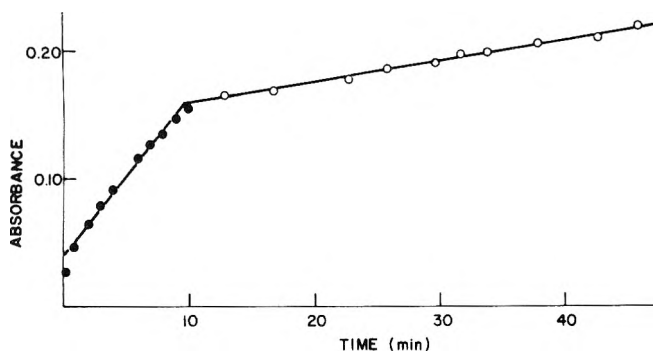


Figure 7. Kinetic plot of growth of carboxyl bands obtained at 275° using 50 Torr of air from time 0 to 10 (●) using 50 Torr of air plus 5 Torr of pyridine from time 10 to 30 (○); using 50 Torr air only from time 30 to 46 (○). Prior to making this plot the alumina was exposed to 10 Torr of propanol at 150° for 6 min.

Pyridine is often used as a diagnostic test for the presence of Lewis acid sites, since it preferentially adsorbs on the stronger sites. Some reactions were carried out for a time with pure alcohol vapor and then pyridine vapor was mixed with the added alcohol vapor. In the presence of pyridine the reaction rate was only about 25% as fast. When the reaction was continued without pyridine vapor added there was only a very slight increase in rate, and the reaction rate was still much less than prior to the pyridine addition. This demonstrates the importance of the Lewis acid sites. The kinetic plots of these experiments were similar to that given in Figure 7.

An air oxidation experiment was done in which propoxyl groups were initially bonded to the surface. After partial reaction pyridine vapor was added to the air and the reaction was allowed to continue. Figure 7 shows that the rate is only about 15% as fast as initially. This demonstrates that with air oxidation the Lewis acid sites are also important for producing the intermediate species required for the oxidation of the alkoxy group to the carboxyl group.

Discussion

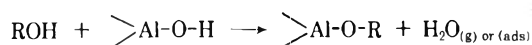
These reactions can be conveniently divided as follows: (1) alcohol bonding reaction to produce alkoxy groups, (2) oxidation of the bonded alkoxy groups to produce carboxyl groups, and (3) the initial fast reaction.

Alkoxy Group Formation. Greenler suggested that the alcohol reacts directly with a surface Al and eliminates hydrogen. In reviewing this work both Little and Hair consider a reaction between the alcohol and surface hydroxyl groups with the elimination of water more likely. This would be exactly analogous to the reactions between alcohols and silanol groups. This point might be resolved by observing spectral changes in the 3700-cm⁻¹ region and detecting water. Kagel's spectra are obscured in this region due to the large amounts of adsorbed water, but he did make a mass spectrometric examination of the gases immediately after the alkoxide formation from EtOD. The gases showed neither hydrogen nor deuterium and the presence of water was questionable, although adsorbed water was observed at room temperature on samples that had been heated to 320° in alcohol vapor. He proposed that the chemisorbed alkoxy groups were formed by adsorption of alcohol on surface oxide ions to form alkoxy and hydroxyl groups. There are difficulties of interpretation under these experimental conditions. In the tempera-

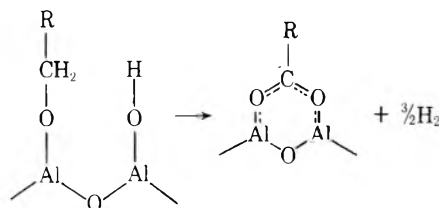
ture region near 300° the catalytic dehydroxylation takes place which produces alkenes and water. Where the temperature was limited to about 170°, where only the alkoxy bonding reaction takes place, the spectra and gas analyses were taken at room temperature. Alumina that has been heated readily adsorbs water on cooling¹⁰ and water might not appear in gas analyses. This adsorbed water (or H bonded OH groups produced by water adsorption) appears as the very broad, strong band from below 3000 to about 3800 cm⁻¹.

Deo and Dalla Lana's spectra show much less initially adsorbed water and the "free" OH bands are well resolved. They examined this region carefully and found that on exposure to alcohol up to 170° the band at 3758 cm⁻¹ disappeared completely and a broad band appeared near 3500 cm⁻¹. This agrees with the results obtained here. Deo and Dalla Lana correctly point out that the bands appearing in this region can be difficult to interpret, but considered this to be indirect evidence of H bonding with the surface. From frequency shifts in the 1060-1250-cm⁻¹ region, they concluded that the alcohol molecules are loosely H bonded through the O of the alcohol to the surface OH. They surmised that the alcohol adsorbs *via* the oxygen of the alcohol to a Al³⁺ site and forms alkoxyate by splitting off a hydrogen ion which is then free to migrate to oxide surface sites and form H₂.

The spectra taken here at reaction temperatures, as well as those taken at 150° followed by raising the temperature to 275°, showed that the alcohol reacts with the free OH groups to produce alkoxy groups stable at 300° *in vacuo*. At this temperature coverage of OH groups *via* H bonding would probably not be important, so that the disappearance of these free OH groups must be due to chemical reaction. The broad band which appears near 3500 cm⁻¹ could, then, be due to adsorbed water produced as a result of the reaction between the alcohol and a surface hydroxyl group. This experimental evidence points to the following reaction



Carboxyl Group Formation. Greenler assumed that the alcohol reacts directly with an oxide atom to form the carboxylate by splitting out three hydrogens. Kagel carried out the reaction at 320° until both propoxide and propionate were formed. He evacuated the system at 150°, cooled it to room temperature, closed the cell, and heated it to 410°. The propoxide disappeared and propionate formed. Gaseous hydrogen was the principal product. Similar results were obtained with butanol and propanol. On the basis of these experiments he concluded that the reaction is



The experiments carried out here demonstrated that the presence of gaseous alcohol is necessary for the alkoxy to carboxyl group reaction to take place. A reaction involving only alkoxy and hydroxyl groups cannot explain the mechanism of this part of the reaction. It was also ob-

served here that at 150°, the temperature at which Kagel evacuated his cell, some loosely bound alcohol is still present. Thus, in the absence of a leaky cell, this adsorbed alcohol desorbs on raising the temperature and readsorbs on the catalytically active sites, thereby leading to carboxylate formation.

Deo and Dalla Lana heated their alumina in propanol vapor for 1 hr, between 170° and 400°, after which only carboxyl groups were observed on the surface. Infrared and mass spectra of the gases formed above 200° showed propylene to be a major product and hydrogen was detected. The gases produced at 400° showed mainly propylene and water. Based on gas analyses, and drawing an analogy with the adsorption of formic acid on nickel oxide, they proposed a bridged carboxylate species similar to Kagel's. The precursor propoxide was considered to be chemisorbed on the electron-abstracting Lewis acid aluminum ion.

The organic product of this surface reaction, an alkene, is the same as that obtained in the catalytic dehydroxylation of alcohols over alumina. The reactive intermediate could be common to both. Generally^{2a} the alcohol is assumed to dissociate into carbonium ions and hydroxyl ions, but specific proof of an ion mechanism is difficult to provide. The catalytic dehydroxylation reactions are usually divided into two main categories: (1) an ether mechanism in which the elements of water are removed from two hydroxyl groups, and (2) an olefin mechanism in which the water molecule that is removed is made up of one OH group together with a hydrogen atom withdrawn from either a CH₂ or CH₃ group. For the alcohols studied here, the methanol proceeds in part *via* the ether mechanism, and the other alcohols completely *via* the olefin mechanism (*cf.* Table II).

Any mechanism proposed has to be consistent with the following experimental observations.

(1) Once the alkoxide is formed at a given temperature, it is perfectly stable in the absence of alcohol vapor or air. Carboxyl groups form only on exposure to these oxidizing agents.

(2) The oxidizing species must add (O).

(3) Two (H) are eliminated from the bonded alkoxy-late. Kagel and Dalla Lana showed that hydrogen is a product of the reaction.

(4) The other gaseous product is (a) an alkene with the same number of carbon atoms as the alcohol, or (b) with methanol an ether and alkanes.

(5) The reaction rate is dependent on the surface coverage of the reactive species (*cf.* Figure 4).

(6) The oxidizing species must be mobile on the surface, since a pseudo-zero-order reaction is observed. If this species were not mobile, the reaction would be first order or greater with respect to the surface sites.

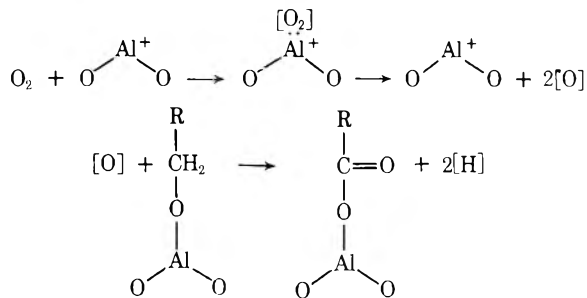
(7) The oxidizing species is produced principally by Lewis acid sites (the Al⁺ atoms). Poisoning with pyridine inhibits the reaction.

(8) With air as an oxidizing agent, the only possible intermediate species are oxygen molecules or atoms (the possibility of a charged species is not excluded). Poisoning with pyridine inhibits the reaction so that the oxygen molecules must interact with the Lewis acid sites and proceed *via* these sites.

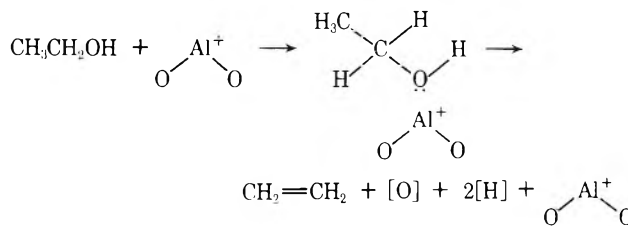
The general picture is that stable alkoxy groups are bonded to the surface. Gaseous alcohol adsorbs on the Lewis acid sites and produces an oxygen-containing species, which is sufficiently mobile to migrate to the

bonded alkoxy and react with this group. As a result of the reaction, two hydrogen atoms are eliminated from the alkoxy and a carboxyl group results.

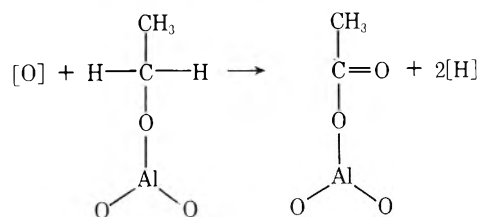
The evidence for carbonium ions is not conclusive and one could write the reaction using any of the following species: (1) carbonium plus hydroxyl ions, (2) alkyl plus hydroxyl radicals, or (3) alkyl radical plus oxygen and hydrogen atoms. Although the experiments carried out here cannot differentiate between these possibilities, the experiments with added air to oxidize the alkoxy group suggest that an oxygen atom is involved.



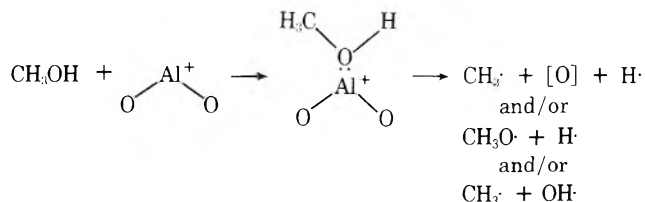
The reactions that take place with the alcohols as oxidants can also be written in a formal manner using oxygen atoms. For ethanol



and



While not proving that the oxygen atom is the reactive species, it is consistent with all the experimental observations, including the mixture of products obtained when methanol is used. For methanol one can write



Combinations of these radicals will lead to ether and alkanes, as is found with methanol. The break which occurs in the reaction curve for methanol could be due to a preponderance of one oxidizing species during the earlier part of the reaction and a different one during the latter part of the reaction.

The reaction scheme proposed is also consistent with the products obtained from the catalytic dehydroxylation of alcohols. When all the surface alkoxy groups have been oxidized to carboxyl groups, or concurrently with this reaction, the species produced by the Lewis acid site will

be an alkene, an oxygen atom, and two hydrogen atoms. On combination of the atoms the final products are an alkene and water.

Initial Fast Reaction. The initial fast reaction appears as a positive intercept on the kinetic plots (or reaction curves) and occurs during the period when the alkoxide builds up to its final constant concentration. At 150° the alcohol bonding reaction takes several minutes. During this time there is a small buildup in the intensities of the C=O bands. Loosely adsorbed alcohol is also oxidized, but on raising the temperature this desorbs and would not be important at higher temperatures. After the first few minutes, no further changes are observed in the intensities of the C=O and CH bands in the presence of alcohol vapor. It is probably that this is the initial fast reaction observed at higher temperatures.

Deo and Dalla Lana proposed that the high-frequency OH groups are catalytically active and that they are removed by NaOH doping, after which the aluminum ion sites assume the primary catalytic role. Under the condi-

tions used here, these high-frequency groups are removed during the initial part of the reaction. A possibility is that this could be the cause of the initial fast reaction. The equation for this reaction would be the same as that proposed by Kagel in his mechanism.

Another possibility is that the water produced by the bonding reaction adsorbs on the strongest Lewis acid sites and deactivates them. Adding water vapor is a common method of partially deactivating alumina supports in gas chromatography.^{11,12}

Acknowledgment. The authors gratefully acknowledge the gift of the Alon C alumina by the Cabot Co., Boston.

(11) C. G. Scott, *J. Inst. Petrol.*, **45**, 118 (1959).

(12) *Note:* An anonymous reviewer suggested the use of a high-temperature H₂ treatment to remove adsorbed O₂. The experiments reported here show that added oxygen does indeed result in formation of the carboxyl groups from the bonded alkoxy groups, but that when the system is evacuated at reaction temperatures no reaction takes place. However, the presence of initially adsorbed oxygen could be the cause of the initial fast reaction observed.

Absorption and Flash Photolysis Kinetic Spectroscopy Studies on Difluoro-, Chlorodifluoro-, Dichlorofluoro-, and Tetrafluorophosphine

Edward G. Skolnik,¹ Robert J. Salesi,² Charles R. Russ, and P. L. Goodfriend*³

Department of Chemistry, University of Maine, Orono, Maine 04473 (Received September 15, 1972)

Absorption studies and flash photolysis kinetic spectroscopy experiments were carried out on HPF₂, P₂F₄, ClPF₂, and FPCl₂. Absorption results were found to disagree with those of other investigators. Upper limits for two dissociation energies were obtained. No transient spectra that could be assigned to PF-containing fragments were observed.

Introduction

The original motivation for the investigations reported here was the desire to detect, identify, and study the electronic absorption spectra of HPF, ClPF, and other unobserved PF-containing radicals by means of flash photolysis kinetic spectroscopy. Although this objective was not realized, information about the absorption spectra and photochemistry of HPF₂, ClPF₂, FPCl₂, and P₂F₄ was obtained. Of particular interest is the fact that results were obtained which disagree strongly with those of other investigators.

Experimental Section

A concentric photolysis flash sample cell arrangement was used in these studies. The concentric arrangement and the delay system are of the same form as previously reported as part of another apparatus.⁴ Delay times of from 0 to 300 μsec were available, and photolysis flashes of energy between 1000 and 2000 J were used. Spectral plates were taken using a Jarrell-Ash F/6.3 75-000 plane grating spectrograph with a reciprocal dispersion of 11

Å/mm. Delay times were monitored using a photodiode and oscilloscope. Sample cells were 65 cm in length except in the P₂F₄ studies where the length was 55 cm.

The wavelengths available for photolysis were limited by the quality of the quartz used to the region above 1900 Å.

Wavelengths (in air) were measured on tracings from a Jarrell-Ash 23-100 recording microphotometer using an iron arc calibration spectrum. Sharp features could be measured to within 1 Å.

Difluoroiodophosphine (PF₂I) was prepared by the reaction of dimethylaminodifluorophosphine with hydrogen iodide as described by Rudolph, Morse, and Parry.⁵ Commercial HI was used. The dimethylaminodifluorophos-

(1) Part of work done by E. G. Skolnik in partial fulfillment of the requirements of the Ph.D. degree at the University of Maine.

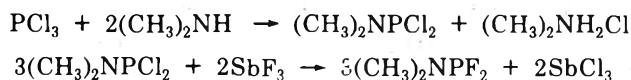
(2) Part of work done by R. J. Salesi in partial fulfillment of the requirements of the M.S. degree at the University of Maine.

(3) To whom correspondence should be addressed.

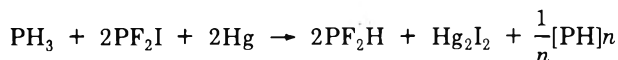
(4) P. L. Goodfriend and H. P. Woods, *Rev. Sci. Instrum.*, **36**, 10 (1965).

(5) R. W. Rudolph, J. G. Morse, and R. W. Parry, *Inorg. Chem.*, **5**, 1464 (1966).

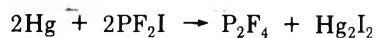
phine was prepared using the following sequence of reactions, the first due to Schmutzler⁶ and the second to Burg and Slota.⁷



Difluorophosphine (HPF₂) was prepared by treating PF₂I with phosphine in the presence of mercury⁸



P₂F₄ was prepared by the method given by Rudolph, Taylor, and Parry.⁹



Purification of the above compounds was carried out by trap to trap distillation in the vacuum line used in their synthesis using appropriate slush baths.

PFCl₂ and PF₂Cl were prepared together by the fluorination of PCl₃ with SbF₃ in the presence of SbCl₅ and then separated by fractional distillation as described by Holmes and Gallagher.¹⁰

Sample identity and purity were monitored by means of infrared spectra obtained using a Perkin-Elmer 457 grating infrared spectrophotometer, except in the case of the HPF₂ studies where an Infracord was used.

Results

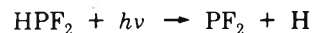
Studies on HPF₂. The only literature reference to the electronic absorption spectrum of HPF₂ is that of Burdett, Hodges, Dunning, and Current,¹¹ who state merely that, "The electronic transitions of PF₂H are centered at 260 mμ and at 218 mμ." A copy of the ultraviolet spectrum of a sample of DPF₂ was supplied to us by Current and showed a very intense absorption near 260 nm. The instrument used by Current, *et al.*, was a Cary Model 11 ultraviolet-visible spectrophotometer.

In our spectrographic studies, it was not found possible to observe this 260-nm absorption in samples of HPF₂. Instead, the absorption of HPF₂ was observed to be continuous, starting at about 3150 Å and increasing in intensity until complete absorption occurred at 2335 Å. The onset of absorption on the long wavelength side did not change in wavelength as the pressure was increased from 20 to 75 Torr. Since sample decomposition is a persistent problem in this system, leading to the formation of the yellow "PF polymer," the absorption was also studied using a Perkin-Elmer 202 visible-uv spectrophotometer so that the infrared spectrum could be observed immediately afterward to confirm the presence of HPF₂ in the sample. Again, the spectrum was without a relative absorption maximum near 260 nm. The chief impurities found in samples of HPF₂ were PH₃ and PF₃. The PF₃ absorption lies entirely below 2000 Å¹² and phosphine absorption begins at almost 2300 Å (at high pressure).¹³ No evidence of molecular fluorine was found in that no maximum of absorption near 2845 Å as found for fluorine by Steunenberg and Vogel¹⁴ was observed. Consequently, the absorption observed is attributed to HPF₂. The missing 2600-Å absorption will be discussed when the results for P₂F₄ are examined.

Flash photolysis kinetic spectroscopy experiments were carried out at delay times between photolysis and source flashes of approximately 0, 80, and 200 μsec. The spectrum in each case was scanned from 2000 to 7000 Å. No features which may be due to transient molecular species

have been observed. If the assignment of the PF₂ absorption spectrum by Cavell, Dobbie, and Tyerman¹⁵ is correct (2200–2300 Å), the spectrum of PF₂, if it occurs in our studies, would be obscured by the sample absorption.

Although failure to observe a spectrum of a radical such as HPF may stem from causes other than the absence of the species, there is reason to believe that the primary process for the photolysis of HPF₂ is as follows



The matrix isolation photolysis studies of Burdett, Hodges, Dunning, and Current¹¹ showed PF₂ as the product of the photolysis and not HPF. From the absorption studies reported here, the onset of continuous absorption is at about 3150 Å, corresponding to about 91 kcal/mol as the upper limit for the dissociation energy of HPF₂ in the photochemical process yielding the continuum. All known PF bond energies¹⁶ are well in excess of 100 kcal/mol. It is clear, therefore, that at least at the onset of continuous absorption the process cannot be dissociation into HPF and an F atom. It can only be the removal of an H atom. Thus, the evidence points to very different behavior for HPF₂ when contrasted with HNF₂ as shown in the flash photolysis kinetic spectroscopy studies of Goodfriend and Woods¹⁷ and of Woodman.¹⁸ It may be that photolysis radiation of wavelength shorter than that accessible to the quartz sample cell could be effective in producing HPF radicals. Better still, a flash discharge apparatus¹⁹ would offer a chance of observing this species.

It is true that Burdett, Hodges, Dunning, and Current¹¹ assert that wavelengths greater than 2500 Å did not decompose HPF₂ in the matrix, but this may be due to the weakness of the continuous absorption in this region.

In this paper absorptions are assigned as continuous if no evidence of structure was observed. It is, of course, conceivable for structure to be present beyond the resolution of the spectrograph used. The presence of vibrational structure would probably be noticed in these spectra unless made very diffuse by predissociation. Predissociation also leads to decomposition, and this situation would not alter the arguments for assigning upper limits to dissociation energies.

An interesting phenomenon was noticed. The sample cell extended beyond the region of the photolyzing flash on both ends, but the buildup of yellow PF polymer was concentrated in the region exposed to the flash.

P₂F₄ Studies. At intermediate pressures, we find the absorption spectrum of P₂F₄ to consist of three regions of

- (6) R. Schmutzler, *Inorg. Chem.*, **3**, 415 (1964).
- (7) A. B. Burg and P. J. Slota, *J. Amer. Chem. Soc.*, **80**, 1107 (1958).
- (8) R. W. Rudolph and H. W. Schiller, *J. Amer. Chem. Soc.*, **90**, 3581 (1968).
- (9) R. W. Rudolph, R. C. Taylor, and R. W. Parry, *J. Amer. Chem. Soc.*, **88**, 3729 (1966).
- (10) R. Holmes and W. P. Gallagher, *Inorg. Chem.*, **2**, 433 (1963).
- (11) J. K. Burdett, L. Hodges, V. Dunning, and J. H. Current, *J. Phys. Chem.*, **74**, 4053 (1970).
- (12) C. M. Humphries, A. D. Walsh, and P. A. Warsop, *Disc. Faraday Soc.*, **35**, 148 (1963).
- (13) G. H. Cheesman and H. J. Emeleus, *J. Chem. Soc.*, 2847 (1932).
- (14) R. K. Steunenberg and R. C. Vogel, *J. Amer. Chem. Soc.*, **78**, 901 (1956).
- (15) R. G. Cavell, R. C. Dobbie, and W. J. R. Tyerman, *Can. J. Chem.*, **45**, 2849 (1967).
- (16) V. I. Vedeneyev, L. V. Gurvich, V. N. Koudrat'Yev, V. A. Medvedev, and Y. L. Frankevich, "Bond Energies Ionization Potentials and Electron Affinities," St. Martin's Press, New York, N. Y., 1966.
- (17) P. L. Goodfriend and H. P. Woods, *J. Mol. Spectrosc.*, **13**, 63 (1964).
- (18) C. M. Woodman, *J. Mol. Spectrosc.*, **33**, 311 (1970).
- (19) G. Herzberg and A. Lagerqvist, *Can. J. Phys.*, **46**, 2363 (1968).

continuous absorption which merge together as the pressure is increased. At high pressures the onset of absorption on the long wavelength side is at 3580 Å. 3580 Å corresponds to 80 kcal/mol. This is again too small to be due to the removal of a fluorine atom. It is, therefore, an upper limit to the dissociation energy of P_2F_4 into two PF_2 radicals. The intermediate absorption region lies between 2800 and 2425 Å, and the absorption region on the violet end of the spectrum begins near 2350 Å and extends beyond the violet end of the range of the apparatus. The highest sample pressure used in the P_2F_4 studies was 100 Torr.

At moderate pressures of P_2F_4 , photochemical activity is manifest by the long wavelength edge of absorption creeping toward the violet with subsequent photolysis flashes. At P_2F_4 pressures sufficiently low to make the region clearly observable, flash photolysis produces a stable substance that absorbs strongly and continuously from 2690 to 2482 Å with a maximum at 2595 Å. The same absorption has also been observed in several "fresh" samples of P_2F_4 . This absorption corresponds in every way with the missing 2600-Å absorption attributed to HPF_2 by Burdett, Hodges, Dunning, and Current.

The only previously reported description of an ultraviolet spectrum for P_2F_4 has been given by Solan.²⁰ Solan describes the ultraviolet absorption spectrum of gaseous P_2F_4 in terms of "three major bands above 220 μ m, one of which is very strong and all of which are broad and partially overlapping." The strongest of the absorptions described by Solan corresponds in every way with the 2600-Å absorption discussed above in connection with the flash photolysis experiments on P_2F_4 . In order to make sure that the 2600-Å absorption is not due to P_2F_4 , ultraviolet spectra were taken on samples of P_2F_4 on the Perkin-Elmer 202 visible-uv spectrophotometer followed immediately by taking infrared spectra. The strong 260-nm absorption was not observed, but the infrared peaks of P_2F_4 were present. Oscillator strengths of strong ultraviolet transitions are so much greater than those of infrared transitions that the observation of the infrared spectrum would imply the observation of the uv absorption.

The nondescript nature of continuous spectra coupled with the difficulties encountered in working with these reactive and unstable substances makes the identity of the carrier of the 2600-Å absorption a mystery. It can be concluded, however, that it is neither HPF_2 nor P_2F_4 . The results presented here indicate that it is a photochemical or photothermal product of P_2F_4 that can also form in other ways, hence explaining its presence in samples of HPF_2 and P_2F_4 .

It does not seem to be a material deposited permanently on the windows of the absorption cell in that the 2600-Å absorption always disappeared on evacuating the cell. Attempts to characterize this substance were unsuccessful, because it was unstable and behaved in a highly erratic manner. It is conceivable that it is an isomer of P_2F_4 .

A number of enigmatic transient absorptions were seen in the flash photolysis kinetic spectroscopy experiments. On one plate at a delay time of 320 μ sec bands were observed at 2564, 2575, 2592, 2602, 2613, 2629, and 2646 Å of which the strongest was the band at 2575 Å which was double headed and red degraded. The absorption at 2575 Å could be due to the CS molecule. The 2575-Å band, but not the others, was seen on another P_2F_4 plate. Other plates showed transients at a delay time of 10 μ sec at 5127 Å on one plate and 5356 Å on another. Since all of these features are not uniformly reproducible, no attempt will be made here to attribute them to PF-containing molecular fragments.

Studies of $CIPF_2$ and $FPCl_2$. In the spectral region accessible to the spectrograph no obvious absorption due to $CIPF_2$, either discrete or continuous, was observed. Absorption was observed, however, in the case of $FPCl_2$. A weak discrete band was found near 2631 Å and a stronger band at 2545 Å which may be shaded to the red. Intensity increases again near 2540 Å, leveling off to an apparently continuous absorption at about 2537 Å. The highest pressure of $FPCl_2$ used in these absorption measurements was 196 mm.

Flash photolysis kinetic spectroscopy experiments on both $CIPF_2$ and $FPCl_2$ were run at a multitude of delay times between 0 and 220 μ sec and throughout the wavelength region accessible to the apparatus. In the case of $FPCl_2$ no transient features were observed. In the case of $CIPF_2$ a transient at 2575 Å was observed which started at 0 μ sec delay and persisted for delays in excess of 220 μ sec. It was, in spite of its long life, a true transient and not a stable substance. Its wavelength and behavior agree with those of the CS molecule. This did not seem unlikely since SO_2 was observed as a frequent impurity in both infrared spectra and ultraviolet spectra (band system in the region 3200–2700 Å). No transients that could be ascribed to the $CIPF$ radical were observed.

Acknowledgment. We are grateful to the National Science Foundation for support under Grant No. GP-12259. We wish to thank Joseph Byrne for independent preparations of samples of HPF_2 and P_2F_4 as an additional check of our conclusions.

(20) D. Solan, Ph.D. Thesis, University of California, Berkeley, 1969.

Disulfide Vibrational Spectra in the Sulfur-Sulfur and Carbon-Sulfur Stretching Region¹

Ernest J. Bastian, Jr., and R. Bruce Martin*

Chemistry Department, University of Virginia, Charlottesville, Virginia 22901 (Received August 25, 1972)

Publication costs assisted by the National Science Foundation

The strong Raman S-S stretching wave number from 498 to 511 cm^{-1} in a variety of disulfides is independent of the dihedral CSSC angle from 20 to near 90°. No correlation exists between the Raman intensity ratio for C-S and S-S stretching bands and the CSS angle. From a proton magnetic resonance analysis of relative rotamer populations in isobutyl disulfide, the molar intensity of the C-S stretching band at 707 cm^{-1} due to a rotamer with anti sulfur and methyl groups is twice that at 665 cm^{-1} due to the rotamer with anti sulfur and hydrogen atoms. The inverse conclusion applies to the intensities in isobutyl chloride where Cl replaces S. Conformational rigidity in *trans*-2,3-dithiadecalin permits assignment of an S-S stretching band at 506 cm^{-1} and a C-S stretching band at 719 cm^{-1} to specific conformers. Identification of C-S wave numbers and rotamers similar to the above is applicable to other disulfides. Unfortunately, cystine and derivatives, known on other grounds to possess significant amounts of each of three ethanic rotamers in solution, exhibit only one C-S stretching Raman band. This result limits the utility of Raman spectra for determination of conformation in cystine and derivatives.

Advantages of Raman spectroscopy for procurement of vibrational spectra in aqueous solutions have been augmented by laser excitation sources, making practical examination of large molecules such as proteins. Despite the overlapping of many bands even in small proteins, the spectral region from 500 to 730 cm^{-1} is relatively clear and includes the S-S and C-S stretching wave numbers. From comparisons among a few disulfide containing compounds it has been suggested that there is a correlation between the intensity ratio of the C-S and S-S stretching wave numbers and the CSS angle. This correlation has been applied to the proteins lysozyme and ribonuclease, each of which contain four disulfide cross links.² In this paper we examine this proposed correlation in more detail.

L-Cystine and derivatives are substituted ethanes, and three staggered rotamers each with distinct energies occur about the C-C bond. Relative populations of these three rotamers have been determined for each of a wide range of L-cystine derivatives in solution by analysis of vicinal coupling constants in proton magnetic resonance spectroscopy and circular dichroism.³ Each one of the three staggered rotamers should in principle exhibit a characteristic C-S stretching frequency, the intensity of which reflects the population of that rotamer. One of the purposes of this paper is to investigate the potentiality of Raman spectroscopy as an additional tool for evaluating rotamer populations of ethanic disulfides in solution.

Experimental Section

The methylated, ester, and cyclic disulfides were synthesized³ by Dr. J. P. Casey, to whom we are grateful. Malformin A was kindly supplied by Professor R. W. Curtis. The other compounds were obtained from commercial sources.

Raman spectra were obtained on the Spex Ramalog Model 1 Raman spectrometer housed in this department.⁴ Usually 514.5-nm laser excitation was employed; no differences were observed with occasional samples run at

488.0 nm. Crystalline, neat liquid, and solution (1-2 M) samples were sealed in standard capillary tubes. Calibration was accomplished by comparison of repeated scans of standard argon fluorescence lines with prominent peaks in the sample spectrum. Resolution was 2-4 cm^{-1} at the exciting line. Strong narrow bands were reproducible to $\pm 1 \text{ cm}^{-1}$. Our Raman results are similar to those pictured² for solids L-cystine and its dihydrohalide salts, but are of better quality with little or no rise in the base line down to 100 cm^{-1} . Generally the Raman spectra of the solids are of higher quality than aqueous solutions, accounting for the greater number of reported lines for the solids. Unfortunately we were unable to obtain a good quality solution spectrum of tetramethylcystine.

Complementary infrared spectra were measured routinely on a Perkin-Elmer 337 grating infrared spectrophotometer. Crystalline samples were run as pressed KBr disks, and neat liquids were placed between two KBr disks. A standard polystyrene film was employed for calibration, and the recorded values are reproducible to $\pm 3 \text{ cm}^{-1}$.

Proton magnetic resonance spectra of the neat liquid isobutyl derivatives were measured on a Varian HA-100 spectrometer operating in HA mode with an internal TMS lock. Interpretation of the spectra by a first-order analysis is straightforward.

Results

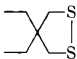

Table I lists a small portion of the Raman and infrared spectra obtained for a wide variety of disulfides. The spectral range quoted from about 480 to about 780 cm^{-1} is

- (1) This research was supported by grants from the National Science Foundation, No. GB-29328 and GP-18251, toward purchase of the Raman spectrometer.
- (2) R. C. Lord and N. T. Yu, *J. Mol. Biol.*, **50**, 509 (1970); **51**, 203 (1970).
- (3) J. P. Casey and R. B. Martin, *J. Amer. Chem. Soc.*, **94**, 6141 (1972).
- (4) D. A. Hatzenbuehler and L. Andrews, *J. Chem. Phys.*, **56**, 3398 (1972).

TABLE I: Vibrational Spectra of Disulfides

	Raman				Infrared	
	Acid solution ^a		Solid ^b		Solid ^b	
	cm ⁻¹	Intensity ^c	cm ⁻¹	Intensity ^c	cm ⁻¹	Intensity ^d
L-Cystine	508	20	498	20	540	s
			541		615	m
			614	1	675	m
	667	14	677	2	777	m
	774	2	784	2		
L-Cystine · 2HCl	Same as above		479	17	475	w
			510	sh	507	m
			518	20		
			587	3	585	w
			664	56	662	w
			751	18	753	m
L-Cystine · 2HBr	Same as above		463	8	458	w
			499	6	503	m
			518	20		
			590	2	588	w
			660	43	658	w
			744	16	741	w
<i>meso</i> -Cystine	506	20	506	s	768	s
					528	m
					558	s
			590	w	590	w
			617	w	618	w
	668	12	660	w	660	w
			683	w	683	w
			785	w	785	m
			482	23	470	w
	L-Cystine dimethyl ester · 2HCl ^e	509	20	508	sh	510
522				20	560	m
					610	m
668		16	669	60	665	m
			755	23	780	s
L-Cystinediamide · 2HCl ^e	508	20			500	w
					580	s
	638	5				
	663	5	659		660	m
					705	w
Glutathione, oxidized ^f	738	2			750	w
	510	20	509	s		
	526	8			531	s
	662	8	659	w	665	s
Malformin A					738	m
					762	m
			487	20	480	w
					496	w
					585	m
			633	6	625	m
					660	s
					707	w
<i>N,N'</i> -Dimethyl-L-cystine			496	20	765	w
	510	20	508	2	504	m
					532	s
			621		615	m
	670	16	684	1	678	m
<i>N,N,N',N'</i> -Tetramethyl-L-cystine	759	3	771	1	767	m
			479	20	474	s
			518	20		
					538	s
			708	52	698	s
					737	s
		776	33	764	m	

TABLE I (Continued)

	Raman				Infrared	
	Acid solution ^a		Solid ^b		Solid ^b	
	cm ⁻¹	Intensity ^c	cm ⁻¹	Intensity ^c	cm ⁻¹	Intensity ^d
<i>N,N,N',N',N'</i> -Hexamethyl-L-cystine	510	20				
	549	13			545	m
L-Homocystine	745	20			680	m
	511	20	510	20	720	m
	640	8	543	5	543	s
L-Homocystine diethyl ester · 2HCl			630	10	626	w
					651	w
			683	2	680	w
			713	4		
			735	2	745	m
					752	m
<i>trans</i> -2,3-Dithiadecalin	509	20	504	20	512	w
	639	9			655	w
	715	5	713	2	714	w
			734	1	734	m
			506	20	512	w
					552	w
			719	5	716	s
			724	sh		
			747	2	746	m
			492	12		
			509	20	508	w
			549	3		
			711	13	654	m
			736	7	734	s
			488	5		
			509	20		
			576	1	576 ^e	w
					649	m
			722	12	720	m
D-Penicillamine disulfide			740	3	735	m
			509	8	518	s
	546	20	556	20	552	s
	579	12			566	m
	650	2	654	4	650	w
Diisobutyl disulfide			680	2	690	w
			748	3	745	m
			487	3		
			511	20		
			525	12	527	w
			665	3	669	w
			707	34	708	m
Isobutyl chloride ^h			744	9	745	m
			523	5		
			689	28		
			730	34		
			805	7		
		819	23			

^a 1–2 M HCl unless otherwise indicated. ^b Solid or neat liquid. ^c Scaled to predominant peak near 510 cm⁻¹ as 20. A blank signifies peak is less than 3% of intensity of 510 cm⁻¹ peak: sh, shoulder. ^d s, strong; m, medium; w, weak. ^e Hydrochloride salt was dissolved in water for acid solution spectrum. ^f Water solution. ^g From ref 8. ^h Raman intensities scaled to 16 for peak at 430 cm⁻¹ which is the value for similar peak in isobutyl disulfide.

intended to include regions commonly assigned to S–S and C–S stretching wave numbers. The former assignments occur from 500 to 530 cm⁻¹ and the latter from 620 to 730 cm⁻¹ in primary aliphatic disulfides.^{5,6} Thus the highest wave numbers quoted in Table I are to be attributed to other vibrations such as a CH₂ rock. For penicillamine disulfide the S–S stretching wave number is increased to near 550 cm⁻¹ and the predominant C–S

stretching wave number in solution reduced to 579 cm⁻¹, typical of a tertiary disulfide.^{5,7} For this compound alone the infrared absorption is strong in the S–S stretching region.

- (5) N. Sheppard, *Trans. Faraday Soc.*, **46**, 429 (1950).
 (6) D. W. Scott and J. P. McCullough, *J. Amer. Chem. Soc.*, **80**, 3554 (1958), and other references of this paper.
 (7) J. H. S. Green, D. J. Harrison, W. Kynaston, and D. W. Scott, *Spectrochim. Acta, Part A*, **25**, 1313 (1969).

TABLE II: Proton Magnetic Resonance Parameters of Isobutyl Derivatives

	Disulfide	Chloride
Chemical Shifts ^a		
CH ₃	98.1	99.0
CH	192.9	193.4
CH ₂	254.7	332.7
Coupling Constants, <i>J</i>		
CH ₂ -CH	6.9	6.2
CH ₃ -CH	6.5	6.6

^a In Hz downfield from internal TMS at 100 MHz and 31°.

The strong Raman bands assigned to S-S stretch usually possess weak or even absent infrared counterparts. This weakness of the S-S stretching vibration in infrared spectra has led to a history of its misassignments to other frequencies.⁸ The S-H stretching vibration is also strong in Raman spectra and notably weak in the infrared. Even the C-S stretching vibration is often more apparent in Raman spectra. If proper identification of stretching frequencies involving sulfur in sulfides and disulfides is to be made, it seems essential to run Raman spectra.

Vicinal coupling constants and chemical shifts derived from proton magnetic resonance spectra of isobutyl disulfide and chloride are presented in Table II. Relative rotamer populations about the CH₂-CH bond of the isobutyl group considered as a substituted ethane may be estimated from the vicinal coupling constant. Of the three staggered ethanic rotamers the two identical ones with anti methyl and sulfur or chlorine atoms (C₁) are designated *g* and the hindered rotamer with a gauche relationship between both methyl groups and a sulfur or chlorine atom (C_s) is termed *h*. By utilizing the experimental value of the vicinal coupling constant for the CH₂-CH bond and the values of *J_G* = 2.5 and *J_T* = 13 Hz, mole fractions of the rotamers may be estimated by standard methods.³ For isobutyl chloride calculation yields mole fractions of 0.70 for rotamers *g* and 0.30 for rotamer *h*, near the expected statistical values. For isobutyl disulfide the mole fractions are 0.84 for rotamers *g* and 0.16 for rotamer *h*. Thus rotamer *h* is only half as populated in the disulfide.

Discussion

The CSSC dihedral angle varies from a low near 26° for the five-membered ring disulfides of Table I, through about 60° for the transdecalin, to near 90° for most of the alicyclic compounds.⁹ Despite this wide variation in dihedral angle, a strong Raman band, identifiable as a S-S stretching frequency, occurs uncorrelated with dihedral angle in the range 496-511 cm⁻¹ in almost all cases of Table I. Exceptions to this range are the two solids tetramethylcystine and malformin A. The disulfide bond in the cystine-containing cyclopentapeptide malformin A is under strain.¹⁰ We conclude that the frequency of the S-S stretching vibration is not indicative of the disulfide dihedral angle.

Of the three rotamers staggered about the C-SS' bond of primary disulfides, one possess a carbon atom anti to the second sulfur, (S') and two possess anti hydrogen atoms. The gauche rotamer where a carbon atom appears in the same direction as the primary carbon on the second sulfur (with about 90° disulfide dihedral angle) has been considered of too high energy to occur with small disul-

fides¹¹ and is sterically impossible for cystine. Thus we anticipate only two rotamers about each XC-SS' bond and designate them *G* for the favored gauche rotamer where X = H is anti to S' and *T* for the anti rotamer where X = C appears anti to S'. Rotamer *G* is favored over rotamer *T* in diethyl disulfide.¹¹

It has recently been suggested that the S-S stretching frequency depends upon whether a hydrogen or carbon atom is anti to the second sulfur atom about the two C-S bonds considered together in XC-SS-CY.¹² For the three possible substitutions of X and Y by hydrogen and carbon, the following representative values were suggested: X = Y = H, 510 cm⁻¹; X = H and Y = C, 525 cm⁻¹; and X = Y = C, 540 cm⁻¹. In the conformationally rigid *trans*-2,3-dithiadecalin, hydrogens are anti to both sulfur atoms and the observed value of 506 cm⁻¹ reported in Table I is consistent with the recent proposal. The interpretations that follow retain this suggestion so that for pairs of C-S rotamers about the disulfide bond we identify *G-G* with about 510 cm⁻¹; *G-T*, 525 cm⁻¹; and *T-T*, 540 cm⁻¹.

Absence of band splitting and presence of only the low wave number vibration in the S-S stretching region for most cases in Table I suggest that usually rotation about the C-S band is hindered and the favored gauche rotational isomer predominates. In these cases the intensity of the C-S stretching band is about half that of the S-S stretching band over a wide range of dihedral and CSS angles in alicyclic and cyclic disulfides of Table I. No correlation is evident between the intensity ratio of the C-S and S-S stretching bands and the CSS angle.

Three ethanic rotamers occur staggered about the carbon-carbon ZC-CS bond, where Z represents the group anti to sulfur. Consistent with our previous formulation, we designate rotamer *h* for Z = H, rotamer *g* for Z = CH₃ or NH₃⁺, and rotamer *t* for Z as any group heavier than NH₃⁺ such as -COOH or a substituted methyl group.

Only one gauche rotamer about the C-S bond exists in crystalline L-cystine¹³ and the dihydrohalide salts of L-cystine.¹⁴ The crystal structures determined for the first three compounds of Table I indicate that in all three cases the dihedral angle about the CC-SS bond is in the direction of the favored gauche rotamer of disulfides but with an angle of 85 ± 4° rather than 60°.¹⁵ Thus no atom is in a position strictly anti to sulfur in these crystals. The large angle may account for deviations from the 510 cm⁻¹ expected for this gauche rotamer,¹² but it does not explain the different values of 498 and 518 cm⁻¹ that are observed. It is possible that the crystalline forms examined by X-ray diffraction and Raman spectra are not the same or that factors in the ionic crystals render the analysis inapplicable. Solid L-cystine is the only compound in Table I with an intensity ratio near 0.1 for the C-S to S-S stretching bands. All three crystals also possess solely rotamer *h* about the C-CS bond with three adjacent gauche

(8) For example, L. Schotte, *Ark. Kemi*, **9**, 309 (1956).

(9) R. Rahman, S. Safe, and A. Taylor, *Quart. Rev., Chem. Soc.*, **24**, 208 (1970).

(10) K. Anzai and R. W. Curtis, *Phytochemistry*, **4**, 263 (1965).

(11) D. W. Scott and M. Z. El-Sabban, *J. Mol. Spectrosc.*, **31**, 362 (1969).

(12) H. Sugeta, A. Go, and T. Miyazawa, *Chem. Lett., Chem. Soc. Jap.*, **83** (1972).

(13) B. M. Oughton and P. M. Harrison, *Acta Crystallogr.*, **12**, 396 (1959). Recalculation indicates that the disulfide dihedral angle of L-cystine is but 74° and the CSS angle 104.5°; F. S. Richardson and John Webb, private communication.

(14) L. K. Steinrauf, J. Peterson, and L. H. Jensen, *J. Amer. Chem. Soc.*, **80**, 3835 (1958); J. Peterson, L. K. Steinrauf, and L. H. Jensen, *Acta Crystallogr.*, **13**, 104 (1960).

(15) F. S. Richardson and J. Webb, private communication.

hydrogens. Taken together the Raman results for the first three solids of Table I suggest a $\nu(\text{C-S})$ from 660 to 677 cm^{-1} that may be assigned to the G h conformation.

The fourth compound in Table I with a prescribed structure is the conformationally rigid *trans*-2,3-dithiadecalin which can exist only as a G t conformer. Only one band, that at 719 cm^{-1} , appears in the $\nu(\text{C-S})$ region. Thus we attribute bands near 719 cm^{-1} to $\nu(\text{C-S})$ characteristic of the G t conformer. In the dithiadecalin this $\nu(\text{C-S})$ band appears relatively weak in Raman spectra and strong in infrared.

One of the goals of this investigation is to test the applicability of the C-S stretching wave numbers for the determination of relative rotamer populations about the C-C bond in substituted ethanic disulfides. The principles involved have been worked out for ethanic chlorides where C-Cl stretching frequencies occur from 679 to 686 cm^{-1} when a primary chlorine atom is anti to a hydrogen on a branched β carbon atom (h) and from 723 to 730 cm^{-1} when a chlorine atom is anti to a carbon atom (g).¹⁶ On this basis the band at 689 cm^{-1} in isobutyl chloride is assigned to rotamer h and that at 730 cm^{-1} to rotamer g. Combination of the results of the pmr population analysis with the intensities of the two Raman bands listed in Table I indicates that for isobutyl chloride the molar intensity of the band due to rotamer h is almost twice that due to rotamer g.

Assignments of $\nu(\text{C-S})$ bands in diisobutyl disulfide are achieved in two ways leading to identical conclusions. First the difference of 41 cm^{-1} between $\nu(\text{C-Cl})$ for the two kinds of rotamers in isobutyl chloride with the similar difference of 42 cm^{-1} for diisobutyl disulfide suggests that the strong Raman band at 707 cm^{-1} may be attributed to rotamers g and the weaker band at 665 cm^{-1} to rotamer h. These assignments are also consistent with those made for isobutylmercaptan where a Raman band at 711 cm^{-1} is assigned to rotamers g and the second at 671 cm^{-1} to rotamer h.¹⁷ Occurrence of two $\nu(\text{S-S})$ Raman bands at 511 and 525 cm^{-1} in diisobutyl disulfide suggests the presence of both GG and GT conformation about the disulfide bond so that four $\nu(\text{C-S})$ bands might be expected corresponding to G h, G g, T h, and T g. The presence of only two sharp Raman bands at less than 730 cm^{-1} in the $\nu(\text{C-S})$ region suggests that G and T isomers do not lead to separate Raman $\nu(\text{C-S})$ bands at less than 730 cm^{-1} . This conclusion appears to be a general one for compounds that are branched at the carbon β to sulfur. Combination of the pmr population analysis with the Raman assignments for diisobutyl disulfide indicates that the molar intensity of $\nu(\text{C-S})$ in each rotamer g is more than twice that of rotamer h. This conclusion is the inverse of that derived for isobutyl chloride.

Compounds that are not branched at the carbon β to sulfur possess lower $\nu(\text{C-S})$ values for rotamer h than do branched compounds. In chlorine compounds $\nu(\text{C-Cl})$ appears about 30 cm^{-1} lower for the unbranched compounds.¹⁶ Thus bands at 642 and 668 cm^{-1} in diethyl disulfide are assigned to conformers G h and T h, respectively. No band appears near 640 cm^{-1} in β -branched disulfides where the G h wave number appears at 665 cm^{-1} in diisobutyl disulfide. Bands appearing at 640 cm^{-1} in

homocystine and its diester (Table I) are assigned to conformer G h. Since only one $\nu(\text{S-S})$ appears in solution, the band near 714 cm^{-1} is attributed to conformer G t. This assignment agrees with that presented above for the dithiadecalin.

Five-membered rings undergo rapid pseudorotation and are sterically prohibited from assuming normal staggered rotamers about C-C bonds. Nevertheless the two five-membered ring disulfides of Table I exhibit $\nu(\text{S-S})$ at 509 cm^{-1} consistent with a GG conformation for a puckered ring and $\nu(\text{C-S})$ at 711 and 722 cm^{-1} , within the range expected for rotamer G t as in the dithiadecalin. Bands at 634 and 684 cm^{-1} in the five-membered ring thioctic acid have been attributed to symmetric and antisymmetric $\nu(\text{C-S})$.² However symmetric and antisymmetric $\nu(\text{C-S})$ are closely spaced and not easily resolved in Raman spectra.¹⁸ Appealing alternative $\nu(\text{C-S})$ assignments are possible for the thioctic acid spectrum. The band at 634 cm^{-1} may be assigned to both the puckered rotamers G h of the homocystine-like portion of the ring and the rotamer with two anti hydrogens with the secondary C-S bond. The higher wave number band at 684 cm^{-1} is reasonably assigned to the rotamer with anti hydrogen and anti carbon with the secondary C-S bond.

In applying the above conclusions to cystine in solution, we note first the presence of only one $\nu(\text{S-S})$ attributable to conformer G-G so that evidently conformers G-T and T-T occur only to a negligible extent, and the G rotamer about the C-S bond predominates. The near identity of the solution Raman spectra for L- and meso-cystine suggests that the two halves of the disulfide may be considered individually. The result also supports the view that no attractive intramolecular interactions occur in either of these molecules in aqueous solutions.³ Since calculations from pmr results yield for L-cystine mole fractions of about 0.50, 0.18, and 0.32 for rotamers t, g, and h, respectively,³ we might expect to observe three Raman $\nu(\text{C-S})$ bands attributable to conformers G t, G g, and G h. In fact only one band appears at 667 cm^{-1} . This position is that expected for the G h conformer and bands for the other two conformers are anticipated at greater than 700 cm^{-1} . The band at 667 cm^{-1} is about 50% broader than $\nu(\text{S-S})$ in cystine, while $\nu(\text{C-S})$ and $\nu(\text{S-S})$ in diisobutyl disulfide are of equal width. The 667- cm^{-1} band of cystine undoubtedly contains contributions from at least two rotamers and still retains intensity at greater than 700 cm^{-1} . However, the shoulder on the other side of the peak at 625 cm^{-1} is stronger, but still weak. Thus it appears likely that $\nu(\text{C-S})$ for rotamers t and g appear under the broad peak at 667 cm^{-1} or are of low intensity. In any case the lack of discrimination among cystine rotamers provided by Raman spectra implies that its utility for determination of rotamer populations in cystine and derivatives, including proteins, appears to be limited.

(16) J. J. Shipman, V. L. Folt, and S. Krimm, *Spectrochim. Acta*, **18**, 1603 (1962).

(17) D. W. Scott, J. P. McCullough, J. F. Messerly, R. E. Pennington, I. A. Hossenlopp, H. L. Finke, and G. W. Waddington, *J. Amer. Chem. Soc.*, **80**, 55 (1958); D. W. Scott and M. Z. El-Sabban, *J. Mol. Spectrosc.*, **30**, 317 (1969).

(18) D. W. Scott, H. L. Finke, M. E. Gross, G. B. Guthrie, and H. M. Huffman, *J. Amer. Chem. Soc.*, **72**, 2424 (1950); S. G. Frankiss, *J. Mol. Struct.*, **3**, 89 (1965).

Nuclear Spin-Lattice Relaxation in Long Chain Viscous Hydrocarbons

J. D. Cutnell,*

Department of Physics, Southern Illinois University, Carbondale, Illinois 62901

R. M. Schisla, and W. C. Hammann

Monsanto Company, St. Louis, Missouri 63166 (Received October 2, 1972)

Publication costs assisted by Southern Illinois University

Nuclear spin-lattice relaxation times T_1 have been measured as a function of temperature (-84 to $+158^\circ$) for seven *gem*-dimethyl-substituted hydrocarbon liquids with carbon chain lengths between C26 and C32. The temperature dependence of the nmr correlation time was Arrhenius in each of the compounds studied. Nonlinear regression analysis of the data showed that the T_1 data (including the T_1 minimum due to overall molecular tumbling) imply either that rotational motions are dominant in the spin-lattice relaxation mechanism or that any translational motions which contribute to T_1 do so in the limit of large translational jumps. Since a single activation energy was sufficient to describe the T_1 data for each compound, rotational and translational correlation times have the same temperature dependence. With the exception of one of the seven compounds the extent to which viscosity determines the nmr correlation time was found to be temperature dependent within the motional narrowing limit. As temperature is increased, a transition to viscosity determined correlation times could not be ruled out on the basis of the experimental data.

Introduction

Nuclear spin-lattice relaxation times T_1 have been used extensively as a probe of molecular motions in studies of systems of a wide variety. The number of such relaxation time studies involving long chain hydrocarbons in the liquid state is surprisingly low, however. Woessner, *et al.*,¹ have studied *n*-dodecane in both the protonated and completely deuterated form in the liquid state and in solution. Agishev² has studied solutions of the normal paraffins with chain lengths of 6, 8, 10, 12, 14, 16, and 18 carbons. Woessner³ has also studied solutions of normal paraffins with chain lengths of 5, 8, 12, and 16 carbons. Cutnell and Stejskal⁴ have studied 6,6,11,11-tetramethylhexadecane, squalane, and squalene as pure liquids. Some of the above mentioned compounds have also been studied in the solid state by Anderson and Slichter,⁵ Douglass and Jones,⁶ and van Putte.⁷ These solid-state studies encompass the normal paraffins with carbon chain lengths between 4 and 94.

It is well known that in the extreme narrowing limit (high temperatures) nmr spin-lattice relaxation rates are proportional to a correlation time which is related to the molecular motions effecting the relaxation. However, from such a limited range of temperatures alone it is not possible to determine whether an exponential correlation function, and hence a single correlation time, is pertinent to the system under study. Spin-lattice relaxation rate data over a wider range of temperatures or as a function of frequency are needed to establish the existence of a nonexponential correlation function. Furthermore, both rotational and translational motions may modulate both intermolecular and intramolecular interactions of nuclear spins. These factors complicate the interpretation of spin-lattice relaxation rates in terms of molecular motions for molecules with appreciable degrees of motional freedom.

The motivation for the present study, then, is threefold: (1) to reduce the relative paucity of such studies for long

chain hydrocarbon liquids, where the relaxation mechanism is complicated by the many degrees of motional freedom possessed by the molecule; (2) to call attention to the importance of translational motions in the overall relaxation mechanism; (3) to provide data on a new group of long chain hydrocarbons.

Experimental Section

1. *Materials.* Each of the *gem*-dimethyl substituted hydrocarbons used in this study has been prepared according to the general method reported by Schisla and Hammann.⁸ The purity of these compounds is at least 99%, as indicated by gas chromatographic techniques. The compounds studied are as follows: 6,6,11,11,16,16,21,21-octamethylhexacosane (compound I); 6,6,11,11,17,17,22,22-octamethylheptacosane (compound II); 6,6,11,11,18,18,23,23-octamethyloctacosane (compound III); 6,6,12,12,18,18,24,24-octamethylnonacosane (compound IV); 6,6,11,11,20,20,25,25-octamethyltriacontane (compound V); 6,6,12,12,21,21,27,27-octamethyldotriacontane (compound VI); and 9,9,18,18-tetramethylhexacosane (compound VII).

2. *Methods.* Each compound was sealed under vacuum in 9-mm o.d. nmr sample tubes after ten freeze-pump-thaw cycles to remove dissolved oxygen. Due to the fact that the vapor pressures of these compounds are not high at the temperatures employed ($\leq 158^\circ$) in this study, no effort was made to reduce the area of the gas-liquid inter-

- (1) D. E. Woessner, B. S. Snowden, Jr., R. A. McKay, and E. T. Strom, *J. Magn. Resonance*, **1**, 105 (1969).
- (2) A. Sh. Agishev, *Zh. Eksp. Teor. Fiz.*, **46**, 3 (1964); [*Sov. Phys. JETP*, **19**, 1 (1964)].
- (3) D. E. Woessner, *J. Chem. Phys.*, **41**, 84 (1964).
- (4) J. D. Cutnell and E. O. Stejskal, *J. Chem. Phys.*, **56**, 6219 (1972).
- (5) J. E. Anderson and W. P. Slichter, *J. Phys. Chem.*, **69**, 3099 (1965).
- (6) D. C. Douglass and G. P. Jones, *J. Chem. Phys.*, **45**, 956 (1966).
- (7) K. van Putte, *J. Magn. Resonance*, **2**, 216 (1970).
- (8) R. M. Schisla and W. C. Hammann, *J. Org. Chem.*, **35**, 3224 (1970).

face, as would be necessary in liquids with low normal boiling points.

All of the T_1 measurements reported here were performed on an NMR Specialties pulsed nmr spectrometer operating at a frequency of 60 MHz. Accuracy is within $\pm 6\%$. The standard $180-90^\circ$ pulse sequence⁹ was used, employing 90° pulse lengths of approximately $3 \mu\text{sec}$. A modified detection system was used which employed a calibrated 6AL5 vacuum tube diode detector¹⁰ and a storage oscilloscope to monitor the magnetization. Temperature control and accuracy¹¹ of $\pm 0.5^\circ$ was achieved *via* a gas flow cryostat¹² utilizing copper-constantan thermocouples.

Kinematic viscosity was measured to within $\pm 5\%$ accuracy using the ASTM D445-T 1960 procedure. Cannon-Manning semimicro viscometers were used. Density measurements were made with a calibrated quartz dilatometer.

Results

Spin-lattice relaxation times for each of the compounds were obtained for temperatures between $\approx 158^\circ$ and temperatures low enough to define the T_1 minimum. At the lowest temperatures each liquid formed a glass.

A plot of spin-lattice relaxation times *vs.* reciprocal temperature is shown in Figure 1 for compound VII. For the compounds studied this plot is typical from several standpoints, namely the presence of a T_1 minimum, the shape of the minimum, and the leveling of T_1 at the lowest temperature shown. In particular each of the compounds studied exhibited the high-temperature linearity indicated in Figure 1. The temperature locations of the T_1 minima were approximately the same at $24 \pm 5^\circ$ for compounds I-V. For compounds VI and VII the T_1 minimum was located at approximately 14 and -6° , respectively. The value of T_1 at the minimum was between 66 and 72 msec for each compound.

The magnetization of the compounds studied did not in general exhibit an exponential return to equilibrium following a 180° pulse. Obvious curvature is present throughout the first decade in typical decay plots for temperatures above that at the T_1 minimum. Two relaxation times T_{1a} and T_{1b} were used, therefore, to fit the decay data according to

$$(M_0 - M_z)/2M_0 = ae^{-\tau/T_{1a}} + be^{-\tau/T_{1b}} \quad (a + b = 1) \quad (1)$$

In this equation a and b denote the relative intensities of the two exponentials, M_z and M_0 denote respectively the z component of the magnetization and its equilibrium value, and τ denotes the time separation between the 180° and 90° pulses. This equation (not its logarithm) was fitted to the data with a nonlinear regression analysis computer program¹³ which produced the parameters a , b , T_{1a} , and T_{1b} . Since automated signal averaging and data collecting are not yet available for the spectrometer used in this work, the quality of the data does not justify reporting these four parameters separately. Where eq 1 is used, only the average spin-lattice relaxation time is employed as a meaningful parameter, according to $(T_1^{-1})_{av} = aT_{1a}^{-1} + bT_{1b}^{-1}$. At temperatures lower than that of the T_1 minimum, where the spin-spin relaxation time T_2 had begun to shorten, a single T_1 was sufficient to describe the decay process for each of the compounds studied. Figure 1 shows the average T_1 values or the single T_1 values depending on temperature.

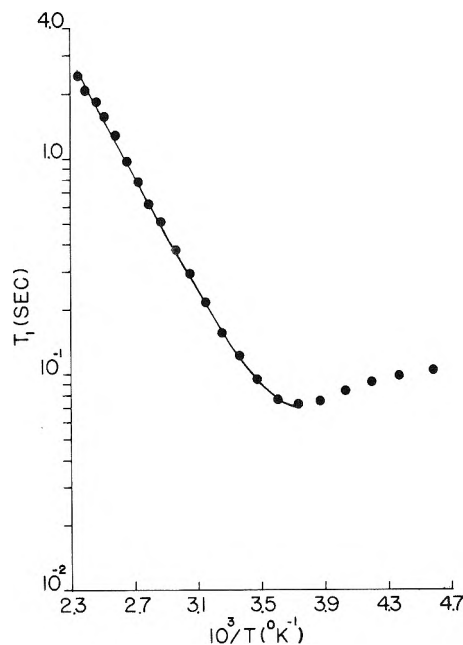


Figure 1. Spin-lattice relaxation time T_1 vs. reciprocal temperature for 9,9,18,18-tetramethylhexacosane: ●, experimental values; solid line, best fit according to eq 2.

Likewise, the parameters given in Table I reproduce within experimental error the T_1 data, as presented in Figure 1, to temperatures down to that at which the T_1 minimum occurs. These parameters were obtained *via* a nonlinear regression analysis of the data using eq 2, which is the usual Bloembergen, Purcell, and Pound¹⁴ (BPP) expression as modified by Kubo and Tomita,¹⁵ together with an Arrhenius temperature dependence for the correlation time.

$$T_1^{-1} = A\tau_c[(1 + \omega^2\tau_c^2)^{-1} + 4(1 + 4\omega^2\tau_c^2)^{-1}] \quad (\tau_c = \tau_0 e^{E/RT}) \quad (2)$$

The resonant frequency is given by ω and the correlation time by τ_c , while A is a constant related to internuclear separation. The dependence on temperature T of the correlation time is determined by the preexponential constant τ_0 and the activation energy E . R is the ideal gas constant. Since the T_1 data span three decades, it was necessary to fit $\ln T_1$ in order to ensure a reasonable convergence criterion for the regression analysis.

A plot of viscosity η *vs.* reciprocal temperature is shown in Figure 2 for compound VII. In this figure η/T is plotted since comparisons of T_1 with viscosity are usually made in this form. The curvature depicted therein is typical of each of the compounds studied. This plot was constructed from kinematic viscosity data and density measurements.

- (9) H. Y. Carr and E. M. Purcell, *Phys. Rev.*, **94**, 630 (1954).
- (10) L. Verduin, M.S. Thesis, Southern Illinois University, Carbondale, Ill., 1972.
- (11) The accuracy of temperature measurements for T_1 data for 6,6,11,11,18,18,23,23-octamethyloctacosane is approximately $\pm 1^\circ$ owing to the inadvertent use and loss of an uncalibrated thermocouple. The standard calibration available in the literature was used.
- (12) L. G. Alexakos, Ph.D. Thesis, University of Wisconsin, Madison, Wis., 1963.
- (13) The program employed in all curve fitting in this study is based upon a subroutine package, entitled GAUSHAUS, which was obtained from the University of Wisconsin Computing Center, Madison, Wis.
- (14) N. Bloembergen, E. M. Purcell, and R. V. Pound, *Phys. Rev.*, **73**, 679 (1948).
- (15) R. Kubo and K. Tomita, *J. Phys. Soc. Jap.*, **9**, 888 (1954).

TABLE I: Spin-Lattice Relaxation Times, Viscosities, and Densities According to Eq 2-4

Compound ^a	T_1 , sec			η , cP ^b			ρ , g/cm ³	
	$10^{-10} A$, sec ⁻²	$10^{14} \tau_0$, sec	E , kcal/mol	η_0 , cP	C , °K	T_0 , °K	ρ_0 , g/cm ³	m , g/cm ³ °K
I	1.97	0.0534	8.76	0.04944	930.2	186.4	0.9956	0.5856
II	1.92	0.720	7.19	0.04984	936.8	185.4	1.0114	0.6307
III	1.87	0.516	7.38	0.05239	941.8	184.0	1.0051	0.6111
IV	1.95	1.29	6.76	0.05059	935.4	184.7	1.0297	0.6953
V	1.94	0.393	7.51	0.05271	974.7	181.1	1.0425	0.6954
VI	1.99	1.50	6.64	0.06634	904.1	186.1	1.0106	0.6078
VII	1.94	1.47	6.15	0.05693	870.7	162.8	1.0002	0.6205

^a See Experimental Section for compound names. ^b Except for compound VII the parameters listed reproduce viscosity for $273 \leq T \leq 533$ °K. For compound VII the temperature range is $255 \leq T \leq 533$ °K.

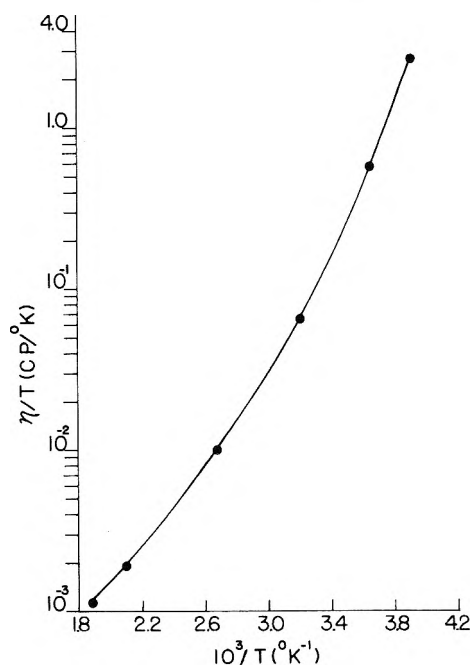


Figure 2. Viscosity η in the form η/T vs. reciprocal temperature T for 9,9,18,18-tetramethylhexacosane: ●, experimental values; solid line, best fit according to eq 4.

Density values are reproduced within experimental error using eq 3. The constants ρ_0 and m , as determined from measurements at two temperatures, are given in Table I. Parameters η_0 , C , and T_0 , reproducing the viscosity data to within 4.5%, are given in Table I also. These parameters were obtained *via* a nonlinear regression analysis of the data using the logarithm of eq 4.¹⁶

$$\rho = \rho_0 - mT/1000 \quad (3)$$

$$\eta = \eta_0 e^{C/(T-T_0)} \quad (4)$$

Discussion

1. *Unresolved Low Temperature T_1 Minimum.* The leveling of the T_1 values shown in Figure 1 at low temperatures indicates the presence of a second minimum at lower temperatures than those studied. Considering the structures of compounds studied, this minimum is probably due to methyl group rotation. The minimum depicted in Figure 1 is due to overall molecular tumbling since it occurs at the higher temperature. Contributions of the methyl rotations in this temperature region are ignored in the subsequent discussion, as no data are available which

would allow a quantitative evaluation of their effect and in view of the fact that the minima appear to be well separated on the reciprocal temperature axis.

2. *Multiple Spin-Lattice Relaxation Times.* The existence of multiple relaxation times, such as implied by eq 1, is well established for pure liquids.^{1,2,4} Interestingly, the data of Woessner, *et al.*,¹ for *n*-dodecane reveal that the protonated species exhibits a single T_1 , whereas the perdeuterio analog exhibits two T_1 's. Thus, motional differences exist between the methyl and methylene deuterons and establish different T_1 's for the two spin systems. The dipole-dipole interactions in the protonated species, however, provide a mechanism effective enough to enable cross relaxation to establish a single T_1 .

Unfortunately, the deuterated analogs of the molecules studied here are not available, so that the questions raised by the work of Woessner, *et al.*,¹ have not been investigated further for these compounds. Since two T_1 's are observed at the higher temperatures for each of the compounds studied, cross relaxation *via* either intermolecular or intramolecular interactions is not strong enough to establish a single T_1 for the methyl and methylene spin systems. Motional differences between these spin systems exist, probably because of the ability of the methyl group to rotate about its threefold symmetry axis. It is not clear why cross relaxation should be so effective in *n*-dodecane and not in the compounds studied here.

3. *On the Use of Eq 2.* Strictly speaking, the BPP formulation of eq 2 may not apply to the molecules studied, for it presumes a single correlation time and a single A value. At least two correlation times, two A values, and a weighted sum of two BPP terms could be expected, due to the presence of methyl and methylene protons. However, in long chain molecules such as those studied, where complicated segmental motion probably predominates, it is questionable whether such a view represents reality more accurately than eq 2. Equally possible is a relaxation mechanism determined by a complicated motional process, but which is determined by a single correlation time and yields an equation of the form of eq 2 as a limiting case. The basic model for the translational motional contribution to T_1 , provided by Torrey,¹⁷ is such an example. (See section 5 below.) The great success of the BPP expression in treating rotational contributions to T_1 should not hide the fact that the form of eq 2 is not specific to a single model for molecular motion.

(16) A. J. Barlow, J. Lamb, and A. J. Matheson, *Proc. Roy. Soc. Ser. A*, **292**, 322 (1966).

(17) H. C. Torrey, *Phys. Rev.*, **92**, 962 (1953).

In cases such as ours, where eq 2 does fit experimental data over a wide enough temperature range (specifically through a T_1 minimum), it provides a useful method for calculating a consistent set of correlation times. Thus, the temperature dependence of the correlation time can be obtained over a wider range of temperatures than that available solely from the high-temperature, motional narrowing region. Of course, the unambiguous interpretation of the correlation time, its temperature dependence, and associated parameters such as an activation energy depends on an unambiguous assignment of a model describing the molecular motions. Even in the absence of such an assignment, the availability of the correlation time over a wider range of temperatures facilitates comparisons with potentially important variables such as viscosity.

4. Temperature Dependence of Nmr Correlation Times and Viscosity. Correlation times can be related to either rotational¹⁸ or translational diffusion^{17,19} constants, and a simple connection between the diffusion constant and viscosity η has been used to justify the calculation of correlation times *via* hydrodynamic models²⁰. According to such models a simple proportionality between the correlation time and η/T is expected, where T denotes the Kelvin temperature. Furthermore T_1^{-1} can be shown to be proportional to the correlation time (average or otherwise) in the motional narrowing limit. Thus in this limit the quantity $T/(T_1\eta)$ should be temperature independent if calculations of nmr correlation times *via* hydrodynamic models are to be meaningful. Values of $T/(T_1\eta)$ can be calculated from the spin-lattice relaxation time and viscosity data for each of the compounds studied. In these compounds, therefore, an evaluation of the role of viscosity in determining the nmr correlation time is possible.

As judged from plots of T_1 vs. $10^3/T$, such as Figure 1, the motional narrowing limit is approximately given by $10^3/T < 3.1$ °K⁻¹ for each of the compounds studied. The highest temperatures for which T_1 was measured were such that $10^3/T \approx 2.3$ °K⁻¹. Viscosity values within the temperature range $2.3 < 10^3/T < 3.1$ may be calculated from eq 4, using the parameters given in Table I. These values may then be combined with the appropriate measured T_1 values to give $T/(T_1\eta)$ as a function of temperature.

Figure 3 shows plots of $T/(T_1\eta)$ vs. $10^3/T$ for compound VII (●'s) and compound IV (×'s). The vertical bars in this figure indicate maximum errors. Similar plots for the other five compounds studied are intermediate in character between those shown in Figure 3 in the following sense. As temperature decreases, each of them exhibits the downward trend beyond experimental error shown in Figure 3 for compound IV (×'s). However, at the high end of the temperature range for which T_1 was measured each of the plots also exhibits the leveling shown in Figure 3 for compound VII (●'s).

If the nmr correlation times were determined solely by viscosity, a plot of $T/(T_1\eta)$ vs. $10^3/T$ would be temperature independent, as discussed above, and thus parallel to the $10^3/T$ axis. With the exception of compound VII, then, the role of viscosity in determining the nmr correlation time depends on temperature for each of the compounds studied within the motional narrowing limit. At low temperatures, but still within the motional narrowing limit, the nmr correlation time is not determined solely by viscosity. However, on the basis of the present work the possibility cannot be ruled out that at the highest temperatures studied viscosity completely determines the

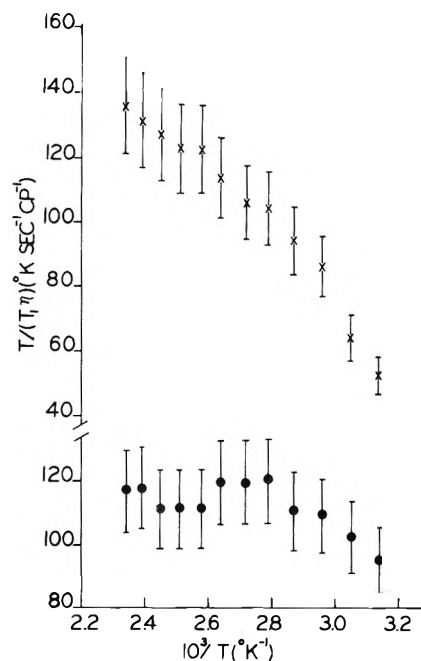


Figure 3. The dependence of $T/(T_1\eta)$ on temperature: ●, 9,9,18,18-tetramethylhexacosane; ×, 6,6,12,12,18,18,24,24-octamethylnonacosane.

nmr correlation time. Experimental error in our results prohibits any quantitative characterization of the temperature range over which the transition occurs to viscosity determined correlation times as temperature increases. Qualitatively it is clear that this transition temperature range is above any liquid-to-solid phase change, since each of the compounds is an oily liquid over the entire range of temperatures shown in Figure 3. For compound VII the deviation from the horizontal in Figure 3 is only slightly beyond experimental error at the lowest temperature shown. Thus, for this compound the data are not sufficiently accurate to rule out complete determination of the nmr correlation time by viscosity within the temperature range for the motional narrowing limit. However, on the basis of the results for the other compounds studied, we may expect that deviations from a completely viscosity determined correlation time would appear as temperature is lowered beyond the motional narrowing limit.

In molecules of relatively simple structure it is known that the temperature dependence of T_1 may disagree with that of the viscosity, due, for example, to intramolecular contributions to T_1 from highly mobile portions of the molecule.²¹ On the other hand, Woessner, *et al.*,¹ have found agreement between the temperature dependence of viscosity and both intermolecular and intramolecular T_1 contributions in *n*-dodecane. Agishev² also found agreement between viscosity and T_1 temperature dependencies for solutions of *n*-hexane, *n*-dodecane, and *n*-octadecane in CCl₄. If intramolecular contributions to T_1 are the cause of the difference in temperature dependence between correlation time and viscosity, then the present study suggests that the number of methyl groups per molecule may be the determining factor. It is not clear why the molecules studied by Cutnell and Stejskal⁴ exhibit re-

(18) A. Abragam, "The Principles of Nuclear Magnetism," Oxford University Press, Oxford, 1961, Chapter 8.

(19) G. J. Kruger, *Z. Naturforsch.*, **24a**, 560 (1969).

(20) See ref 1 and references contained therein.

(21) J. G. Powles and R. Figgins, *Mol. Phys.*, **10**, 155 (1966).

sults contrary to those found here, especially in view of the similarity of the saturated hydrocarbons involved.

Fiorito and Meister²² have implicated hydrogen bonding in the lack of agreement between the pressure dependence of viscosity and diffusion constants. Since the liquids studied here are not hydrogen bonded, any cooperative effects, such as ascribed to hydrogen bonding by Fiorito and Meister, must be related to restricted mobility *via* entanglement between the long chain hydrocarbon molecules.

The Arrhenius temperature dependence of the nmr correlation time allows the determination of activation energies E according to eq 2. These activation energies are shown in Table I and compare with the value of 2.9 kcal/mol determined by Agishev² for CCl_4 solutions of the normal paraffins hexane, dodecane, and octadecane as well as the value of 3.7 kcal/mol determined for *n*-dodecane by Woessner, *et al.*¹ The larger values measured here are no doubt due to the increased chain length, although no simple dependence of activation energy on chain length is apparent. Excluding compound VII, which has the shortest chain length and smallest activation energy, the greater the separation between methyl groups within the molecule, the smaller the activation energy. It is also interesting to note that the activation energies shown in Table I are appreciably larger than the maximum of 3–4 kcal/mol found for rotation of a methyl group about its three-fold axis. On the other hand, the values found for E by Agishev² and Woessner, *et al.*¹ for normal hexane, dodecane, and octadecane are compatible with the 3–4 kcal/mol maximum. Thus a dominance of the relaxation mechanism by methyl rotation cannot be ruled out in hydrocarbon liquids of chain lengths up to 18 carbons. In the compounds studied, however, the greater chain lengths evidently lead to a reduction in the importance of methyl rotation to the overall relaxation mechanism. Other motions provide more efficient possibilities for relaxation, most likely motions of methylene protons resulting from complicated segmental movements of the molecule.

Within the temperature range studied the Arrhenius temperature dependence of T_1 in the high-temperature limit rules out any significant contribution to the spin-lattice relaxation rate from spin-rotation interaction,²³ for spin-rotation interaction would result in a positive slope in the high-temperature region of Figure 1. The absence of a noticeable T_1 contribution from spin-rotational interaction applies for each of the compounds studied and is consistent with the observation of Woessner, *et al.*¹ for *n*-dodecane. Evidently spin-rotation interaction is not a sufficiently efficient spin-lattice relaxation mechanism to compete favorably with other such mechanisms in liquids where the molecules possess many degrees of motional freedom.

The non-Arrhenius temperature dependence of eq 4 prohibits the determination of activation energies and generally is related to a free volume theory for viscosity.¹⁶ Furthermore, the glass transition temperatures of these compounds may be expected to be somewhat higher than the T_0 values shown in Table I.

5. *Rotational vs. Translational Contributions to T_1 .* It is well known that both rotational and translational motions can provide a mechanism for spin-lattice relaxation in liquids. In long chain hydrocarbons such as studied here, one cannot uniquely identify rotational with intramolecular contributions to T_1 , nor translational with intermolecular contributions to T_1 . Such simplification is not possi-

ble because of the high degree of motional freedom possessed by long chain molecules. In general one may expect the nuclear spins of such a molecule to exhibit as much relative translation as rotation, both motions contributing to the intramolecular part of T_1 . It is unlikely, therefore, that studies of such molecules in solution in their completely deuterated analogs would yield a separation of rotational and translational contributions to T_1 . Such studies provide at present the only direct experimental method with which to attack this problem. The results of Woessner, *et al.*,¹ show, for example, that intermolecular interactions yield approximately 28% of the total spin-lattice relaxation rate for *n*-dodecane.

In order to assess, then, the importance of rotational *vs.* translational contributions to T_1 , a direct fit of theoretical models to the T_1 data would appear to be the best approach. Fiorito and Meister²² have recently taken this approach in their study of hydrogen bonded liquids. The contribution to T_1 due to rotational diffusion of nuclear spins is given by eq 2. Torrey¹⁷ has provided the basic treatment for the translational contribution to T_1 , while Kruger¹⁹ has provided a corrected version of Torrey's results. These expressions are bulky and need not be given here. It is sufficient to say that in these expressions T_1 is determined by the translational diffusion constant, the distance d of closest approach to which the spins come, and a parameter $\alpha = \langle r^2 \rangle / 12d^2$. The mean-square jump distance exhibited by the spins is given by $\langle r^2 \rangle$. It should be noted that in the limit that $\alpha \rightarrow \infty$ eq 2 is obtained with a different constant A . Thus, the temperature dependence of T_1 implied by eq 2 does not establish the dominance of rotational contributions to T_1 , unless it can be shown independently that α is small.

A three-parameter nonlinear regression analysis of the T_1 data employing eq 2 produces a fit to within experimental error in each case. The parameters obtained are given in Table I. Such a fit implies that if translational contributions to T_1 are significant, then the translational motions are in the limit of $\alpha \rightarrow \infty$. Furthermore, the high-temperature linearity of the T_1 data as exhibited in Figure 1 implies that if the translational and rotational correlation times are both important, then they have the same Arrhenius temperature dependence. It is reassuring to note the near identity of the values for A in Table I, for A is determined by an internuclear separation and except for the position of the methyl groups, the molecules studied are structurally similar.

Since the parameter α in the Torrey theory provides yet a fourth variable parameter compared to the three in eq 2, a meaningful application of the Torrey-Kruger equations requires very accurate data. However, the importance of α as a repository of information about the translational motions justifies an attempt to obtain it from data of even limited accuracy. Except for compound VII,²⁴ a four-parameter nonlinear regression analysis of our data produces extremely large values for α , consistent with the above mentioned appropriateness of eq 2 in fitting the data. The fit is to within the experimental error in each case and virtually identical in quality with that obtained using eq 2. Virtually identical values for the activation energy are

(22) R. B. Fiorito and R. Meister, *J. Chem. Phys.*, **56**, 4605 (1972).

(23) P. S. Hubbard, *Phys. Rev.*, **131**, 1155 (1963).

(24) For compound VII a value of $\alpha \approx 0.7$ was obtained. Although this value is not reliable it is mentioned because it is surprisingly close to the $\alpha \approx 0.2$ value used by Fiorito and Meister²² for 2-methyl-2,4-pentanediol.

obtained from this fit as are given in Table I. However, the values for α are not reliable enough to report, because of the experimental error in our data and the insensitivity of the Torrey-Kruger function to α in the limit of large α . (Indeed, the confidence limits on α and the correlation coefficient matrix provided by our analysis indicate that extreme caution must be exercised in assigning approximate fixed values to α .) Interestingly enough, Fiorito and Meister²² report small values of α to be appropriate in fit-

ting T_1 data in hydrogen-bonded liquids. The lack of motional restrictions from such bonding in the molecules studied here is consistent with the expectation that the spins may be free to exhibit larger translational jumps. Large values of α would then be appropriate in calculating T_1 from the Torrey theory.

Acknowledgment. We wish to acknowledge gratefully the thorough the helpful comments of the reviewer.

Thermodynamics of the Helix-Coil Transition of Polypeptides in Binary Solvent Systems

F. E. Karasz* and G. E. Gajnos

Polymer Science and Engineering, University of Massachusetts, Amherst, Massachusetts 01002 (Received December 7, 1972)

Publication costs assisted by The National Science Foundation

The thermodynamics of the helix-coil conformational transition for polypeptides in mixed organic solvents is analyzed in terms of the temperature dependent free energies of the helix disruption and preferential coil-solvent binding reactions. Transition enthalpies, transition temperature-solvent composition relationships, and fractional degrees of binding are calculated as a function of the respective individual enthalpy and entropy parameters. The effect of these parameters and of solvent composition on the direction of the thermally induced transition is demonstrated. The observed width of the transition either in the temperature or solvent composition planes is also related to these parameters. The theory is used to analyze available experimental data for the helix-coil transition for three systems: poly- γ -benzyl-L-glutamate in dichloroacetic acid-1,2-dichloroethane and poly- β -benzyl-L-aspartate in dichloroacetic acid-chloroform, and in dimethyl sulfoxide-dioxane. The respective enthalpy and entropy parameters are compared in terms of postulated concepts for the transition mechanism.

Introduction

The heat and entropy associated with an order-disorder transition in biopolymers have been of interest mainly in relation to theories of the cooperativity of this transformation. There has been comparatively little discussion of the significance of these parameters *per se*. This can be attributed to the long-standing appreciation of the fact that these measured quantities represent the net effect of more than one process contributing to the transition, and in the absence of a general method of analysis by which the individual enthalpic or entropic contributions could be resolved, such discussion is inopportune. However, the helix-coil transition of polypeptides in mixed organic solvents presents a special case in which a more detailed examination may be fruitful, for it is not too unreasonable to assume, at least initially, that the transition can be described in terms of only two steps: the formation or disruption of intramolecular hydrogen bonds stabilizing the helical conformation, and a preferential interaction of solvent molecules with backbone sites on the polypeptide exposed by the disordering of the helix. Such a model dates from the earliest considerations of the helix-coil transition^{1,2} and is necessary to account, for example, for the so-called "inverse" (coil-to-helix) thermal transitions that

are found in the majority of polypeptide-mixed organic solvent systems studied to date.³

The aim of this paper is to demonstrate how the observed thermodynamic data are related to the individual reaction parameters and consequently how such data may be analyzed to provide a greater insight into the effect of molecular structure on the transition. In addition, this general framework will explain the basis for a rather wide range of phenomena encountered. Specifically we will be interested first in the enthalpy and entropy of what may be termed the intrinsic polypeptide disruption step, *i.e.*, the quantities which would be measured if the transition could be observed in an inert solvent system. Indeed if this were possible, the effect of side chain interaction, chirality, and other parameters affecting helical stability could be assessed by direct comparison. In practice this cannot be done, basically because the ordered conformations of all polypeptides of interest are somewhat too stable to be disrupted in noninteracting solvents—the transition temperatures are too high. The role of the second, in-

(1) J. A. Schellman, *J. Phys. Chem.*, **62**, 1485 (1958).

(2) L. Peller, *J. Phys. Chem.*, **63**, 1199 (1959).

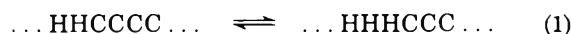
(3) G. D. Fasman in "Poly- α -Amino Acids," Vol. 1, G. D. Fasman, Ed., Marcel Dekker, New York, N. Y., 1967.

teracting, component in a mixed solvent system is thus in effect to lower the transition temperature to an experimentally observable range. The conditions which make this possible and how this depression can result in an inversion of the direction of the observed thermal transition are of interest. The theory developed here also permits a discussion of the effect of the relative free energies of the two reactions on the transition temperature-solvent composition relation, *i.e.*, on the phase diagrams. Finally, an analysis of some available data will be used to illustrate the concepts employed.

Theoretical Section

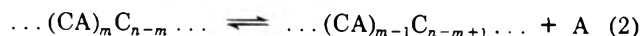
The model employed is one that has been used in more or less equivalent form by several authors^{1,2,4-6} and we describe it only briefly. The mixed solvent system is in general assumed to contain one of each of two classes of solvents: inert solvents (I) whose interaction with the solute molecules is indifferent to the conformational state of the latter, and active solvents (A) which can interact preferentially with the disordered conformation. The nature of this interaction need not be further specified at present. As already stated, active solvents depress the transition temperature, T_c , of a polypeptide relative to its value in a pure inert solvent, T_c^0 . A corollary of this model is thus that, for a given polypeptide, T_c^0 is the same for any inert solvent. Furthermore, we assume the interaction between the active solvent molecule and peptide groups in the disordered conformation to be governed by the mass action law and postulate noninteraction between bound solvent molecules, equivalent therefore to a Langmuir adsorption model.

The overall transition can thus be described in two steps. The first may be represented by



where the state of each peptide group within a chain is represented by either H (helical or ordered) or C (coil, random). Following Zimm and Bragg⁷ and similar treatments,⁸ we consider the sequence nucleation and growth steps within a macromolecule separately, and in this section consider only the latter. The nucleation process which governs the width of either the solvent or thermally-induced transition will be introduced into the theory at a later stage. Equation 1 thus represents the net growth of an existing helical sequence by one peptide unit.

The second step describes the interaction of a coil or disordered peptide group with an active solvent molecule A



In eq 2 the $n - m$ (or $n - m + 1$) unbound peptide groups are assumed to be distributed at random among any set of n residues. The equilibrium constant for the addition of one peptide unit to an existing sequence, K_1 , in the absence of A is related to the respective heat and entropy by

$$K_1 = \exp[-(\Delta H_1 - T \Delta S_1)/RT] \quad (3)$$

The equilibrium constant for the binding reaction (eq 2) is given by

$$K_2 = x_C x_A / x_{CA} \quad (4)$$

where we assume ideal solution behavior and hence use mole fractions instead of activities. Thus x_A is the mole

fraction of A in the A-I solvent mixture, and we assume that $x_A \gg x_C$ throughout the transition. The ratio of ordered to total random residues K_1' is given by

$$K_1' = x_H / (x_C + x_{CA}) \quad (5)$$

which yields, for the equilibrium constant s describing the addition of a peptide unit in the presence of A^{5,7}

$$s = K_1 K_2 / (K_2 + x_A) \quad (6)$$

which can be written, with the usual assumption concerning the temperature dependence of equilibrium constants

$$RT \ln s = -(\Delta H_1 - T \Delta S_1) - RT \ln \{1 + x_A \exp[(\Delta H_2 - T \Delta S_2)/RT]\} \quad (7)$$

Equation 7 (see also ref 2), relates the transition temperature T to the solvent composition x_A for given values of the enthalpy and entropy (ΔH_1 and ΔS_1) of the interpeptide reaction, eq 1, and of the peptide-solvent reaction (ΔH_2 and ΔS_2), eq 2, and at a given value of s .

In particular, we may let $s = 1$ and obtain phase boundaries in the T, x_A plane along which the fraction of helical conformation, f_H , present is $1/2$, separating ordered and disordered conformations. Where necessary, we denote the parameters associated with these special solutions by the subscript c , but defer the consideration of these diagrams themselves to a later section.

The calorimetric heat of transition is defined as

$$\Delta H_{\text{cal}} = RT_c^2 (\partial \ln s / \partial T)_{x_{A,c}} \quad (8)$$

which, combined with eq 7, reduces to the simple form

$$\Delta H_{\text{cal}} = \Delta H_1 + \{x_{A,c} / (x_{A,c} + K_2)\} \Delta H_2 \quad (9)$$

We note that the coefficient of ΔH_2 in eq 9 is equal to F_c , the fraction of coil groups bound to A at $f_H = 1/2$

$$F_c = \frac{x_{CA}}{x_C + x_{CA}}$$

and from eq 4

$$F_c = \frac{x_{A,c}}{x_{A,c} + K_2} \quad (10)$$

thus

$$\Delta H_{\text{cal}} = \Delta H_1 + F_c \Delta H_2 \quad (11)$$

Equation 11, which has been derived previously in similar form^{3,6} can be invoked to explain the observation of a so-called inverse thermal transition if ΔH_1 and ΔH_2 are of opposite sign and $|\Delta H_2| > |\Delta H_1|$. With the conventions adopted in eq 1 and 2, we indeed expect both ΔH_1 and ΔS_1 to be negative and ΔH_2 and ΔS_2 to be positive in relevant situations of interest. These conditions will be assumed to hold in the ensuing discussion. F_c , of course, is a function of T_c , decreasing with increasing transition temperature if ΔH_2 and ΔS_2 are positive.

The reversible binding of A to coil residues C may be viewed as a "freezing" of A; in these terms the transition temperature-solvent composition curve may be regarded

- (4) J. Applequist, *J. Chem. Phys.*, **38**, 934 (1963).
- (5) G. Giacometti in "Structural Chemistry and Molecular Biology," A. Rich and N. Davidson, Ed., W. H. Freeman and Co., San Francisco, Calif., 1968.
- (6) M. Bixon and S. Lifson, *Biopolymers*, **4**, 815 (1966).
- (7) B. H. Zimm and J. K. Bragg, *J. Chem. Phys.*, **31**, 526 (1959).
- (8) D. C. Poland and H. A. Scheraga, "Theory of Helix-Coil Transition in Biopolymers," Academic Press, New York, N. Y., 1970.

as a "melting-point" depression curve for A,⁹ whose activity is being lowered by the addition of the diluent I. Thus, a transition enthalpy ΔH_{comp} may be defined from the effect of solvent composition on T_c :

$$\Delta H_{\text{comp}} = RT_c^2 (\partial \ln x_A / \partial T)_c \quad (12)$$

From eq 12 and 7 we obtain

$$\Delta H_{\text{comp}} = \Delta H_1 / F_c + \Delta H_2 \quad (13)$$

Equations 11 and 13 represent respectively the overall enthalpy change associated with the transfer of one mole of peptide residues from an ordered to a disordered conformation and with one mole of A from a free to a bound state, as can be seen by inspection. These two quantities will be equal in the limiting case of stoichiometric or "tight" binding (*i.e.*, $F_c = 1$). In general, this will not be the case, however, and thus the condition $\Delta H_{\text{comp}} > \Delta H_{\text{cal}}$ may be anticipated, as is seen by combining eq 13 and 11

$$F_c = \Delta H_{\text{cal}} / \Delta H_{\text{comp}} \quad (14)$$

Equation 14 is a useful result, not only because it enables us to estimate the fraction of bound peptide units from a measurement of ΔH_{cal} and of T_c as a function of $x_{A,c}$, but also because it permits a calculation of K_2 (eq 10) and hence of K_1 (eq 6) along the phase boundary. Thus, if F_c can be determined as a function of temperature, the important parameters, ΔH_1 , ΔS_1 , ΔH_2 , and ΔS_2 may be calculated. In this manner the relative contributions of the intramolecular and the intermolecular peptide-solvent bond to the conformational stability of the helix may be evaluated. The special case $\Delta H_{\text{cal}} = \Delta H_{\text{comp}}$ would be of some interest in that it would permit a noncalorimetric determination of the net transition enthalpy,⁹ but would offer no opportunity for estimating the separate inter- and intramolecular contributions.

Phase Diagrams. The solution of eq 7 with the condition $s = 1$ yields T_c as a function of $x_{A,c}$. In general, this solution cannot be obtained in closed form, but numerical solutions may be readily found.¹⁰ As already anticipated from the discussion of eq 11 and 13 we find two possibilities. If $|\Delta H_1| \geq |\Delta H_2|$ only one meaningful solution exists, separating low- and high-temperature fields of stability in which, respectively, the ordered and disordered conformations predominate. Thus any thermally induced transition will in this case be of the helix-to-coil ("normal") type. The isothermal, solvent-induced transition (*i.e.*, the transition induced by the addition of the active solvent A to the solution of the polypeptide in I) will invariably be of the helix-to-coil type because of the negative slope of the phase boundary. Figure 1 shows solutions of eq 7 for this case for a number of sets of parameters. For the case $|\Delta H_1| < |\Delta H_2|$, a more complex situation prevails. If the intermolecular peptide-solvent bond is only moderately stronger than the intramolecular peptide-peptide bond, two distinct branches of the phase boundary exist, separating a low- and high-temperature disordered conformational domain from an intermediate temperature ordered or helical state, Figure 2. Thus, the direction of any thermal transition experimentally observed depends on which of these boundaries fell broadly within the experimentally accessible temperature region. For most systems, this is generally in the range from 0 to 100°; at higher temperatures polymer degradation occurs, and at lower temperatures polymer solubility or other problems prevail. The

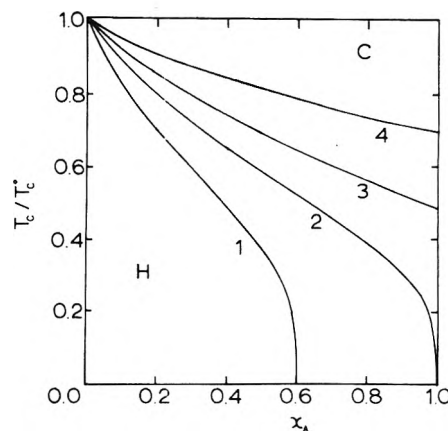


Figure 1. Reduced transition temperatures as a function of solvent composition for $|\Delta H_1| \geq |\Delta H_2|$. All curves: $\Delta H_1 = -1000$ cal/mol, $\Delta S_1 = -2$ eu. ($T_c^0 = 500^\circ\text{K}$); $-\Delta H_2/\Delta H_1$ and $-\Delta S_2/\Delta S_1$, for curves 1-4 are 1.0, 0.5; 1.0, 1.0; 0.8, 1.0; and 0.25, 1.0, respectively. H and C represent regions of helical and random-coil stability, respectively.

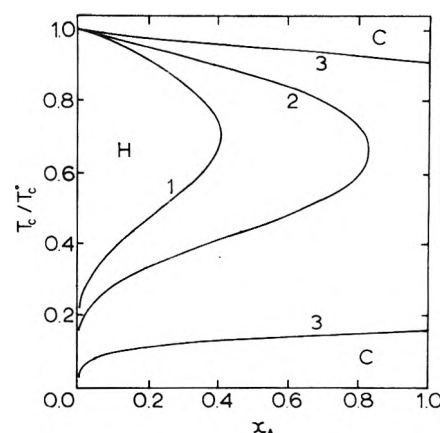


Figure 2. Reduced transition temperatures as a function of solvent composition for $|\Delta H_2| > |\Delta H_1|$. All curves: $\Delta H_1 = -1000$ cal/mol, $\Delta S_1 = -2$ eu. ($T_c^0 = 500^\circ\text{K}$). $-\Delta H_2/\Delta H_1$ and $-\Delta S_2/\Delta S_1$ for curves 1-3 are 3.0, 4.0; 2.5, 4.0; and 1.5, 4.0 (two branches), respectively. H and C represent regions of helical and random-coil stability, respectively.

distinction between the high-temperature and low-temperature coiled conformation lies, of course, in the relative proportions of CA groups.

For conditions in which the peptide-solvent bond is relatively stronger, the two branches will merge at $x_{A,c} \leq 1$ and a more limited region of stability for the ordered form is observed. For a given polypeptide, the size of this domain decreases with increasing ΔH_2 (see Figure 2). The above qualitative discussion in enthalpic terms is based on an implicit assumption of constant ΔS_2 (and ΔS_1). This of course need not be so and we also show (Figure 3) a set of solutions in which ΔS_2 is varied with the other parameters fixed.

A given polypeptide may thus be characterized by values of ΔH_1 and ΔS_1 ; the ratio $\Delta H_1/\Delta S_1$ is equal to the

(9) F. E. Karasz and J. M. O'Reilly, *Biopolymers*, **5**, 27 (1967).

(10) The solution of eq 7 in the case $K_2^{-1}x_A \gg 1$, corresponding to "tight binding," or saturation of C sites by A molecules, is

$$T_c = \frac{\Delta H_1 + \Delta H_2}{\Delta S_1 + \Delta S_2 - R \ln x_A} \quad (7)$$

Normally, this solution will only be valid at low temperatures. It is interesting to note it is of the same form as the well-known "ceiling (or floor) temperature" equation describing monomer-polymer equilibrium. In this case, the process is the formation of sequences of A (*i.e.*, A "polymer") by "adsorption" on adjacent "C" sites.

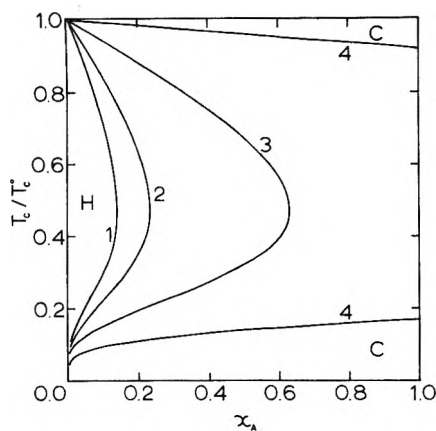


Figure 3. Reduced transition temperatures as a function of solvent composition, showing effect of change in ΔS_2 . All curves: $\Delta H_1 = -1000$ cal/mol, $\Delta S_1 = -2$ eu ($T_c^0 = 500^\circ\text{K}$), $\Delta H_2/\Delta H_1 = -1.5$, $-\Delta S_2/\Delta S_1$ for curves 1-4 are 0.5, 1.0, 2.0, and 4.0 (two branches), respectively. H and C represent regions of helical and random-coil stability, respectively.

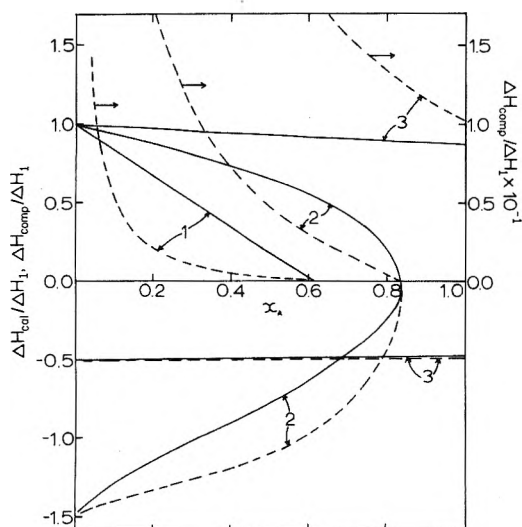


Figure 4. Reduced calorimetric, $\Delta H_{\text{cal}}/\Delta H_1$ (full lines) and composition, $\Delta H_{\text{comp}}/\Delta H_1$ (dashed lines) transition enthalpies as function of solvent composition. All curves: $\Delta H_1 = -1000$ cal/mol, $\Delta S_1 = -2$ eu, $-\Delta H_2/\Delta H_1$ and $-\Delta S_2/\Delta S_1$ for curves 1-3 are 1.0, 0.5; 2.5, 4.0; and 1.5, 4.0 (two branches), respectively. Note change of scale for reduced composition transition enthalpies in higher temperature branch (upper half of figure) only.

transition temperature of the thermally induced helix-to-coil transition for the polypeptide in an inert solvent (*i.e.*, T_c^0). It may be anticipated that the solvent interaction parameters ΔH_2 and ΔS_2 are also a function of the structure of the polypeptide substrate, though perhaps to a relatively small degree. Figure 1 therefore represents the case in which a given polypeptide interacts with a number of comparatively weakly binding active solvents; in Figure 2 the effect of a number of more strongly interacting solvents on the same polypeptide is shown.

Figures 2 and 3 clearly provide the rationale for an inverse thermal transition (which has necessarily to be accompanied by a normal direction conformational change at a higher temperature) and indicate the possibility that a given polypeptide may display thermal transitions of opposite directions at about the same temperature if different solvent systems are used.

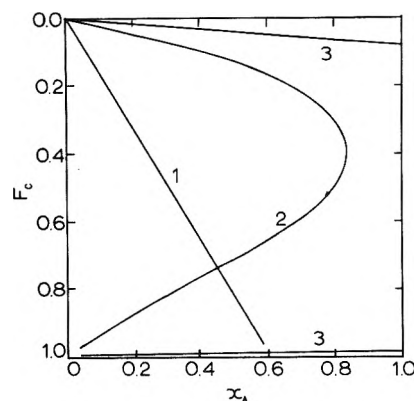


Figure 5. Fractional solvent binding, F_c , for three sets of parameters used in Figure 4. Curve numbering corresponds to that used in Figure 4.

The transition enthalpies, ΔH_{cal} and ΔH_{comp} , may be calculated for any given set of parameters along the T_c , $x_{A,c}$ phase boundaries from eq 10, 11, and 13. The results of such calculations are shown in Figure 4 for sets of parameters selected from those used in calculating the phase boundaries shown in Figures 1 and 2. According to eq 11, ΔH_{cal} assumes a limiting value of ΔH_1 at $T_c = T_c^0$, $x_{A,c} = 0$ in the upper branch of the phase diagram. If a low-temperature branch exists, *i.e.*, if $|\Delta H_2| > |\Delta H_1|$, ΔH_{cal} approaches the limit $\Delta H_1 + \Delta H_2$, and $\Delta H_{\text{comp}} = \Delta H_{\text{cal}}$. This limit obviously cannot be attained; the formalism becomes invalid when $x_A \sim 0(x_C)$. In the limit $T_c \rightarrow T_c^0$, $\Delta H_{\text{comp}} \rightarrow 0$, reflecting the absence of solvent interaction. The ratio F_c , along the phase boundaries, is also shown for the several cases in Figure 5; as already pointed out, for the most likely situations, in terms of the signs of the respective parameters, the fraction of solvent bound residues decreases with increasing temperature.

Relation to Transition Width

The theory discussed above deals essentially with the thermodynamic changes in the complete transformation from one conformational state to another, while the phase boundaries represent the loci of the midpoints of the transitions, $f_H = 0.5$. A discussion of the finite transition width for this process requires the introduction of a sequence initiation or co-operativity parameter. In the Zimm-Bragg⁷ treatment this parameter, σ , is a direct measure of the average sequence length (n) of either H or C residues at $f_H = 0.5$; *i.e.*, $n = \sigma^{-1/2}$. We consider the necessary relations in terms of both the thermal and solvent-induced transitions.

Thermal Transition. From a determination of f_H vs. T in a thermally induced transition at constant solvent composition the van't Hoff transition enthalpy ΔH_{VH} may be found

$$\left(\frac{\partial f_H}{\partial(1/T)} \right)_{f_H=1/2} = \frac{\Delta H_{\text{VH}}}{4R} \quad (15)$$

$$= \frac{\Delta H_{\text{cal}}}{4R\sigma^{1/2}} \quad (16)$$

The essential relation between f_H and s has been given by Applequist⁴ in terms of the Zimm and Bragg treatment

$$f_H = \frac{1}{2} + \frac{s-1}{2\{(1-s)^2 + 4\sigma s\}^{1/2}} \quad (17)$$

or, in more restricted form, valid around $f_H = 1/2$

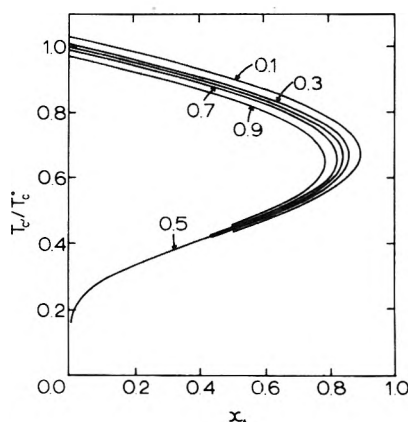


Figure 6. Reduced transition temperatures T_c'/T_c^0 at fractional helical contents shown as function of solvent composition. (T_c' represents solutions of eq 7 for any f_H). $\Delta H_1 = -1000$ cal/mol, $\Delta S_1 = -2$ eu, $\Delta H_2/\Delta H_1 = -2.5$, $\Delta S_2/\Delta S_1 = -4$. Zimm-Bragg⁷ parameter $\sigma = 10^{-4}$.

$$\partial f_H = \frac{\partial \ln s}{4\sigma^{1/2}} \quad (17')$$

Thus, assuming σ is known, phase boundaries corresponding to any required f_H may be found by using eq 17 or 17' to calculate the corresponding value of s and solving eq 7 as before.

Solvent-Induced Transition. The experimental quantity $\partial f_H/\partial \ln x_A$ at $f_H = 1/2$ in an isothermal solvent-induced transition is related to the transition enthalpies and to σ as follows. From eq 6 we find

$$\ln s = \ln K_1 K_2 - \ln(x_{A,c} + K_2)$$

Thus

$$\left(\frac{\partial \ln s}{\partial \ln x_A}\right)_{T_c} = -\frac{x_{A,c}}{x_{A,c} + K_2} \quad (18)$$

Combining this result with eq 17' yields

$$-\left(\frac{\partial f_H}{\partial \ln x_A}\right)_{T_c} = \frac{F_c}{4\sigma^{1/2}}$$

This is equivalent to a result obtained by Birshtein and Ptitsyn,^{11a} and by Giacometti^{11b} for the special "tight-binding" case of $F_c = 1$. As isothermal f_H vs. x_A data in the transition range are frequently available, it provides some added flexibility in the determination of F_c and hence of ΔH_1 , ΔH_2 , etc., from solvent-induced transition data. The broadening of the isothermal transition with increasing T_c (i.e., decreasing F_c) even at constant σ , is apparent in the example presented in Figure 6. The possibility of less than complete conversion to the helical form in the case of thermal transitions in solvent compositions around the critical value corresponding to the change in sign of $\partial T_c/\partial x_A$ is also indicated.

Applications

The theory presented above provides a basis for characterizing the conformational transition of a polypeptide in an inert-active solvent system in terms of four parameters, ΔH_1 and ΔS_1 and ΔH_2 and ΔS_2 . These parameters can be interpreted at least semiquantitatively in terms of known concepts. Thus, ΔH_1 can be identified with the stabilization enthalpy of a given polypeptide by interpeptide hydrogen bond formation, modified, as the case may be, by the interactions of pendant groups. ΔS_1

TABLE I: Calculated Thermodynamic Parameters for PBG and PBA and for Their Interactions with DCA and DMSO

	PBG-DCA	PBA-DCA	PBA-DMSO
ΔH_1 , cal/mol of residue	-845	-390	-390
ΔS_1 , eu	-1.55	-0.9	-0.9
T_c^0 , °K	545	425	425
ΔH_2 , cal/mol	2920	3030	800
ΔS_2 , eu	9.3	8.1	4.3

can be identified with the molar entropy lost upon the formation of a rigid helical conformation from a random coil. Both these quantities will reflect the effect of variations in side-chain structure. The solvent-peptide binding enthalpy ΔH_2 is a measure of the interaction of a given active solvent with a peptide group. This interaction will again be perturbed by the nature of the side chain if only through the presumed variation in accessibility of the solvent molecule to the CO and NH groups assumed to be involved in the binding process. For a tightly bound peptide-solvent complex, the entropy ΔS_2 in the model should reflect the loss of translational freedom of the solvent molecule in the binding process; we might thus expect ΔS_2 to approach values characterizing fusion entropies for the solvent species A.

We have analyzed below three polypeptide-solvent systems for which appropriate data are available. These are poly- γ -benzyl-L-glutamate (PBG) in dichloroacetic acid and 1,2-dichloroethane (DCA-DCE), and poly- β -benzyl-L-aspartate (PBA) in DCA-CHCl₃ and in DMSO-dioxane. In principle an analysis to yield the four parameters could be carried out purely from a consideration of T_c vs. $x_{A,c}$ data; because of the form of eq 7, however, it develops that neither the range nor the precision of such data is sufficient in practice to unequivocally determine ΔH_1 , etc. A more satisfactory approach is to use such data to calculate ΔH_{comp} as a function of temperature and combine this with available values of ΔH_{cal} . This approach was used in an analysis of the PBG system. By combining calorimetric¹² and solvent composition data,⁹ F_c (eq 14) and K_2 (eq 10) as a function of T_c were obtained. K_1 along the phase boundary was then found from eq 6. The enthalpies and entropies were derived from the equilibrium constants in the normal manner and are presented in Table I. Figure 7 shows the phase diagram for PBG in DCA-DCE calculated using these parameters, while Figure 8 depicts the corresponding values of ΔH_{cal} and ΔH_{comp} . The experimental data over the relatively limited range for which it is available are also included. While it is obvious that the good agreement between these data and the calculated results is in part a reflection of the use of the former in the analysis, the self-consistency of the results is a more independent check of the validity. The probable errors in the calculated parameters are at least $\pm 15\%$.

Several qualitative features of the experimental data are satisfactorily explained by the results obtained. For example, according to the present treatment PBG is seen to form a very stable helix in inert solvents, with a predicted transition temperature of about 270°. This stability

(11) (a) T. M. Birshtein and D. B. Ptitsyn, *Mol. Biol. (USSR)*, **3**, 121 (1969); (b) G. Giacometti, A. Turolla, and R. Boni, *Biopolymers*, **6**, 441 (1968).

(12) (a) F. E. Karasz, J. M. O'Reilly, and H. E. Bair, *Nature (London)*, **202**, 693 (1964); (b) F. E. Karasz and J. M. O'Reilly, *Biopolymers*, **4**, 1015 (1966).

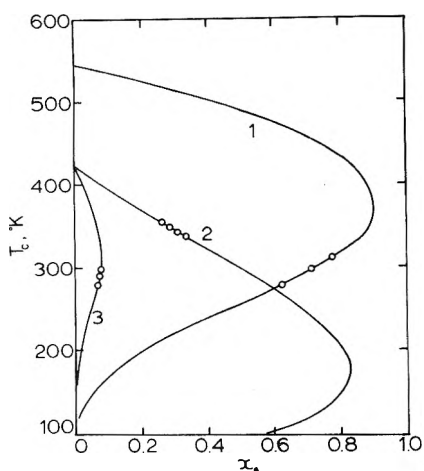


Figure 7. Transition temperatures for PBG-DCA-DCE (curve 1), PBA-DMSO-dioxane (curve 2) and PBA-DCA-CHCl₃ (curve 3) systems calculated using parameters shown in Table I. Filled circles represent available data (see text for sources).

has been amply demonstrated in the work of Franzen, *et al.*,¹³ who studied the high-temperature optical rotation of PBG in a number of solvents. In 1-chloronaphthalene, which might reasonably be expected to be inert in the context used here, no transition was observed up to the temperature of degradation, about 200°. There was some evidence, from infrared spectra, for the onset of a transition at somewhat higher temperatures, in the vicinity of 255°.

The observed direction of the thermal conformational transition for PBG in DCA-DCE around room temperature (and, according to these results, up to about 100°) is evident from the calculated phase diagram, as is the basis for the observed pronounced upward curvature in the T_c vs. $x_{A,c}$ data above ambient temperatures.^{12,14} The phase diagram also predicts that a "normal" helix-to-coil thermal transition should be found in this solvent system at higher temperatures in compositions containing less than 92 mol % DCA. It would be necessary to extend measurements to the vicinity of 200° to obtain a complete transformation to the coiled conformation, however. As already pointed out, it would, in principle, also be possible to find an active solvent which depresses the transition temperature sufficiently for a helix-to-coil transition to be observed around room temperature. Conditions for this occurrence, in terms of sets of necessary ΔH_2 and ΔS_2 values, can be readily calculated.

The calculated values of ΔH_{cal} and ΔH_{comp} for the PBG-DCA-DCE system (Figure 8) reflect the observed large negative temperature coefficients in these quantities in the temperature range studied. It is important to note that in this model the large apparent molar heat capacity arises not from an enthalpic difference in the conformations themselves but from a change in solvent binding with temperature. At $T_c = 25^\circ$ we calculate the fraction, F_c , of available "C" sites bound to DCA to be 0.45. This is in excellent agreement with the value of 0.48 obtained by Ptitsyn and Birshtein^{11a} though it should be noted that in deriving this result they used the somewhat higher value of ΔH_{cal} obtained by Ackermann.¹⁴

The numerical results shown in Table I indicate that the stabilization enthalpy of PBG in an inert solvent is less than one kilocalorie per peptide residue which, considering the known variability of hydrogen bonding in

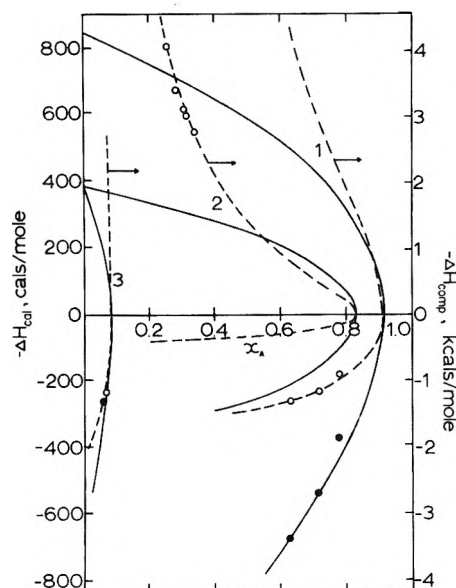


Figure 8. Calorimetric (full line) and compositional (dashed line) transition enthalpies for PBG-DCA-DCE (curve 1), PBA-DMSO-dioxane (curve 2) and PBA-DCA-CHCl₃ (curve 3) systems calculated using parameters shown in Table I. Filled circles (ΔH_{cal}) and open circles (ΔH_{comp}) represent available data (see text for sources).

these systems, is a very acceptable estimate. The corresponding molar entropy, 1.5 eu, is lower than has been postulated for the unsubstituted polypeptide chain, *i.e.*, polyglycine,¹⁵ but this decrease is to be expected in view of the extended nature of the PBG random coil.¹⁶ It would seem better to defer further discussion on the absolute values of these parameters until a comparison with several other peptide structures can be made. It is seen also that the absolute value of the DCA-peptide interaction enthalpy, ΔH_2 , is much greater than the intramolecular term, possibly a result, in part, of the often-postulated formation of two hydrogen bonds per residue;²⁻⁵ the corresponding entropy is also substantial, in accord with the loss of translational mobility concept suggested above.

In the case of PBA, the conformational change is of particular interest because of the observation that the thermal transition may be in either direction, according to the solvent system used. This suggests that the PBA helix is weak relative to PBG, but nevertheless it is also known that the disruption cannot be induced in an inert solvent below the temperature at which polypeptide degradation becomes significant, *i.e.*, around 90°. The instability of the PBA helix has also been inferred from the relatively low concentration of DCA necessary to induce the transition, but from a consideration of the phase diagrams for the more complicated inverse transitions as shown in Figure 2 for example, one concludes that this correlation is not necessarily correct in all cases.

We have used available data for PBA in DCA-chloroform^{17,18} and in DMSO-dioxane¹⁷ to calculate the respective parameters for these cases. In the former solvent

(13) J. S. Franzen, J. B. Harry, and C. Bobik, *Biopolymers*, **5**, 193 (1967).

(14) T. Ackermann and E. Neumann, *Biopolymers*, **5**, 649 (1967).

(15) J. A. Schellman, *C. R. Trav. Lab. Carlsberg, Ser. Chim.*, **29**, 230 (1955).

(16) D. A. Brant and P. J. Flory, *J. Amer. Chem. Soc.*, **87**, 2788 (1965).

(17) P. Dubin and F. E. Karasz, *Biopolymers*, **11**, 1745 (1972).

(18) R. H. Karlson, K. S. Norland, G. D. Fasman, and E. R. Blout, *J. Amer. Chem. Soc.*, **82**, 2268 (1960).

system an inverse thermal transition is found around ambient temperature; in the latter a helix-to-coil change may be observed in the range 60–90°. For neither solvent system considered here are there sufficient calorimetric data available to permit a direct calculation of the parameters *via* F_c , etc. However, it was possible to extrapolate the available $x_{A,c}$, T_c data for the DMSO–dioxane system to $x_{A,c} = 0$, *i.e.*, to pure dioxane, and thus obtain the ratio $\Delta H_1/\Delta S_1$, ($T_c^0 = 425^\circ\text{K}$). For PBA in the DCA–chloroform solvent system transition temperatures as a function of solvent composition are at present only available over a quite limited range,¹⁷ but these, combined with an available estimate of ΔH_{ca1} within this range,¹⁹ sufficed to determine F_c and thus K_2 and K_1 at 20°. The analysis was then completed by combining T_c^0 with K_1 to yield ΔH_1 and ΔS_1 individually, and ultimately derive ΔH_2 and ΔS_2 for both the DMSO–dioxane and DCA–chloroform systems. The complete numerical results are shown in Table I, while phase diagrams and transition enthalpies calculated on the basis of these parameters are shown in Figures 7 and 8. The relative instability of the PBA helix postulated above, and previously attributed to the unique chirality of this molecule,^{3,20} is confirmed. The conformational entropy change ΔS_1 is even lower than that found for PBG perhaps, in part, attributable to the same cause. For the DCA–chloroform solvent system the DCA binding parameters are surprisingly close to those found for the PBG–DCA complex. An assessment of whether ΔH_2 and ΔS_2 are indeed independent of peptide structure will again have to be deferred until a wider range of polypeptide–solvent systems can be analyzed. The relatively weak binding capability of DMSO to the PBA residues is also established; perhaps the low value of ΔH_2 calculated may be related to the fact that only one site for hydrogen bonding per residue is available. It is tempting to use the fact that the calculated ΔS_2 for DMSO is only about half the corresponding parameter for DCA with either PBG or PBA to lend further weight to this premise.

Further Discussion

The theory detailed above is able to account for many of the phenomena related to the helix–coil transition in polypeptides in organic solvent systems that have been described. In particular it provides a rational basis for the frequently observed coil-to-helix thermal transition and for the role of the active, binding, solvent in the thermodynamics of the overall process. Furthermore, we believe

this theory has some use in more directly relating the effect of side-chain structure on the intrinsic stabilization of the ordered conformation.²¹ For the first time, it has been possible to estimate the appropriate thermodynamic parameters unperturbed by preferential solvent binding effects.

Several simplifications in the theory are apparent and reduce the number of parameters which have to be evaluated from the limited experimental data. One of the more obvious simplifications is the substitution of activities by molar fractions in eq 4 and those that follow. This has the effect, among others, of omitting a partial molar enthalpy correction to the term ΔH_2 .⁶ Also the latter term will require redefinition if the active solvent participates in a monomer–dimer equilibrium ($2A \rightleftharpoons A_2$) as might occur with strong carboxylic acids. However, the same formalism can be retained unless the presence of the polypeptide significantly depletes the concentration of the monomer species A in the solvent mixture. Further, we have chosen to ignore the undoubted differences between the carbonyl and amine binding sites in the polypeptide backbone; the enthalpy and entropy terms as well as the equilibrium constants must therefore be regarded as averages for the two sites. The possible interaction of bound A molecules on adjacent “C” sites has also been entirely neglected. This in effect removes a possible element of cooperativity from the transition process; however, the effect will be reflected in the overall parameter σ . Thus, this is a mechanism which would explain the variation in σ observed for a given polypeptide (PBA) in different solvent systems.¹⁹ It is possible that the reported considerable temperature sensitivity of σ may also be a consequence of this point.^{12b,14}

Possible extensions of the model (albeit at the expense of simplicity) are also apparent. It would be a comparatively straightforward extension of the formalism to include the cases of a copolypeptide and/or competing active solvents. This will be done in a subsequent report.

Acknowledgment. We thank Mrs. K. Paranya for invaluable assistance with the numerical computations. This work was supported by NSF Grant GB 33484.

- (19) Y. Hayashi, A. Teramoto, K. Kawahara, and H. Fujita, *Biopolymers*, **8**, 403 (1969).
- (20) M. Goodman, C. M. Deber, and A. M. Felix, *J. Amer. Chem. Soc.*, **84**, 3773 (1962).
- (21) F. Gaskin and J. T. Yang, *Biopolymers*, **10**, 631 (1971).

Crystal Structure of Methylenediphosphonic Acid

D. DeLaMatter, J. J. McCullough, and C. Calvo*

Department of Chemistry, McMaster University, Hamilton, Ontario, Canada (Received September 27, 1972)

Publication costs assisted by The National Research Council of Canada

Methylenediphosphonic acid is monoclinic with space group $P2_1/c$ and has lattice parameters $a = 7.840(9)$, $b = 5.494(3)$, $c = 13.746(6)$ Å and $\beta = 103.69(7)^\circ$, with $Z = 4$. The structure was refined by full-matrix least squares to a final R value of 0.032 with 1173 reflections measured with a Syntex automatic diffractometer. The P-C bonds are 1.790(3) and 1.794(3) Å in length with a P-C-P angle of $117.2(1)^\circ$. The P-O bond lengths are 1.494(2) and 1.503(2) Å while the average P-O(-H) bond length is 1.546 Å. Each of the oxygen atoms involved in the former bonds is an acceptor for two hydrogen bonds.

Introduction

The study of the structure of a substantial number of diphosphates has as its goal the understanding of the nature of the bonding in this anion. The role and the nature of the π bonding within the anion still remains obscure. In addition the nature of the motion of the bridging atom remains unresolved.¹ The study of the methylenediphosphonates was undertaken because the bridging bonds, since they involve P-C, should be devoid of π bonding and because the motion of the bridging group can be studied over a large temperature range by nmr techniques. The crystal structure of the acid has been resolved as the first step in this study, although a recent report on the structure of ethane-1-hydroxy-1,1-diphosphonic acid monohydrate² uses some unpublished results on an early study of the structure of methylene diphosphonic acid by Lovell.³

Experimental Section

Methylenediphosphonic acid was prepared by hydrolysis of the tetraisopropyl ester with hydrochloric acid, according to the method of Roy.⁴ The acid gave colorless crystals from 1-butanol, which melted in the range $192-204^\circ$ (lit. mp $203-206^\circ$). The nmr spectrum of the acid was obtained at 100 MHz in D_2O , and showed a triplet for the methylene group at 5.16 ppm with $J_{PH} = 21$ Hz.

Crystals large enough for a structure determination were obtained by the slow evaporation of a saturated solution of isopropyl alcohol. One of these was ground into a sphere having a diameter of 0.25 mm and used to collect all the data. The unit cell parameters were determined by least squares from 15 values of 2θ determined with a Syntex P1 automatic diffractometer using graphite monochromatized Mo $K\alpha$ radiation (λ 0.71069 Å).

Crystal Data. The formula weight was 176.01; $a = 7.840(9)$, $b = 5.494(3)$, $c = 13.746(6)$ Å, $\beta = 103.69(7)^\circ$, unit cell volume 575.26 Å³, $Z = 4$, space group $P2_1/c$, calculated density = 2.03 g/cm³, experimental density = 2.05 g/cm³(3).

Data were collected in a quadrant up to a 2θ angle of 50° with a standard reflection measured after every 50 reflections. Peaks were scanned at a rate varying from 2 to 24° /min, depending upon the peak intensity, and backgrounds were measured at fixed angles at either side of the peak and for the same time interval as used to scan the peak. Intensities whose measure after background correction were negative were dropped from the refinement to save computational time. Those whose intensity ex-

ceeded 3σ were regarded as observed and the remainder as unobserved with a maximum possible value of 3σ . The data set contained 1170 symmetry independent reflections with 898 of these regarded as observed. These data were corrected for Lorentz, polarization, extinction, and absorption ($\mu R = 0.1$).

A trial structure was generated using the sign determination routines in X-ray 67. The phosphorus positions were readily identified in the subsequently prepared electron density maps and the oxygen atom positions resolved by the use of difference syntheses. The structure was refined using full-matrix least squares utilizing a program written for the CDC-6400 by J. S. Stephens. Atomic scattering curves were obtained from the "International Tables for X-Ray Crystallography."⁵ Weights, ω , were chosen so that $\omega\Delta F^2$, with ΔF the difference between the observed and calculated structure factor, was independent of F_o . Those unobserved reflections with F_c less than the assigned maximum possible structure factor were given zero weight in the refinement. When convergence had been obtained with isotropic temperature factors, anisotropic components were allowed to vary. An R value of 0.042 was obtained, at this stage, with $\omega R = 0.052$. Finally hydrogen atoms were assigned to the carbon atom, and to those oxygen atoms with the longer P-O bond lengths. Although these atoms seemed to appear in the difference synthesis their positions were assigned as lying 1 Å removed from its nearest neighbors and with idealized angular geometry. The refinement was carried to convergence, with all shifts less than $1/5\sigma$, with isotropic thermal parameters for the hydrogen atoms. The final R value is 0.032 and $\omega R = 0.035$. The final atomic parameters are in Table I and the thermal parameters are in Table II.⁶

Description of the Structure. Methylenediphosphonic acid deviates by about 30° from an eclipsed configuration

- (1) B. E. Robertson and C. Calvo, *Can. J. Chem.*, **46**, 605 (1968).
- (2) V. A. Uchtman and R. A. Gloss, *J. Phys. Chem.*, **76**, 1298 (1972).
- (3) F. M. Lovell, Abstracts of the American Crystallographic Association Meeting, July, 1964.
- (4) C. H. Roy, U. S. Patent No. 3,251,907; *Chem Abstr.*, **65**, 3908d (1966).
- (5) "International Tables for X-Ray Crystallography," Vol. III, Kynoch Press, Birmingham, 1963.
- (6) The final atomic parameters and the thermal parameters, Tables I and II, respectively, as well as a listing of the observed and calculated structure factors will appear following these pages in the microfilm edition of this volume of the journal. Single copies may be obtained from the Business Operations Office, Books and Journals Division, American Chemical Society, 1155 Sixteenth St., N.W., Washington, D. C. 20036. Remit check or money order for \$3.00 for photocopy or \$2.00 for microfiche, referring to code number JPC-73-1146.

TABLE III: Interatomic Distances and Angles with Standard Errors^a for Methylene-diphosphonic Acid

Bond	Length, Å	Bond	Length, Å
P(1a)-C(a)	1.790(3)	P(2a)-C(a)	1.794(3)
-O(1a)	1.546(2)	-O(2a)	1.545(2)
-O(3a)	1.547(2)	-O(4a)	1.548(2)
-O(5a)	1.494(2)	-O(6a)	1.500(2)
C(a)-O(1a)	2.656(3)	C(a)-O(2a)	2.728(3)
-O(3a)	2.631(3)	-O(4a)	2.715(3)
-O(5a)	2.749(3)	-O(6a)	2.685(3)
O(1a)-O(3a)	2.486(3)	O(2a)-O(4a)	2.406(3)
-O(5a)	2.539(3)	-O(6a)	2.542(3)
O(3a)-O(5a)	2.544(3)	O(4a)-O(6a)	2.562(3)
H(1a)-O(1a)	0.73(6)	H(2a)-O(2a)	0.68(6)
-O(5c)	1.87(6)	-O(5b)	1.93(6)
O(1a)-O(5c)	2.605(3)	O(2a)-O(5b)	2.603(3)
H(3a)-O(3a)	0.73(4)	H(4a)-O(4a)	0.85(5)
-O(6d)	1.95(4)	-O(6b)	1.74(5)
O(3a)-O(6d)	2.675(3)	O(4a)-O(6b)	2.577(3)
C(a)-H(5a)	0.91(4)		
-H(6a)	0.93(4)		

Angle	Degree	Angle	Degree
C(a)-P(1a)-O(1a)	105.4(1)	C(a)-P(2a)-O(2a)	109.1(1)
-O(3a)	103.2(1)	-O(4a)	108.2(1)
-O(5a)	113.6(1)	-O(6a)	109.3(1)
O(1a)-O(3a)	107.0(1)	O(2a)-O(4a)	102.2(1)
-O(5a)	113.3(1)	-O(6a)	113.2(1)
O(3a)-O(5a)	113.5(1)	O(4a)-O(6a)	114.5(1)
P(1a)-C(a)-P(2a)	117.2(1)	H(5a)-C(a)-H(6a)	112(3)
O(5c)-H(1a)-O(1a)	177(6)	O(3a)-H(3a)-O(6d)	172(4)
O(5b)-H(2a)-O(2a)	178(6)	O(4a)-H(4a)-O(6d)	171(4)

^a Includes errors in the unit cell lengths. Atom position X(ln) is derived from those in Table I by the transformations $a = x, y, z$; $b = -x, \frac{1}{2} + y, \frac{1}{2} - z$; $c = x, -y, -z$; $d = x, \frac{1}{2} - y, \frac{1}{2} + z$.

when viewed along the P-P vector. The carbon atom is bonded to two phosphorus atoms and two hydrogen atoms and these atoms are distributed nearly tetrahedrally about the carbon atom. The P-C-P angle is $117.2(2)^\circ$. The carbon atom is displaced from colinearity with the two phosphorus atoms such that it lies nearly equidistant from all the oxygen atoms in the molecule. These distances range from 2.621 to 2.750 Å. Table III contains the pertinent bond distances and angles. Each molecule is bonded through hydrogen atoms to eight neighbors, four at each end. Groups of four molecules hydrogen bond to form rings about the inversion center, *e.g.*, $\frac{1}{2}0\frac{1}{2}$ in Figure 1, by the bonding of O(6) to O(3) and O(4) through H(3) and H(4), respectively. These rings then form ribbons running parallel to the $-b + c$ direction with adjacent ribbons joined by means of a centrosymmetrically related pair sharing H(1) and H(2) between O(5) and O(1) and O(2). The structure shows chains $O \cdots H-O-P-O-H \cdots O$ at each end running parallel to the $-a + b$ direction with the acceptor oxygen atoms in a trans arrangement.

The individual P-C bond lengths, at 1.790(3) and 1.794(3) Å, differ insignificantly. The P-O bond lengths fall into two distinct classes. The shorter ones involve

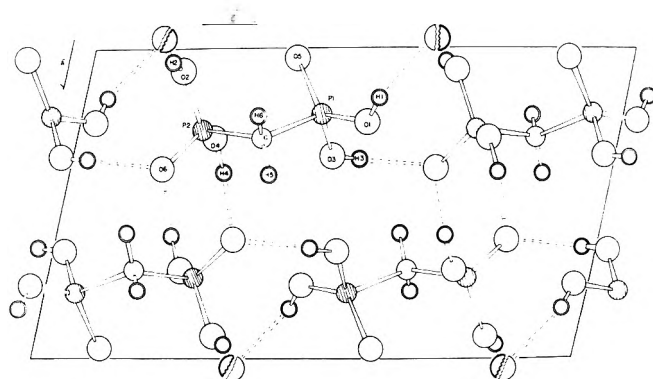


Figure 1.

O(5) and O(6) and are 1.494(2) and 1.500(2) Å long while the remaining ones, which in fact are POH groups, all lie between 1.545(2) and 1.548(2) Å. All the C-P-O bond angles on side 2 lie with 1.5° of the ideal tetrahedral value while those on side 1 range from 103.2 to 113.6°. Two of the three O-P-O bond angles on each side are larger than ideal and one is smaller. The smallest of these lies on side

2 and has a value of $102.2(1)^\circ$. Each tetrahedra has as its shortest O-O edge that one containing the two OH groups.

Discussion

Uchtman and Gloss² indicated that in $C(CH_3)(OH)(PO_3H_2)_2$ (I), $NH^+(CH_2PO_2H_2)_2(CH_2PO_3H)$ (II), and Lovell's results on $CH_2(PO_2H_2)_2$ (III) that as the P-O(-H) bond strengthened, as measured by its bond length, so does the hydrogen bond, as measured by the donor-acceptor O-O contact. In addition these authors noted that a decrease in the P-O bond length paralleled a decrease in the P-O(-H) bond length which shared a common P atom. The present refinement breaks the pattern since the P-O(-H) bond lengths differ insignificantly while the O-H...O distances are different. The second effect does not seem universal either since the average P-O(-H) bonds in I and III are identical while III has the shorter P-O bonds.

I has a nearly eclipsed configuration when viewed down the P-P axis, with C-P-O and O-O bond angles on one

side of the molecule (side 1) consistent with a displacement of the P from an ideal tetrahedron toward the plane of the oxygen atoms. On the other side of the P atom (side 2) the P is also displaced away from the edge containing the two OH groups. In contrast methylenediphosphonic acid distorts in a manner consistent with a displacement of the phosphorus atom away from the edge containing the two OH groups. A further difference between I and III concerns the P-C bond lengths (1.832 and 1.840 Å in I) although the P-C-P bond angles (115° in I) are similar. As indicated by Uchtman and Gloss² this difference is not consistent with a steric effect. Careful molecular orbital calculations might sort out the various effects leading to these differences and reflect on Uchtman and Gloss² suggestion that the dihedral angle collapses because of the repulsion arising when functional groups replace the hydrogen atoms on the carbon atom.

Acknowledgment. This research was supported through a grant from the National Research Council of Canada.

A Far-Infrared Study of the Association of Benzoic Acid with Substituted Ammonium Halides in Benzene

R. A. Work, III, and R. L. McDonald*

Department of Chemistry, University of Hawaii, Honolulu, Hawaii 96822 (Received December 27, 1972)

Tetraheptyl- and tri-*n*-octylammonium chlorides and bromides were studied by far-infrared techniques in benzene solutions containing small amounts of benzoic acid. Both cation-anion and anion-acid stretching vibrations can be observed simultaneously in the region below 400 cm^{-1} . An internal OCO deformation mode of benzoic acid which absorbs in the far-infrared was used to estimate anion-acid association constants. Although ion pair-ion pair association of the tetraheptylammonium salts is decreased by benzoic acid solvation of the anion, in no case was any evidence of cation-anion separation observed.

Several recent papers¹⁻³ have described the interaction of ion pairs with hydrogen-bonding molecules in aprotic organic solvents. Taylor and Kuntz^{1b} used nmr and mid-infrared techniques to study the interaction of various ion pairs with phenol in several different solvents. Phenol-anion association constants were computed from "free" ν_{OH} intensities, and it was suggested that solvent separation of the ion pairs occurs on addition of phenol. Martin, *et al.*,^{2c} used similar nmr and infrared techniques to study the association of tetra-*n*-butylammonium halides with various alcohols in CCl_4 . They concluded that 1:1 alcohol-anion complexes were formed in solution. Diamond, *et al.*,³ studied the coordination of water-insoluble phenols and alcohols with tetraalkylammonium fluoride and chloride in toluene by extraction techniques. Up to four alcohol or phenol molecules were found to coordinate to the halide ion in the organic phase.

Although far-infrared instruments have been commercially available for more than a decade, surprisingly few

far-infrared studies of ion pair-molecule interactions in solution have been reported. We have found that in favorable cases both cation-anion and anion-molecule stretching vibrations can be observed simultaneously in the region below 400 cm^{-1} for systems consisting of an ion pair and a hydrogen-bonding molecule in an "inert" diluent. Most polar solvents are unsuitable as diluents because they exhibit intense, broad absorptions in the far-infrared region due to dipole-dipole interactions.⁴ On the other hand, benzene is an excellent solvent. It is transparent, it

- (1) (a) R. P. Taylor and I. D. Kuntz, Jr., *J. Amer. Chem. Soc.*, **92**, 4813 (1970); (b) *J. Phys. Chem.*, **74**, 4573 (1970).
- (2) (a) R. D. Green and J. S. Martin, *J. Amer. Chem. Soc.*, **89**, 5549 (1967); (b) J. S. Martin, J.-I. Hayami, and R. U. Lemieux, *Can. J. Chem.*, **46**, 3263 (1968); (c) R. D. Green, J. S. Martin, W. B. McG. Cassie, and J. B. Hyne, *Can. J. Chem.*, **47**, 1639 (1969).
- (3) D. J. Turner, A. Beck, and R. M. Diamond, *J. Phys. Chem.*, **72**, 2831 (1968); T. Kenjo, S. Brown, E. Held, and R. M. Diamond, *J. Phys. Chem.*, **76**, 1775 (1971).
- (4) R. J. Jakobsen and J. W. Brasch, *J. Amer. Chem. Soc.*, **86**, 3571 (1964).

TABLE I: Far-Ir Data for Benzene Solutions of THA^+X^- , TOAH^+X^- , and $\text{C}_6\text{H}_5\text{CO}_2\text{H}^a$

Species	OCO def.	$\text{C}_6\text{H}_5\text{CO}_2\text{H-X}^-$	C^+-A^- stretch	C^+-A^- bend
$(\text{C}_6\text{H}_5\text{CO}_2\text{H})_2$	281s
THA^+Cl^-	118s	...
			91s	
$\text{THA}^+\text{Cl}^- \text{HO}_2\text{CC}_6\text{H}_5$	251s	154s	ca. 120s, br	...
TOAH^+Cl^-	197s	85m
$\text{TOAH}^+\text{Cl}^- \text{HO}_2\text{CC}_6\text{H}_5$	247s	150s γ	183s	ca. 87mw, br
THA^+Br^-	84ms	...
			75ms	
$\text{THA}^+\text{Br}^- \text{HO}_2\text{CC}_6\text{H}_5$	243s	100s	ca. 73sh	...
TOAH^+Br^-	139ms	61mw
$\text{TOAH}^+\text{Br}^- \text{HO}_2\text{CC}_6\text{H}_5$	242s	130sh	132ms	ca. 60w, br

^a All data in cm^{-1} ; s, strong; m, medium; w, weak; sh, shoulder; br, broad.

dissolves a wide variety of hydrogen-bonding molecules and ionic compounds containing substituted ammonium cations, and it interacts only very weakly with most substances.

In spite of the limitations, far-infrared spectroscopy is a powerful method for studying these systems. It enables one to identify the species present, to estimate the strengths of the bonds formed and, in some cases, to determine formation constants. It was mostly for this last reason that benzoic acid was chosen for this study. The internal OCO deformation mode of benzoic acid which appears in the far-infrared region obeys Beer's law; it was used to obtain "solvation" numbers and formation constants. The effect of this solvation on the ion-pair bond was observed simultaneously.

Experimental Section

Reagents. Eastman White Label tetra-*n*-heptylammonium chloride (THA^+Cl^-) was purchased as a liquid which crystallized after several weeks *in vacuo*; it was used without further purification. Eastman White Label tetra-*n*-heptylammonium bromide (THA^+Br^-) was recrystallized from *n*-hexane. Eastman tri-*n*-octylammonium chloride (TOAH^+Cl^-) was recrystallized once from ether and twice from *n*-hexane. Tri-*n*-octylammonium bromide (TOAH^+Br^-) was prepared by slowly bubbling HBr through a cold dilute solution of Eastman Yellow Label tri-*n*-octylamine in *n*-hexane. The product was purified in the same manner as TOAH^+Cl^- . All alkylammonium salts were stored in a vacuum desiccator. Mallinckrodt Reagent Grade benzoic acid and Nanograde benzene were used without further purification.

Solutions. Approximately 0.4 *M* stock solutions of THA^+Cl^- , THA^+Br^- , TOAH^+Cl^- , TOAH^+Br^- , and benzoic acid were prepared in benzene that had previously been dried with activated Linde 3A molecular sieve. The molecular sieve was activated before use by heating in a vacuum oven at 200° for 48 hr. After preparation, the alkylammonium salt stock solutions were stored over the molecular sieve. Solutions were prepared between 0.02 and 0.10 *M* in benzoic acid and between 0.02 and 0.20 *M* alkylammonium salt by quantitative mixing of the two stock solutions and benzene. The choice of concentrations was determined by the infrared intensities and the degree of association of the ion pair and benzoic acid. Stock solution concentrations were determined by two-phase titrations: benzoic acid was titrated with 0.1000 *N* NaOH to a

phenolphthalein end point; the alkylammonium salts were determined by the Mohr method.⁵

Ir Spectra. Spectra in the region 4000–600 cm^{-1} were obtained with a Beckman IR-9 infrared spectrophotometer fitted with KBr optics. Far-infrared spectra in the region 400–40 cm^{-1} were determined with an R.I.I.C. Model FS-720 Fourier spectrometer equipped with an FTC 100/7 Fourier transform computer and wave analyser. In the 4000–600- cm^{-1} region 0.1-mm NaCl cells were used for the solutions containing chloride and 0.08-mm KBr cells were used for the solutions containing bromide; in the 400–40- cm^{-1} region a Beckman vacuum cell with polyethylene windows and a 1-mm Teflon spacer was used. All band positions are believed accurate within $\pm 3 \text{ cm}^{-1}$ unless otherwise stated. The solutions were run *vs.* solvent as a reference. Multiple spectral runs were made of each solution.

Results

The far-infrared spectra data are given in Table I and representative spectra are shown in Figures 1 and 2. The important maxima in the mid-infrared region due to both benzoic acid and the alkylammonium cations are presented in Table II.^{6,7} Force constants for the stretching vibrations were estimated (see Discussion) and are listed in Table III. Association constants for the association of benzoic acid with the ion pairs are given in Table IV⁸ along with the molar absorptivities of the OCO deformation mode employed in their computation.

Discussion

The self-association of benzoic acid in benzene solution is well known.⁹ The equilibrium between monomeric benzoic acid and the hydrogen-bonded cyclic dimer has been thoroughly studied; the dissociation constant of the dimer is 1.53×10^{-3} at 297°K.⁹ At a benzoic acid concentration of 0.1 *M* about 10% of the acid is in the monomer form.

The far-infrared spectrum of a benzoic acid solution shows but one absorption maximum (Figure 1C). This has

- (5) I. M. Kolthoff and E. B. Sandell, "Textbook of Quantitative Analysis," 3rd ed, Macmillan, New York, N. Y., 1952, p 542.
- (6) D. Hadzi and M. Pintar, *Spectrochim. Acta*, **12**, 162 (1958).
- (7) R. A. Work, III, and R. L. McDonald, *J. Inorg. Nucl. Chem.*, **34**, 3123 (1972).
- (8) F. E. Croxton, "Elementary Statistics," Dover, New York, N. Y., 1953, p 114.
- (9) F. T. Wall and J. A. Banes, *J. Amer. Chem. Soc.*, **67**, 898 (1945).

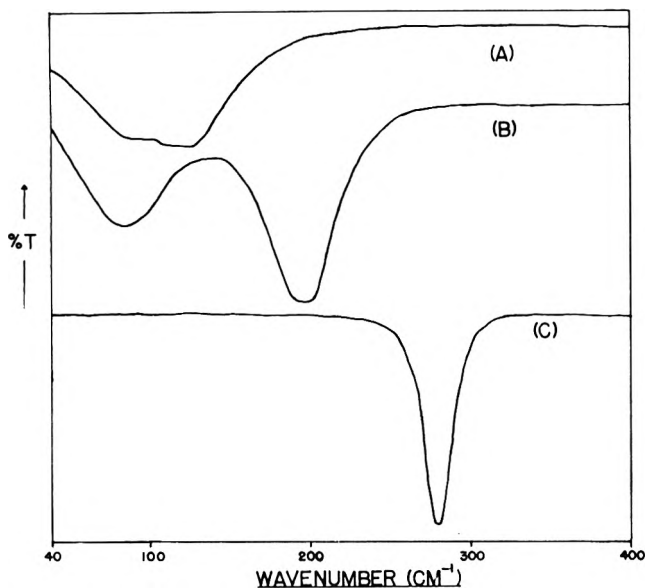


Figure 1. Far-infrared spectra of (A) 0.10 M THA+Cl⁻; (B) 0.10 M TOAH+Cl⁻; (C) 0.10 M C₆H₅COOH in benzene.

TABLE II: Mid-Ir Data For Benzene Solutions of THA+X⁻ or TOAH+X⁻ and C₆H₅CO₂H^a

Species	N-H st	C=O st	OH def	C-O st
(C ₆ H ₅ CO ₂ H) ₂	...	1700	1418	1288
C ₆ H ₅ CO ₂ H	...	1742	(1340) ^b	(1075) ^b
THA+Cl ⁻ -HO ₂ CC ₆ H ₅	...	1705	1383	1228
TOAH+Cl ⁻ -HO ₂ CC ₆ H ₅	ca. 2500 ^c	1707	1379	1224
THA+Br ⁻ -HO ₂ CC ₆ H ₅	...	1711	1373	1219
TOAH+Br ⁻ -HO ₂ CC ₆ H ₅	ca. 2500 ^c	1712	1368	1216
TOAH+Cl ⁻	ca. 2100 ^d
TOAH+Br ⁻	ca. 2400 ^d

^a All data in cm⁻¹. ^b Reference 6. ^c Approximate band centers ±30 cm⁻¹. ^d Reference 7. Very broad and structured absorptions, approximate band center given.

TABLE III: Force Constants for Ion-Pair and H Bond-Anion Vibrations

Bond	k, mdyn/Å
THA ⁺ -Cl ⁻	0.27 ^a
THA ⁺ -Cl ⁻ -HO ₂ CC ₆ H ₅	ca. 0.28
THA ⁺ Cl ⁻ -HO ₂ CC ₆ H ₅	0.38
TOAH ⁺ -Cl ⁻	0.74
TOAH ⁺ -Cl ⁻ -HO ₂ CC ₆ H ₅	0.64
TOAH ⁺ Cl ⁻ -HO ₂ CC ₆ H ₅	ca. 0.36
TOAH ⁺ -Cl ⁻ -HAOT	0.68
THA ⁺ -Br ⁻	0.28 ^a
THA ⁺ -Br ⁻ -HO ₂ CC ₆ H ₅	ca. 0.21
THA ⁺ Br ⁻ -HO ₂ CC ₆ H ₅	0.28
TOAH ⁺ -Br ⁻	0.74
TOAH ⁺ -Br ⁻ -HO ₂ CC ₆ H ₅	0.67
TOAH ⁺ Br ⁻ -HO ₂ CC ₆ H ₅	ca. 0.30

^a The higher frequency ion-pair band was used in the computation.

been attributed to a deformation mode of the OCO group of benzoic acid in the dimer form.¹⁰ It obeys Beer's law when the concentrations are corrected for dimer dissociation. Figure 3 shows least-square plots of absorbance vs. both the total acid concentration and that calculated for

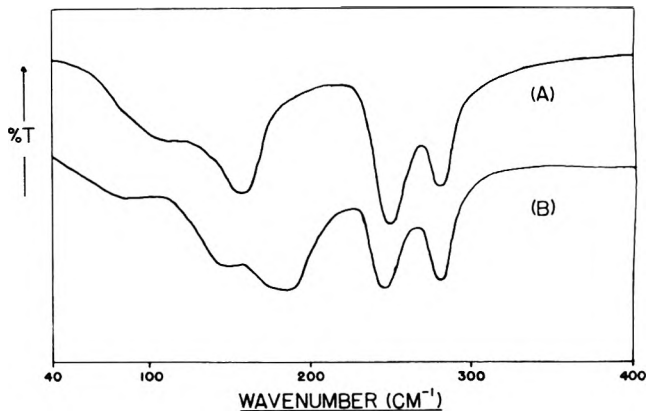


Figure 2. Far-infrared spectra of (A) 0.044 M THA+Cl⁻; (B) 0.060 M TOAH+Cl⁻ and 0.10 M C₆H₅COOH in benzene.

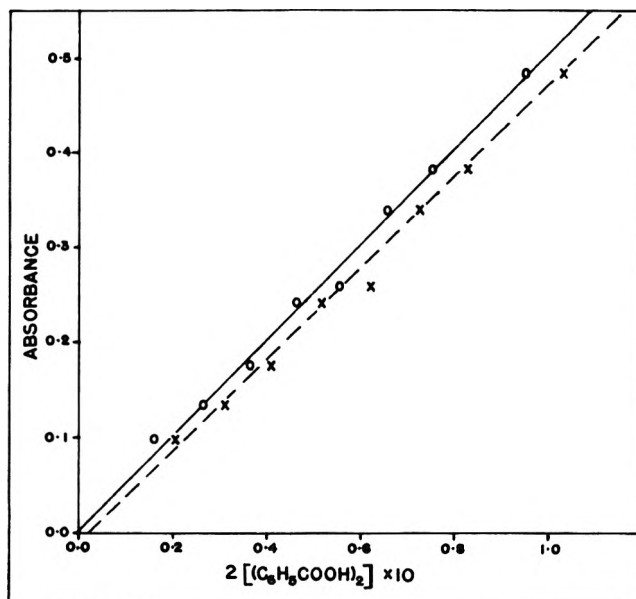


Figure 3. Beer's law plots of benzoic acid concentration vs. absorbance (OCO deformation mode) of the acid in benzene: X, stoichiometric acid concentration; O, benzoic acid dimer concentration × 2.

TABLE IV: Molar Absorptivities of the OCO Deformation Mode and Association Constants for Amine Halides and Benzoic Acid in Benzene^a

Salt	ε, l./mol cm ^b	K ₁	K ₂ ^c
None	5.01 ± 0.01 ^d
THACl	4.91 ± 0.01 ^d	> 10 ⁴	14 ± 4
TOAHCl	4.72 ± 0.35	700 ± 400	...
THABr	3.08 ± 0.15	> 10 ⁴	...
TOAHBr	2.66 ± 0.19	50 ± 30	...

^a See text for the form of the equations used. ^b Mean value ± standard deviation from the mean. ^c Dash indicates no evidence for a second association was detected. ^d Most probable value ± standard estimate of error from a least-squares plot (see ref 8).

the dimer. The latter plot, which extrapolates through the origin, confirms the absence of monomer absorption and was used for subsequent equilibrium constant calculations.

(10) W. R. McWinnie. *Spectrochim. Acta*, **22**, 501 (1966).

In addition to internal vibrations, benzoic acid in the dimer form should exhibit vibrational modes characteristic of the hydrogen bond. Solid-state spectra have been reported in which three such absorptions were observed.¹¹ They were assigned as the antisymmetric hydrogen-bond stretching mode at 107 cm^{-1} and two bending modes at *ca.* 70 and 39 cm^{-1} . For the solutions used here, no evidence of these bands was found. They are apparently too weak to be observed in our concentration range.

Tetra-*n*-heptylammonium chloride and bromide and tri-*n*-octylammonium chloride and bromide were chosen as the halide-containing salts primarily because they are sufficiently soluble in benzene to permit far-infrared studies to be done easily. They exist in solution as ion pairs or higher aggregates at the concentrations studied here.^{12a}

The spectrum of tetra-*n*-heptylammonium chloride in benzene (Figure 1A) shows one broad band with two poorly resolved maxima. For a simple X^+-Y^- type ion pair only one vibration would be anticipated.¹³ Evans and Lo^{12a} proposed that the basic ionic unit of quaternary ammonium halides in benzene solution is the ion-quadruplet possessing D_{2h} symmetry. This species has six normal vibrational modes, three of which are infrared active, two ring stretching modes, and one out-of-plane bending mode. The two overlapping maxima observed for THA^+Cl^- and THA^+Br^- correspond to the ring stretching modes; the out-of-plane bending mode is expected to be below 40 cm^{-1} . Further aggregation beyond the ion-quadruplet is assumed not to affect the far-infrared spectrum.

Tertiary ammonium salts possess considerably different spectra. McDonald, *et al.*,^{12b} studied several different tertiary ammonium salts in various low dielectric constant solvents. In all cases two maxima were observed, as shown in Figure 1. The higher frequency band was assigned as an ion-pair (hydrogen bond) stretching mode and the lower one as a hydrogen bond bending mode. These spectra do not reflect ion pair-ion pair aggregation as do the quaternary salts. Ion pair-ion pair and solvent-ion pair interactions were found to have a relatively small effect on band frequencies and no appreciable effect on band intensities.^{12b}

Spectra of mixtures of THA^+Cl^- and benzoic acid and TOAH^+Cl^- and benzoic acid (Figure 2) show bands similar to those of the salts alone in benzene and of benzoic acid alone in benzene. However, two new maxima at 251 and 154 cm^{-1} and 247 and *ca.* 150 cm^{-1} , respectively, are also present. The higher frequency band near 250 cm^{-1} has a band shape nearly identical with that of the benzoic acid dimer OCO deformation at 281 cm^{-1} . Furthermore, it increases in intensity with increasing salt concentration while the dimer band decreases in intensity. We have assigned the 250 cm^{-1} band to the OCO deformation mode of a single benzoic acid molecule hydrogen-bonded to the halide ion. The new maximum at about 150 cm^{-1} increases in intensity as the concentration of benzoic acid bound to chloride increases, and it appears at about the same position for both salts. We have assigned this band to the benzoic acid to chloride hydrogen bond stretching mode. These assignments are substantiated upon comparison with the corresponding spectra of the bromide salts (Table I). The bands shift to lower frequencies with the heavier halide ion, but the spectra are otherwise identical.

Modifications are observed in the ion-pair vibrations of both types of salts when benzoic acid is added. The lower

band in the doublet exhibited by THA^+Cl^- and THA^+Br^- appears to decrease in intensity with the addition of more and more benzoic acid, while the higher frequency band appears to be unchanged. This is due to breaking up of the ion-pair aggregates which is known to occur when polar molecules are added.¹⁴ These results support the assumption that the doublet is indeed due to aggregation. The ion-pair stretching modes in TOAH^+Cl^- and TOAH^+Br^- do not decrease in intensity as benzoic acid is added but the maxima do shift to slightly lower frequencies. This shift is a result of a decrease in ion-pair hydrogen bond strength upon solvation of the anion by benzoic acid.^{12b} More importantly, in none of these solutions is there any evidence of cation-anion separation when benzoic acid is present. We conclude that all four salts exist in solution as solvent- (*i.e.*, benzoic acid) shared and not solvent-separated ion pairs.

The mid-infrared spectra ($4000\text{--}600\text{ cm}^{-1}$) of each solution showed three maxima characteristic of the COOH group of benzoic acid: the carbonyl stretch; a mode considered as primarily an O-H deformation but highly coupled to the other modes in the COOH group; a third mode considered primarily a C-O stretch, but which is also highly coupled.⁶ For solutions containing halide, the frequencies of these bands lie between those of the dimer and the monomer of benzoic acid. The frequencies of the OH def, C-O st, (and OCO def) increase: monomer < TOAH^+Br^- < THA^+Br^- < TOAH^+Cl^- < THA^+Cl^- < dimer; the carbonyl stretch varies in the reverse order. This agrees with the expected order of benzoic acid hydrogen bond strength: $\text{Cl}^- > \text{Br}^-$ and weak ion pair (THA^+X^-) > strong ion pair (TOAH^+X^-). Finally, the N-H stretching bands of TOAH^+Cl^- and TOAH^+Br^- were found to shift to higher frequency (indicating a weakening of the N-H hydrogen bond to halide) upon solvation by benzoic acid.

Difficulties are encountered when one tries quantitatively to correlate ion-pair and hydrogen-bond vibrational data with bond strengths. First we must decide whether a few atoms or the entire masses of the molecules and ions are involved in the vibration. Examples of both types have been reported in the literature.¹⁵ For ion-pair vibrations of the type involved here, inclusion of the entire mass of both anion and cation in the reduced mass expression of the harmonic oscillator approximation¹³ leads to acceptable results^{12b} (Table III). The inclusion of only part of the cation mass would lead to force constants of unreasonably high values compared to other systems.¹⁶ Benzoic acid in the dimer form exhibits a hydrogen bond stretching mode which behaves similarly, that is as a vibration of one rigid molecule against the other.¹¹ Therefore we propose that a treatment which assumes all internal cation and acid vibrational force constants are infinite (*i.e.*, a rigid molecule approximation) should apply to the systems being discussed here.

(11) A. E. Stanevich, *Opt. i Spektrosk.*, **16**, 446 (1964).

(12) (a) J. C. Evans and G. Y.-S. Lo, *J. Phys. Chem.*, **69**, 3223 (1965); (b) J. R. Kludt, G. Y. W. Kwong, and R. L. McDonald, *ibid.*, **76**, 339 (1972).

(13) K. Nakamoto, "Infrared Spectra of Inorganic and Coordination Compounds," 2nd ed, Wiley-Interscience, New York, N. Y., 1970, p. 8.

(14) A. Allerhand and P. von R. Schleyer, *J. Amer. Chem. Soc.*, **85**, 1233 (1963).

(15) (a) G. C. Pimentel and A. L. McClellan, "The Hydrogen Bond," Freeman, San Francisco, Calif., 1960; (b) G. C. Pimentel and A. L. McClellan, *Annu. Rev. Phys. Chem.*, **22**, 347 (1971).

(16) M. J. French and J. L. Wood, *J. Chem. Phys.*, **49**, 2338 (1968).

The simplest model for the solvated ion pair is $C^+ \cdots A^- \cdots HO_2CC_6H_5$, a linear triatomic model of the XYZ type. Two stretching and one bending mode are required, all of which are infrared active. However, a valence force field calculation¹⁷ of force constants using the entire masses of the species involved yields imaginary force constants. An alternative approach is to assume two simple diatomic systems very weakly coupled. First the solvated ion pair is treated as simply a weakened ion pair. This should be true if the solvent-anion force constant is small, which of course it must be. The solvent-anion vibration is then treated in a similar manner, ignoring the cation-anion bond. That is, the reduced mass expressions include only the two bodies directly involved in the vibration with zero contribution, *i.e.*, zero coupling, from the third body. The force constants so calculated are included in Table III. The inclusion of any significant mass contribution from the benzoic acid in the reduced mass expression for the solvated ion pair would yield a higher force constant for the solvated ion pairs than for the unsolvated ion pairs. This result is to us unreasonable.

It is difficult to compare the k values for solvated *vs.* unsolvated quaternary ammonium halides (Table III); there are large uncertainties in the values for the solvated salts. It can be said that there appears to be no drastic change in bond strength. This is not true for the tertiary ammonium salts. Both show a marked decrease in cation-anion bond strength when solvation occurs, the bromide salt being somewhat less affected than the chloride. For comparison, the mixed dimer⁷ $(TOAH)_2Cl^+$ force constant computed in the same manner is included. The k ion-pair values decrease in the order $TOAH^+Cl^- > (TOAH^+)_2Cl^- > TOAH^+Cl^-HO_2CPh$.

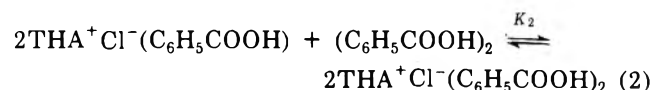
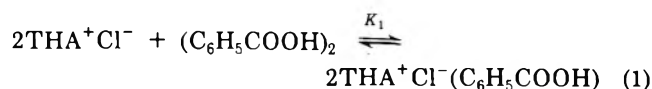
The anion-benzoic acid bond strengths show very little cation dependence but substantial anion dependence. The chloride-acid bond is stronger than the bromide-acid bond as expected. Both the magnitudes and trends in the force constant values seem reasonable and support the view that the two body approximation is applicable to systems of this type.

Formation constants of hydrogen-bonded systems are often determined by utilizing the "free" or nonhydrogen bonded O-H stretching maximum in the mid-infrared region.^{15,18} For the present study we chose instead to use another internal mode of the acid, the OCO deformation of the dimer at 281 cm^{-1} . This proves to be a particularly powerful approach since the OCO deformation of the acid hydrogen-bonded to a halide ion also obeys Beer's law; the concentration of dimer and of acid hydrogen-bonded to halide ion can be determined independently. The equilibrium constant for the monomer-dimer is also known; thus the monomer concentration can be computed and the sum of the three can be compared with the total acid present in the solution.

Errors in species concentrations obtained in this way come largely from the selection of a base line. A successive approximation method was developed to correct the originally chosen base line so as to normalize the sum of the three acid concentrations to the total acid concentration. This correction is small (usually about 0.01 absorbance unit) and was added to or subtracted from the absorbances of both the dimer and the acid hydrogen bonded to halide ion. This reduced considerably the average deviations in absorbances measured repeatedly for the same solutions.

The molar absorptivity of the OCO deformation for acid bound to THA^+Cl^- was determined directly by varying the amount of acid from 0.02 to 0.06 *M* keeping the THA^+Cl^- concentration at 0.1 *M*. Under these conditions essentially all of the acid is bound to the chloride ion. For the other cases it was necessary to use a less precise technique. The molar absorptivities were determined for each spectrum by choosing a base line, estimating the dimer and monomer concentrations, and computing the concentration of acid bound to halide ion by difference. The average values (of several determinations) of the molar absorptivities so calculated were then used to recalculate new base lines and species concentrations as before. The calculated mean values of the final OCO deformation molar absorptivities and their standard deviations from the mean are listed in Table IV. The values obtained for $TOAH^+Cl^-$ and $TOAH^+Br^-$ have the greatest uncertainties due to the overlapping ion-pair stretching band.

Over the concentration ranges studied, the average number of acids bound to halide, \bar{n} , was never greater than unity except with THA^+Cl^- . For this salt an attempt to compute the two successive association constants by standard methods¹⁹ was not successful; the first association constant is too large. For THA^+Cl^- the equilibria are



For the other salts only eq 1 is required. The values of K_i so calculated are independent of salt concentration; they are listed in Table IV. As expected, the weaker ion pair appears to require solvation more, as does the smaller anion.

(17) G. Herzberg, "Molecular Spectra and Molecular Structure. II. Infrared and Raman Spectra of Polyatomic Molecules," Van Nostrand, New York, N. Y., 1945, p 173.

(18) J. Wenograd and R. A. Spurr, *J. Amer. Chem. Soc.*, **79**, 5844 (1957).

(19) F. J. C. Rossotti and H. Rossotti, "The Determination of Stability Constants," McGraw-Hill, New York, N. Y., 1961, p 89.

Photolysis of Nitrogen Dioxide to Produce Transient O, NO₃, and N₂O₅

Alan B. Harker and H. S. Johnston*

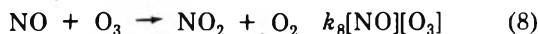
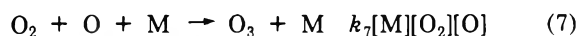
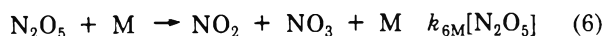
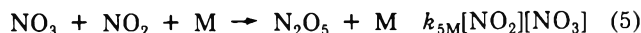
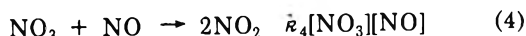
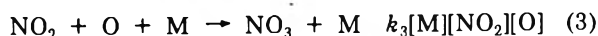
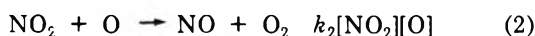
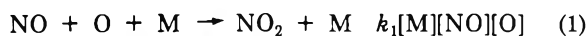
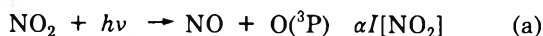
Department of Chemistry and Inorganic Materials Research Division, Lawrence Berkeley Laboratory, University of California, Berkeley, California 94720 (Received December 27, 1972)

Publication costs assisted by The University of California

Nitrogen dioxide was photolyzed at room temperature in a long-path infrared cell. The concentrations of nitrogen dioxide and nitrogen pentoxide (N₂O₅) were followed as a function of time, and the molecular modulation spectrum of nitrogen dioxide was obtained in a steady-flow experiment. With 1 atm of nitrogen, the observations were the rate constant ratios and standard deviations: $k_1[M]/k_2 = 0.18 \pm 0.01$, $k_3[M]/k_2 = 0.22 \pm 0.01$, $k_4/K = 0.71 \pm 0.05 \text{ sec}^{-1}$ where (1) $\text{NO} + \text{O} + \text{M} \rightarrow \text{NO}_2 + \text{M}$; (2) $\text{NO}_2 + \text{O} \rightarrow \text{NO} + \text{O}_2$; (3) $\text{NO}_2 + \text{O} + \text{M} \rightarrow \text{NO}_3 + \text{M}$; (4) $\text{NO}_3 + \text{NO} \rightarrow 2\text{NO}_2$; $K = ([\text{N}_2\text{O}_5]/[\text{NO}_2][\text{NO}_3])_{\text{eq}}$. By using literature values for k_1 ($6.9 \times 10^{-32} \text{ cm}^3 \text{ molecule}^{-1} \text{ sec}^{-1}$) and for K ($1.24 \times 10^{-11} \text{ cm}^{-3}$), the values of the elementary rate constants are $k_2 = 9.2 \times 10^{-12} \text{ cm}^3 \text{ molecule}^{-1} \text{ sec}^{-1}$, $k_3 = 8.2 \times 10^{-32} \text{ cm}^6 \text{ molecule}^{-2} \text{ sec}^{-1}$, and $k_4 = 8.7 \times 10^{-12} \text{ cm}^3 \text{ molecule}^{-2} \text{ sec}^{-1}$.

Introduction

The photolysis of nitrogen dioxide is a key reaction in photochemical air pollution,¹ is important in stratospheric photochemistry,² and is often used in the laboratory to measure light intensity between 300 and 400 nm. The reaction is complex, and there is disagreement in the literature as to the value of certain rate constants and rate-constant ratios. There is agreement in the literature³⁻⁵ that the following mechanism describes the overall kinetics of the photolysis of small amounts of NO₂ in an inert carrier gas



where α includes the absorption cross section σ and the quantum yield ϕ . The purpose of this study was to examine this system with the molecular modulation technique,⁶ and in particular to focus on the rate constants for reactions 2, 3, and 4 at room temperature.

Quantities measured in this study were the decay of NO₂, the buildup and decay of N₂O₅, and the molecular modulation of NO₂ during intermittent illumination of a steady-flow system. In terms of the mechanism these measurements give the following information. At low pressures (below 50 Torr) the M gas dependent reactions (1 and 3) become negligible compared to reaction 2, and the decay of nitrogen dioxide can be described by

$$\left(\frac{d[\text{NO}_2]}{dt}\right)_{t \rightarrow 0} = -\alpha I \quad (\text{I})$$

At 1 atm total pressure and with small initial NO concentration, the disappearance of NO₂ is given (by reactions a, 1, 2, 3, and 5) as a good approximation by

$$\ln \frac{[\text{NO}_2]}{[\text{NO}_2]_0} = \frac{-2\alpha I t}{(1 + k_3[\text{M}]/k_2)} = -k_a t \quad (\text{II})$$

where k_a is the empirical, first-order, decay constant. If the initial concentration of nitric oxide is close to zero, the initial rate of formation of dinitrogen pentoxide is

$$\left(\frac{d[\text{N}_2\text{O}_5]}{dt}\right)_{t \rightarrow 0} = \frac{\alpha I [\text{NO}_2]}{(1 + k_2/k_3[\text{M}])} \quad (\text{III})$$

At an early stage of the reaction ($t = t^*$) dinitrogen pentoxide goes through a maximum, at which point

$$\left(\frac{[\text{N}_2\text{O}_5]}{[\text{NO}_2]}\right)^* = \frac{\alpha I (K/k_4)}{(1 + k_2/k_3[\text{M}])} \left(\frac{[\text{NO}_2]}{[\text{NO}]}\right)^* \quad (\text{IV})$$

where reactions a and 1-6 are included and where $K = k_5/k_6$. The modulation amplitude of nitrogen dioxide in a steady-flow system illuminated with square-wave photolyzing light of frequency f is

$$\frac{\Delta[\text{NO}_2]}{[\text{NO}_2]} = \frac{4\alpha I / \pi^2 f}{1 + \frac{k_1[\text{NO}]}{k_2[\text{NO}_2]} + \frac{k_3[\text{M}]}{k_2}} \quad (\text{V})$$

It can be seen that eq I gives αI ; with αI so determined, eq II and III give two independent measures of the ratio k_2/k_3 ; the combination of eq I, II, and V gives k_1/k_2 .

Thus by solving the five experimental relationships simultaneously, it is possible to obtain values for αI , k_4/K , k_1/k_2 , and k_3/k_2 , with one equation redundant to use as a check. By taking the literature values for k_1 and for the

- (1) A. J. Hagen-Smit, *Ind. Eng. Chem.*, **44**, 1342 (1952).
- (2) (a) M. Nicolet, *J. Geophys. Res.*, **70**, 679 (1965); (b) P. J. Crutzen, *Quart. J. Roy. Met. Soc.*, **96**, 320 (1970); (c) H. S. Johnston, *Science*, **173**, 517 (1971).
- (3) T. C. Hall, Jr., "Photochemical Studies of Nitrogen Dioxide and Sulfur Dioxide," Ph.D. Thesis, University of California, Los Angeles.
- (4) H. W. Ford and N. Endow, *J. Chem. Phys.*, **27**, 1156, 1277 (1957).
- (5) J. Troe, *Ber. Bunsenges. Phys. Chem.*, **73**, 906 (1969).
- (6) H. S. Johnston, G. E. McGraw, T. T. Paukert, L. W. Richards, and J. Van den Bogaerde, *Proc. Nat. Acad. Sci., U.S.A.*, **57**, 1146 (1967).

equilibrium constant K , it is possible to obtain the elementary rate constants k_2 , k_3 , and k_4 . Reactions 7 and 8 are not significant in this system.

Experimental Section

The instrument used in this work is a long-path molecular modulation infrared spectrometer. A block diagram of the apparatus is shown in Figure 1. The reaction cell is a cylindrical quartz tube 91 cm long and 28.7 cm in diameter, with a volume of 67.0 l. The cell is equipped with gold-coated multiple-reflection mirrors which give it a spectroscopic path length adjustable from 4 to 40 m. The source of the ir radiation is a Nernst glower which is chopped at 400 cps by an American Time Products tuning fork. The monochromator is a McPherson Model 2051, 1-m grating monochromator equipped with a 150-line per mm grating and order sorting filters. The ir detector is a liquid helium cooled, copper-doped germanium photoconductor produced by the Santa Barbara Research Center.

The photolytic light for these experiments was supplied by four, 32-in. G.E. 30-W, F30T8/BL black lamps. The photolytic photon flux in the cell is on the order of 10^{16} photons/cm² sec. The photolysis lamp output for the cell is monitored by a phototransistor, which can be used as a reference to detect fluctuations in the lamp intensities. The photolysis lamps are driven by a regulated power supply which can electronically switch them on and off in response to a reference square wave from a crystal oscillator.

The electronics for the instrument are designed to detect the periodic concentration fluctuations in the absorbing gases in the cell which are induced by the flashing of the photolysis lamps. This is done by two sequential stages of demodulation. The 400-cps ac signal from the detector carries the modulation information on sidebands at $400 \pm f$ cps, where f is the frequency of the flashing lamps. The first demodulation is carried out by a 400-cps lock-in amplifier which produces a dc signal directly proportional to the spectroscopic light intensity. Riding on this dc signal as a low-frequency ripple is the modulation information. This dc signal is split in two with one component being recorded while the other is ac coupled, filtered, and sent into the second stage of demodulation. The second-stage demodulator is a set of two lock-ins, operating at frequency f , with one lock-in reference in

phase with the photolysis lamps and one reference exactly 90° out of phase. The outputs of these two lock-ins represent the amplitude of the sine and cosine components of the first fundamental of the modulation signal. From these values the phase shift and amplitude of the modulation signal can be calculated. The output of all three lock-in amplifiers are recorded and time averaged in a signal averaging computer.

The carrier gases used in the experiments were high-purity nitrogen and argon, both of which are passed through a Matheson water-and-particulate removal filter before use. The nitrogen dioxide used in the closed cell photolysis experiments was prepared by vacuum distillation from bulk liquid N₂O₄. The NO₂ used in the flow experiments was commercial mixed gas supplied by Matheson. The gas was analyzed by ir and uv spectroscopy in this laboratory and found to contain 970 ± 5 ppm of NO₂ and 38 ± 4 ppm of NO, with the remainder being N₂. The concentrations of all NO_x species involved in this work were determined spectroscopically from calibration curves measured in this laboratory.

Results

A series of experiments was carried out in the closed cell with low total pressure, 19–56 Torr. The decay of NO₂ was first order throughout an experiment, and the results are listed in Table I. When NO₂ is photolyzed in a closed cell at 1 atm, the initial decay is first order, but deviations from first-order kinetics appear at later times, as illustrated by Figure 2. (The concentration of NO₂ was followed by infrared absorption at 1600 cm⁻¹.) Data for a series of experiments of this type are included in Table I.

The buildup and decay of N₂O₅ is illustrated by Figure 3 for conditions at 1 atm total pressure (N₂) and 24°. The concentration of N₂O₅ was followed by infrared absorption at 1238 cm⁻¹. The initial rate of formation of N₂O₅ is given in Table II, and the concentrations of NO, NO₂, and N₂O₅ at the maximum value of N₂O₅ are given in Table III. A plot of $([N_2O_5]/[NO_2])^*$ against $([NO_2]/[NO])^*$ is given as Figure 4 (compare eq IV).

Along with these conventional measurements, a molecular-modulation study of NO₂ photolysis was carried out. The molecular-modulation method consists of monitoring the periodic concentration fluctuations induced in the reacting species by flashing the photolysis lamps on and off. In this work the NO₂ modulation was studied in a steady-flow system with the photolysis lamps flashing at 1 cps. Under these conditions the NO₃ radicals and oxygen atoms will be at their steady-state concentrations and N₂O₅ will be equilibrium.

The behavior of the concentration modulation of NO₂ can be described by a differential equation with the flashing lamps represented by the Fourier series for a square wave

$$\frac{d[NO_2]}{dt} = \frac{F}{V} \{ [NO_2]_{in} - [NO_2]_{out} \} - \left(\frac{k_2[NO_2]^2}{k_1[NO][M] + (k_2 + k_3[M])[NO_2]} \right) \times \left(\frac{2\alpha\pi}{I} \sum_{\text{odd } n} \frac{1}{n} \sin(n\omega t) + \alpha I \right) \quad (VI)$$

with F = flow rate of chemicals; V = volume of the reaction cell; $[NO_2]_{in}$ = the NO₂ concentration flowing into the cell; $[NO_2]_{out}$ = the NO₂ concentration flowing out of

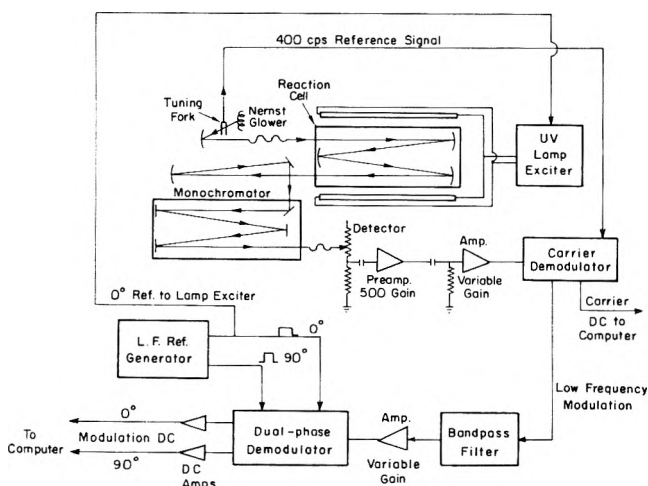
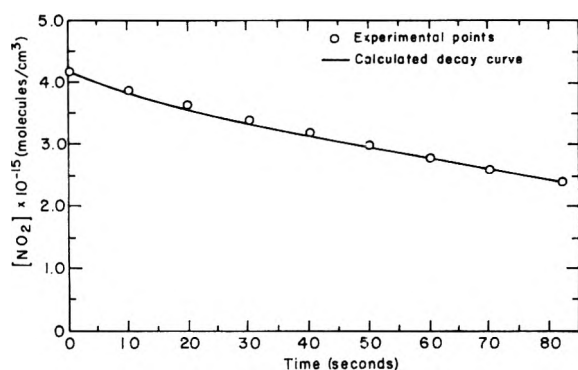
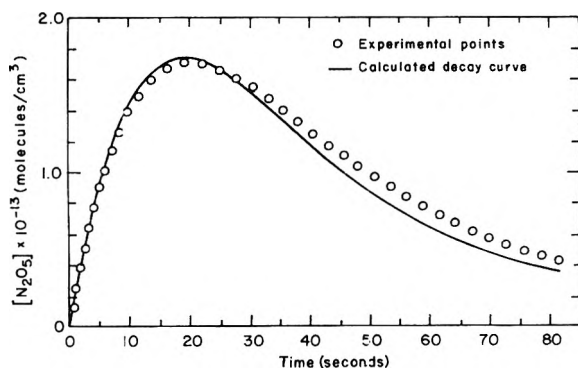


Figure 1. Schematic diagram of experimental apparatus.

TABLE I: Initial Rate of Decay of NO₂ as a Function of Pressure^a

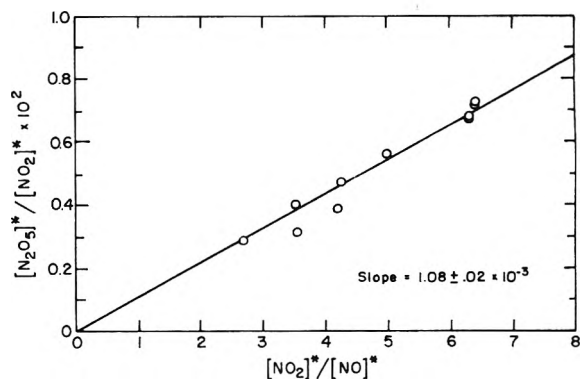
[NO ₂], molecules cm ⁻³	Total pressure, Torr	Relative light nt.	k _a , sec ⁻¹ (eq II)
8.6 × 10 ¹⁴	19.5	1.00	1.47 × 10 ⁻²
8.8 × 10 ¹⁴	19.5		1.44 × 10 ⁻²
4.8 × 10 ¹⁴	22		1.50 × 10 ⁻²
8.8 × 10 ¹⁴	27		1.52 × 10 ⁻²
12 × 10 ¹⁴	56		1.52 × 10 ⁻²
6.7 × 10 ¹⁴	756	1.00	1.23 × 10 ⁻²
9.6 × 10 ¹⁴	756		1.20 × 10 ⁻²
10.5 × 10 ¹⁴	756		1.25 × 10 ⁻²
11.6 × 10 ¹⁴	756		1.22 × 10 ⁻²
2.1 × 10 ¹⁴	756	0.56	0.69 × 10 ⁻²
2.4 × 10 ¹⁴	756		0.71 × 10 ⁻²
3.1 × 10 ¹⁴	756		0.68 × 10 ⁻²
19.7 × 10 ¹⁴	756		0.68 × 10 ⁻²

^a Temperature, 24°; NO₂ followed by infrared absorption at 1600 cm⁻¹

Figure 2. NO₂ decay; comparison of experimental points and calculated curve based on rate constants in Table VIII. Initial concentration of [NO₂] = 4.2 × 10¹⁵ and [NO] = 2.05 × 10¹⁴

Figure 3. N₂O₅ decay as observed by infrared absorption at 1237 cm⁻¹; comparison of experimental points and calculated curve based on rate constants in Table VIII. Initial concentration of NO₂ = 2.8 × 10¹⁵ molecules cm⁻³ and [NO] = 0.

 the cell; $\omega = 2\pi/T$, where T is the period of the square wave.

This equation neglects the ozone reactions, since the system contains no initial oxygen and the O₃ buildup will not be significant. Under these conditions the flow system has reached a steady state with respect to reactants and products, so the unmodulated or dc terms in eq VI cancel leaving only the modulation or ac terms

$$\frac{d[\text{NO}_2]_{AC}}{dt} = \frac{-\alpha I 2k_2[\text{NO}_2]^2 \sum_{\text{odd } n} \frac{1}{n} \sin(n\theta)}{\pi^2 f \{k_1[\text{NO}][\text{M}] + (k_2 + k_3[\text{M}])[\text{NO}_2]\}} \quad (\text{VII})$$



The * indicates the concentration at the time of the N₂O₅ concentration maximum, t*

Figure 4. Concentration ratios where nitrogen pentoxide is a maximum (eq IV).

TABLE II: Initial Rate of Formation of N₂O₅

[NO ₂], molecules cm ⁻³	lim(d[N ₂ O ₅]/dt) _{t→0} /[NO ₂], sec ⁻¹	[NO ₂], molecules cm ⁻³	lim(d[N ₂ O ₅]/dt) _{t→0} /[NO ₂], sec ⁻¹
1.91 × 10 ¹⁵	0.73 × 10 ⁻³	2.8 × 10 ¹⁵	0.63 × 10 ⁻³
2.5 × 10 ¹⁵	0.69 × 10 ⁻³	3.3 × 10 ¹⁵	0.70 × 10 ⁻³
2.6 × 10 ¹⁵	0.64 × 10 ⁻³	3.3 × 10 ¹⁵	0.79 × 10 ⁻³

TABLE III: Conditions at Maximum Concentration of N₂O₅

Initial concn		Concn at N ₂ O ₅ maximum		
[NO ₂] × 10 ⁻¹⁵ , molecules cm ⁻³	[NO], × 10 ⁻¹⁴ , molecules cm ⁻³	[N ₂ O ₅] × 10 ⁻¹³ , molecules cm ⁻³	[NO ₂] × 10 ⁻¹⁵ , molecules cm ⁻³	Ratio [NO][N ₂ O ₅]/[NO ₂] ² × 10 ³
3.28	0.0	2.1	2.82	1.14
3.26	0.0	2.0	2.79	1.13
2.50	0.0	1.43	2.13	1.06
2.84	0.0	1.66	2.43	1.08
1.85	8.1	0.89	1.59	1.11
1.61	10.2	0.65	1.37	1.11
2.56	16.5	0.84	2.21	0.91
2.56	25.2	0.68	2.19	0.87
2.26	25.8	0.80	1.95	1.16
2.36	40.8	0.57	2.00	1.05

where $d\theta = 2\pi f dt$; $\theta = \omega t$; and f = flashing frequency.

Selecting the conditions so that the modulation will be less than one part per thousand leaves the reactant concentrations essentially constant, allowing eq VII to be integrated in closed form to give

$$[\text{NO}_2]_{AC} = \frac{-\alpha I [\text{NO}_2]^2 k_2 \sum_{\text{odd } n} n^{-2} \cos(n\theta)}{\pi^2 f \{k_1[\text{NO}][\text{M}] + (k_2 + k_3[\text{M}])[\text{NO}_2]\}} \quad (\text{VIII})$$

By electronically filtering out all but the first Fourier component of the modulation signal, and taking the peak-to-peak amplitude gives the experimental relationship

$$[\text{NO}_2]_{\text{mod}} = \frac{4\alpha I k_2 [\text{NO}_2]^2}{\pi^2 f \{k_1[\text{NO}][\text{M}] + (k_2 + k_3[\text{M}])[\text{NO}_2]\}} \quad (\text{IX})$$

Comparison of eq VIII and VI shows the NO₂ modulation wave form to be triangular, phase shifted 90° from the exciting light. The amplitude of this wave form and its phase shift from the exciting light can be determined experimentally and related to eq IX

TABLE IV: Data for NO₂ Modulation at 1 atm Total Pressure, 24°

Carrier gas	Steady-state concn		$k_a, \text{sec}^{-1} \times 10^3$	Phase shift, deg	$\Delta [\text{NO}_2]_{\text{mod}}, \times 10^{-11}$	$k_1[M]/k_2$
	$[\text{NO}_2], \times 10^{-14}$	$[\text{NO}], \times 10^{-15}$				
N ₂	1.02	0.74	8.3	93.6	1.43	0.163
N ₂	1.19	1.22	8.3	89	1.31	0.179
N ₂	0.68	1.49	8.3	70	1.40	0.189
N ₂	1.13	2.04	8.3	82	0.83	0.185
N ₂	1.87	2.12	8.3	80	1.62	0.190
N ₂	1.68	1.60	7.2	94	1.68	0.178
Ar	1.55	1.38	8.3	88.2	1.78	0.190
Ar*	2.12	1.30	4.6	87.8	1.65	0.206
Ar	1.34	1.34	8.3	91.8	1.41	0.198

TABLE V: Observed Rate Constant and Rate-Constant Ratios

Rate constant function	Observed value	Based on eq	Source of data	Condition
αI	$7.45 \times 10^{-3} \text{ sec}^{-1}$	I	Table I	
k_a	$1.22 \times 10^{-2} \text{ sec}^{-1}$	II	Table I	1 atm of N ₂
$k_3[M]/k_2$	0.22	II	Table I	1 atm of N ₂
k_3/k_2	8.9×10^{-21}	II		N ₂ = M
$k_3[M]/k_2$	0.20	III	Table II	1 atm of N ₂
k_3/k_2	8.1×10^{-21}	III		N ₂ = M
k_4/K	0.71 sec^{-1}	IV	Table III, Figure 4	
$k_1[M]/k_2$	0.18	V	Table IV	1 atm of N ₂
k_1/k_2	7.3×10^{-21}	V		N ₂ = M
$k_1[M]/k_2$	0.20	V	Table IV	1 atm of Ar
k_1/k_2	8.1×10^{-21}	V		Ar = M

TABLE VI: Comparison of the Results of This Work with the Literature Values^a

$k_1[M]/k_2$	$k_3[M]/k_2$	$k_4/K, \text{sec}^{-1}$	$T, ^\circ\text{K}$	Ref
0.18 ± 0.01	0.221 ± 0.005	0.71 ± 0.02	296	This work
0.18 ± 0.004	0.33 ± 0.08		296	7
0.10 ± 0.05	0.27 ± 0.03		295	5
0.36	1.9		300	4
		0.60 ± 0.06	296	8

^a Total pressure = 1 atm, M gas = nitrogen.

A summary of the steady-state concentrations with the phase shift and amplitude measurements are recorded in Table IV. The photolytic light intensity for the modulation experiments was found to be 11.2% greater than in the initial slope experiments, when measured by the phototransistor mounted in the cell, and the values of αI have been normalized by this factor.

Discussion

The observed rate constant ratios are assembled in Table V. The two independent values of k_3/k_2 agree within 10%; the value based on eq II was more precise and is preferred. The three observed ratios, k_1/k_2 , k_3/k_2 , and k_4/K , are compared with values reported in the literature in Table VI.^{4,5,7,8}

This study gives only rate ratios. To evaluate absolute values of rate constants, either k_1 , k_2 , or k_3 must be taken from the literature. Of the three, the most extensive and most precise data are those for k_1 . Literature values are

TABLE VII: Observed Values of k_1 ^a

$k_1, \text{cm}^6 \text{ molecule}^{-2} \text{ sec}^{-1}$	M gas	$T, ^\circ\text{K}$	Ref
$7.0 \pm 0.08 \times 10^{-32}$	O ₂ , N ₂ , Ar	296	9
$7.6 \pm 0.05 \times 10^{-32}$	Ar, O ₂	300	10
$6.4 \pm 0.8 \times 10^{-32}$	O ₂	297	11
$7.3 \pm 0.9 \times 10^{-32}$	N ₂	297	11
$5.1 \pm 0.2 \times 10^{-32}$	O ₂ , He, Ar	293	12
5.3×10^{-32}	Ar	298	13
6.1×10^{-32}	N ₂	298	14
$10.0 \pm 0.14 \times 10^{-32}$	N ₂	296	15

^a Average value = $6.9 \times 10^{-32} \text{ cm}^6/\text{molecule}^2/\text{sec}$.

TABLE VIII: Elementary Rate Constants for Nitrogen Dioxide Photolysis (297°K, 1 atm of N₂)

Constant	Value	Source	Ref
k_1	$6.9 \times 10^{-32} \text{ cm}^6 \text{ sec}^{-1}$	Literature	9-15
k_2	$9.2 \times 10^{-12} \text{ cm}^3 \text{ sec}^{-1}$	$k_1, k_1/k_2$	Table V
k_3	$8.2 \times 10^{-32} \text{ cm}^6 \text{ sec}^{-1}$	$k_2, k_3/k_2$	Table V
K	$1.24 \times 10^{-11} \text{ cm}^{-3}$	Literature	16
k_4	$8.7 \times 10^{-12} \text{ cm}^3 \text{ sec}^{-1}$	$K, k_4/K$	Table V
k_{6M}	0.104 sec^{-1}	Literature	17
k_{5M}	$1.29 \times 10^{-12} \text{ cm}^3 \text{ sec}^{-1}$	K, k_{6M}	
k_7	$6.24 \times 10^{-34} \text{ cm}^6 \text{ sec}^{-1}$	Literature	18
k_8	$2.1 \times 10^{-14} \text{ cm}^3 \text{ sec}^{-1}$	Literature	19

summarized in Table VII,⁹⁻¹⁵ and the value $6.9 \times 10^{-32} \text{ cm}^6 \text{ molecule}^{-2} \text{ sec}^{-1}$ was taken for N₂ as foreign gas at room temperature. The observed quantity k_4/K is reduced to k_4 by the literature value of K . With these values of K and k_1 , the elementary rate constants k_2 , k_3 , and k_4 are evaluated and listed in Table VIII⁹⁻¹⁹ with the other eight elementary rate constants in this system.

With these eight elementary reactions, a computer program was written that integrated the simultaneous rate equations to give NO₂ and N₂O₅ as a function of time. In Figures 2 and 3 the circles represent observations and the smooth curves are those calculated from the elementary rate constants in Table VIII. There is good agreement between the calculated and observed curves over the full course of observations.

Acknowledgment. This work was supported in part by the U. S. Atomic Energy Commission through the Inorganic Materials Research Division, Lawrence Berkeley Laboratory, and in part by AP-104 Air Pollution Control Office, Environmental Protection Agency.

- (7) E. A. Schuck, E. R. Stephens, and R. R. Schrock, *J. Air Pollut. Contr. Ass.*, **16**, 695 (1966).
- (8) I. C. Hisatsune, B. Crawford, Jr., and R. A. Ogg, Jr., *J. Amer. Chem. Soc.*, **79**, 4648 (1957).
- (9) F. Kaufman, *Proc. Roy. Soc., Ser. A*, **247**, 123 (1958).
- (10) P. Hastek, R. R. Reeves, and G. G. Mannella, Air Force Cambridge Research Center, Technical Report No. AFCRC-TR60-264 (1960).
- (11) M. A. A. Clyne and B. A. Thrush, *Proc. Roy. Soc., Ser. A*, **269**, 404 (1962).
- (12) E. A. Ogryzlo and H. I. Schiff, *Can. J. Chem.*, **37**, 1690 (1959).
- (13) S. Takahashi and S. Miyazaki, *Mem. Def. Acad., Jap.*, **8**, 611 (1968).
- (14) S. Takahashi, *Mem. Def. Acad., Jap.*, **8**, 777 (1968).
- (15) F. S. Klein and J. T. Herron, *J. Chem. Phys.*, **41**, 1285 (1964).
- (16) G. Schott and N. Davidson, *J. Amer. Chem. Soc.*, **80**, 1841 (1958).
- (17) R. L. Mills and H. S. Johnston, *J. Amer. Chem. Soc.*, **73**, 938 (1951).
- (18) H. S. Johnston, "Gas Phase Reaction Kinetics of Neutral Oxygen Species," NSRDS-National Bureau of Standards, 20.
- (19) H. S. Johnston and H. J. Crosby, *J. Chem. Phys.*, **22**, 689 (1954).

Torsional Frequencies and Conformational Equilibria of Ortho-Substituted Phenols

Gerald L. Carlson*

Mellon Institute of Science, Carnegie-Mellon University, Pittsburgh, Pennsylvania 15213

and William G. Fateley

Department of Chemistry, Kansas State University, Manhattan, Kansas 66506 (Received January 8, 1973)

In a recent publication [*J. Phys. Chem.*, **76**, 1553 (1972)], the use of torsional frequencies in determining the enthalpy differences between the cis and trans forms of the ortho halophenols was described. This study has now been extended to include several additional ortho-substituted phenols. Torsional frequencies and barriers to internal rotation are presented for *o*-methoxy-, -ethoxy-, -phenyl-, -cyano-, -*tert*-butyl-, -methyl-, -trifluoromethyl-, -2-*tert*-butyl-6-methyl-, -2,6-dimethyl-, and -2,3-diphenylphenols. For those molecules where cis and trans isomers are possible, the enthalpy differences between the isomeric forms are evaluated and compared.

Introduction

In a recent paper, we reported on the value of far-infrared torsional frequencies in the study of intramolecular hydrogen bonding and cis-trans isomerism in *o*-halophenols.¹ However, in addition to the halogens, there are many other groups which also give rise to the possibility of cis and trans forms for ortho-substituted phenols. Putnam² and Krueger and Thompson³ have examined the OH stretching frequencies of a number of ortho-substituted phenols and have found that ortho groups, such as cyano, phenyl, ethoxy, *tert*-butyl, and hydroxyl, give rise to two OH stretching frequencies while for methoxy and all other alkyl substituents only one OH stretching frequency is observed. The number of OH stretching bands observed was generally taken to be indicative of the number of isomers present for a particular substituent. Ingold and Taylor have discussed the geometrical isomerism in a number of ortho-alkyl-substituted phenols and determined energy differences between the cis and trans forms of *o*-methylphenol and several *o-tert*-alkylphenols.⁴ More recently, Allinger, Maul, and Hickey⁵ have calculated the conformational properties of *o-tert*-butylphenol from dipole moment measurements and have discussed the internal rotation barriers and conformational equilibria for other ortho-alkyl-substituted phenols.

In the present study, we have observed the phenolic-OH torsional frequencies for *o*-methyl-, -trifluoromethyl-, -*tert*-butyl-, -methoxy-, -ethoxy-, -cyano-, -phenyl-, -2,6-dimethyl-, -2,6-diphenyl-, and -2-*tert*-butyl-6-methylphenol. These frequencies have been used to calculate internal rotation barriers as well as conformational equilibria for the cases where cis and trans forms are possible.

Experimental Section

Most of the phenols studied were available commercially in good purity; a few were obtained through the courtesy of Dr. A. W. Baker of the Dow Chemical Co. Authenticity of the samples was checked by comparison of their infrared spectra with published reference spectra. The *o*-methylphenol sample was also analyzed by gas-liquid chromatography and found to be 98.9% pure.

Low-frequency infrared spectra of the phenols and their phenol-OD derivatives as dilute (0.01–0.03 *M*) solutions in cyclohexane were obtained on a Digilab FTS-14 Fourier

transform spectrometer employing a 3- μ Mylar beamsplitter to cover the range 650–100 cm^{-1} . The experimental details were the same as described previously.^{1,6}

Infrared spectra in the OH stretching region for a few of the compounds were obtained on a Beckman IR-9 spectrophotometer employing 5-cm quartz cells and CCl_4 solutions. Raman spectra and depolarization ratios for *o*-methylphenol were recorded on a Cary 83 laser Raman spectrophotometer.

Results

The low-frequency infrared spectra of the ten ortho-substituted phenols are given in Table I. The frequencies for the analogous OD compounds are included. The accuracy of these frequencies will be determined by the error in choosing the band maxima, for the frequency accuracy of the Digilab FTS-14 is better than $\pm 1 \text{ cm}^{-1}$.

Far-infrared data for some of these phenols in the monomeric state have been reported previously; the torsional frequencies for *o*-phenyl- and *o*-methoxyphenol in CCl_4 solution have been given by Nyquist;⁷ torsional frequencies for *o*-methyl-, *o-tert*-butyl-, 2,6-dimethyl-, and 2-*tert*-butyl-6-methylphenol in polyethylene matrix by Jakobsen and Brasch;⁸ and the far-infrared spectra of *o*-methylphenol and 2,6-dimethylphenol by Green, *et al.*⁹ Our results, although in generally good agreement with this data, are considerably more detailed.

Our assignments of the torsional frequencies were confirmed by their shift on deuteration of the phenolic OH group. The $\nu_{\text{OH}}/\nu_{\text{OD}}$ ratios fell in the range 1.31–1.35. The torsions for *o*-cyanophenol-OH and *o*-trifluoromethyl-

- (1) G. L. Carlson, W. G. Fateley, A. S. Manocha, and F. F. Bentley, *J. Phys. Chem.*, **76**, 1553 (1972).
- (2) N. A. Putnam, *J. Chem. Soc.*, 5100 (1960).
- (3) P. J. Krueger and H. W. Thompson, *Proc. Roy. Soc., Ser. A*, **250**, 22 (1959).
- (4) K. U. Ingold and D. R. Taylor, *Can. J. Chem.*, **39**, 471 (1961); **39**, 481 (1961).
- (5) N. L. Allinger, J. J. Maul, and M. J. Hickey, *J. Org. Chem.*, **36**, 2747 (1971).
- (6) G. L. Carlson, W. G. Fateley, and F. F. Bentley, *Spectrochim. Acta Part A*, **28**, 177 (1972).
- (7) R. A. Nyquist, *Spectrochim. Acta*, **19**, 1655 (1963).
- (8) R. J. Jakobsen and J. W. Brasch, *Spectrochim. Acta*, **21**, 1753 (1965).
- (9) J. H. S. Green, D. J. Harrison, and W. Kynaston, *Spectrochim. Acta, Part A*, **27**, 2199 (1971); **28**, 33 (1972).

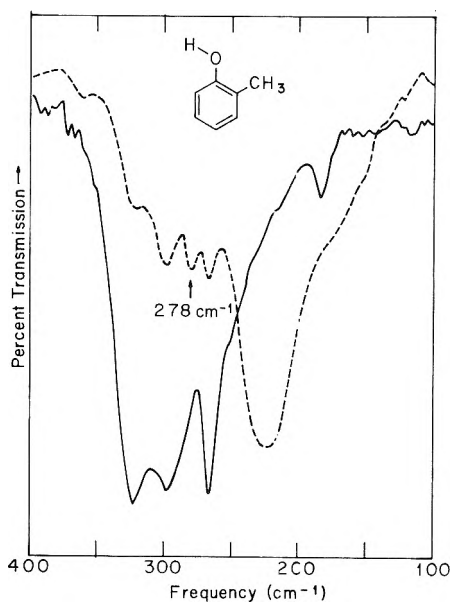


Figure 1. Far-infrared spectra of *o*-methylphenol (solid curve) and *o*-methylphenol-OD (dashed curve) in cyclohexane solution: sample concentrations $\sim 0.04 M$ path length 5 mm.

2,6-dimethyl-, and 2-*tert*-butyl-6-methylphenol-OD appear as doublets apparently due to Fermi resonance with other nearby modes. In the case of 2-*tert*-butyl-6-methylphenol only one OH torsional frequency could be found, although the presence of two OH stretching bands indicates the existence of both *cis* and *trans* forms.

The OH torsional region for *o*-methylphenol is abnormally complex and shows unusual behavior upon deuteration. The possibility that this complexity is due to impurity bands is ruled out because gas chromatographic analysis of the sample showed the purity to be 98.9%. Consequently, both the infrared and Raman spectra were studied in considerable detail in order to determine the number and positions of the torsional frequencies. The results of these studies are given in Figure 1 and Table II.

Discussion

It is well known that the phenol molecule is planar with a twofold barrier to internal rotation of about 3.5 kcal/mol.¹⁰ For ortho-substituted phenols, the presence of the ortho substituent may introduce a V_1 term in the potential function for internal rotation resulting in an unsymmetrical barrier and the possibility of *cis* and *trans* conformers. If the ortho substituent is capable of hydrogen bonding with the phenolic OH group, the *cis* form is stabilized by an energy corresponding to the strength of the intramolecular hydrogen bond. This is the usual case and the form of the potential curve for *o*-cyanophenol is shown in Figure 2. However, in the case of *o*-*tert*-butylphenol, the steric effects of the bulky *tert*-butyl group favors the *trans* isomer although the *cis* isomer still exists apparently due to the fitting of the phenolic hydrogen into the *tert*-butyl group.⁴

In a previous paper, we reported our observations of torsional frequencies for both the *cis* and *trans* forms of the ortho halophenols and showed how these frequencies could be used to evaluate the enthalpy differences between the isomeric forms.¹ We have now used the method outlined in that paper to calculate barrier heights (V_1 and V_2) and conformational equilibria for other ortho-substituted phenols which exist as mixtures of *cis* and *trans* forms. For

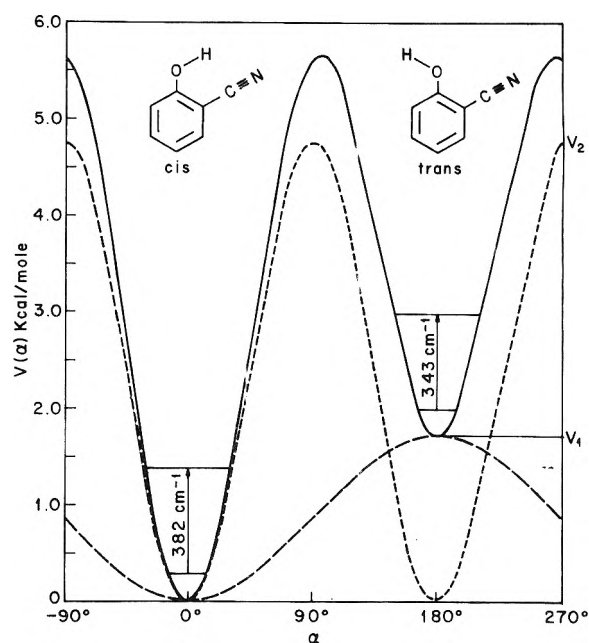


Figure 2. Potential curve for internal rotation in *o*-cyanophenol: $V(\alpha)$ (kcal/mol) = $1.73(1 - \cos \alpha)/2 + 4.76(1 - \cos 2\alpha)/2$.

2,6-dimethyl- and 2,6-diphenylphenol, where V_1 must be zero, the calculation of V_2 followed standard methods employing the Mathieu equation.¹¹ The reduced moment of inertia, $F(\alpha)$, for each phenol was calculated using the structural data for the phenol framework given by Pederson, *et al.*¹⁰ As a consequence of the center of mass of the O-H rotor falling on the internal rotation axis, $F(\alpha)$ was found to be the same for both the *cis* and *trans* isomers and virtually insensitive to the mass of the substituent group. A value of 22.47 cm^{-1} was used in all cases.

The results of the barrier calculations will be discussed in the following sections.

o-Methoxy-, -Ethoxy-, -Cyano-, and -Phenylphenol. All of these phenols except the *o*-methoxy compound show two OH stretching bands. Puttnam² has discussed the assignment of these two bands to the *cis* and *trans* orientation of the O-H group with respect to the ortho substituent for the cyano and ethoxy derivatives, and attributes the absence of the second, weaker OH stretch in the *o*-methoxy compound to an unusually low intensity in the *trans* isomer. *o*-Phenylphenol also exists in *cis* and *trans* forms with the *cis* form stabilized by an intramolecular hydrogen bond with the π electrons of the *o*-phenyl group.¹² For all of these phenols, the major portion of the sample exists in the bonded (*cis*) form.

Torsional frequencies attributable to both the *cis* and *trans* forms were observed and confirmed by their shifts on deuteration for each of these phenols. By analogy with the *o*-halophenols,¹ the intense, higher frequency band is assigned to the *cis* form. The assignment of the *trans* torsion for *o*-phenylphenol is somewhat tenuous because the 319-cm^{-1} band is considerably weaker than normal. However, the fact that an analogous shifted band could be found in the OD compound and the absence of the band in 2,6-diphenylphenol gives some support to its reality.

(10) T. Pederson, N. W. Larsen, and L. Nygaard, *J. Mol. Struct.*, **4**, 59 (1969).

(11) D. R. Herschbach, *J. Chem. Phys.*, **31**, 91 (1959).

(12) A. W. Baker and A. T. Shulgin, *J. Amer. Chem. Soc.*, **80**, 5358 (1958).

TABLE III: OH Stretching and Torsional Frequencies and Internal Rotation Barriers for Ortho-Substituted Phenols^a

Phenol	OH stretch, cm ⁻¹ (CCl ₄ soln) ^b		OH torsion, cm ⁻¹ (cyclohexane soln)		V ₁ , kcal/mol	V ₂ , kcal/mol	
	Cis	Trans	Cis	Trans			
<i>o</i> -Methoxy	3557 s	—	428 s	388 w	2.00	5.94	
<i>o</i> -Ethoxy	3555 s	3613 w	432 s	386 w	2.31	5.97	
<i>o</i> -Cyano	3559 s	3595 w	~382 s ^c	343 w	1.73	4.76	
<i>o</i> -Phenyl	3565 s	3605 w	383 s	319 w?	2.73?	4.52?	
2,6-Diphenyl	3558 s	<i>d</i>	389 s	<i>d</i>	0	5.42	
<i>o</i> - <i>tert</i> -Butyl	3647 w	3607 s	307 s	341 w-m	1.38 ^e	—	
			277 ^e	307 s			or
			264 ^e	297 s			
2- <i>tert</i> -Butyl-6-methyl	3649 w	3617 s	297 s	325 ^e	1.05 ^e	—	
			or				
<i>o</i> -CF ₃		3622 s		300 s ^f	<i>g</i>	~3.34	
<i>o</i> -Methyl		3614 s		297 s	<i>g</i>	3.29	
2,6-Dimethyl	3620 s	<i>d</i>	303 s	<i>d</i>	0	3.41	

^a s = strong, w = weak. ^b Frequencies taken from ref 3 and 4 except for *o*-CF₃ and 2,6-diphenyl which were measured in this work. ^c Weighted average of Fermi doublet. ^d Not observable since molecules exist as cis form only. ^e Predicted values, see text. ^f Broad, asymmetric band. ^g See text.

The calculated values of V_1 and V_2 for *o*-methoxy, -ethoxy-, -cyano-, and -phenylphenol in cyclohexane solutions are summarized in Table III. The magnitude of V_2 , the twofold barrier, arises mainly from the overlap between the π orbitals of the phenolic oxygen and the aromatic ring, and the utility of this data in the study of π -electron densities in aromatic rings will be discussed in a future paper. In the present study, the value of V_1 is more pertinent because it is the energy difference between the cis and trans forms and is a direct measure of the strength of the intramolecular hydrogen bond. To our knowledge, the only previous data on intramolecular hydrogen bond strengths in these four phenols are ΔH values of 1.45 and 0.91 kcal/mol for *o*-phenylphenol in CCl₄ solution given by Oki and Iwamura¹³ and Plourde,¹⁴ respectively.

A comparison of the bridge bond strengths for these four phenols with those determined previously for the *o*-halophenols¹ is given in Table IV.¹⁵ According to these data, in cyclohexane solution, the alkoxy, cyano, and phenyl groups all form stronger intramolecular hydrogen bonds than the halogens.

o-Phenylphenol is the only example we have studied which involves hydrogen bonding to π electrons. This type of intramolecular hydrogen bonding has been discussed by Baker¹² and Oki and Iwamura.¹³ Our value of ΔH for this compound is two-three times that reported in previous studies.^{13,14} An effort was made to resolve this discrepancy by repeating the work of Oki and Iwamura on the temperature-dependent change in intensity of the OH stretching vibrations. Because of the great difference in intensity of the two bands, accurate intensity measurements are very difficult. Also, since CCl₄ was employed as the solvent, only a 50° temperature range was possible and over this temperature range the change in the intensity ratio was exceedingly small. This observation implies that ΔH for this cis \rightleftharpoons trans conversion is either very large (>2.5 kcal/mol) or very small (<0.5 kcal/mol). Furthermore, if we use the cis torsional frequency of 383 cm⁻¹ and Oki and Iwamura's ΔH value of 1.45 kcal/mol, we can predict the trans torsional frequency to be 351 cm⁻¹. No band is observed at this position although a weak band could conceivably be lost in the wing of the intense 383-cm⁻¹ band. We, therefore, cannot determine with certainty the energy difference between the cis and trans forms of *o*-phenyl-

phenol; however, both our torsional assignments and our temperature dependence study appear to favor a higher ΔH value than that given previously.¹⁶ On the other hand, a large ΔH would seem to be in disagreement with the observed intensities of the OH stretching bands. Baker and Shulgin¹² have noted that the intensity of the bonded OH stretching band is about six times that of the free OH. This would indicate that the concentration of trans isomer would be on the order of 10%, whereas a ΔH of 2.7 kcal/mol would imply a much smaller concentration. This apparent discrepancy might be reconciled if the bridge bond formation were accompanied by an entropy decrease of 4–5 eu. A decrease of this magnitude may not be unreasonable because the hydrogen bond formation would result in a restriction of rotation and/or vibration around the pivot bond between the two phenyl rings.

o-*tert*-Butylphenol and 2-*tert*-Butyl-6-methylphenol. Both of these phenols show a strong OH stretching band near 3610 cm⁻¹ with a weaker band at approximately 3650 cm⁻¹. Ingold and Taylor demonstrated that the two bands are due to the presence of cis and trans forms and measured the energy differences between the two isomers. For *o*-*tert*-butylphenol in CCl₄ solution the free energy change (ΔG) for the cis-trans conversion was found to be 1.57 kcal/mol while for 2-methyl-6-*tert*-butylphenol values for ΔG (1.06 kcal/mol), ΔH (1.05 kcal/mol), and ΔS (-0.1 eu) were reported.⁴ These results for the *o*-*tert*-butyl compound have been confirmed by the dipole moment study of Allinger, *et al.*,⁵ which showed that the trans form accounts for 91% of the mixture, indicating a ΔG of 1.38 kcal/mol at 300°K. These authors have also calculated an enthalpy difference between the cis and trans forms of gaseous *o*-*tert*-butylphenol of 3.04 kcal/mol and predict a lower value of ΔH (2.22 kcal/mol) for the 2-methyl-6-*tert*-butyl compound.

(13) M. Oki and H. Iwamura, *Bull. Chem. Soc. Jap.*, **33**, 717 (1960).

(14) G. R. Plourde, Thesis, University of Wisconsin, 1961; *Diss. Abstr.*, **22**, 400 (1961).

(15) A. W. Baker and A. T. Shulgin, *Can. J. Chem.*, **43**, 650 (1965).

(16) We tend to disregard the 0.91 kcal/mol value obtained from a temperature-dependence study on the overtone bands of the OH stretching frequencies by Plourde¹⁴ because in this same work the bridge bond strengths found for *o*-chloro- and *o*-bromophenol were also much lower than the more generally accepted values.¹

For *o*-*tert*-butylphenol in cyclohexane solution, we observe an intense band at 307 cm^{-1} and a weaker band at 341 cm^{-1} both of which appear to shift by a value of ~ 1.35 on deuteration. Since this compound is known to exist predominantly in the trans form, it would seem that the intense 307-cm^{-1} band should be attributed to the trans torsion and the weak 341-cm^{-1} band to the cis. However, this assignment of the torsional frequencies cannot be correct because then the lower frequency is attributed to the more stable form. We could disregard the intensities of the two bands and reverse the assignment. Using 341 cm^{-1} for the trans torsional frequency and 307 cm^{-1} for the cis, V_1 and V_2 are calculated to be 1.34 and 3.87 kcal/mol, respectively, and the agreement of our V_1 (1.34 kcal/mol) with an energy difference of 1.38 kcal/mol given by Allinger is excellent. However, we are reluctant to disregard the intensity data and have examined the far-infrared spectrum of 2,6-di-*tert*-butylphenol in cyclohexane solution to determine the approximate position of the O-H torsional frequency for the cis form. The far-infrared spectrum of the 2,6-di-*tert*-butyl compound shows bands at 320, 285, 245, and 154 cm^{-1} all of which disappear on deuteration of the O-H group with the appearance of only two bands (208 and 148 cm^{-1}) in the O-D compound. Although the complexity of these spectra precludes an accurate assignment of the cis O-H torsional frequency, the data for the O-D compound suggest that this frequency is significantly lower than 300 cm^{-1} ($208\text{ cm}^{-1} \times 1.35 = \sim 280\text{ cm}^{-1}$).

If we use 307 cm^{-1} as the trans torsional frequency for *o*-*tert*-butylphenol and Allinger's energy difference value of 1.38 kcal/mol as an estimate of V_1 , we calculate a cis torsional frequency of $\sim 277\text{ cm}^{-1}$. We do not observe a band in this region although a weak band near 280 cm^{-1} could be hidden in the wing of the intense 307-cm^{-1} band, and, in fact, some asymmetry on the low-frequency side of the 307-cm^{-1} band is discernible.

Thus, if we disregard the band intensities, we obtain a reasonable V_1 term using the 307- and 341-cm^{-1} bands. On the other hand, it would seem more reasonable to assume that the cis torsional frequency should be lower than 307 cm^{-1} but is not observed because of low intensity; however, this assumption would not explain the shift of the 341-cm^{-1} band with deuteration. A third explanation which would rationalize the assignment of 307 cm^{-1} (trans) and 341 cm^{-1} (cis) on an intensity basis is suggested by Ingold's reasoning on the O-H stretching frequencies for the cis and trans forms of *o*-*tert*-butylphenol.⁴ Ingold explained the observation that the stretching frequency for the cis form was higher than the trans on the basis of a repulsion of the phenolic hydrogen by the *tert*-butyl group which results in a narrowing of the potential well and a raised frequency. If this same reasoning were applied to the torsional vibration, a higher frequency for the less stable form might be expected. Obviously, if this is the case, the torsional motion could not be characterized by a simple potential function, and we would not be able to evaluate a V_1 term. Thus, the data for *o*-*tert*-butylphenol presented in Table III should be viewed as very speculative.

For 2-*tert*-butyl-6-methylphenol, only one deuteration-sensitive band at 297 cm^{-1} was observed. The problem for this compound is much the same as for *o*-*tert*-butylphenol. If we assume that 297 cm^{-1} is the trans torsional frequency (here cis and trans refer to the orientation of the O-H rotor with respect to the *tert*-butyl group), the use of the ΔH value of 1.05 kcal/mol given by Ingold and Taylor for this molecule⁴ allows us to calculate a cis torsional frequency

TABLE IV: Intramolecular Hydrogen Bond Strengths for Ortho-Substituted Phenols in Solution

Phenol	Enthalpies of H bond formation, $-\Delta H$, kcal/mol	
	Torsional method, cyclohexane solution	Temperature dependence method, CCl ₄ solution
<i>o</i> -Phenyl	2.73?	1.45 ^a
<i>o</i> -Ethoxy	2.31	
<i>o</i> -Methoxy	2.00	
<i>o</i> -Cyano	1.73	
<i>o</i> -Chloro	1.62	1.44 ^b
<i>o</i> -Bromo	1.57	1.21
<i>o</i> -Iodo	1.45	1.08
<i>o</i> -Fluoro	1.44	

^a Reference 13. ^b Reference 15.

of 264 cm^{-1} . We do observe a weak band at 266 cm^{-1} but this band is also present in the O-D compound. On the other hand, if 297 cm^{-1} is assigned to the cis torsion our calculation using $V_1 = 1.05\text{ kcal/mol}$ would predict 325 cm^{-1} for the trans torsional frequency, which is also not apparent in our spectrum. These data for the 2-*tert*-butyl-6-methyl compound are included in Table III but should also be regarded as speculative.

o-Methyl-, *o*-Trifluoromethyl-, 2,6-Dimethyl-, and 2,6-Diphenylphenol. The presence of only one band in the OH stretching region for these phenols in dilute CCl₄ solution would seem to indicate the existence of just one isomeric form and certainly this must be the case for the 2,6-disubstituted compounds. However, Ingold and Taylor⁴ have pointed out that the half-band width of the O-H stretch for *o*-methylphenol is greater than the corresponding half-band widths for phenol and 2,6-dimethylphenol. These measurements are substantiated by the work of Krueger and Thompson,³ and are interpreted by Ingold and Taylor as being indicative of two unresolved O-H stretching bands in *o*-methylphenol.

In addition, Ingold and Taylor have taken the decrease in ΔG on going from *o*-*tert*-butylphenol ($\Delta G_{\text{soln}} = 1.57\text{ kcal/mol}$) to 2-*tert*-butyl-6-methylphenol ($\Delta G_{\text{soln}} = 1.06\text{ kcal/mol}$) as a measure of the difference in free energy of the cis and trans forms of the *o*-methyl compound. A ΔG value of 0.5 kcal/mol indicates that *o*-methylphenol exists as $\sim 70\%$ trans isomer and 30% cis in CCl₄ solution at 300°K. More recently, Allinger, *et al.*,⁵ have approached the conformational equilibrium in *o*-methylphenol via a force field calculation and have predicted an energy difference between the cis and trans forms of 0.86 kcal/mol. These authors also postulate the existence of two trans forms arising from the orientation of the methyl hydrogens with respect to the hydroxyl group.

For 2,6-dimethylphenol and 2,6-diphenylphenol, we observe only the expected single torsional frequency in each case. These frequencies have been used to calculate the V_2 barriers given in Table III. It is noteworthy that the value of V_2 found for 2,6-dimethylphenol (3.41 kcal) is almost unchanged from the 3.5 kcal value of phenol.¹⁰ This is contrary to the prediction by Allinger⁵ that the steric effects of the methyl groups would reduce the barrier in 2,6-dimethylphenol from what it is in phenol itself by about 1 kcal/mol.

The torsional region for *o*-methylphenol in dilute cyclohexane solution is considerably more complex than for any other phenol we have studied and contains three bands of

about equal intensity as shown in Figure 1. All three bands disappear on deuteration; however, only one reasonably sharp and symmetric OD torsional band appears. We have therefore carried out a detailed study of the low-frequency infrared and Raman spectra of *o*-methylphenol in an attempt to explain the origin of these three bands and to determine whether we are observing more than one torsional frequency. The results of this study are summarized in Table II.

Green, *et al.*, have recently published a vibrational assignment for *o*-methylphenol.⁹ Their assignment was made on the basis of the trans conformer, and only one band at 1219 cm^{-1} was suggested as possibly being due to the cis form. Thus the bands at 322 and 297 cm^{-1} were attributed to the torsional mode of the trans isomer, and the 266- cm^{-1} band was assigned as the lowest in-plane bending mode. This explanation is not satisfactory because it does not account for the disappearance of the 266- cm^{-1} band with deuteration nor does it justify the presence of two torsional frequencies (322 and 297 cm^{-1}) for the O-H compound and only one (224 cm^{-1}) for the O-D compound.

Our Raman spectrum of *o*-methylphenol shows two bands in the 250-350- Δcm^{-1} region (Table II). The polarization of the 310- Δcm^{-1} band and the persistence of the 277- Δcm^{-1} band in the O-D compound show that neither are associated with a torsional mode, and furthermore the 277- cm^{-1} band does not shift appreciably on going from the liquid to dilute cyclohexane solution. However, the infrared spectrum of *o*-methylphenol in the 250-350- cm^{-1} region changes dramatically on going from the liquid to cyclohexane solution. The strong, broad absorption in the 300-400- cm^{-1} region of the liquid becomes two bands at 297 and 322 cm^{-1} and the 275- cm^{-1} liquid band appears to shift to 266 cm^{-1} . These same three bands are evident in the spectrum of the vapor although they are broader and not as well defined as in the solution spectrum. We have also compared the intensities of the 322, 297, and 266 cm^{-1} bands at +24 and -30° (pentane solution); only a slight relative increase of the peak intensity of the 322- cm^{-1} band was observed on lowering the temperature.

Upon deuteration of the OH group, the 322-, 297-, and 266- cm^{-1} bands all decrease greatly in intensity and a fourth weak band at 278 cm^{-1} becomes evident (see Figure 2). We feel that this 278- cm^{-1} band is the counterpart of the 275- cm^{-1} liquid band observed in both the infrared and Raman spectra, and that the 266- cm^{-1} band observed in solution is associated with a torsional mode and not a shifted 275- cm^{-1} band as had been assigned by Green.⁹

Our solution (and vapor-phase) spectra and the deuteration experiment therefore seem to indicate that the three bands, 322, 297, and 266 cm^{-1} , must be associated with the torsional mode(s) of monomeric *o*-methylphenol. However, the assignment of the bands as the torsional modes of cis and trans forms is clouded by the observation of only one O-D torsional band at 224 cm^{-1} in *o*-methylphenol-OD. Furthermore, the half-band width of the 224- cm^{-1} band is exactly the same as the half-band width of the O-D torsional band in 4-methylphenol-OD where there is no possibility for cis and trans isomers. (This comparison was made with the 4-methyl analog rather than with phenol or 2,6-dimethylphenol because the O-D torsional region for these compounds is complicated by Fermi resonance.)

We are thus presented with a paradox. Earlier studies^{4,5} have supported the existence of appreciable quantities of

cis and trans forms of *o*-methylphenol, and we have observed what appear to be at least two and possibly three O-H torsional bands. On the other hand, Green, *et al.*,⁹ have found very little spectral evidence for more than one form, and the single O-D torsional band is strong evidence for the existence of only one isomeric form. We have considered the following possibilities in attempting to rationalize these observations.

(1) *o*-Methylphenol-OH exists as a mixture of isomeric forms while there is only one stable form for *o*-methylphenol-OD. The 322-, 297-, and 266- cm^{-1} bands might then be the torsional frequencies of the cis and two trans forms described by Allinger, Maul, and Hickey.⁵ This, however, seems highly unlikely because in none of the other ortho-substituted phenols which we have studied has there been a significant difference between the O-H and O-D compounds. Even for the *o*-*tert*-butyl compound where any steric effects of the larger deuterium atom might be important, no significant change in geometrical isomerism with deuteration was found. However, it should be noted that if we choose the 322- and 297- cm^{-1} bands as the torsional frequencies of cis and trans forms, the value of V_1 (ΔH) derived from these frequencies is 0.85 kcal/mol which is in almost perfect agreement with the 0.86 value calculated by Allinger.⁵

(2) There is only one torsional frequency for *o*-methylphenol (as well as for *o*-methylphenol-OD) and two of the three bands in the O-H torsional region have some alternate explanation. Although it seems very unlikely, we have considered the possibility that the three bands arise from the 0 \rightarrow 1, 1 \rightarrow 2, and 2 \rightarrow 3 torsional transitions of the O-H rotor. Using 322 cm^{-1} as the 0 \rightarrow 1 transition and assuming a V_2 barrier only, we calculate, by the method of Herschbach,¹¹ the 1 \rightarrow 2 and 2 \rightarrow 3 transitions at 294 and 266 cm^{-1} , respectively. Although the agreement with the observed frequencies is good, we feel this explanation is unsatisfactory for several reasons: (a) assuming a V_2 barrier only ignores any V_1 contribution from the *o*-methyl group; (b) it is very unlikely that upper state transitions would be observed in the solution phase with intensities almost as great as the fundamental; and (c) the complete lack of evidence for the upper state transitions in the O-D analog. Therefore, if there is only one torsional frequency for *o*-methylphenol, the 297- cm^{-1} band would be the most likely candidate based on the shift on deuteration ($\nu_{\text{OH}}/\nu_{\text{OD}} = 1.33$). The 322- and 266- cm^{-1} bands would then require an assignment which would account for their disappearance on deuteration of the O-H group. The only apparent explanation which would fit this requirement would have to involve other fundamentals or combination tones in Fermi resonance with the torsion. Examination of the vibrational assignment given by Green, *et al.*, for *o*-methylphenol⁹ shows two other fundamentals in this region, 275 and 310 cm^{-1} . Since we have found the 310- cm^{-1} band to be Raman polarized (Table II), only the 275- cm^{-1} band is of the right symmetry to enter into Fermi Resonance with the torsion (a''). The fact that we see the 275- cm^{-1} band as well as vestiges of the 322-, 297-, and 266- cm^{-1} bands (Figure 1) after deuteration is evidence that the 275- cm^{-1} band is not involved in a Fermi Resonance situation. Further consideration of Green's vibrational assignment for monomeric *o*-methylphenol also suggests no possible combination tones which would fall in this region. One could postulate a number of difference tones which would fall near 300 cm^{-1} ; however, in this case Fermi Resonance interaction with a

torsion near 300 cm^{-1} would not be possible. Our low-temperature experiment described above was aimed at determining whether difference tones could be involved; however, the small intensity changes observed did not permit any conclusion to be drawn.

We cannot, therefore, offer a reasonable explanation for the presence of three bands in the O-H torsional region of *o*-methylphenol. However, our observations on *o*-methylphenol-OD forces us to conclude that only one of these bands (297 cm^{-1}) is due to the torsion. With only one torsional frequency available, only the V_2 barrier can be evaluated. Using 297 cm^{-1} as the torsional frequency, we find V_2 to be 3.29 kcal/mol . This value is slightly lower than the V_2 barriers found for phenol and 2,6-dimethylphenol. This conclusion implies that the V_1 contribution of the *o*-methyl group is not significantly greater than that of hydrogen. If we use our ΔH value of 1.34 kcal/mol for the *cis* \rightarrow *trans* isomerism in *o*-*tert*-butylphenol and the value of 1.05 kcal/mol given by Ingold⁴ for 2-*tert*-butyl-6-methylphenol, the predicted ΔH value for *o*-methylphenol would be 0.29 kcal/mol . Using this as an estimate of V_1 and a *trans* torsional frequency of 297 cm^{-1} , we can predict a *cis* torsional frequency of $\sim 285\text{ cm}^{-1}$. If the *cis* and

trans torsional frequencies are this close together in the -OH compound, it is conceivable they might be even closer in the -OD analog and give the appearance of only a single band.

The same situation is found for *o*-trifluoromethylphenol. Again, only one torsional frequency is observed, although the band is considerably broader and more asymmetric than for most other phenols. A further complication is the apparent Fermi Resonance in the O-D torsional region. For this molecule, a torsional frequency of 300 cm^{-1} yields a V_2 value of 3.34 kcal/mol .

Acknowledgment. Support for this work was provided by the United States Air Force, Wright-Patterson Air Force Base, Contract No. F 33 615-71-C-1157, and Carnegie-Mellon University. The authors are also grateful to Dr. A. W. Baker of the Dow Chemical Co. for providing some of the samples used in this study and to Dr. E. C. Tuazon and Mr. A. S. Manocha for assistance with the barrier calculations. The use of the Model 83 Raman spectrometer was provided through the courtesy of Cary Instruments.

A Study of Methyl Methacrylate in γ -Irradiated Organic Glasses at 77 K

Tomas Gillbro,*¹ Hitoshi Yamaoka, and Seizo Okamura

Research Reactor Institute, Kyoto University, Kumatori-cho, Sennan-gun, Osaka, Japan (Received February 7, 1972)

Publication costs assisted by The Research Reactor Institute of Kyoto University

After γ -irradiation at 77 K in the dark organic glasses of 2-methyltetrahydrofuran and 3-methylpentane containing methyl methacrylate give rise to esr spectra consisting of three lines with a coupling constant of $11.0 \pm 0.2\text{ G}$, which overlaps the spectra from the pure glasses. The paramagnetic species formed is probably the radical anion of methyl methacrylate as supported by simple MO calculations. Methyl methacrylate in small concentration (0.05 mol %) scavenges the trapped electrons in the two glassy systems. The radical anion is bleached by visible light in the 2-methyltetrahydrofuran glass and methyl radicals derived from the methoxy group are produced. The methyl radicals so formed abstract hydrogen atoms from 2-methyltetrahydrofuran. In the 3-methylpentane glass the radical anion is bleached by ir light and no methyl radicals are observed. The mechanisms of radical anion formation upon γ -irradiation and decay following photobleaching in the two glassy systems are discussed.

Introduction

When pure methyl methacrylate (MMA) is irradiated in the polycrystalline solid state radicals are formed by hydrogen addition to the double bond.² At 77 K these radicals give a typical seven-line esr spectrum with a hyperfine coupling constant of about 23 G. Similar radicals were recently found in a single-crystal study on MMA,³ but in this case additional strongly anisotropic esr lines were discovered and interpreted as coming from pairs of radicals situated close to each other ($\leq 5.45\text{ \AA}$). A mechanism for the formation of radicals in pairs was proposed which involved a local ionization of several molecules sit-

uated close to each other as the primary event, followed by a proton transfer process between neighboring ions.

The present study was made in order to find out whether radical ions of MMA can be produced using γ -irradiation and also to study their chemical properties as well as their esr and optical absorption spectra.

- (1) Address correspondence to The Swedish Research Councils' Laboratory, Studsvik, Fack, S-311 01 Nyköping 1, Sweden.
- (2) (a) R. Bensasson, A. Bernas, M. Bodard, and R. Marx, *J. Chim. Phys.*, **60**, 950 (1963); (b) T. Komatsu, T. Seguchi, H. Kashiwbara, and J. Sohma, *J. Polym. Sci., Part C*, **16**, 535 (1967).
- (3) T. Gillbro, P.-O. Kinell, A. Lund, *J. Polym. Sci., Part A2*, **9**, 1495 (1971).

It is well known that electrons are produced and trapped in some organic glasses, for example, 2-methyltetrahydrofuran (MTHF) and 3-methylpentane (3MP), when these are irradiated at 77 K.⁴ If these electrons react with solute molecules, anions are formed, which may be stable or undergo some decay. In the case of alkyl chlorides the following reaction scheme occurs: $\text{RCl} + e^- \rightarrow \text{R}\cdot + \text{Cl}^-$.⁵ Some solutes such as methyl vinyl ether have a low reactivity toward electrons produced by γ -irradiation in MTHF, but when the trapped electrons are optically bleached they react with methyl vinyl ether according to the reaction $\text{CH}_2=\text{CHOCH}_3 + e^- \rightarrow \text{CH}_2=\text{CHO}^- + \cdot\text{CH}_3$.⁶ In the present case it was found that MMA reacts easily with electrons produced by irradiation in MTHF and gives anions which are stable in the dark. Upon bleaching with visible light the MMA^- decays by different mechanisms in the two systems. In the MTHF glass methyl radicals are formed, but in the 3MP glass no methyl radicals were discovered.

A matrix of *n*-butyl chloride is often used to stabilize positive ions. The positive holes formed in the alkyl chloride upon irradiation migrate in the glassy matrix, and are trapped by solute molecules with a lower ionization potential than that of the solvent. With MMA as solute no positive MMA ions were detected. This suggests that the ionization potential for MMA is higher than that for *n*-butyl chloride.

Experimental Section

The monomers methyl methacrylate (MMA), methyl acrylate (MA), and ethyl acrylate (EA) of Nakarai reagent grade were all purified from stabilizer by extraction with a 4 *N* NaOH solution and distilled water. They were then fractionally distilled twice and dried twice over a molecular sieve (Linde 3A) baked at 400° for about 15 hr. The final drying of the monomers was always made under vacuum. The solvents 2-methyltetrahydrofuran (MTHF), Nakarai guaranteed reagent, and 3-methylpentane (3MP), Aldrich Chemicals, puriss grade, were fractionally distilled twice and dried twice, first over CaH_2 or a molecular sieve and then on a sodium-potassium mirror under vacuum. The criterion for purity was the observation of the singlet esr signal from trapped electrons in the pure γ -irradiated glasses at 77 K. Since the experiments were made on samples containing rather high concentrations (~1 mol %) of solutes of high electron affinity, small amounts of impurities should not influence the results. The *n*-butyl chloride (*n*-BuCl) was fractionally distilled twice and dried twice over a baked molecular sieve. The mixed samples were prepared in Suprasil esr tubes or Spectrosil optical absorption cells under vacuum. The electron scavenger biphenyl was used as received (Nakarai, extra pure reagent). The deuterated MMA ($\text{CH}_2=\text{C}(\text{CH}_3)\text{COOCD}_3$, MMA- d_3) was prepared by a conventional technique. Methacrylyl chloride was added to a solution of tetradeuteriomethanol (Merck) in carbon tetrachloride under stirring.⁷ The MMA- d_3 was then purified by fractional distillation. The chemical purity as measured by gas chromatography was 97.8%, CCl_4 being the main impurity, and the degree of deuteration was 100% according to nmr measurements. The esr measurements were made using the Varian E-3 spectrometer operated at X-band using 100-kHz magnetic field modulation. The bleaching of the samples was carried out directly in the esr cavity with a 1000-W tungsten lamp mounted in a projector with its front lens 9 cm from the sample tube.

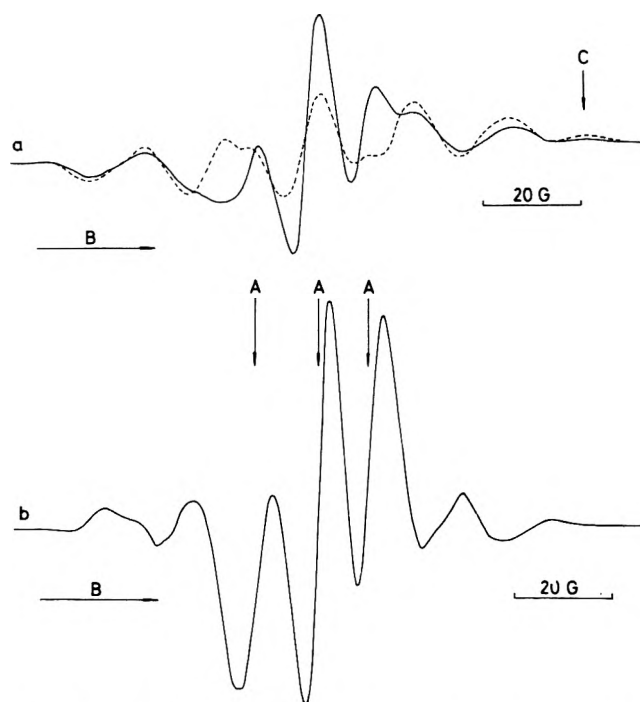


Figure 1. (a) ESR spectrum of a γ -irradiated MTHF glass containing 1 mol % MMA as measured in the dark at 77 K. The dotted spectrum was obtained from the same sample after photobleaching. (b) The difference between the spectra in 1a. The lines on the wings of the spectrum are due to MTHF radicals formed during the photobleaching.

All optical filters used were from the Toshiba Co. Difference spectra were obtained by electronic subtraction using a time averaging computer (Varian). The optical absorption measurements were carried out using a Shimadzu multipurpose spectrometer (MPS-50 L) equipped with a special dewar at 77 K. The γ -irradiation was carried out for 5 or 10 min in the dark at 77 K and the dose rate of the ^{60}Co γ source was 2.4 Mrads/hr.

Results

MMA-MTHF System. After irradiation at 77 K in the dark the esr spectrum in Figure 1a of a sample containing 2 mol % MMA was recorded. When the sample was illuminated with visible light from the projector the seven-line spectrum, which is typical for irradiated pure MTHF, remained (dotted line in Figure 1a). By subtracting the dotted curve from the solid curve the spectrum shown in Figure 1b was obtained. The spectrum is characterized by three central lines with a hyperfine coupling constant $a = 11.2$ G. There is also an approximate doubling in intensity of the spectrum attributed to MTHF radicals, when the sample is photobleached. If the spectrum of a MMA-MTHF sample is recorded during or immediately after photobleaching, another spectrum consisting of four lines with a splitting of 22.4 G between the lines is clearly observed (the lines marked B in Figure 2a). This spectrum is attributed to the methyl radical and it decays with "com-

- (4) See, for example, the review articles by (a) J. E. Willard in "Fundamental Processes in Radiation Chemistry," P. Ausloos, Ed., Interscience, New York, N.Y., 1968; (b) W. H. Hamill in "Radical Ions," Kevan and Kaiser, Ed., Interscience, New York, N.Y., 1967; (c) L. Kevan, "Actions Chimiques et Biologiques des Radiations," Vol. 15, M. Haissinsky, Ed., Masson, Paris.
- (5) T. Shida and W. H. Hamill, *J. Chem. Phys.*, **44**, 4372 (1966).
- (6) M. Irie, K. Hayashi, S. Okamura, and H. Yoshida, *J. Phys. Chem.*, **75**, 476 (1971).
- (7) I. Lal and R. Green, *J. Org. Chem.*, **20**, 1954 (1955).

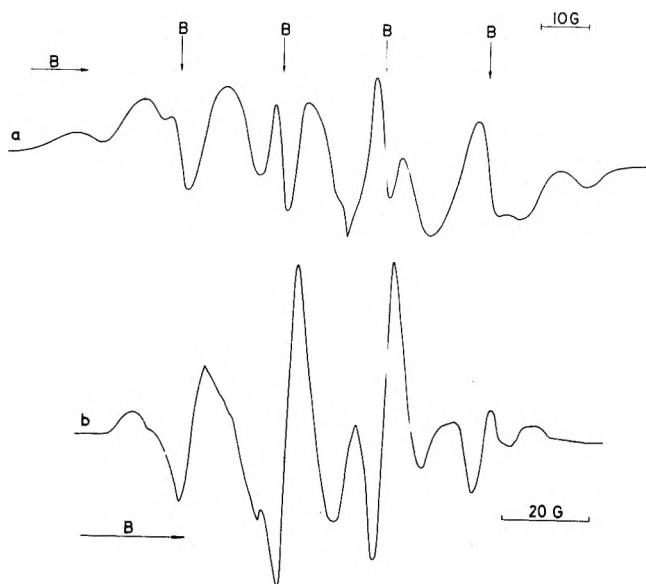


Figure 2. (a) ESR spectrum recorded during photobleaching of an irradiated 2 mol % MMA-MTHF sample. (b) The decaying part of the spectrum in 2a.

posite" first-order kinetics on standing in the dark. As shown in Figure 3 the decay can approximately be divided into two first-order decays with half-lives of about 10 and 1.6 min, respectively. A second-order plot also gave a straight line, but the half-life of the methyl radicals as measured in two samples irradiated for 5 and 2 min, respectively, and then photobleached for 1 min each was approximately the same (1.6 and 1.7 min, respectively). In the case of a second-order reaction the half-lives would change as $1/kc_0$, where c_0 is the initial methyl radical concentration in the bleached sample, which is assumed to be proportional to the dose. Spectrum A is not bleached with red light ($\lambda > 630$ nm). The change in MTHF radical concentration following a 1-min photobleaching is shown in Figure 3. Here the amplitude of the peak C (see Figure 1a) has been subtracted from the peak height at completed growth and plotted as a function of the time elapsed after the light was switched off. The kinetics of methyl radical decay and MTHF radical growth are essentially the same. Samples containing different concentrations of MMA (0.3–5 mol %) showed no significant change in the intensity of spectrum A relative to the MTHF radical spectrum after the same irradiation. No difference in the methyl radical concentration was observed after the same photobleaching of the different samples. From this it can be concluded that the methyl radicals were not produced by direct photolysis of MMA.

At extremely low MMA concentrations (0.05 mol %), however, the central peak in spectrum A is more intense by comparison with the outer two lines. After bleaching with $\lambda > 630$ nm (Toshiba filter VR-63), the central peak decreased and the surrounding two lines increased in intensity (see Figure 4). No methyl radicals could be detected. A comparison with irradiated pure MTHF glass showed that the photobleaching ($\lambda > 630$ nm) of the central line is about three times faster when 0.05 mol % MMA is added to the glass. When the microwave power was increased from 0.25 to 1.0 mW the central line was slightly saturated. A further increase of the microwave power to 16.0 mW saturated spectrum A while the MTHF radical spectrum remained unsaturated.

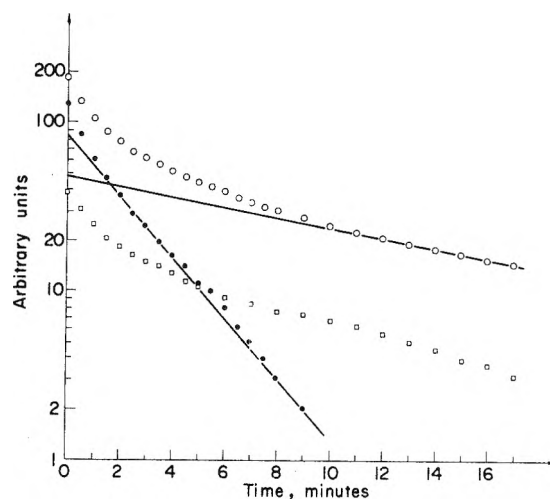


Figure 3. Decay curve of methyl radicals in 1 mol % of MMA-MTHF glass immediately after photobleaching for 1 min is indicated by circles. This curve can be divided into two first-order decays as shown by the straight lines. The squares show the MTHF radical concentration at completed growth minus the concentration at a given time, t , after the conclusion of 1 min of photobleaching.

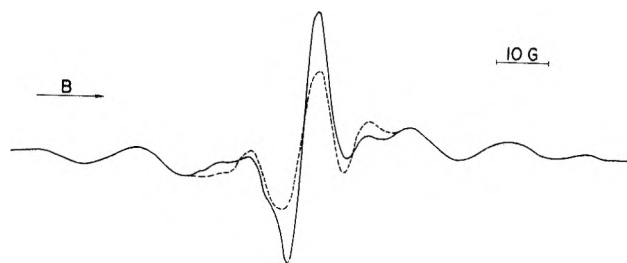


Figure 4. ESR spectrum of a 0.05 mol % MMA-MTHF sample γ -irradiated for 5 min. The dotted line shows the spectrum after illumination with $\lambda > 6300$ Å for 3 min.

If the MTHF glass contains MA or EA instead of MMA there is no difference in the ESR spectra as recorded in the dark after irradiation. The optical spectra of irradiated MA-MTHF glass were identical with those found for MMA-MTHF glasses. When bleached, the glass containing MA is found to contain methyl radicals. When the EA-MTHF glass is bleached, however, further outer spectral lines are produced, which can be attributed to ethyl radicals. The bleaching rate of spectrum A in the irradiated sample is about three times slower in the glass containing EA. When a MTHF glass containing allyl methacrylate (AMA) is irradiated spectrum A is obtained. The ESR spectrum from the photobleached sample is shown in Figure 5a, together with the spectrum from a bleached pure MTHF glass. The difference spectrum between these two spectra consists of five lines as can be seen in Figure 5b. The coupling constant is 14.3 G. The radical produced in the photobleached AMA-MTHF glass is obviously the allyl radical and it does not decay at 77 K. A MTHF glass with 1 mol % MMA- d_3 also gave spectrum A when irradiated. After photobleaching no methyl radicals were discovered. It was found, however, that if the photobleaching had been interrupted the central peak continued to decay with a half-life of about 2 min. This was attributed to the decay of trideuteriomethyl radicals produced during the photobleaching, which are supposed to give a broad singlet in the glassy state.

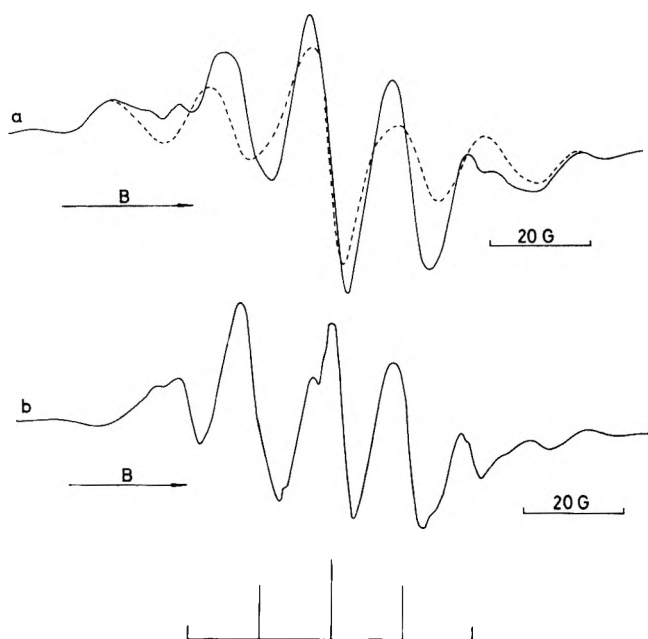


Figure 5. (a) ESR spectrum from a photobleached MMA-MTHF sample. The dotted line shows the spectrum from a pure photobleached MTHF glass. (b) The difference between the spectra in Figure 5a and a stick plot using four equivalent protons with $a = 14.3$ G.

Optical measurements at 77 K on an irradiated 2 mol % MMA-MTHF sample gave the spectrum in Figure 6. The figure also shows the difference in optical density between the irradiated and unirradiated samples. The absorption maximum for the radiation-produced species is at about 320 nm. It is possible to calculate the molar extinction coefficient, ϵ , for the absorbing species if its G value is assumed to be 2.55, *i.e.*, the same as that for the trapped electrons in MTHF glass. Since the optical density for a radiation dose of 1.2×10^{19} eV/g was 2.75, ϵ was calculated to be $6400 \text{ M}^{-1} \text{ cm}^{-1}$. Upon illumination with visible light the absorption band was bleached. In the range 800–1500 nm, where the electrons trapped in MTHF absorb, no absorption band was detected, and no change was observed in this range after photobleaching. The rate of bleaching of the optical absorption band at 320 nm is of the same order of magnitude as that found for ESR spectrum A, *i.e.*, the half-time is about 2 min. However, no correction was made for differences in dewar and sample geometries in the two cases.

The addition of *n*-BuCl to a MTHF glass with 1 mol % MMA reduces the magnitude of spectrum A in the irradiated sample. However, the *n*-BuCl concentration has to be about 5 mol % before spectrum A is reduced to half of the value obtained for a glass without *n*-BuCl. If biphenyl is added to MTHF glass containing MMA no decrease in spectrum A is noted, even when the ratio biphenyl:MMA is as high as 20:1. When a small amount (about 0.2 mol %) of MMA is added to an MTHF glass with 1.0 mol % biphenyl, the optical absorption from the biphenyl anion at 620 nm is reduced by 30% compared to a sample not containing any MMA. Obviously MMA is a very strong electron scavenger in MTHF glass as compared to biphenyl.

When 0.02 mol % CCl_4 was added to a 1 mol % MMA-MTHF glass, spectrum A was formed on γ -irradiation and on photobleaching spectrum B was clearly observed. A 5 mol % MMA-MTHF glass containing 0.5 mol % CCl_4

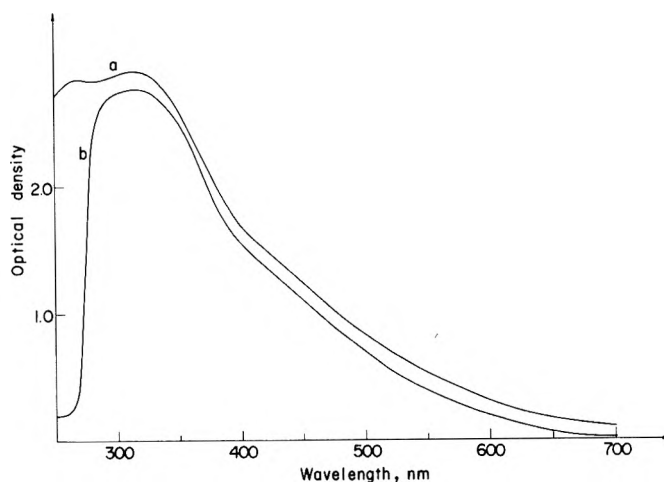


Figure 6. (a) The optical absorption spectrum of a 2 mol % MMA-MTHF sample γ -irradiated for 5 min. (b) Difference spectrum between irradiated and unirradiated samples.

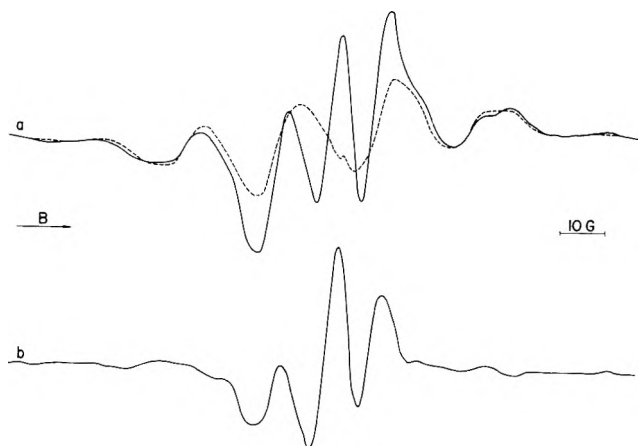


Figure 7. (a) ESR spectrum of an irradiated 3MP glass containing 0.04 mol % of MMA. Dotted line obtained after photobleaching of the sample. (b) The difference between the spectra in 6a. The lines on the wings of the spectrum are due to decrease of 3MP radicals during photobleaching.

showed no spectrum A when irradiated, neither did the spectrum change on photobleaching. CCl_4 is obviously a stronger electron scavenger as compared to MMA in this system.

MMA-3MP System. The ESR spectrum of an irradiated 0.05 mol % MMA-3MP sample is shown in Figure 7 together with the spectrum from the bleached sample (dotted line). The difference spectrum has the same three lines (spectrum A) with a hyperfine coupling constant $a = 10.8$ G close to that found for the MMA-MTHF system. The intensities of the three peaks, starting from the low-field side, are in the ratio 0.8:2.0:1.1. In contrast to irradiated MMA-MTHF glass, the irradiated MMA-3MP glass is also bleachable with $\lambda > 630$ nm. When UV light only ($300 < \lambda < 400$ nm) is used the bleaching is a very slow process. Even at a very low concentration of MMA (0.05 mol %) no singlet due to trapped electrons could be detected. When 2.4 mol % of the electron scavenger *n*-BuCl was added to 1.6 mol % MMA-3MP spectrum A disappeared almost completely. The addition of biphenyl had no noticeable effect on spectrum A. The methyl radical spectrum could not be detected in an irradiated MMA-3MP sample after photobleaching. After complete bleaching of spectrum A the high-field peak, which is de-

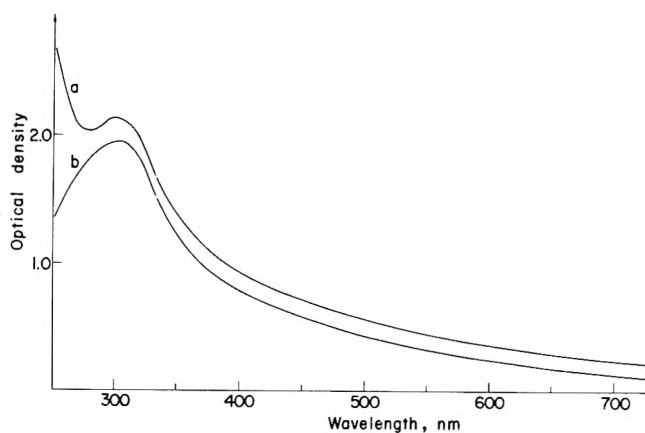


Figure 8. (a) The optical absorption spectrum of an irradiated 0.1 mol % MMA-3MP sample. (b) Difference spectrum between irradiated and unirradiated samples.

rived from the 3MP radicals, showed a 30% decrease. A comparison of the rates with which the central spectra are bleached with visible light in irradiated glasses of MMA-3MP and MMA-MTHF shows that the bleaching is ten times faster in the MMA-MTHF system. Optical absorption spectra measured for a sample containing 0.1 mol % of MMA (higher concentrations gave milky glasses) are shown in Figure 8. The absorption band has a maximum at 305 nm and is in fairly good agreement with the absorption band obtained for the irradiated MMA-MTHF system. Photobleaching with $\lambda > 630$ nm for 1 min reduced the intensity of the 305-nm band by 60%, as compared to a reduction of only about 5% in the 320-nm band in the MMA-MTHF glass bleached in the same way. The irradiated MMA-3MP glass showed no absorption band from trapped electrons at higher wavelengths.

MMA-*n*-BuCl System. BuCl glasses containing different amounts of MMA were γ -irradiated at 77 K in the dark. The recorded esr spectra only showed absorption from *n*-butyl radicals and no MMA⁺ was detected. The optical absorption spectra showed typical absorption peaks from BuCl⁺ at 380 and 540 nm,⁶ which were easily photobleached. The remaining absorption at 430 nm is difficult to photobleach.

Discussion

The electrons produced in the pure MTHF and 3MP glasses by γ -irradiation will be trapped in the glasses in the dark at 77 K. These electrons will also give characteristic esr and optical absorption spectra. When MMA was present in the MTHF and 3MP glasses during γ -irradiation, the optical absorption or esr spectra from the trapped electrons could not be detected, except in the case of a very low concentration of MMA (0.05 mol %) in MTHF, in which case the esr signal from the trapped electrons was observed. These results indicate that the MMA molecule reacts very effectively with the electrons formed in the MTHF and 3MP glasses upon γ -irradiation. The product of this reaction gives rise to the three-line esr spectrum A (Figure 1b) with $a = 11.0 \pm 0.2$ G (medium) in the MMA-MTHF and MMA-3MP glasses, and also to the uv absorption at 320 nm in the MMA-MTHF glass and at 305 nm in the MMA-3MP glass. It is reasonable to believe that the species formed is the MMA anion radical, $\text{CH}_2=\text{C}(\text{CH}_3)\text{COOCH}_3^-$, (MMA⁻). A theoretical calculation of the spin densities in this anion radical was made using the Hückel method. As can be seen in Table I the

TABLE I: Calculated Electron Spin Densities in MMA^{-a}

Method	$\text{CH}_2=\text{C}(\text{CH}_3)\text{COOCH}_3$				a, G
	1	2	4	3	
Huckel	0.34	0.10	0.34	0.007	7.8
McLachlan	0.47	0.01	0.41	0.003	10.8
ω method	0.42	0.08	0.36	0.005	9.7
First iteration					
Second iteration	0.43				9.9

^a The following parameters were used in the calculations (cf. ref 9): $h_0 = 2$, $h(\text{CH}_3) = 2$, $h(\text{OCH}_3) = 0.5$; $k(\text{C}=\text{C}) = 1.10$, $k(\text{C}-\text{C}) = 0.87$, $k(\text{C}=\text{O}) = 1.41$, $k(\text{C}-\text{CH}_3) = 0.7$, and $k(\text{C}-\text{OCH}_3) = 0.6$; $\omega = 1.4$.

calculated spin density on the carbon atom C-1 with two coupling hydrogen atoms is 0.34. A substitution of this value into the McConnell relation, $a = \rho Q$ where $Q = 23$ G, gives $a = 7.8$ G. If, however, the Coloumb integrals used in the Hückel method are corrected according to the ω technique,⁸ where the decrease in the Coloumbic attraction on a carbon atom with negative charge is considered, the new coupling constant obtained after two iterations will be 9.9 G. This value is more in accord with the experimental value of $a = 11.0 \pm 0.2$ G. The McLachlan method⁹ gave a calculated coupling constant $a = 10.8$ G, in excellent agreement with the experimental data. The relative ease with which the esr spectrum is saturated also indicates that the absorbing species is a radical ion rather than a neutral radical.

At low concentrations the esr signal from the trapped electron is observed in the MTHF glass. This signal is easily bleached with $\lambda > 630$ nm light; this is in contrast to the MMA⁻ spectrum in the same sample, which is bleached with uv light. When the trapped electrons are bleached the MMA⁻ concentration increases. The electrons consequently react with the MMA molecule to form anion radicals. This reaction must be very efficient as is confirmed by the relatively small effect caused by the addition of an electron scavenger (*n*-BuCl) as well as by the increase in the photobleaching rate of the trapped electrons when MMA is added to the MTHF glass.

The disappearance of MMA⁻ in MTHF after bleaching is related to the appearance of a new four-line spectrum with coupling constant $a = 22.4$ G. This spectrum evidently arises from methyl radicals formed when MMA⁻ dissociates as a consequence of photobleaching by light in the uv range. The small divergence in coupling constant compared to 23 G, which is normally found for the methyl radical, is most probably due to an error in the measurement because of the broad overlapping spectrum from MTHF radicals. However, some influence by the solvent on the electronic structure of the methyl radical can not be excluded. There are two possible ways in which methyl radicals can be formed by a bond rupture in MMA, and therefore MA was also used as a solute. In MA methyl radicals can only be formed by bond cleavage between carbon and oxygen in the methoxy group. Since methyl radicals were found in this case also, when the sample was bleached, it is reasonable to believe that the methyl radicals in MMA also derive from the methoxy group. In the case of EA no methyl radicals are expected, but instead ethyl radicals should be formed. Spectral lines were in

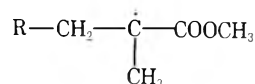
- (8) A. Streitwieser, Jr., "Molecular Orbital Theory for Organic Chemists," Wiley, New York, N.Y., 1961, p 115.
 (9) A. D. McLachlan, *Mol. Phys.*, 2, 361 (1959).

fact detected in the bleached sample which indicated that ethyl radicals had been formed. The fact that the photobleaching of EA⁻ is 2.5 times slower than that of MMA⁻ indicates that the size of the ester group has some effect on the bleaching process.

The results obtained for the AMA-MTHF glass clearly demonstrate that allyl radicals are produced from AMA⁻ on illumination. The allyl radicals do not react in contrast to the methyl radicals with the MTHF molecules in our system. The mean value of the coupling constants for the four α protons as given by Fessenden and Schuler¹⁰ in the liquid state is 14.38 G, which is very close to the coupling constant of 14.3 G found by us (Figure 5b). The additional splitting of 4.06 G from the β proton is not resolved in our spectrum due to the broad line width ($\Delta H \approx 6$ G) in the glassy matrix.

When MMA-*d*₃ was used, photobleaching gave no methyl radicals. The deuteriomethyl radical with its small hyperfine coupling constant¹⁰ (3.58 G) is expected to give a broad central line in the glassy matrix, since typical line widths in such a matrix are in the order of 5 G. The continued decay of the central peak in the esr spectrum, even when the photobleaching is interrupted, indicates that deuteriomethyl radicals are indeed present. The low content of CCl₄ (2.2%) in MMA-*d*₃ as an impurity will not influence this result, since no influence was noted for non-deuterated MMA containing the same amount of CCl₄. Besides, at high CCl₄ concentrations the spectrum of the MMA-*d*₃ radical ions should not be formed.

A dimerization or polymerization of MMA initiated by MMA⁻, which is very unlikely, would give the polymer radical



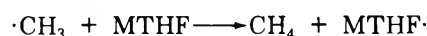
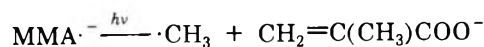
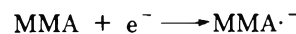
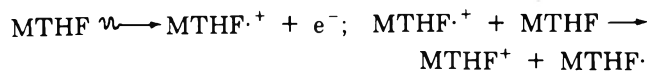
The esr spectrum of this radical is well known in the literature¹¹ and it consists of nine lines due to the nonequivalent couplings from the methylene protons. Spectrum B consisting of an even number of lines can thus not be ascribed to a polymer or dimer radical.

A careful analysis of data from photobleached MMA-MTHF (Figure 3) shows that the methyl radicals decay with "composite" first-order kinetics,¹² which means that the methyl radicals react with the surrounding solvent molecules or that the methyl radicals combine with some other species produced in their close vicinity in the spur. The increase in the MTHF radical concentration by a factor of 2 when the sample is bleached, as well as the very good agreement between the kinetics for methyl radical decay and MTHF radical build-up, strongly suggests that methyl radicals abstract hydrogen from MTHF. Since the decay can be divided into at least two first-order reactions it is suggested that the methyl radicals have different reactivities, depending on how they are formed in the MTHF matrix. The half-life of about 2 min for deuteriomethyl radicals is somewhat longer than that found for methyl radicals (1.6 min) but on the basis of the present data it is not possible to ascribe this definitely to a lower reactivity toward MTHF; this is because the decay of CD₃ is followed by an increase in the MTHF radical concentration, as is the case for methyl radicals. The esr spectra from these radicals overlap severely, which render an exact evaluation of the half-life of the deuteriomethyl radicals more difficult.

The growth in MTHF radical concentration even when the bleaching of MMA⁻ is interrupted indicates that

methyl radicals with thermal energy are also reactive in this system. This is also in agreement with the composite first-order decay found for methyl radicals in the dark.

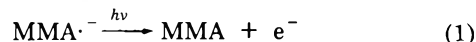
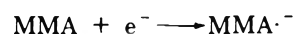
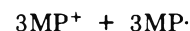
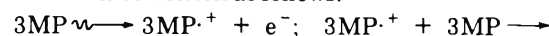
A study by Irie, *et al.*,⁶ showed that methyl radicals in MTHF decay thermally with second-order kinetics at 77 K, although methyl radicals produced from methyl vinyl ether by a dissociative electron capture process react with the solvent molecules in a first-order process. The methyl radicals produced by optical bleaching of MMA⁻ are consequently of this reactive type. The processes occurring in the MMA-MTHF system after γ -irradiation and subsequent photobleaching can be summarized as follows.



One surprising discovery was the fact that biphenyl does not scavenge the MMA⁻ ion at all, even at high concentrations. One explanation for this could be that biphenyl scavenges "hot" electrons less effectively than MMA or that electrons are transferred from the biphenyl anions to nearby MMA molecules.

The fate of MMA⁻ in the 3MP glass is less well understood and the decay does not follow the same path as in the MTHF glass. To begin with, the decay during photobleaching can be divided into two first-order processes, which indicates that the decay mechanism is connected with the structure of the trapping sites as in the case of trapped electrons. Secondly, illumination with $\lambda > 630$ nm easily bleaches the MMA⁻ in the 3MP glass, in contrast to the case for the MTHF glass, and methyl radicals are not formed. According to Willard and Claridge¹³ the half-life of methyl radicals in 3MP glass is 16 min, so if once formed they should be easy to detect. There is obviously a broad absorption band in irradiated MMA-3MP at longer wavelengths, as can be seen in Figure 8. This band is not bleached with $\lambda > 630$ nm, however.

There are at least three possible mechanisms that can account for the observed reaction. The MMA anion can be ionized by the ir light in 3MP or the positive holes in 3MP can be mobilized and recombine with the MMA anions. The 3MP matrix is less polar than the MTHF matrix. This leads to a more heterogeneous distribution of MMA in the 3MP glass (the glass gets milky at higher (~1 mol %) concentrations of MMA). This can lead to ion pair formation (MMA⁻...MMA⁺) and neutralization will then occur upon bleaching with ir light. These three mechanisms can be written as follows.

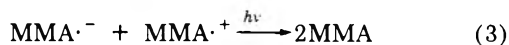
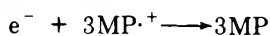
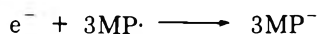


(10) R. W. Fessenden and R. H. Schuler, *J. Chem. Phys.*, **39**, 2147 (1963).

(11) See, for example, (a) I. H. O'Donnell, B. McGarvey, and H. Morawetz, *J. Amer. Chem. Soc.*, **86**, 2325 (1964); (b) Y. Sakai and M. Iwasaki, *J. Polym. Sci., Part A-1*, **7**, 1749 (1969); (c) V. G. Vasil'ev, N. V. Verein, G. A. Ozerova, and A. K. Piskunov, *High Energy Chem.*, **5**, 108 (1971).

(12) W. G. French and J. E. Willard, *J. Phys. Chem.*, **72**, 4604 (1968).

(13) R. F. C. Claridge and J. E. Willard, *J. Amer. Chem. Soc.*, **87** 4992 (1965).



Judging from the 30% decrease in 3MP radical concentration, which is similar to that formed when trapped electrons are photobleached in pure 3MP glass,¹⁴ ionization mechanism 1 seems to be the most acceptable. However, positive hole transfer mechanism 2 could also explain the decrease in 3MP radicals as shown in the reaction scheme. It is also necessary to account for the fact that the methoxy bond of the MMA⁻ ion does not break in the 3MP glass. In order to explain this the hole migration theory is more convenient since the hole migrates in the 3MP glass but not in the MTHF glass and neutralization will occur before the MMA⁻ has a chance to dissociate. The role of the polarity of the medium as such is not clearly understood, but it is probable that a polarization of the methoxy bond of MMA⁻ by the MTHF matrix could facilitate bond rupture.

As had been expected, MMA⁻ was not found in the *n*-BuCl glass since the electrons react easily with *n*-BuCl to give *n*-butyl radicals and chlorine ions. The positive MMA ion would be formed in the glass if the MMA ionization potential were lower than that for *n*-BuCl. Since MMA⁺ was not discovered it is believed that the ionization potential for MMA is higher than that for *n*-BuCl,

i.e., 10.67 eV. The results show that if MMA⁺ is formed it must be very unstable.

Conclusion

Anions of MMA formed by electron capture by the MMA molecule are stable in the MTHF and 3MP glassy matrices at 77 K. In MTHF the anion radical of MMA is bleached by visible light and the methyl radicals so formed abstract hydrogen atoms from the solvent. The anion radicals in 3MP are bleached by ir light but no methyl radicals are formed in this case. The MMA⁻ is therefore believed to combine with positive holes in 3MP before bond rupture can occur.

The positive radical ion of MMA could not be detected in an *n*-BuCl glass. It is therefore concluded that the radical ion is either unstable or the ionization potential of MMA is higher than for *n*-BuCl.

Acknowledgments. T. Gillbro is grateful to the Japan Society for the Promotion of Science for a fellowship that made this work possible. The support of the staff at the Research Reactor Institute of Kyoto University is also gratefully acknowledged. Special thanks are due to Mr. Noda and Mr. Warashina for their kind assistance in many experiments. Thanks are also due to Dr. A. Lund for his assistance in the molecular orbital calculations and to Dr. Yoshida for stimulating discussions. Mrs. I. Edvardsson handled the manuscript with her usual expertise.

(14) A. Ekstrom, R. Suenram and J. E. Willard, *J. Phys. Chem.*, **74**, 1888 (1970).

Pulse Radiolytic Investigations of the Catalyzed Disproportionation of Peroxy Radicals. Aqueous Cupric Ions¹

Joseph Rabani,* Dina Klug-Roth,

Department of Physical Chemistry, The Hebrew University of Jerusalem, Jerusalem 91 000, Israel

and J. Lilie

Hahn-Meitner-Institut für Kernforschung Berlin GmbH, Sektor Strahlenchemie, 1 Berlin 39 (Received October 30, 1972)

Publication costs assisted by the Hahn-Meitner-Institut

The catalytic effect of Cu²⁺ in enhancing the dismutation of the peroxy radicals HO₂ and O₂⁻ has been investigated. Cu²⁺ ions react with O₂⁻ ($k = 8 \times 10^9 M^{-1} \text{sec}^{-1}$) and with HO₂ radicals ($k \cong 1 \times 10^8 M^{-1} \text{sec}^{-1}$). The catalytic effect involves alternate reduction and oxidation of the copper. Cu⁺ reacts with O₂⁻ with a rate constant of $\sim 10^{10}$. HO₂ oxidizes Cu⁺, $k > 10^9 M^{-1} \text{sec}^{-1}$. The uv absorption spectrum of Cu⁺ has been measured in formate and in methanol solutions.

Introduction

Catalysis of superoxide dismutation has been suggested several years ago.² The biological significance of such catalysis became evident from the work of McCord and Fridovich,³ who discovered recently that a group of enzymes, superoxide dismutases, act as catalysts for O₂⁻ dismutation. Since the work of McCord and Fridovich, several pa-

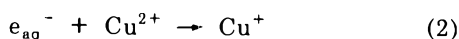
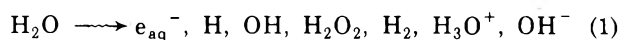
pers appeared in which the rate and mechanism for the enzymatic catalysis were investigated.⁴⁻⁷ The most investigated enzyme bovine superoxide dismutase contains two

- (1) The research has been supported in part by the Authority for Research and Development, The Hebrew University of Jerusalem, P.O.B. 1255, Jerusalem, Israel.
- (2) J. Rabani and S. O. Nielsen *J. Phys. Chem.*, **73**, 3736 (1969).
- (3) J. M. McCord and I. Fridovich, *J. Biol. Chem.*, **244**, 6049 (1969).

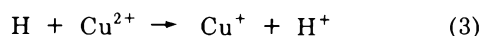
copper atoms which are the active centers.^{3,8} In view of this it was desired to investigate the catalysis by copper ions as such, as well as the effect of complexing agents. Previous results indicated that copper ions are able to catalyze the dismutation of superoxide radicals.⁹ In the present manuscript we report results obtained in $\text{Cu}(\text{ClO}_4)_2$ solutions containing formate. $\text{Cu}(\text{ClO}_4)_2$ was used in both catalytic amounts, as well as in large excess over the superoxide radicals.

The radiation chemistry of cupric solutions has been previously studied by several groups. Schwarz¹⁰ used CuSO_4 solutions for the measurements of the H_2 yields. Several groups¹¹ reported that cupric ions were reduced to cuprous ions by H atoms and organic free radicals. The reaction rate constants of cupric ions with e_{aq}^- ,^{12,13} H,¹⁴ and OH^{15} have been reported as 3×10^{10} , 5×10^8 , and $3 \times 10^8 \text{ M}^{-1} \text{ sec}^{-1}$, respectively.

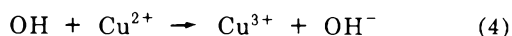
In the presence of both cupric and formate ions at near neutral pH's, the following reaction sequence is expected upon irradiation.



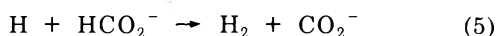
$$k = 3 \times 10^{10} \text{ M}^{-1} \text{ sec}^{-1} \quad (12,13)$$



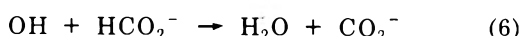
$$k = 1.5 \times 10^9 \text{ M}^{-1} \text{ sec}^{-1} \quad (14)$$



$$k = 3 \times 10^8 \text{ M}^{-1} \text{ sec}^{-1} \quad (15)$$



$$k = 5 \times 10^8 \text{ M}^{-1} \text{ sec}^{-1} \quad (16)$$

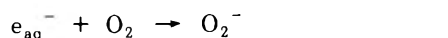


$$k = 3 \times 10^9 \text{ M}^{-1} \text{ sec}^{-1} \quad (17)$$

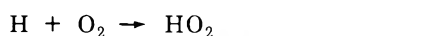


At sufficiently high formate concentrations the net result of these reactions is the reduction of cupric to cuprous ions, with a yield of $G = G_e + G_H + G_{\text{OH}} \cong 6$ ions per 100 eV of radiation.

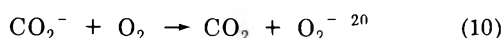
When oxygen is also present, it competes with cupric ions for e_{aq}^- and CO_2^- , and with both cupric ions and formate ions for H atoms.



$$k = 2 \times 10^{10} \text{ M}^{-1} \text{ sec}^{-1} \quad (18)$$



$$k = 2 \times 10^{10} \text{ M}^{-1} \text{ sec}^{-1} \quad (19)$$

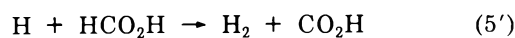


In acidic solutions, similar reactions take place. However, several of the transients involved are acids and their acid-base forms, and equilibria must be considered. CO_2^- is converted to CO_2H in acid solution. The $\text{p}K$ of CO_2H is 3.9,²⁰ similar to the $\text{p}K$ of formic acid, which is 3.75. OH reacts with formic acid similarly as with formate ions according to



$$k_{6'} = 1.3 \times 10^8 \text{ M}^{-1} \text{ sec}^{-1} \quad (17)$$

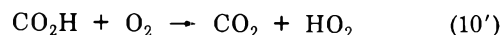
The reaction of H with formic acid according to



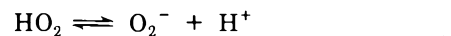
$$k < 10^6 \text{ M}^{-1} \text{ sec}^{-1} \quad (21)$$

is relatively slow.

The radical CO_2H is also capable to reduce O_2 according to^{20,21}



HO_2 is in equilibrium with O_2^-



$$K_{11} = 1.6 \times 10^{-5} \text{ M} \quad (2,21)$$

In solutions containing formate (or formic acid), O_2 , and $\text{Cu}(\text{ClO}_4)_2$, it is possible to choose concentrations such that the reactions of e_{aq}^- , H, and OH with cupric ions are minimized. Under such conditions, the radiation-induced primary free radicals are converted into HO_2 and O_2^- . The reactions of peroxy radicals with the cupric ion can be followed from the decay of the optical absorbance of the peroxy radicals in the uv. The purpose of this manuscript is to present the results of such measurements. The reduction of Cu^{2+} by O_2^- has already been postulated by other authors.²² In oxygen free solutions, Cu^{2+} is reduced by the hydrated electron and CO_2^- . Similarly, reduction by methanol radicals occurs in solutions where formic acid is substituted by methanol.

Experimental Section

The pulse radiolysis set ups at the Hahn-Meitner-Institute and at the Hebrew University have been used. A 4-cm cell with one or three light passes was used. Pulse durations ranged between 5 nsec (10 A, 10 MeV) and 1.5 μsec (200 mA, 5 MeV). Tektronix 556 dual-beam and 549 memory scopes were used. The light sources were 450-W Xe-Hg and 60 W D_2 lamps; Carl Zeiss M4QIII prism

(4) G. Rotilio, R. C. Bray, and E. M. Fielden, *Biochim. Biophys. Acta*, **268**, 605 (1972).

(5) D. Klug, J. Rabani, and I. Fridovich, *J. Biol. Chem.*, **247**, 4839 (1972).

(6) J. Rabani, D. Klug, and I. Fridovich, "Molecular Basis of Radiation Biology," G. Stein, Ed., Weizmann Press, Israel, 1972, p 1095.

(7) D. Klug-Roth, I. Fridovich, and J. Rabani, *J. Amer. Chem. Soc.*, in press.

(8) G. Rotilio, L. Morurgo, C. Giovagnoli, L. Calabrese, and B. Mondovi, *Biochemistry*, **11**, 2187 (1972).

(9) I. Fridovich, private communication.

(10) H. A. Schwarz, *J. Amer. Chem. Soc.*, **77**, 4960 (1955).

(11) (a) J. H. Baxendale and D. Smithies, *Z. Phys. Chem.*, **6**, 6242 (1956); (b) E. J. Hart and P. D. Walsh, *Radiat. Res.*, **1**, 498 (1954); (c) O. Micić and I. Draganić, *J. Phys. Chem.*, **70**, 2212 (1966).

(12) S. Gordon, E. J. Hart, M. S. Matheson, J. Rabani, and J. K. Thomas, *Discuss. Faraday Soc.*, **36**, 193 (1963).

(13) J. H. Baxendale, E. M. Fielden, C. Capellos, J. M. Francis, J. V. Davies, M. Ebert, C. W. Gilbert, J. P. Keene, E. J. Land, A. J. Swallow, and J. M. Nosworthy, *Nature (London)*, **201**, 468 (1964).

(14) G. Scholes and M. Simic, *J. Phys. Chem.*, **68**, 1738 (1964).

(15) J. H. Baxendale, E. M. Fielden, and J. P. Keene, "Pulse Radiolysis," M. Ebert, J. P. Keene, A. J. Swallow, and J. H. Baxendale, Ed., Academic Press, New York, N.Y., 1965, p 217.

(16) (a) J. Rabani, *J. Phys. Chem.*, **66**, 361 (1962); (b) J. Rabani and D. Meyerstein, *J. Phys. Chem.*, **72**, 1599 (1968).

(17) M. S. Matheson, W. A. Mulac, J. L. Weeks, and J. Rabani, *J. Phys. Chem.*, **70**, 2092 (1966).

(18) (a) J. P. Keene, *Radiat. Res.*, **22**, 1 (1964); (b) S. Gordon, E. J. Hart, M. S. Matheson, J. Rabani, and J. K. Thomas, *J. Amer. Chem. Soc.*, **85**, 1375 (1963).

(19) (a) J. P. Sweet and J. K. Thomas, *J. Phys. Chem.*, **68**, 1363 (1964); (b) H. Fricke and J. K. Thomas, *Radiat. Res. Suppl.*, **4**, 35 (1964).

(20) A. Fojtik, G. Czapski, and A. Henglein, *J. Phys. Chem.*, **74**, 3204 (1970).

(21) D. Behar, G. Czapski, L. M. Dorfman, J. Rabani, and H. A. Schwarz, *J. Phys. Chem.*, **74**, 3209 (1970).

(22) (a) E. J. Hart, *Radiat. Res.*, **2**, 33 (1955); (b) J. H. Baxendale, *Advan. Catal.*, **4**, 31 (1952).

monochromator with the Xe-Hg lamp or B and L grating monochromator with the D₂ lamp were employed. Scattered light was measured by adjusting the monochromator on a wavelength where no light was expected (*e.g.*, 180 nm). Any light signal was attributed to scattered light. Practically no scattered light was found.

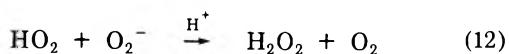
A syringe technique²³ or a flow system have been employed. When the flow system was used to fill the cell, the solution was pushed by oxygen or argon, depending on whether an oxygenated or argon-saturated solution was used. In order to guarantee removal of radiation products, the irradiation cell was emptied and refilled after each pulse (air was used to empty the cell in the case of oxygenated solutions, argon in the argon saturated solutions).

In all cases, blank experiments were carried out as described previously⁵ to make sure that impurities did not have an important role in the peroxy reactions. The pH of the solutions was always measured before irradiation. The temperature ranged between 20 and 25°. A shutter between the analyzing light source and the irradiation cell was opened shortly (~1 sec) before pulsing, to minimize photolysis.

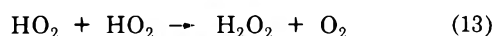
Materials. Either triply distilled or five times distilled water was used. Unless otherwise stated, triply distilled water has been used. All the materials used were of high purity grade and were used as received. Cu(ClO₄)₂ was Fluka, purum, CuSO₄ Merck, p.e., HCO₂Na Riedel de Haen, pa., HClO₄ Riedel de Haen, pa., methanol Merck, pa.

Results and Discussion

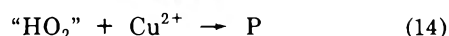
Unless otherwise stated the solutions were O₂ saturated. In the absence of a catalyst, peroxy radicals decay away by a second-order process. In neutral and in acid solutions, reactions 12 and 13^{2,21} are important. In the presence of cupric ions the decay of absorbance due to HO₂ and O₂⁻ became first order in peroxy and approximately first-order in cupric ions concentration. Typical oscilloscope traces are given in Figure 1. At relatively low Cu²⁺ concentrations such as in Figure 1a, the optical absorption due to HO₂ and O₂⁻ decays away by a single process. At higher concentrations, such as in Figures 1b and 1c, two processes can be observed. The rate of the first one increases with the Cu²⁺ concentration and we attribute this process (in the following will be referred to as "A") to a reaction between the equilibrium mixture of HO₂ and O₂⁻ ("HO₂" in the following) with Cu²⁺ ions. P represents the products of reaction 14. The nature of P will be discussed later. The second process ("B") whose rate seems to be independent of [Cu²⁺] will be described further.



$$k = 8.5 \times 10^7 \text{ M}^{-1} \text{ sec}^{-1}$$



$$k = 6.7 \times 10^5 \text{ M}^{-1} \text{ sec}^{-1}$$



The absorbance change does not normally decay away to its value before pulsing. An absorbance change (in following the "residual absorbance") remains at least for a period of 1 min. The magnitude of the residual absorbance depends on the formate concentration and on the wavelength. The effect of pH has not been investigated.

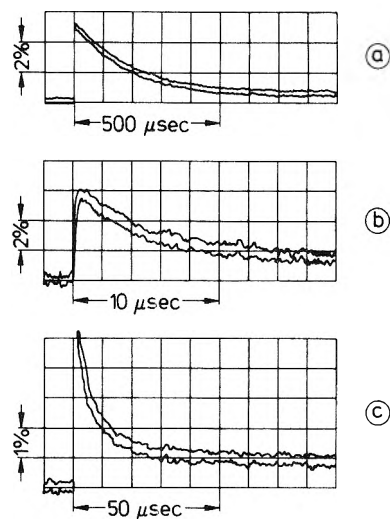


Figure 1. Oscilloscope traces representing the decay of HO₂ + O₂⁻ in O₂ saturated cupric ions solutions (4-cm cell, one pass, 245 nm, 10-nsec pulse producing 4 μM (O₂⁻ + HO₂), 22°): (a) pH 4.5, 1.4 μM Cu(ClO₄)₂ + 1.1 mM sodium formate + 1.8 × 10⁻⁴ M HClO₄; (b and c) 3.5 × 10⁻⁵ M Cu(ClO₄)₂ + 9.2 × 10⁻⁴ M formate + 1.43 × 10⁻⁵ M HClO₄, pH 5.1

As will be seen later, we have reasons to conclude that the residual absorbance is due to Cu⁺ ions.

Catalysis at Low Cu²⁺ Concentrations. At low copper concentrations, such that [Cu²⁺] < ["HO₂"], only one decay process is observed. From the effect of [Cu²⁺] on the rate of decay we identify this as the decay A. Plots of ln (D_t - D_∞) vs. time were linear. D_t is the absorbance change at time *t* after the electron pulse. D_∞ was zero or close to zero at low [Cu²⁺].

This linearity was not varied when ["HO₂"] ranged between 2 and 200 μM. It strongly suggests a reaction first order in "HO₂." The slopes of such lines were proportional to the Cu²⁺ concentration at a given pH. Corrections were sometimes necessary (up to 25%, but usually much less). The corrections were estimated from the decay of HO₂ and O₂⁻ in each of the solutions, before Cu²⁺ ions were added. We conclude that the overall rate of reaction 14 at low [Cu²⁺] is first order in both ["HO₂"] and [Cu²⁺]. Thus, a second-order rate constant for reaction 14 can be calculated. It is pH dependent as demonstrated in Figure 2.

Since the concentration of Cu²⁺ was much lower than the initial "HO₂" concentration after the pulse, the reaction must be a catalytic one. There must be some mechanism for Cu²⁺ regeneration during the catalysis, apparently *via* reactions of the products P with "HO₂." In the case of such a catalytic reaction one can expect that Cu²⁺ decays away partially, and reaches a steady concentration. Steady-state concentrations of products, which may be Cu⁺, Cu⁰, or complexes of Cu²⁺ with "HO₂," should correspondingly be established at the expense of [Cu²⁺]. Due to the very low concentrations of the initially present Cu²⁺, only minor absorbance changes can take place as a result of the establishment of steady-state concentrations, and the only observable effect is the enhanced decay of "HO₂."

Reaction at Higher [Cu²⁺]/["HO₂"] Ratios and at Various pH's. In Table I we present data which show the effects of [Cu²⁺], [formate], [H⁺], and ["HO₂"]₀ (the initial ["HO₂"]) on *k*₁₄ at constant pH. *k*₁₄ decreases somewhat

(23) C. Senvar and E. J. Hart, *Proc. 2nd Intern. Conf. Peaceful Uses At. Energy*, **29**, 19 (1958).

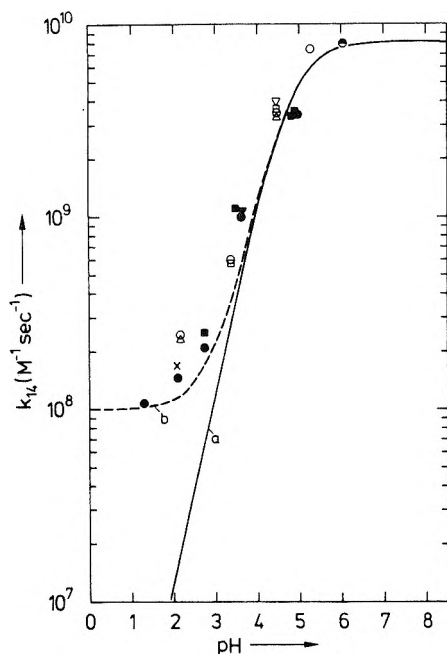
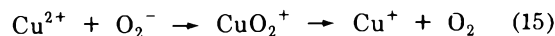


Figure 2. Second-order rate constant of the reaction of "HO₂" with Cu²⁺ as a function of pH at low ratio [Cu²⁺]/["HO₂"]₀ (unless otherwise stated, O₂ saturated solutions, 20–24°, 4-cm cell, one or three passes used, 245 nm, five times distilled water): O, 4 μM Cu²⁺, 4 μM ["HO₂"]₀, 1.2 mM formate; □, 4 μM Cu²⁺, 28 μM ["HO₂"]₀, 1.2 mM formate; Δ, 2 μM Cu²⁺, 4 μM ["HO₂"]₀, 1.1 mM formate; ▽, 1.4 μM Cu²⁺, 29 μM ["HO₂"]₀, 1.1 mM formate; X, 1.0 μM Cu²⁺, 30 μM ["HO₂"]₀, no formate; ●, 1.2 μM Cu²⁺, 3.6 μM ["HO₂"]₀, 4.5 mM formate; ○, 2 μM Cu²⁺, 150 μM ["HO₂"]₀, 10 mM formate; ▼, 2 μM Cu²⁺, 150 μM ["HO₂"]₀, 10 mM formate, aerated; ■, 1 μM Cu²⁺, 150 μM ["HO₂"]₀, 10 mM formate. The full points are results at the higher ionic strengths because of the high formate concentration. Lines are calculated using $k_{15} = 8.0 \times 10^9 \text{ M}^{-1} \text{ sec}^{-1}$, $pK_{\text{HO}_2} = 4.83$, and neglecting ionic strength effects: (a) k_{15}' and k_{16}' assumed as zero, k_{16} assumed equal to k_{15} ; (b) $k_{15}' = 1 \times 10^8 \text{ M}^{-1} \text{ sec}^{-1}$, k_{16} assumed equal to k_{15} , k_{16}' assumed equal to k_{15} .

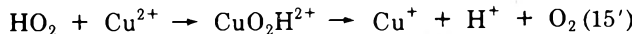
as the concentration of "HO₂" increases. ["HO₂"]₀ has an effect on k_{14} ; at constant pH, [Cu²⁺], and [formate], k_{14} increases somewhat at higher pulse intensities. These effects are relatively small, but are systematically observed, and must be attributed, generally, to real chemical effects, and not to experimental scatter of the results. The effect of [Cu²⁺] seems to be stronger at low pH. Thus, at pH 3.35 an increase of 100-fold in [Cu²⁺] causes an approximately twofold decrease in k_{14} , while at pH 6.05 a similar increase in [Cu²⁺] seems to effect k_{14} by 0–20%. The small changes and the scatter in the data makes it difficult to treat these effects quantitatively. In addition, in some cases, due to poor time separation between decays A and B, there might be an additional error in k_{14} . All the rate constants in Table I were obtained as $(1/[\text{Cu}^{2+}])(d/dt) \ln (D_t - D_\infty)$, where D_∞ is the absorbance at the end of the decay of fraction A. D_∞ was measured directly when there was a good separation between decays A and B or when the decay B was absent. Otherwise D_∞ was chosen so that the plot of $\ln (D_t - D_\infty)$ vs. t is linear. Values of D_∞ so chosen were nearly identical with the extrapolated absorbances from the kinetics of the decay B. The decay B was absent in the following cases: (a) less than 10^{-5} M Cu²⁺; (b) relatively slow decay A ($\tau_{1/2} > 10 \mu\text{sec}$); (c) at formate concentrations higher than 10^{-2} M , at least 98% of the decaying absorbance was the decay A.

Mechanism. The results agree with the following mech-

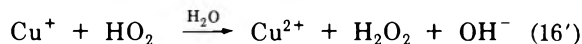
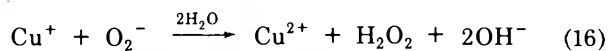
anism. Suppose that O₂⁻ reduces Cu²⁺ to Cu⁺ (perhaps via a complex CuO₂⁺) according to the reaction



HO₂ may also be able to reduce Cu²⁺, but it is reasonable to assume that k_{15}' is much smaller than k_{15} , as indicated by the decrease in k_{14} at pH values below the pK of HO₂ in Table I.



Let us assume now that the product Cu⁺ is reactive toward both O₂⁻ and HO₂.



In near neutral solutions, when Cu²⁺ is present at a large excess over O₂⁻ reaction 15 has no competition. The results of Table I at high Cu²⁺ concentrations show that k_{15} is nearly diffusion controlled. At relatively low initial Cu²⁺ concentrations (Figure 2 and Table I), values of k_{14} close to $10^{10} \text{ M}^{-1} \text{ sec}^{-1}$ are measured at near neutral pH. Under such conditions, both reaction 15 and 16 are important. k_{16} cannot be lower than k_{15} since otherwise (16) would become the rate-determining step at low [Cu²⁺] and the catalytic process would be slower as reaction 15, which is not the case. We therefore conclude that $k_{16} \cong k_{15}$.

Since the oxidizing power of HO₂ is stronger than that of O₂⁻ and since reaction 16 is already practically diffusion controlled, the reaction of Cu⁺ with "HO₂" is expected to be fast also at lower pH values when HO₂ is predominant in the equilibrium of eq 11. We propose that at lower pH values reaction 15 of Cu²⁺ with "HO₂" is rate determining and the decrease in the apparent rate constant k_{14} is due to the decreasing concentration of O₂⁻ in the equilibrium of eq 11.

The apparent changes in k_{14} with changing Cu²⁺ concentration and pulse intensity described above can be rationalized on the basis of the proposed mechanism. Let us at first consider solutions at low pH where HO₂ is mainly present in the equilibrium of eq 11. At high [Cu²⁺], only reaction 15 is responsible for the disappearance of "HO₂." The rate constant will then be $k_{15}[\text{O}_2^-]/[\text{"HO}_2\text{"}]$ (O₂⁻ being supplied by the dissociation of HO₂). At low Cu²⁺ concentration or high dose, a certain amount of Cu⁺ will accumulate that undergoes reaction with HO₂ according to eq 16'. If $k_{16}' > k_{15}[\text{O}_2^-]/[\text{"HO}_2\text{"}]$, the replacement of Cu²⁺ by Cu⁺ enhances the overall rate for "HO₂" decay in agreement with the results. If $k_{16} \gg k_{15}[\text{O}_2^-]/[\text{"HO}_2\text{"}]$, the enhancement may occur even at relatively high Cu²⁺ concentration. In the case of solutions of pH > 5.5 where the equilibrium of eq 11 is shifted toward the side of O₂⁻ and Cu²⁺ and Cu⁺ have nearly equal reactivities toward "HO₂," little effect of [Cu²⁺] on k_{14} is expected. This expectation is in agreement with the observations described above.

On the basis of our above discussion, it is apparent that k_{15} is equal to the measured apparent rate constant k_{14} only at high ratios [Cu²⁺]/["HO₂"]₀. In Figure 3, we present the pH dependency of k_{14} at high ratio [Cu²⁺]/["HO₂"]₀. A comparison with Figure 2, where the ratio [Cu²⁺]/["HO₂"]₀ was low, shows that at pH values below the pK of HO₂ all points lie above the calculated curves in Figure 3.

The lines a and b in Figures 2 and 3 were calculated

TABLE I: Effect of $[\text{Cu}^{2+}]$, pH, and Pulse Intensity on k_{14}^a

pH ^b	$[\text{Cu}^{2+}]$, μM	$k_{14}^c \times 10^7$ $\text{M}^{-1} \text{sec}^{-1}$	$[\text{HO}_2^\bullet]_0$, $\mu\text{M}/\text{pulse}$	[Sodium formate], mM	pH ^b	$[\text{Cu}^{2+}]$, μM	$k_{14}^c \times 10^7$ $\text{M}^{-1} \text{sec}^{-1}$	$[\text{HO}_2^\bullet]_0$, $\mu\text{M}/\text{pulse}$	[Sodium formate], mM
0.80	210	5.6	4.5	1.03	3.50	83	44	2.1	1.30
0.80	210	7.2	33	1.03	3.50	83	51	11.3	1.30
0.80	210	6.3	4.5	8.1	3.50	122	40	2.1	1.30
0.80	210	9.4	45	8.1	3.50	203	32	1.9	1.30
1.30	193	6.5	150	10	3.50	203	48 ^e	4.8	1.30
1.40	210	12.0	4.5	1.03	3.50	203	40	4.8	1.30
1.40	210	16.5	36	1.03	4.43	1.4	330	4.1	1.09
2.15	2.6	24	4.5	1.03	4.43	1.4	410	29	1.09
2.15	2.6	23	35	1.03	4.43	4.7	320	4.1	1.09
2.15	8.3	28	4.5	1.03	4.43	4.7	310	29	1.09
2.15	8.3	24	35	1.03	4.43	9.3	380	4.1	1.09
2.15	31	22	4.5	1.03	4.43	9.3	450	29	1.09
2.15	31	23	35	1.03	4.43	30.3	260	4.1	1.09
2.15	85	19	4.5	1.03	4.43	30.3	350	29	1.09
2.15	85	22	35	1.03	4.43	77	230	4.1	1.09
2.15	210	17	4.5	1.03	4.43	77	260	29	1.09
2.15	210	19	35	1.03	4.43	77	170	4.1	14.0
2.70	410	16	4.0	15	4.43	77	200	29	14.0
2.70	410	21	27	15	5.10	47	550	3.9	0.92
3.35	4.1	60	3.4	1.28	5.10	95	450	3.9	0.92
3.35	4.1	59	28	1.28	5.10	190	460	3.9	0.92
3.35	14.2	48	3.4	1.28	5.10	190	380 ^f	3.9	0.92
3.35	14.2	64 ^d	28	1.28	5.27	3.1	740	4.1	1.07
3.35	14.2	56	3.4	1.28	5.27	11.5	640	4.1	1.07
3.35	46	46	3.4	1.28	5.27	46	600	4.1	1.07
3.35	120	45	3.4	1.28	5.27	46	430	4.1	17
3.35	120	44	28	1.28	5.40	104	440	3.0	3.85
3.35	410	28	3.4	1.28	5.40	104	380	3.0	11.7
3.35	410	35	28	1.28	5.40	246	320	3.0	11.7
3.35	410	38	41	1.28	6.05	1.23	800	4.1	4.5
3.50	14	75	1.2	1.30	6.05	6.5	600	4.1	4.5
3.50	35	45	1.2	1.30	6.05	39	820	4.1	4.5
3.50	83	34	1.2	1.30	6.05	106	650	4.1	4.5

^a Measured at 245 nm, using light path of 4 cm, O₂ saturated. Each result represents an average of three-six runs. Temperature was 20–23°. ^b Before pulsing. ^c Corrected for the decay of peroxy radicals in the blanks. ^d The solution was illuminated with the analyzing light beam for 2 min prior to pulse irradiation. ^e Twentieth pulse. ^f Aerated.

assuming a large excess in $[\text{Cu}^{2+}]$ over $[\text{HO}_2^\bullet]$ according to

$$k_{14} = k_{15}/(1 + [\text{H}^+]/K_{11}) + k_{15}'(1 + K_{11}/[\text{H}^+]) \quad (17)$$

where K_{11} is the equilibrium constant of eq 11. Reasonable agreement with the experimental points in Figure 3 is obtained using $k_{15} = 8 \times 10^9$ and $k_{15}' = 1 \times 10^8 \text{ M}^{-1} \text{ sec}^{-1}$. Somewhat lower rate constants are observed at higher formate concentrations. This can be accounted for at least in part by an ionic strength effect on reaction 15. We were unable to observe any significant effect of complex formation between Cu^{2+} and formate²⁴ on the rate of reaction 15 under our concentration conditions. When Cu^{2+} is present in catalytic amounts, a steady state can be assumed for Cu^{2+} and Cu^+ . It can be shown that under such conditions equation 18 must hold.

$$k_{14} = 2r_{15}r_{16}/(r_{15} + r_{16}) \quad (18)$$

where $r_i = k_i/(1 + [\text{H}^+]/K_{11}) + k_i \cdot (1 + K_{11}/[\text{H}^+])$. Note that r_i is an effective rate constant for peroxy radicals with cupric ions (r_{15}) and with cuprous ions (r_{16}).

At sufficiently high acidities, if k_{16}' becomes significantly larger than $k_{15}[\text{O}_2^-]/[\text{HO}_2^\bullet]$, eq 18 can be written as

$$k_{14} \cong 2r_{15} \quad (19)$$

On the other hand, we have shown that at high ratio $[\text{Cu}^{2+}]$

$[\text{HO}_2^\bullet]$, $k_{14} = r_{15}$ (see eq 17). Hence, the use of catalytic amounts of Cu^{2+} may increase the apparent reactivity toward HO_2^\bullet by up to a factor of 2. This is indeed observed when one compares the data for the lower pH values in Figures 2 and 3. Many of the results in Figure 2 have been measured in 10 mM formate, and a correction for the ionic strength effect is expected to increase k_{14} in these experiments.

In near neutral solutions, $r_{15} \cong r_{16}$ and $k_{14} \cong r_{15} \cong r_{16} \cong k_{15} \cong k_{16}$ in both low and high $[\text{Cu}^{2+}]/[\text{HO}_2^\bullet]$. Little or no $[\text{Cu}^{2+}]$ effect on the apparent reaction rate k_{14} is expected.

Process B. The decay process B amounts to 0–15% of the initial O_2^- absorbance at 245 nm. It is observed only at the higher $[\text{Cu}^{2+}]$. Its magnitude becomes lower at higher formate concentrations, from ~15% at 1 mM to less than 2% at 10 mM formate. The half-life of this process is 5–10 μsec , independent on $[\text{O}_2]$ (air and O₂ saturated solutions were tested) and on $[\text{Cu}^{2+}]$ (tested at pH 5.1, $9.2 \times 10^{-4} \text{ M}$ formate, 3.5×10^{-5} – $1.9 \times 10^{-4} \text{ M}$ $\text{Cu}(\text{ClO}_4)_2$). Due to the relatively small amount of decay and to the poor separation from the decay A in many experiments under our conditions, no systematic investigation of this process was made. The lack of process B at

(24) H. M. Hershenson, R. T. Brooks, and M. E. Murphy, *J. Amer. Chem. Soc.*, **79**, 2046 (1957).

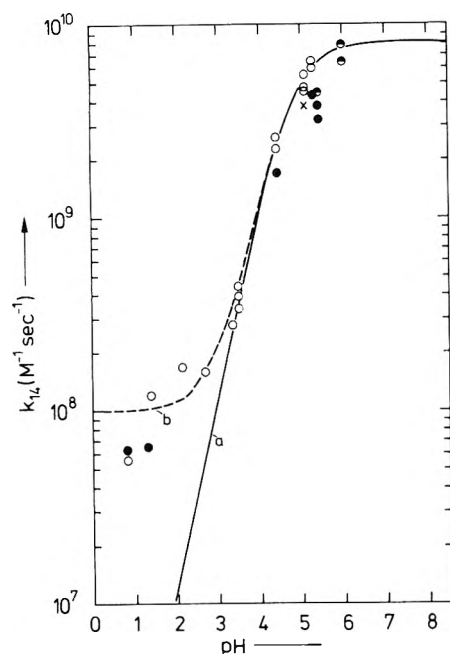
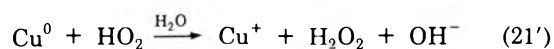
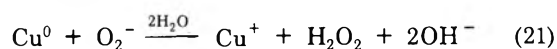
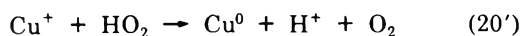
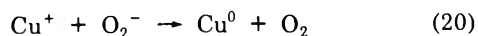


Figure 3. The reactivity of Cu^{2+} toward HO_2 at high ratio $[\text{Cu}^{2+}]/[\text{HO}_2]_0$. Data taken from Table 1. The temperature ranged between 20 and 24°: O, about 1 mM formate; ●, about 4 mM formate; ●, 8–15 mM formate. The full points are results at high ionic strength because of the high formate concentration. The calculated lines a and b are the same as in Figure 2. As we have here a large excess of Cu^{2+} , reactions 16 and 16' can be neglected without respect what are their rate constants.

lower $[\text{Cu}^{2+}]$ and at low pH where the decay A is relatively slow may indicate that decay B is not independent, but is consecutive to the decay A.

These observations could perhaps be explained by the formation of a complex CuO_2^+ as already indicated in eq 15 whose lifetime is 5–10 μsec . The decay B would have to be attributed to the decay of this complex according to eq 15. No satisfactory explanation can be given for the fact that the complex could not be observed at higher formate concentrations.

Alternative Mechanism of Catalysis. In the mechanism of catalysis, according to eq 15, 15', 16 and 16', Cu^{2+} and Cu^+ are the active valence states of copper that participate. One could conceive of another mechanism, in which Cu^+ and Cu^0 are the active intermediates for catalysis. After formation of Cu^+ via reaction 15 or 15', the following processes could take place



Both mechanisms 15–16' and 15, 20–21' could occur simultaneously.

Let us discuss first the more acidic pH range, where HO_2 is predominant. HO_2 radicals are relatively strong oxidizing and relatively poor reducing species. Therefore, it is likely that reaction 16' will compete efficiently with 20', and practically no Cu^0 will be produced in these solutions. In the solutions at near neutral pH, mechanism of equations 20–21' could be feasible if reaction 21 is nearly diffusion controlled. The standard redox potential of the system $\text{O}_2^-/\text{H}_2\text{O}_2$ is not known. Since the standard po-

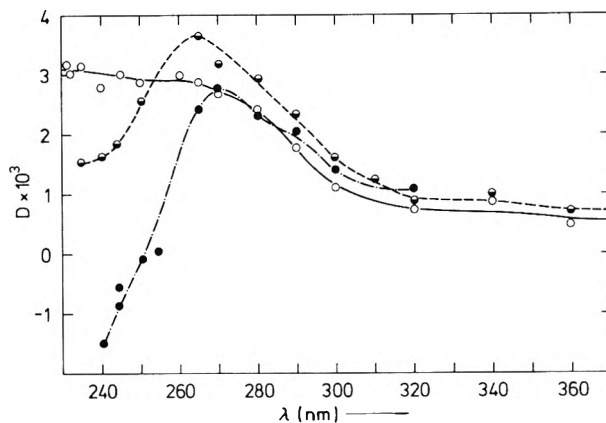


Figure 4. The residual absorption spectra obtained in oxygenated Cu solutions. The spectra were measured 100 μsec after an electron pulse, using a 4-cm light path: O, 3.5×10^{-5} M $\text{Cu}(\text{ClO}_4)_2$, 9.2×10^{-4} M formate, $[\text{HO}_2]_0 = 3.9 \mu\text{M}$, pH 5.55, optical density normalized to $[\text{HO}_2]_0 = 2.83 \mu\text{M}$, 20°; ● and ●, 1.04×10^{-4} M $\text{Cu}(\text{ClO}_4)_2$, $[\text{HO}_2]_0 = 2.83 \mu\text{M}$, pH 5.40, 22°; ●, 3.85 mM formate; ●, 11.7 mM formate.

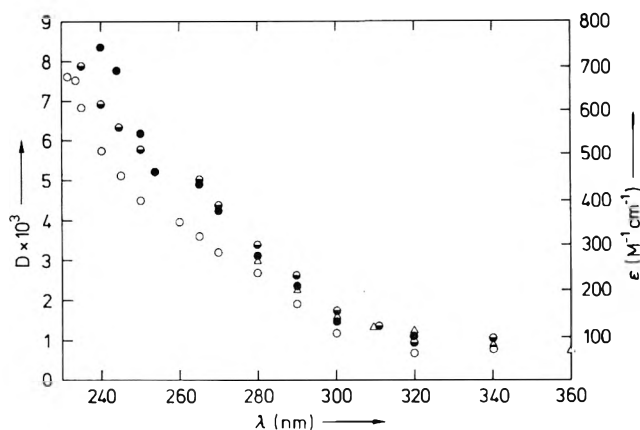


Figure 5. The absorption spectrum of Cu^+ . The spectra were obtained using the results of Figure 4 and correcting for the bleaching of the Cu^{2+} absorbance (see text): O, ●, ●, see Figure 4; Δ, corrected and normalized absorbances obtained in a 1.04×10^{-4} M $\text{Cu}(\text{ClO}_4)_2$, 3.8 mM formate, $[\text{HO}_2]_0 = 3.8 \mu\text{M}$, pH 5.30, 24°, O_2 saturated solution. A filter to protect from uv light below 280 nm was used. The uncorrected data appear in Figure 6.

tential of Cu^+/Cu^0 (0.52 V) is much more positive than that of $\text{Cu}^{2+}/\text{Cu}^+$, it seems conceivable that O_2^- can oxidize Cu^+ efficiently, but not Cu^0 . HO_2 is known to be an efficient oxidation agent. It is likely, therefore, that mechanism 15–16' prevails in both neutral and acidic solutions.

Spectrum of Cu^+ and the Identification of Cu^+ as the Product of (15). The nature of the final product of reaction 15 was investigated by means of its absorption spectrum. The absorption spectrum obtained in $\text{Cu}(\text{ClO}_4)_2$ -formate- O_2 solutions, immediately after the pulse, was identical with the spectrum of the equilibrium mixture $\text{HO}_2 + \text{O}_2^-$.²¹

The spectrum of the residual absorption depends strongly on the concentration of formate. This is demonstrated in Figure 4, where spectra obtained after 70 μsec in 3.85 and 11.7 mM formate at pH 5.4 and in 9.2×10^{-4} M formate at pH 5.5 are presented. This is due to the bleaching of the Cu^{2+} absorbance, which depends on the formate concentration. The amount of bleaching of the Cu^{2+} absorbance depends on the formate concentration. This is due to ion pair formation between Cu^{2+} and for-

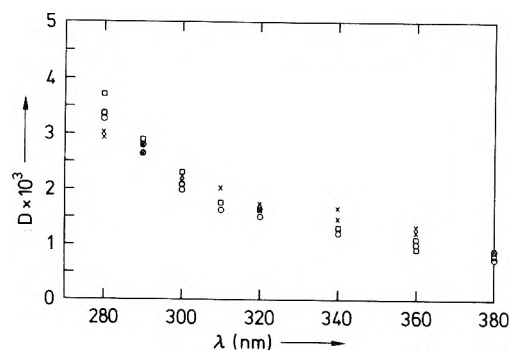


Figure 6. Comparison of spectra in the presence and absence of O_2 . The spectra were taken at 24° 400 μ sec after the electron pulse, $[^{\cdot}HO_2]_0 = 3.8 \mu M$. A filter to protect from uv light below 280 nm was used: O, $1.04 \times 10^{-4} M$ $Cu(ClO_4)_2$, 3.8 mM formate, saturated O_2 at pH 5.30; \square , $1.04 \times 10^{-4} M$ $Cu(ClO_4)_2$, 3.8 mM formate, deaerated, pH 5.30; X, $3.80 \times 10^{-4} M$ $Cu(ClO_4)_2$, $4.1 \times 10^{-2} M$ methanol, deaerated, pH 5.3.

mate, which have higher absorbance as compared with Cu_{aq}^{2+} . We carried out spectral measurements in unirradiated solutions containing both Cu^{2+} and formate ions. At 244 nm, the extinction coefficient of a $1.04 \times 10^{-4} M$ $Cu(ClO_4)_2$ solution was found to be ϵ 115 $M^{-1} cm^{-1}$. Upon the addition of 3.85 mM formate at pH 5.40 the apparent extinction coefficient of Cu^{2+} became 390 $M^{-1} cm^{-1}$, while in a $1.17 \times 10^{-2} M$ formate (same pH) it was 740 $M^{-1} cm^{-1}$.

Similar effects have been observed at other wavelengths, as well as in a solution containing $9.3 \times 10^{-4} M$ formate and $3.5 \times 10^{-5} M$ $Cu(ClO_4)_2$ where an apparent ϵ 205 $M^{-1} cm^{-1}$ was measured at 244 nm. From such results, an equilibrium constant $K = [copper\ formate]/[Cu^{2+}][formate] = 50 M^{-1}$ could be calculated. This is in agreement with polarographic measurements²⁴ which yielded $K = 37 M^{-1}$ at ionic strength $\mu = 2.00$. The association of a second formate ion can be neglected under our conditions.²⁴ Under our conditions, only 5% of the Cu^{2+} ions form ion pairs at 1 mM formate, while 33% form ion pairs at 10 mM formate. We have measured the absorbance spectra of the Cu^{2+} formate under the conditions of Figure 4, and corrected the spectra of the residual absorbance for the bleaching of the Cu^{2+} formate absorbance.

The corrected spectra are presented in Figure 5. The agreement between the corrected spectra is good. Therefore we conclude that the corrected residual absorbance spectrum represents the absorption spectrum of the product of reaction 15. Apparently the same product is obtained in all three formate concentrations which have been tested. The lower absorption in $3.5 \times 10^{-5} M$ $Cu(ClO_4)_2$ may be due to some oxidation of the product Cu^+ , due to the relatively low $[Cu^{2+}]$.

In Figure 6 we present the spectra (uncorrected for cu-

pric bleaching) obtained in solutions of $Cu(ClO_4)_2$ containing formate and O_2 , formate in the absence of O_2 , and methanol in the absence of O_2 . These spectra are identical within experimental error. As we observed a strong photolytic effect, which strongly affects the radiation results in the deoxygenated solutions, an appropriate light filter was used in these experiments, which prevented us from measurements below 280 nm. Note that the results in the oxygenated formate solutions were corrected for bleaching and plotted in Figure 5, where they are shown to be identical with similar results obtained in O_2 solutions without light protection. In the absence of O_2 , the product of irradiation is Cu^+ ions. Cu^+ is formed upon the reduction of Cu^{2+} by e_{aq}^- . In the absence of O_2 , all e_{aq}^- are expected to be scavenged by Cu^{2+} . H atoms may also react with Cu^{2+} , or react with the organic solutes and produce the organic radicals $CO_2^{\cdot-}$ and CH_2OH^{\cdot} in the formate and methanol solutions, respectively. These organic radicals are expected to be formed also as a result of the attack by OH radicals. Eventually, Cu^{2+} will be reduced with $G = G_e + G_H + G_{OH}$. Reduction of Cu^{2+} by various organic radicals has been reported previously.^{11,25} The residual absorption in pulse irradiated $1.93 \times 10^{-4} M$ $Cu(ClO_4)_2$ in $10^{-2} M$ formate at pH 1.3 was still found to be present after 1 min (tested at 245 nm). Some of the absorbances in Figure 6 were tested and found to be stable for at least 5 msec. This is in agreement with the known fact that the metastable solutions of Cu^+ can be used for some time without an appreciable disproportionation of Cu^+ .²⁶ The agreement between all three spectra in Figure 6 indicates that Cu^+ is obtained also in the oxygenated solutions, namely, that Cu^+ is the final product of reaction 15. It is known that Cu^+ solutions are sensitive to O_2 . Apparently, oxidation by O_2 does not take place within the time range of our measurements under our conditions.

The spectra in Figure 6 have not been corrected for copper bleaching. This correction is relatively small above 280 nm (up to about 30%). We preferred to avoid the correction, as no accurate data concerning the extinction coefficient of Cu^{2+} and Cu^{2+} -formate were available above 280 nm. Our measurements showed, however, that Cu^{2+} and Cu^{2+} -formate ion pairs under the conditions of Figure 6 had nearly the same extinction coefficients above 280 nm. Therefore the comparison of the three spectra is meaningful.

Acknowledgment. The authors are indebted to M. Wilhelm, E. Janata, and Y. Ogdan for careful operation and maintenance of the linacs. We would like to thank Professor A. Henglein for many helpful discussions and for critical comments on the manuscript.

(25) A. MacLachlan, *J. Phys. Chem.*, **71**, 4132 (1967).

(26) J. H. Espenson, K. Shaw, and O. J. Parker, *J. Amer. Chem. Soc.*, **89**, 5730 (1967).

Electron Scavenging and Product Formation in the γ -Radiolysis of Nitrous Oxide–Liquid Xenon Solutions¹

Stefan J. Rzad* and George Bakale²

Radiation Research Laboratories and Center for Special Studies, Mellon Institute of Science, Carnegie-Mellon University, Pittsburgh, Pennsylvania 15213 (Received December 4, 1972)

Publication costs assisted by Carnegie-Mellon University

γ -Irradiation of solutions of nitrous oxide in liquid xenon at 164°K results in the formation of nitrogen and oxygen, the latter being ~10% of the former. At low $[\text{N}_2\text{O}]$ both products increase with increasing N_2O concentration then level off between 10^{-2} and 10^{-1} M nitrous oxide ($G(\text{N}_2) \sim 8$) and increase again above 10^{-1} M N_2O where they become dependent on the square of the nitrous oxide concentration. The addition of sulfur hexafluoride to the system completely inhibits the formation of both products indicating that the electron is the primary precursor of both species. For a given nitrous oxide concentration the yields of nitrogen increase with decreasing dose rate indicating that the electrons are homogeneously distributed in liquid xenon. Carbon dioxide decreases the yield of nitrogen to a constant value of $G(\text{N}_2) = 4.3$ which is found to correspond to the yield of electrons produced by γ -irradiation of liquid xenon (*i.e.*, $W = 23.3$). The following mechanism is found to be consistent with all of the data: $\text{Xe} \rightarrow \text{e}^- + \text{Xe}^+$; $\text{e}^- + \text{N}_2\text{O} \rightarrow \text{N}_2\text{O}^-$ (k_3'); $\text{N}_2\text{O}^- + \text{N}_2\text{O} \rightarrow \text{N}_2 + (\text{N}_2\text{O})\text{O}^-$ (k_{10}); $\text{N}_2\text{O}^- + \text{CO}_2 \rightarrow \text{N}_2 + \text{CO}_3^-$ (k_6'); $(\text{N}_2\text{O})\text{O}^- + \text{Xe}^+ \rightarrow 2\text{NO} + \text{Xe}$ (k_{11}); $(\text{N}_2\text{O})\text{O}^- + \text{N}_2\text{O} \rightarrow (\text{N}_2\text{O})_2\text{O}^-$ (k_{12}); $(\text{N}_2\text{O})_2\text{O}^- + \text{Xe}^+ \rightarrow \text{N}_2 + 2\text{NO} + \text{O} + \text{Xe}$ (k_{13}); $(\text{N}_2\text{O})_2\text{O}^- + 2\text{N}_2\text{O} \rightarrow (\text{N}_2\text{O})_3\text{O}^- + \text{N}_2\text{O}$ (k_{14}); $(\text{N}_2\text{O})_3\text{O}^- + \text{Xe}^+ \rightarrow 2\text{N}_2 + 2\text{NO} + \text{O}_2 + \text{Xe}$ (k_{15}). From such treatment of the data k_{10} is estimated to be diffusion controlled and of the order of $\sim 10^{10}$ $\text{M}^{-1} \text{sec}^{-1}$, $k_{11} \approx k_{13} \sim 1.6 \times 10^{11}$ $\text{M}^{-1} \text{sec}^{-1}$, $k_{12} \approx 8.3 \times 10^4$ $\text{M}^{-1} \text{sec}^{-1}$, $k_{14} \approx 4.7 \times 10^3$ $\text{M}^{-2} \text{sec}^{-1}$, and $k_6'/k_{10} = 2.5$.

Introduction

Conductivity measurements^{3,4} and electron scavenging studies⁵ in irradiated liquid hydrocarbons have shown that most of the electrons undergo geminate recombination and only a small fraction becomes free and homogeneously distributed throughout the medium. The increase of this fraction when going from linear to branched hydrocarbons is accompanied by an increase in the mobility of the negative charge carrier^{4,6} (*e.g.*, *n*-hexane $G_{\text{fi}} = 0.13$,³ $\mu_e = 0.09$ $\text{cm}^2 \text{V}^{-1} \text{sec}^{-1}$,⁶ 2,2,4-trimethylpentane, $G_{\text{fi}} = 0.322$,³ $\mu_e = 7$ $\text{cm}^2 \text{V}^{-1} \text{sec}^{-1}$,⁶ and neopentane, $G_{\text{fi}} = 0.857$,³ $\mu_e = 55$ $\text{cm}^2 \text{V}^{-1} \text{sec}^{-1}$). Recently it has been shown that in liquid argon a large fraction of the electrons escape geminate recombination.⁷⁻⁹ Fuochi and Freeman⁹ estimated a free ion yield of $G_{\text{fi}} = 2.0$ at 87°K in liquid argon which is characterized by an electron mobility of 475 $\text{cm}^2 \text{V}^{-1} \text{sec}^{-1}$ ¹⁰ at this temperature. In liquid Xe the electron mobility is 2200 $\text{cm}^2 \text{V}^{-1} \text{sec}^{-1}$ ¹⁰ and therefore if the increase of the free ion yield with increase in mobility is real, one would expect most of the electrons to be free in irradiated liquid xenon. In such a case the scavenging of these electrons should follow simple homogeneous kinetics in contrast with the complex kinetics which are applicable in liquid hydrocarbons.⁵ Such scavenging studies are very important for the understanding of the ion recombination processes in irradiated liquids. With this in mind we have undertaken the study of the electron scavenging processes in irradiated N_2O -xenon solutions at 164°K.

Experimental Section

Air Products and Chemicals Research Grade xenon was degassed at liquid nitrogen temperature, stored under vacuum, and used without further purification (stated pu-

urity >99.995%). Matheson's nitrous oxide, sulfur hexafluoride, and carbon dioxide were purified by low-temperature distillation and stored under vacuum.

The irradiation cells were Pyrex U-shaped tubes of a total volume of *ca.* 0.5 cm^3 fitted with breakseals for removal of gases noncondensable at 77°K. A known amount of xenon (usually 0.36 cm^3) was introduced into the irradiation cell and condensed at 77°K. The amount of additive was measured by *PV* and distilled into the cell. The vessel was then sealed off and allowed to warm for 30 min in an ethyl iodide bath ($T = 164^\circ\text{K}$). The solubility of N_2O and CO_2 in liquid xenon at 164°K can be estimated from the thermodynamic data on the solubility of solids in cryogenic solvents given by Prausnitz and coworkers.¹¹⁻¹³ One can estimate that at saturation the mole fraction of the solute is 0.067 and 0.37 for CO_2 and N_2O , respectively. Since xenon is 28.6 M the solutes were completely in solution at the highest amounts used, *i.e.*, ~ 0.5 M.

- (1) Supported in part by the U. S. Atomic Energy Commission.
- (2) Present address: Hahn-Meitner-Institut, Berlin, Germany.
- (3) W. F. Schmidt and A. O. Allen, *J. Chem. Phys.*, **52**, 2345 (1970).
- (4) P. H. Tewari and G. A. Freeman, *J. Chem. Phys.*, **49**, 4394 (1968).
- (5) For example, see (a) J. M. Warman, K.-D. Asmus, and R. H. Schuler, *J. Phys. Chem.*, **73**, 931 (1969); (b) S. J. Rzad and J. M. Warman, *J. Chem. Phys.*, **49**, 2861 (1968); (c) S. J. Rzad and K. Bansal, *J. Phys. Chem.*, **76**, 2374 (1972); (d) M. G. Robinson and G. R. Freeman, *J. Chem. Phys.*, **55**, 5644 (1971); (e) K. Horacek and G. R. Freeman, *ibid.*, **53**, 4486 (1970).
- (6) W. F. Schmidt and A. O. Allen, *J. Chem. Phys.*, **52**, 4788 (1970).
- (7) N. V. Klassen and W. F. Schmidt, *Can. J. Chem.*, **47**, 4786 (1969).
- (8) P. H. Tewari and G. R. Freeman, *J. Chem. Phys.*, **51**, 1276 (1969).
- (9) P. C. Fuochi and G. R. Freeman, *J. Chem. Phys.*, **56**, 2333 (1972).
- (10) L. S. Miller, S. Howe, and W. E. Spear, *Phys. Rev.*, **166**, 871 (1968).
- (11) G. T. Preston and J. M. Prausnitz, *Ind. Eng. Chem., Process Des. Develop.*, **9**, 264 (1970).
- (12) E. W. Lychman, C. A. Eckert, and J. M. Prausnitz, *Chem. Eng. Sci.*, **20**, 703 (1965).
- (13) A. L. Myers and J. M. Prausnitz, *Ind. Eng. Chem., Fundam.*, **4**, 209 (1961).

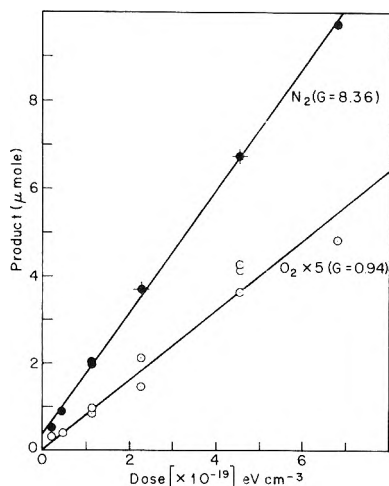


Figure 1. Dose dependence of the yield of nitrogen (●) and oxygen (○) at a dose rate of $2.28 \times 10^{18} \text{ eV cm}^{-3} \text{ min}^{-1}$ and $[\text{N}_2\text{O}] = 0.1 \text{ M}$. Flagged points represent several undistinguishable measurements.

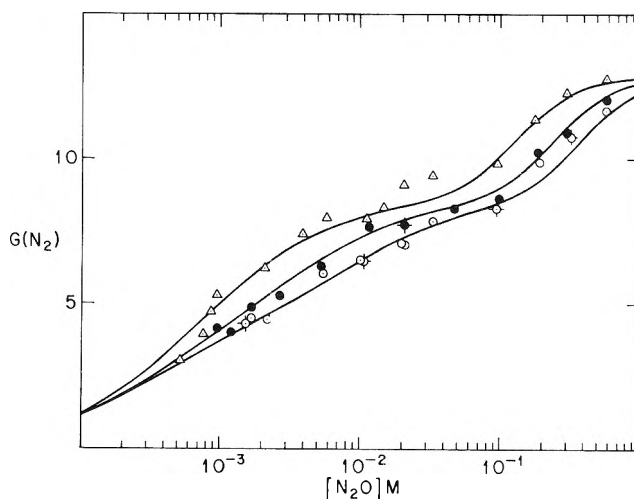


Figure 2. Nitrous oxide concentration dependence of the yield of nitrogen at three different dose rates: (Δ) 3.49×10^{16} , (●) 3.95×10^{17} , and (○) $2.28 \times 10^{18} \text{ eV cm}^{-3} \text{ min}^{-1}$. Flagged points represent G values obtained from yield dose plots as in Figure 1. Solid lines are calculated with eq III and the parameters given in the text.

The samples were ^{60}Co γ-irradiated at 164°K using a Gamma Cell 220 or a point source. Two different dose rates were obtained in the Gamma Cell by using a lead shielding. The dose rates were determined from the Fricke dosimeter correcting for the pertinent electron densities and soft radiation absorption (10%) by the xenon in the γ cell experiments where no lead shielding was present.¹⁴⁻¹⁶ The three dose rates studied were in units of $\text{eV cm}^{-3} \text{ min}^{-1}$ in xenon 2.28×10^{18} , 3.95×10^{17} , and 3.49×10^{16} .

After irradiation the gas noncondensable at 77°K was toepled into a gas buret and the pressure measured. The gas was then analyzed for composition by mass spectrometry.

Dose dependences were carried out at a dose rate of $2.28 \times 10^{18} \text{ eV cm}^{-3} \text{ min}^{-1}$ and N_2O concentrations of 1.5×10^{-3} , 10^{-2} , 0.1, and 0.3 M and at a dose rate of $3.95 \times 10^{17} \text{ eV cm}^{-3} \text{ sec}^{-1}$ and a N_2O concentration of $2 \times 10^{-2} \text{ M}$. The yield-dose plots were linear (Figure 1) both for nitrogen and oxygen. However, at 10^{-2} M N_2O and above small intercepts of nitrogen appear. *e.g.*, 0.37 μmol at 0.1 M N_2O . Except for the above-mentioned points all G values were calculated from single experiments corrected for the intercept which applies at this particular concentration range. The total dose delivered to the samples was $2.28 \times 10^{18} \text{ eV cm}^{-3}$ at concentrations below 10^{-2} M , $6.84 \times 10^{18} \text{ eV cm}^{-3}$ between 10^{-2} and 10^{-1} M , and $4.56 \times 10^{19} \text{ eV cm}^{-3}$ above 0.1 M.

Results

The gas noncondensable at 77°K was composed exclusively of nitrogen and oxygen. The yields of these products were linear with dose as is illustrated in Figure 1 for a 0.1 M N_2O solution at a dose rate of $2.28 \times 10^{18} \text{ eV cm}^{-3} \text{ min}^{-1}$. As can be seen on this figure the reproducibility of the oxygen data is much poorer. The oxygen yields increased from 5 to 10 to ~15% of that of nitrogen when the N_2O concentration increased from 0.01 to 0.1 to 0.3 M, respectively. The yields of nitrogen and oxygen increased with increasing N_2O concentration, Figures 2 and 3, and reached a plateau at $\sim 10^{-2} \text{ M}$ N_2O ($G(\text{N}_2) \sim 8$, $G(\text{O}_2) \sim 0.6$). A further increase in the yields occurred above 0.1 M N_2O . The yields of nitrogen also show a dose rate dependence (Figure 2). At a given N_2O concentration the $G(\text{N}_2)$ increases with decreasing dose rate. Such a dose rate de-

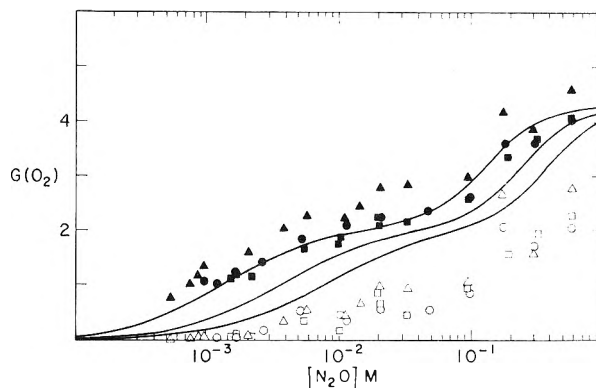


Figure 3. Nitrous oxide concentration dependence of the yield of oxygen at three different dose rates: (Δ,▲) 3.49×10^{16} , (○,●) 3.95×10^{17} , and (□,■) $2.28 \times 10^{18} \text{ eV cm}^{-3} \text{ min}^{-1}$. The open points are the experimental data. The solid points are calculated by eq VII as described in the text. Solid lines are calculated with eq V and the parameters given in the text.

pendence is less noticeable for oxygen due to the much larger scatter of the experimental data. The addition of SF_6 , a very efficient electron scavenger, decreased the yield of nitrogen and oxygen from N_2O -xenon solutions irradiated at a dose rate of $2.28 \times 10^{18} \text{ eV cm}^{-3} \text{ min}^{-1}$. No nitrogen or oxygen is formed in a solution of 0.22 M SF_6 and 0.0071 M N_2O in xenon while the yields of nitrogen and oxygen from a solution of 1.1 M SF_6 and 0.3 M N_2O are respectively $G(\text{N}_2) = 1.9$ and $G(\text{O}_2) \cong 0.01$ (compared to 10.8 and 1.94 when no SF_6 is present). It should be pointed out here that in the former experiment the ratio of sulfur hexafluoride to N_2O is 31 while in the latter it is only 3.7. The addition of CO_2 to a solution of 0.011 M N_2O in xenon, irradiated at a dose rate of $3.95 \times 10^{17} \text{ eV cm}^{-3} \text{ min}^{-1}$, decreased the yield of nitrogen to a constant value of $G(\text{N}_2) = 4.3$. This is illustrated in Figure 4. The oxygen was essentially unaffected by the presence of CO_2 .

(14) W. Bernstein and R. H. Schuler, *Nucleonics*, **13**, 110 (1955).
 (15) D. R. Davis, W. F. Libby, and L. Kevan, *J. Amer. Chem. Soc.*, **87**, 2766 (1965).
 (16) J. A. Stone, *Can. J. Chem.*, **46**, 1267 (1968).

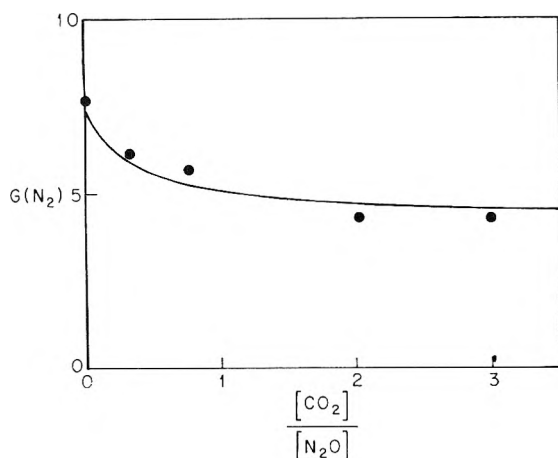
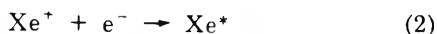
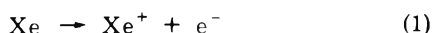


Figure 4. Nitrogen yield as a function of the ratio $[\text{CO}_2]/[\text{N}_2\text{O}]$ for increasing CO_2 concentration and $[\text{N}_2\text{O}] = 0.011 \text{ M}$. Solid line calculated with eq IX and the parameters given in the text.

Discussion

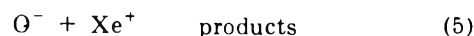
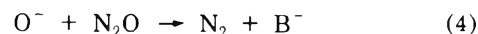
The fact that SF_6 , a very efficient electron scavenger, decreases drastically the yield of nitrogen and oxygen from γ -irradiated N_2O -xenon solutions, indicates that these products have ionic precursors. Charge transfer from Xe^+ to N_2O should not occur because of the difference in the gas-phase ionization potentials: $\text{IP}(\text{Xe}) = 12.1 \text{ eV}$ and $\text{IP}(\text{N}_2\text{O}) = 12.9 \text{ eV}$. It should be noted that ionization potentials in liquids may well be different from those in the gas phase. However, these differences are not expected to be very large since yields of electrons similar to that in the gas phase have been found in the γ -radiolysis of many liquid hydrocarbons.⁵ Such a conclusion is also reached for xenon in the present work (see Discussion). Moreover since the positive ion in liquid xenon has been shown to be $(\text{Xe})_2^+$ ¹⁷ the charge transfer to N_2O is even more unlikely. These facts point to the electron as the primary precursor of the nitrogen and oxygen yields. As shown in Figure 2 the nitrogen yield increases with N_2O concentration and more or less levels off between 10^{-2} and 10^{-1} M . While dose-rate dependent during this rise, the nitrogen yields converge to the same value at low N_2O concentration $\sim 10^{-3} \text{ M}$, where $G(\text{N}_2) \sim 4.0$. The dose-rate dependence indicates that the electron is not correlated with the positive ion, *i.e.*, the ion pairs are homogeneously distributed in liquid xenon. The dose-rate independence at the low concentration of N_2O indicates that at these concentrations the electron scavenging by N_2O results always in the formation of one nitrogen molecule without competition from recombination between the electron and Xe^+ .¹⁸ Quite generally one would have that



The product of reaction 3 could be N_2O^- , this is irrelevant for the moment, all we are interested in is that the end product is a nitrogen molecule. Some comments on the nature of the secondary ions will be made later. From the experimental data it appears then that at the concentrations of N_2O studied in the present work reaction 2 cannot compete with reaction 3. This is not unreasonable. Taking $G(\text{e}^-) \sim 4.0$ the production rate of electrons at the highest dose rate, $2.28 \times 10^{18} \text{ eV cm}^{-3} \text{ min}^{-1}$, is $\sim 2.5 \times 10^{-6} \text{ M sec}^{-1}$. Debye has shown¹⁹ that for low dielec-

tric constant liquids the rate constant for the recombination of two ions is given by $k_r = (4\pi e/\epsilon)\mu$ where μ is the sum of the mobilities of the ions and ϵ is the dielectric constant of the liquid. The Debye equation has been assumed to be applicable to the electron ion recombinations^{4,6,8,9} and, therefore, since $\mu_e \gg \mu_+$, one has that $\mu \approx \mu_e = 2200 \text{ cm}^2 \text{ V}^{-1} \text{ sec}^{-1}$ for the electron in liquid xenon¹⁰ and $\epsilon = 2.11$ for liquid xenon.²⁰ On the other hand one can assume that as in other dielectric liquids^{5a,5c} the rate constant for electron scavenging by N_2O is diffusion controlled. Then using the mobility of the electron in liquid xenon quoted above together with a reaction radius of 5 \AA ^{5c} one gets a rate constant $\sim 10^{16} \text{ M}^{-1} \text{ sec}^{-1}$ for the electron scavenging by N_2O . The half-life for recombination is then $\sim 4 \times 10^{-13} \text{ sec}$ while the half-life for scavenging at $10^{-3} \text{ M N}_2\text{O}$ is $\sim 7 \times 10^{-14} \text{ sec}$ or almost an order of magnitude shorter than the former. This difference will be greater if one has in xenon as in argon an efficiency factor < 1 in the neutralization reaction.⁹

The nitrogen yield increases to a value of the order of $G \sim 8$ at $3 \times 10^{-2} \text{ M N}_2\text{O}$. From the gas-phase W value of xenon = 21.8²¹ the yield of electrons is $G(\text{e}^-) = 4.6$. This value is not expected to change appreciably when going to liquid xenon, since yields of electrons similar to that in the gas phase have been found in the γ -radiolysis of many liquid hydrocarbons.⁵ Moreover Klassen and Schmidt found that in gaseous and liquid argon the W values are essentially the same.⁷ This together with the electronic origin of N_2 strongly suggests that secondary reactions of the anion produced in reaction 3 lead to nitrogen formation. Moreover, since reaction 2 does not compete with reaction 3, the dose rate dependence of the nitrogen yields can then be explained in terms of a competition between the reaction with N_2O of the secondary ion O^- (N_2O^-) produced in reaction 3 and its recombination



Again it should be pointed out that reaction 4 does not represent the actual reaction of $\text{O}^- + \text{N}_2\text{O}$ but indicates that whatever the path, the end product is one nitrogen molecule. A steady-state treatment of reactions 1-5 gives for the yield of nitrogen

$$G(\text{N}_2) = G(\text{e}) \left[1 + \frac{1}{1 + \frac{B}{[\text{N}_2\text{O}]}} \right] \quad (I)$$

The constant B in units of M is given by $[(D/W)(k_5/N)]^{1/2}(1/k_4)$ where N is Avogadro's number, D is the dose rate in $\text{eV l}^{-1} \text{ sec}^{-1}$, and W is the energy in eV required to form an ion pair. A plot of $G(\text{e})/[G(\text{N}_2) - G(\text{e})]$ vs. $1/[\text{N}_2\text{O}]$ should be a straight line with an intercept of 1 and a slope B . However, one does not know accurately the value of $G(\text{e})$ in liquid xenon. A first estimate can be made by plotting $1/G(\text{N}_2)$ vs. $1/[\text{N}_2\text{O}]$. The intercept of such a plot should give $\sim 1/2G(\text{e})$. From this plot one finds that $G(\text{e}) \sim 4.3$. Another way to find the yield of

(17) H. T. Davis, S. A. Rice, and L. Meyer, *J. Chem. Phys.*, **37**, 947 (1962).

(18) Although the ion undergoing recombination is most probably $(\text{Xe})_2^+$ ¹⁷ we will write Xe^+ in order to keep the equations as simple as possible. At any rate this is inconsequential as to the conclusions reached in the discussion.

(19) P. Debye, *Trans. Electrochem. Soc.*, **82**, 265 (1942).

(20) G. A. Cook, Ed., "Argon, Helium and the Rare Gases," Interscience, New York, N. Y., 1961, p 370.

(21) G. G. Meisels, *J. Chem. Phys.*, **41**, 51 (1964).

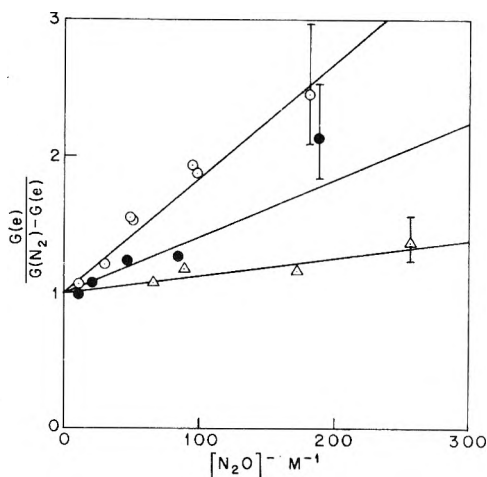


Figure 5. Reciprocal plot of eq I for intermediate nitrous oxide concentrations at three different dose rates (Δ) 3.49×10^{16} , (\bullet) 3.95×10^{17} , and (\circ) 2.28×10^{18} eV cm $^{-3}$ min $^{-1}$.

$G(e)$ is to suppress the secondary reactions and measure the nitrogen yield. CO_2 has been shown to react very efficiently with the secondary ion O^- (possibly N_2O^-) in the gas phase according to²²⁻²⁷



The addition of CO_2 to a 0.011 M solution of N_2O in liquid xenon decreased the nitrogen to a constant $G(\text{N}_2) = 4.3$ (Figure 4). This value agrees surprisingly well with that obtained from the reciprocal plot (see above) and is very similar to that obtained in the gas phase²¹ $G(e) = 4.6$. Taking $G(e) = 4.3$ one can plot $G(e)/[G(\text{N}_2) - G(e)]$ vs. $1/[\text{N}_2\text{O}]$. This is illustrated in Figure 5 for the three dose rates studied and N_2O concentrations between 4×10^{-3} and 0.1 M. Indeed a linear dependence is observed and from an analysis of the data values of B are obtained, i.e., 8.3×10^{-3} , 3.73×10^{-3} , and 1×10^{-3} M at dose rates of 2.28×10^{18} , 3.95×10^{17} , and 3.49×10^{16} eV cm $^{-3}$ min $^{-1}$, respectively. Since $B = [(D/W)(k_5/N)]^{1/2}(1/k_4)$ it should be proportional to the square root of the dose rate. Within experimental errors such a proportionality is obtained. It should be noted that below 4×10^{-3} M deviation from linearity occurs for the plot of $G(e)/[G(\text{N}_2) - G(e)]$ vs. $1/[\text{N}_2\text{O}]$. This together with the fact that at the three different dose rates the nitrogen yields become essentially the same at low N_2O concentrations and decrease with a concentration decrease, seems to indicate that at low concentrations ($\sim 10^{-3}$ M N_2O) an impurity starts competing with N_2O for the electrons. In such a case the real yield of nitrogen should be given by

$$G(\text{N}_2) = \frac{G(e)}{1 + \frac{A}{[\text{N}_2\text{O}]}} \left[1 + \frac{1}{1 + \frac{B}{[\text{N}_2\text{O}]}} \right] \quad (II)$$

with $A = k_1[I]/k_3$ where k_1 is the rate of scavenging by the impurity present at a concentration $[I]$. From a best fit of eq II to the experimental data obtained at a dose rate of 3.97×10^{17} eV cm $^{-3}$ min $^{-1}$ (see below) one gets $A = 3 \times 10^{-4}$ M. If $k_1 = k_3$ the electron scavenging impurity is present in liquid xenon at a concentration of the order of 3×10^{-4} M. This impurity level is reasonable since it is within 0.2 times that stated in the supplier's analysis of the xenon.

At concentrations above 0.1 M the nitrogen yields increase again and tend toward a value of $3G(e)$. These

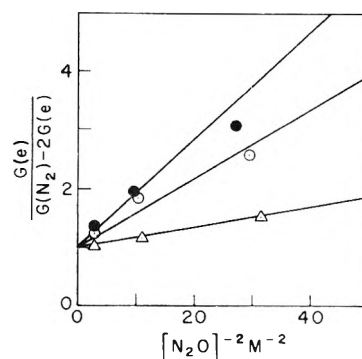


Figure 6. Reciprocal plot of eq IV for high nitrous oxide concentrations and $n = 2$ at three different dose rates: (Δ) 3.49×10^{16} , (\bullet) 3.95×10^{17} , and (\circ) 2.28×10^{18} eV cm $^{-3}$ min $^{-1}$.

yields are also dose rate dependent. It is readily seen from Figure 2 that the nitrogen yield concentration dependence is higher than first order with respect to the N_2O concentration. One can write then quite generally



A steady-state treatment of these reactions together with reactions 1-5 gives

$$G(\text{N}_2) = \frac{G(e)}{1 + \frac{A}{[\text{N}_2\text{O}]}} \left[1 + \frac{1}{1 + \frac{B}{[\text{N}_2\text{O}]}} \left(1 + \frac{1}{1 + \frac{C}{[\text{N}_2\text{O}]^n}} \right) \right] \quad (III)$$

where $C = [(D/W)(k_7/N)]^{1/2}(1/k_8)M^n$. For high N_2O concentrations $[\text{N}_2\text{O}] \gg B$ and A , and eq III reduces to

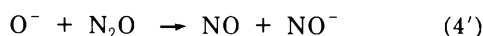
$$G(\text{N}_2) = G(e) \left[2 + \frac{1}{1 + \frac{C}{[\text{N}_2\text{O}]^n}} \right] \quad (IV)$$

and $G(e)/[G(\text{N}_2) - 2G(e)]$ plotted vs. $1/[\text{N}_2\text{O}]^n$ should be a straight line with a slope C and an intercept of 1. This is illustrated in Figure 6 for $n = 2$ and gives a fair linear dependence considering the small numerical differences in the N_2 yields and the error introduced in squaring N_2O . The slopes obtained are 0.088, 0.058, and 0.016 M 2 at dose rates of 2.28×10^{18} , 3.95×10^{17} , and 3.49×10^{16} eV cm $^{-3}$ min $^{-1}$. The values obtained from reciprocal plots of Figures 5 and 6 used together with eq III should describe the data over the whole concentration range. Actually the fitting procedure used was the following. We have taken the nitrogen yields at the dose rate of 3.95×10^{17} eV cm $^{-3}$ min $^{-1}$. From the reciprocal plots we know that $B = 3.73 \times 10^{-3}$ M, $C = 0.058$ M, and $n = 2$ and with these values a first calculation was made. It was found that a value of $B = 3.4 \times 10^{-3}$ M gave a better fit in the intermediary concentration range $\sim 10^{-2}$ - 10^{-1} M. Then the constant A was introduced to account for the faster drop when going to lower N_2O concentrations. As anticipated above, the best fit was obtained for $A = 3 \times 10^{-4}$ M. Once the experimental data at the dose rate of 3.95×10^{17} eV cm $^{-3}$ min $^{-1}$ were fitted and values of B and C so obtained, the

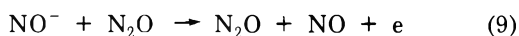
(22) W. L. Fite and J. A. Rutherford, *Disc. Faraday Soc.*, **37**, 192 (1964).
 (23) T. L. Moruzzi and A. V. Phelps, *J. Chem. Phys.*, **45**, 4617 (1966).
 (24) J. M. Warman, *J. Phys. Chem.*, **71**, 4066 (1967).
 (25) J. M. Warman, *J. Phys. Chem.*, **72**, 52 (1968).
 (26) S. J. Rzad and J. M. Warman, *J. Phys. Chem.*, **72**, 3013 (1968).
 (27) D. A. Parkes, *J. Chem. Soc., Faraday Trans. 1*, **68**, 627 (1972).

parameters pertinent to the other two dose rates were obtained by multiplying the values obtained above by the square root of the appropriate ratio of the dose rates since B and C by definition are both proportional to the square root of the dose rate. Of course the parameter A remains the same at the three dose rates. Hence the solid lines in Figure 2 were calculated with eq III and the following parameters $G(e) = 4.3$, $A = 3 \times 10^{-4} M$, $n = 2$; $B = 8.1 \times 10^{-3} M$, and $C = 0.14 M^2$ at $2.28 \times 10^{18} \text{ eV cm}^{-3} \text{ min}^{-1}$; $B = 3.4 \times 10^{-3} M$ and $C = 5.8 \times 10^{-2} M^2$ at $3.95 \times 10^{17} \text{ eV cm}^{-3} \text{ min}^{-1}$; $B = 1 \times 10^{-3} M$ and $C = 1.7 \times 10^{-2} M^2$ at $3.49 \times 10^{16} \text{ eV cm}^{-3} \text{ min}^{-1}$. The agreement between the calculated and experimental data is fairly good. It should be pointed out again that the fit was done only at one dose rate and then extended to the other dose rates by using the dependence of the constants B and C on the square root of the dose rate. The slight differences between the values obtained for B and C from reciprocal plots and from the curve fitting is due to the fact that the impurity depresses the yields at low concentrations and that the low and high concentration regions overlap.

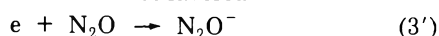
At this point some comments concerning the ions involved in reactions 1-8 are in order. First arises the question of whether reaction 3 leads to $N_2 + O^-$ or to N_2O^- . If gas-phase data can be extrapolated to liquid xenon then one would have to rule out the formation of O^- in reaction 3. Indeed the temperature dependence of the rate constant for the reaction leading to $N_2 + O^-$ has been studied by Warman and coworkers²⁸ and is describable by $k_3 = 4.3 \times 10^{13} \exp(-4.8 \times 10^3/T) M^{-1} \text{ sec}^{-1}$. This gives $k_3 \sim 10 M^{-1} \text{ sec}^{-1}$ at 164°K and reaction 3 could not compete with electron recombination. Moreover, if O^- is produced, it can further react with N_2O according to²⁹



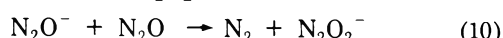
NO^- would then undergo a collisional detachment with N_2O to give^{28,30}



Although the gas-phase rate for this reaction is of the order of $10^8 M^{-1} \text{ sec}^{-1}$ at 164°K ,²⁸ it seems unlikely in the liquid phase, since in the gas phase it probably involves some sort of activation or energy transfer process. Moreover we do not observe a chain reaction as that which would be generated through reactions 3, 4', and 9. Within the assumption that gas-phase data apply to our system one can say that reaction 3 produces N_2O^- . This is not unreasonable since at high pressures in the gas phase, electron capture has been shown to be a three-body process²⁸⁻³¹ leading most probably to N_2O^- . Since in a liquid molecules are essentially in a collisional state, one would expect such a process to dominate.³² Recently Mishra and Symons have presented esr spectroscopic evidence which suggests that N_2O^- is stable at 77°K in a carbon disulfide matrix.³³ Moreover, Dainton and coworkers interpreted their pulse radiolysis studies of N_2O -cyclohexane solutions in terms of a N_2O^- ion stable for at least $20 \mu\text{sec}$ ³⁴ at room temperature. From the above arguments the formation of N_2O^- seems to be favored

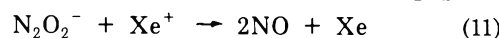


This would be followed by the analog of reaction 4' with the production of a stable $N_2O_2^-$ ion.³²

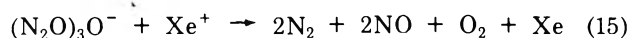
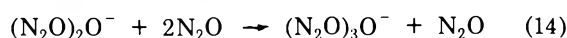
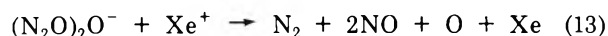
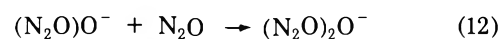


This species has been observed by Moruzzi and Dakin³⁵ who explained their data in terms of a collisional stabili-

zation of the intermediate of reaction 4'. Since there is no excess nitrogen produced in reaction 10 the dose rate effect on the secondary nitrogen formation has to come as the competition between the recombination of the $N_2O_2^-$



and its further reaction with N_2O as required by the general mechanism proposed above. The reaction of the $N_2O_2^-$ as well as those following could be regarded as a clustering of N_2O molecules around the O^- . $N_2O_2^-$ itself can be regarded as an N_2O molecule attached to O^- ($(N_2O)O^-$). Clustering of the O^- ion has been proposed previously to explain results obtained in the gas phase.³⁶ We would have then



In this mechanism since the equivalent of reaction 4, *i.e.*, reaction 12, does not give nitrogen, one has to have two nitrogen molecules produced in reaction 15 to account for a total of $3G(e)$. The kinetic equations of reactions 1, 2, 3', and 10-15 are evidently identical with those given above. It should be pointed out here that the mechanism presented above does not necessarily represent reality nor is it unique in explaining the experimental data, however, it is consistent with the known reactions observed in the gas phase.

Since the oxygen atoms produced in reaction 13 will not react with N_2O at the temperature of the experiment,³⁷ they will recombine to give O_2 . Taking this under consideration a steady-state treatment of the mechanism proposed above gives for the yields of O_2 and NO

$$G(O_2) = \frac{\frac{1}{2}G(e)}{1 + \frac{A}{[N_2O]}} \left[\frac{1}{1 + \frac{B}{[N_2O]}} \left(1 + \frac{1}{1 + \frac{C}{[N_2O]^2}} \right) \right] \quad (V)$$

$$G(NO) = \frac{2G(e)}{1 + \frac{A}{[N_2O]}} \quad (VI)$$

Since all the parameters necessary for the evaluations of eq V and VI are known, one can calculate the yields of NO and O_2 at the different dose rates. The solid lines in Figures 3 and 7 are calculated in such a way. However, the experimental yield of oxygen is much smaller than the calculated values and no NO is observed in our experiments. Moreover if N_2 and O_2 were the only products the stoichiometry of $2N_2$ for one O_2 is not obeyed. Obviously a product is missing and that product is most probably NO .

(28) J. M. Warman, R. W. Fessenden, and G. Bakale, *J. Chem. Phys.*, **57**, 2702 (1972).

(29) E. E. Ferguson, *Advan. Electron. Phys.*, **24**, 23 (1968).

(30) M. McFarland, D. B. Dunkin, F. E. Fehsenfeld, A. L. Schmeltekopf, and E. E. Ferguson, *J. Chem. Phys.*, **56**, 2358 (1972).

(31) (a) A. V. Phelps and R. E. Voshall, *J. Chem. Phys.*, **49**, 3246 (1968); (b) J. M. Warman and R. W. Fessenden, *ibid.*, **49**, 4718 (1968).

(32) J. M. Warman, K.-D. Asmus, and R. H. Schuler, *Advan. Chem. Ser.*, **No. 82**, 25 (1968).

(33) S. P. Mishra and M. C. R. Symons, *J. Chem. Soc., Chem. Commun.*, 510 (1972).

(34) F. S. Dainton, P. O'Neill, and G. A. Salmon, *J. Chem. Soc., Chem. Commun.*, 1001 (1972).

(35) J. L. Moruzzi and J. T. Dakin, *J. Chem. Phys.*, **49**, 5000 (1968).

(36) J. L. Redpath and M. Simic, *J. Phys. Chem.*, **73**, 2809 (1969).

(37) F. Kaufman, *Progr. React. Kinet.*, **1**, 1 (1961).

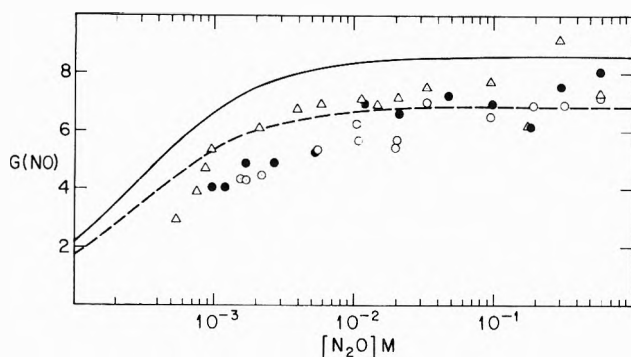


Figure 7. Nitrous oxide concentration dependence of the yield of nitric oxide, calculated by eq VIII as described in the text, at three different dose rates: (Δ) 3.49×10^{16} , (●) 3.95×10^{17} , and (○) 2.28×10^{18} eV cm⁻³ min⁻¹. Solid line calculated with eq VI and the parameters given in the text. Dashed line is the solid line multiplied by an arbitrary factor of 0.8.

NO has been shown to react very efficiently with O₂ at low temperatures and the reaction is mercury catalyzed.³⁸



Mercury is present in our system since the samples are prepared on a mercury line. Moreover, after irradiation the gas noncondensable at 77°K is toepled through cold traps containing mercury. Recently it has been shown^{39,40} that NO₂ produced in reaction 16 further reacts with NO



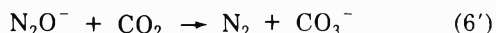
In such a case four NO disappear for one O₂ and the real yields should be given by

$$G(\text{O}_2) = \frac{1}{2}G(\text{O}_2)_m + \frac{1}{4}G(\text{N}_2) \quad (\text{VII})$$

$$G(\text{NO}) = G(\text{N}_2) - 2G(\text{O}_2)_m \quad (\text{VIII})$$

where $G(\text{O}_2)_m$ is the experimentally measured yield of oxygen. The yields of O₂ and NO calculated by eq VII and VIII are shown in Figures 3 and 7. The agreement between the yields expected from the mechanism and those estimated from the stoichiometry is fairly good considering all the assumptions involved. To illustrate the accurate form of the N₂O concentration dependence of NO as predicted by eq VI we have multiplied the solid line by an arbitrary factor of 0.8 and this is presented as the dashed line in Figure 7.

Within the framework of the mechanism presented above the effect of CO₂ can be understood in terms of a reaction analogous to reaction 6



A steady-state treatment of the mechanism including reaction 6' gives for the yield of nitrogen in the presence of CO₂

$$G(\text{N}_2)_{\text{CO}_2} = \frac{G(e)}{1 + \frac{A}{[\text{N}_2\text{O}]}} \times$$

$$\left[1 + \frac{1}{1 + \frac{K[\text{CO}_2]}{[\text{N}_2\text{O}]}} \frac{1}{1 + \frac{B}{[\text{N}_2\text{O}]}} \left(1 + \frac{1}{1 + \frac{C}{[\text{N}_2\text{O}]^2}} \right) \right] \quad (\text{IX})$$

where $K = k_6'/k_{10}$. Since all the other parameters are known K can be obtained by fitting eq IX to the experimental data presented in Figure 4. Such a fit with $K = 2.5$ is illustrated as the solid line in Figure 4. This ratio of rate constants is an order of magnitude smaller than that

of 44 obtained in the gas phase by Warman⁴¹ for the ratio of the rate constants of O⁻ (possibly N₂O⁻) reaction with CO₂ to that for reaction with N₂O. This difference will be commented on below. The fact that the presence of CO₂ does not affect the yield of oxygen is not surprising since the neutralization of CO₃⁻ will lead to the formation of oxygen. Due to this complication it is very difficult to estimate the real yield of oxygen originating from N₂O-CO₂-Xe solutions.

From the knowledge of the recombination rate constants for reactions 11 and 13 one can estimate the rates for reactions 12 and 14. The magnitude of these recombination rate constants can be obtained in the following fashion. The recombination rate constant for two ions is given according to Debye by $k_r = (4\pi e/\epsilon)\mu$,¹⁹ or making use of the Nernst-Einstein relationship, $k_r = (4\pi e^2/\epsilon kT)D$, where D is the sum of the diffusion coefficients of the two ions. The diffusion coefficient of (Xe)₂⁺ at 164°K, i.e., 2.3×10^{-6} cm² sec⁻¹, is obtained from the work of Davis, *et al.*¹⁷ On the other hand, the diffusion coefficients of (N₂O)O⁻ and (N₂O)₂O⁻ can be deduced from the value of 2.8×10^{-6} cm² sec⁻¹ reported for O₂⁻ in liquid xenon by Davis, *et al.*⁴² Since the diffusion coefficient is inversely proportional to the radius σ of the diffusing species and since the radius of O₂⁻ is known to be 1.8 Å⁴² and that of (N₂O)O⁻ and (N₂O)₂O⁻ can be approximated as 2 and 3 Å, respectively,⁴³ we calculate the diffusion coefficients of these two latter species as 2.5×10^{-6} and 1.7×10^{-6} cm² sec⁻¹, respectively. This in turn gives for the recombination rate constants $k_{11} = 1.7 \times 10^{11}$ M⁻¹ sec⁻¹ and $k_{13} = 1.5 \times 10^{11}$ M⁻¹ sec⁻¹. Since $B = [(D/W)(k_{11}/N)]^{1/2}(1/k_{12})$ and $C = [(D/W)(k_{13}/N)]^{1/2}(1/k_{14})$ one gets immediately $k_{12} = 8.3 \times 10^4$ M⁻¹ sec⁻¹ and $k_{14} = 4.7 \times 10^3$ M⁻² sec⁻¹. $W = 100/4.3 = 23.3$ has been used in the calculations. Such a rate constant of 8.3×10^4 M⁻¹ sec⁻¹ is much lower than the diffusion-controlled rate of $\sim 10^{10}$ M⁻¹ sec⁻¹ in liquid xenon at 164°K. This is not surprising since one would expect the clustered O⁻ to be more stable than N₂O⁻ and hence react at a slower rate with nitrous oxide. At this point two more comments should be made. The rate for recombination of N₂O⁻ is also of the order of $\sim 2 \times 10^{11}$ M⁻¹ sec⁻¹, while reaction 10 of N₂O⁻ with N₂C is expected to be diffusion controlled in liquid xenon, i.e., $\sim 10^{10}$ M⁻¹ sec⁻¹ since it has been shown to be diffusion controlled in dielectric liquids such as cyclohexane⁴⁴ and 2,2,4-trimethylpentane.^{5c} Since the ion production rate is 2.5×10^{-6} M⁻¹ sec⁻¹ one finds that the half-life with respect to recombination is $\sim 2 \times 10^{-6}$ sec while that for reaction with N₂O present at 10^{-3} M is $\sim 7 \times 10^{-8}$ sec. Therefore, as assumed in the mechanism proposed above, one does not expect any appreciable competition between reaction 10 and the recombination of N₂O⁻. The fact that reaction 10 is expected to be diffusion controlled also explains the small ratio of k_6'/k_{10} , since reaction 6' cannot be much faster than reaction 10, possibly a factor of 2 but certainly not a factor of 44.

(33) N. Sasaki and Y. Hiraki, *Proc. Imp. Acad. (Tokyo)*, **16**, 303 (1940).

(39) R. I. Greenberg and J. Heicklen, *Int. J. Chem. Kinet.*, **2**, 185 (1970).

(40) M. C. Dodge and J. Heicklen, *Int. J. Chem. Kinet.*, **3**, 269 (1971).

(41) J. M. Warman, *J. Phys. Chem.*, **71**, 4066 (1967).

(42) H. T. Davis, S. A. Rice, and L. Meyer, *J. Chem. Phys.*, **37**, 2470 (1962).

(43) See, for example, L. Pauling, "The Nature of the Chemical Bond," Cornell University Press, Ithaca, N. Y., 1948.

(44) P. P. Infelta and R. H. Schuler, *Int. J. Appl. Radiat. Phys. Chem.*, **5**, 41 (1973).

Conclusions

The results presented above show that most of the electrons produced by γ -irradiation of liquid xenon at 164°K behave as free electrons and are homogeneously distributed throughout the liquid which allows the use of simple homogeneous kinetics in contrast to the complex kinetics used in liquid hydrocarbons.⁵ The yield of these free electrons, $G_{fi}(e^-) = 4.3$, is higher than that obtained for liquid argon⁹ where $G_{fi}(e^-) = 2.0$. This observation with xenon provides further evidence for the increase of G_{fi} with the electron mobility in dielectric liquids and is in line with previous results, e.g., $G_{fi} = 0.13$,³ $\mu_e = 0.09 \text{ cm}^2 \text{ V}^{-1} \text{ sec}^{-1}$,⁶ $G_{fi} = 0.332$,³ $\mu_e = 7 \text{ cm}^2 \text{ V}^{-1} \text{ sec}^{-1}$,⁶ $G_{fi} = 0.857$,³ $\mu_e = 55 \text{ cm}^2 \text{ V}^{-1} \text{ sec}^{-1}$,⁶ $G_{fi} = 2.0$,⁹ $\mu_e = 475 \text{ cm}^2 \text{ V}^{-1} \text{ sec}^{-1}$,¹⁰ and $G_{fi} = 4.3$, $\mu_e = 2200 \text{ cm}^2 \text{ V}^{-1} \text{ sec}^{-1}$,¹⁰ for *n*-hexane, 2,2,4-trimethylpentane, neopentane, argon, and xenon, respectively. This yield of electrons of $G(e) =$

4.3 should be compared to that obtained in the gas phase $G(e) = 4.6^{21}$ and indicates, as in the case of hydrocarbons,⁵ that the yields of electrons (*i.e.*, the *W* values) are similar in both phases.

The product formation is understood in terms of the electron scavenging by N_2O to give N_2O^- and the secondary reaction of the latter to give $(\text{N}_2\text{O})\text{O}^-$. This ion recombines or yields one excess nitrogen by further reacting with N_2O . The resulting anion $(\text{N}_2\text{O})_2\text{O}^-$ reacts in competition with its recombination with two nitrous oxide molecules to give two excess nitrogen molecules. While the reaction of N_2O^- with nitrous oxide is thought to proceed with a diffusion-controlled rate, that of $(\text{N}_2\text{O})\text{O}^-$ is only $8.3 \times 10^4 \text{ M}^{-1} \text{ sec}^{-1}$. The three-body reaction involving $(\text{N}_2\text{O})_2\text{O}^-$ is estimated to be $4.7 \times 10^3 \text{ M}^{-2} \text{ sec}^{-1}$. Finally, the ratio of the rate constant for reaction of N_2O^- with CO_2 to that for reaction with N_2O is 2.5 indicating that the reaction with CO_2 is also diffusion controlled.

Reaction of Atomic Oxygen with Hydrogen Bromide

G. A. Takacs and G. P. Glass*

Department of Chemistry, Rice University, Houston, Texas 77001 (Received January 8, 1973)

Publication costs assisted by the Petroleum Research Fund

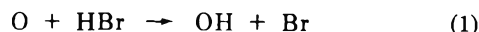
The reaction of atomic oxygen with HBr was studied in a fast discharge flow system by monitoring epr spectra of $\text{O}(^3\text{P}_2)$, $\text{Br}(^2\text{P}_{3/2})$, $\text{OH}(^2\pi_{3/2})$, and $\text{H}(^2\text{S}_{1/2})$ at various reaction times. The experimental results were found to be in accord with the mechanism, $\text{O} + \text{HBr} \rightarrow \text{OH} + \text{Br}$ (1), $\text{OH} + \text{HBr} \rightarrow \text{H}_2\text{O} + \text{Br}$ (2), $\text{OH} + \text{O} \rightarrow \text{H} + \text{O}_2$ (3), $\text{H} + \text{HBr} \rightarrow \text{H}_2 + \text{Br}$ (4), and k_1 was measured at 298 K as $4.4 \pm 1.0 \times 10^{-14} \text{ cm}^3 \text{ molecule}^{-1} \text{ sec}^{-1}$. The radical intermediate, $\text{OH}(^2\pi_{3/2})$, was detected in both the ground state, and in the first vibrationally excited state. Measurements on the relative population of these states allowed a lower limit of 0.3 to be placed on the ratio $k_{1(b)}/k_{1(a)}$, $\text{O} + \text{HBr} \rightarrow \text{OH}(\nu = 0) + \text{Br}(^2\text{P}_{3/2})$ (1a) and $\text{O} + \text{HBr} \rightarrow \text{OH}(\nu = 1) + \text{Br}(^2\text{P}_{3/2})$ (1b).

Introduction

This paper reports part of a general study of reactions of hydrogen halides with simple free radicals (*e.g.*, O, H, and OH).¹ Such reactions play an important role in the inhibition of flame and combustion processes.^{2,3}

No previous direct experimental study has been made of the reaction of atomic oxygen with HBr. However, the reaction has been investigated theoretically by Mayer and Schieler⁴ using the BEBO method introduced by Johnston and Parr. They calculated the rate constant for reaction 1 as $3.15 \times 10^{-12} T^{1/2} \exp(-300/RT) \text{ cm}^3 \text{ molecule}^{-1} \text{ sec}^{-1}$. Only one other estimate of this rate constant has appeared in the literature. In a study of the inhibition of the second explosion limit of the $\text{H}_2\text{-O}_2$ reaction by HBr, Clark, *et al.*,⁵ simulated the course of the reaction by numerical integration of the rate equations pertaining to a mechanism that included reaction 1. A reasonable fit to experiment at 773 K was obtained when k_1 was set equal

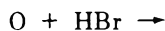
to $4.15 \times 10^{-11} \text{ cm}^3 \text{ molecule}^{-1} \text{ sec}^{-1}$. However, the fit was not sensitive to the actual value of k_1 if chosen within large limits.



In this study the reaction was followed directly in a fast flow system using epr detection. Spectra of $\text{O}(^3\text{P}_2)$, $\text{OH}(\nu = 0)$, $\text{OH}(\nu = 1)$,⁶ $\text{H}(^2\text{S}_{1/2})$, $\text{Br}(^2\text{P}_{3/2})$, and $\text{Br}(^2\text{P}_{1/2})$ ⁷

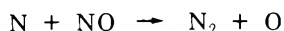
- (1) G. A. Takacs and G. P. Glass, *J. Phys. Chem.*, accepted for publication.
- (2) R. N. Butlin and R. F. Simmons, *Combust. Flame*, **12**, 447 (1968).
- (3) W. E. Wilson, Jr., J. T. O'Donovan, and R. M. Fristrom, *Symp. Combust. 12th*, 929 (1969).
- (4) S. W. Mayer and L. Schieler, *J. Phys. Chem.*, **72**, 236 (1968).
- (5) D. R. Clark, R. F. Simmons, and D. A. Smith, *Trans. Faraday Soc.*, **66**, 1423 (1970).
- (6) P. N. Clough, A. H. Curran, and B. A. Thrush, *Chem. Phys. Lett.*, **7**, 86 (1970).
- (7) P. B. Davies, B. A. Thrush, A. J. Stone, and F. D. Wayne, *Chem. Phys. Lett.*, to be submitted for publication.

were recorded. An attempt was made to identify the primary reaction from the following possible choices



Experimental Section

The construction and operation of the discharge flow system and epr spectrometer have been described previously.^{1,8} Atomic oxygen was produced by either microwave discharge of O₂-Ar mixtures, or, in the absence of O₂, by NO titration of atomic nitrogen⁹



HBr was added to the 20-mm i.d. quartz flow tube through a small movable inlet probe. Concentrations of O, Br, H, and OH were measured absolutely by epr using the O₂ reference method. The initial concentration of HBr was estimated from its measured flow rate. Prior to each set of experiments, the flow tube was treated with a fluorinated halocarbon coating¹⁰ that has previously been shown to inhibit wall recombination of atomic bromine and many other free-radicals species.¹

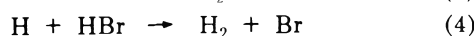
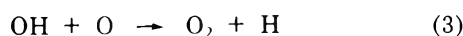
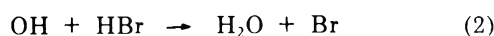
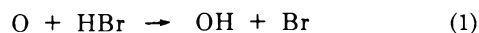
The corrosive reaction products were trapped at 77 K in a U-tube positioned immediately upstream of the pump. A large brass dump tank placed between the flow tube and the liquid nitrogen trap effectively removed all trace of ozone. In the absence of this tank, a highly explosive mixture of ozone and reaction products was condensed.

For this study the epr system was slightly modified to improve its sensitivity. A new cylindrical cavity, operating in the TE₀₁₂ mode, and having end plates that can be screwed in or out to change its length, was constructed. Improved sensitivity was obtained by adjusting the end plates until the position of maximum microwave field was superimposed on that of maximum modulating magnetic field. With this cavity OH concentrations of 10¹¹ molecule/cm³ could be detected, although accurate quantitative measurements were not possible at this concentration.

Results

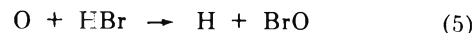
In this study the growth of Br(²P_{3/2}) and the decay of atomic oxygen was followed as a function of reaction time in 12 different mixtures for which the ratio of the initial concentration of HBr to that of atomic oxygen varied from 2.02 to 34.6. The concentration of OH and of atomic hydrogen was also monitored in several of the more stoichiometric mixtures.

The results of these measurements were classified and tabulated using the following reaction mechanism

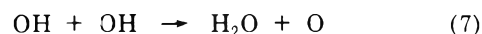


Reactions 2, 3, and 4 are well known, and their rate constants have been measured as 5.1×10^{-12} , 4.3×10^{-11} , and 3.4×10^{-12} cm³ molecule⁻¹ sec⁻¹, respectively.^{1,8}

The alternative reactions of atomic oxygen with HBr, namely



were dismissed since reaction 5 is 31 kcal/mol endothermic, and reaction 6 produces a 3 atom complex whose lifetime is too short for it to be collisionally deactivated. Reactions 7 and 8 were neglected because they are too slow to be of significance in the presence of atomic oxygen. Under the present conditions, atomic bromine should be unreactive since wall recombination is effectively inhibited by the fluorinated halocarbon wall coating, third-order recombination is slow at pressures below 1 Torr, and the abstraction reactions with HBr, O₂, and H₂ are very endothermic.



The correctness of the mechanism was tested by (i) comparing the kinetic data on oxygen atom decay and Br(²P_{3/2}) growth with that predicted by the mechanism, (ii) determining the concentration of the predicted intermediates (H and OH), and (iii) measuring the reaction stoichiometry.

An analysis of the kinetic behavior predicted by the mechanism is straight forward only when HBr is present in large excess. In this limiting case, all OH reacts *via* reaction 2, and reactions 3 and 4 can be neglected. Since the concentration of excess HBr remains effectively constant throughout the reaction, atomic oxygen undergoes pseudo-first-order decay, and its concentration at any time *t* is given by the equation

$$\ln (\text{O})_t / (\text{O})_0 = k_1(\text{HBr})t \quad (9)$$

where (O)₀ represents the initial oxygen atom concentration. If $k_2 \gg k_1$, reaction 1 will be rapidly followed by reaction 2, and two bromine atoms will be produced for each oxygen atom reacted. Thus $(\text{Br}) = 2[(\text{O})_0 - (\text{O})]$, $(\text{Br})_\infty = 2(\text{O})_0$, and

$$\ln (\text{Br})_\infty / [(\text{Br})_\infty - (\text{Br})] = k_1(\text{HBr})t \quad (10)$$

Equations 9 and 10 predict that plots of $\ln (\text{O})$ or $\ln [(\text{Br})_\infty - (\text{Br})]$ against reaction time should be linear, and have identical slopes of magnitude $k_1(\text{HBr})$. Figure 1 illustrates such plots for two reaction mixtures: one with $(\text{HBr})_0 / (\text{O})_0 = 34.6$, and the other with $(\text{HBr})_0 / (\text{O})_0 = 15.5$. For these mixtures $(\text{Br})_\infty$ was estimated as the bromine atom concentration determined at the longest measured reaction time plus twice the atomic oxygen concentration remaining at that time.

Values of k_1 estimated from Figure 1 and other similar plots are tabulated in Table I. Also included in this table are values of k_1 computed from experimental data, assuming the reaction mechanism to be composed of reactions 1-4. The computed values are chosen to minimize the difference between the experimentally measured oxygen atom concentrations and those calculated by integrating the rate equations pertaining to reactions 1-4. A simple Newtonian integration method was used with a step size of 10⁻⁴ sec. In order to avoid the mixing zone, inte-

(8) J. E. Breen and G. P. Glass, *J. Chem. Phys.*, **52**, 1082 (1970).

(9) F. Kaufman, *J. Chem. Phys.*, **28**, 992 (1958).

(10) Coating supplied by Marchem Inc., P. O. Box 6914, Houston, Tex. 77005. The properties of this coating are fully described in ref 1.

TABLE I: Kinetics of the Reaction of Atomic Oxygen with HBr

(Ar), 10 ¹⁶ molecule cc ⁻¹	(HBr) ₀ , 10 ¹⁴ molecule cc ⁻¹	(O) ₀ , 10 ¹⁴ molecule cc ⁻¹	$k, 10^{-14} \text{ cc molecule}^{-1} \text{ sec}^{-1}$			(Br formed/ O reacted)	(Br formed/ O reacted) _{calcd}
			O decay	Br growth	Calcd ^a		
1.24	3.84	1.71				1.15	1.24
1.95	11.3	2.10	5.9		4.9	1.61	1.35
2.33	22.7	3.84	3.6		2.6	1.55	1.45
2.36	21.3	2.40	3.7		2.8	1.62	1.52
2.17	18.5	1.75	5.1		3.8	1.91	1.60
2.32	17.1	1.36	3.7		3.6	1.52	1.61
2.04	13.4	0.90 ^b	6.6		5.5		
2.02	26.7	1.72	5.7		4.6	1.71	1.73
2.21	19.6	0.97 ^b	5.7	5.7	4.8	1.76	1.74
3.20	29.7	1.25 ^b	6.4	6.3	5.7	1.65	1.76
2.64	25.4	0.98 ^b	7.1	7.5	5.6	2.00	1.82
1.83	35.4	1.02 ^b	5.3	5.4	4.4	1.98	1.88

^a $k(\text{calcd}) = 4.4 \pm 1.0 \times 10^{-14} \text{ cm}^3 \text{ molecule}^{-1} \text{ sec}^{-1}$. ^b For these mixtures O was produced in the absence of O₂ by NO titration.

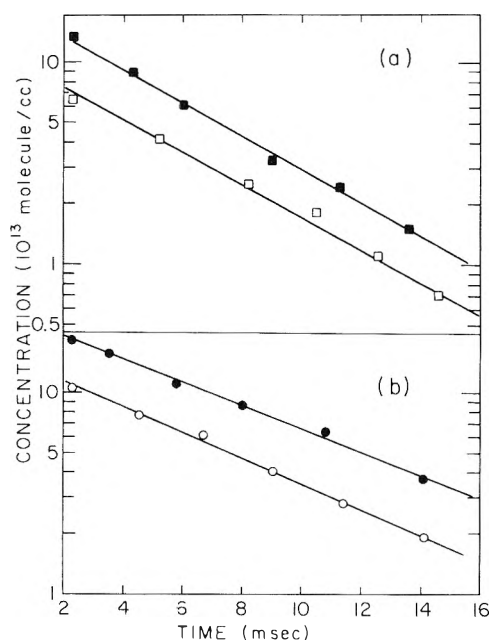


Figure 1. Plot of log (O) [open circles and squares] and log ((Br)_∞ - (Br)) [closed circles and squares] vs. reaction time: (a) (HBr)₀ = 3.54 × 10¹⁵, (O)₀ = 1.02 × 10¹⁴ molecule/cc; (b) (HBr)₀ = 2.67 × 10¹⁵, (O)₀ = 1.72 × 10¹⁴ molecule/cc.

gration was begun at the first measured point. The rate constants k_2 , k_3 , and k_4 were not varied during computation, and were chosen as 4.3×10^{-11} , 5.1×10^{-12} , and $3.4 \times 10^{-12} \text{ cm}^3 \text{ molecule}^{-1} \text{ sec}^{-1}$, respectively.^{1,8} k_1 was varied in increments of $10^{-15} \text{ cm}^3 \text{ molecule}^{-1} \text{ sec}^{-1}$ until the best fit between experiment and calculation was obtained. In order to reduce computation time the initial trial value of k_1 was set equal to the value estimated from Figure 1.

It is clear from Table I that, in general, the computed value of k_1 is less than the value obtained by pseudo-first-order oxygen atom decay. This is to be expected since the overall reaction stoichiometry changes with the (HBr)/(O) ratio, being governed by the relative rates of reactions 2 and 3. When HBr is in great excess, all OH is consumed by reaction 2, and thus the rate of removal of O is equal to the rate of reaction 1. If more atomic oxygen is present, some OH is consumed in reaction 3, and the rate of removal of atomic oxygen is then greater than the rate of

reaction 1. When this occurs the rate constant obtained by pseudo-first-order oxygen decay (graphically) is greater than k_1 . Since $k_3/k_2 = 8.4$, even a mixture with an 8.4-fold excess of HBr reacts to form (initially) equal amounts of H₂O and O₂, and with a pseudo-first-order rate constant (measured using the early points) 50% greater than k_1 .

A successful search was made for the two intermediates, OH and H, predicted by the mechanism. Unfortunately, due to their low concentration they could be detected only at short reaction times and only using stoichiometric mixtures. Under these conditions their spectra were observed with S/N ratios of between 2 and 5, and only rough estimates could be made of their absolute concentrations. These estimates are recorded in Table II together with values of (OH) and (H) that were calculated from the mechanism using the value of k_1 measured in this study, namely, $4.4 \times 10^{-14} \text{ cm}^3 \text{ molecule}^{-1} \text{ sec}^{-1}$, and the relationships

$$(\text{OH}) = k_1(\text{O})(\text{HBr})/k_2(\text{HBr}) + k_3(\text{O}) \quad (11)$$

and

$$(\text{H}) = k_3(\text{O})(\text{OH})/k_4(\text{HBr}) \quad (12)$$

which were derived using the steady-state approximation. This approximation can be applied to OH since $k_1 \ll k_2$ and k_3 , and to H since $k_1 \ll k_4$, and reaction 3 is clearly slower than reaction 1.

In this study, OH(²π_{3/2}) was observed in both the ground and the first vibrationally excited state. The concentration of the ground state was determined by comparing its integrated epr spectra to that of a known pressure of NO, using the intensity relationships developed by Westenberg.¹¹ The intensity relationship pertinent to OH($\nu = 1$) is not in the literature, but can be readily evaluated using the relationship

$$\int x_{ij} dH = \frac{h}{g_{eff}\beta} \left[\frac{w_0}{kT} \right] \frac{N}{Z} \exp(-E_i/kT) |\mu_{ij}|^2$$

which is derived in Westenberg's paper. Here $\int x_{ij} dH$ is the total integrated absorption, μ_{ij} is the matrix element of the transition dipole between states i and j , N is the number of absorbing molecules, Z is the partition function, and E_i is the energy of the absorbing state. The only

(11) A. A. Westenberg and N. deHaas, *J. Chem. Phys.*, **40**, 3087 (1964).

TABLE II: Comparison of Measured and Calculated (OH)

Pressure, Torr	Time, msec	10 ¹⁴ molecule cm ⁻³				10 ¹¹ molecule cm ⁻³					
		(HBr) ₀	(O) ₀	(O)	(Br)	(HBr) ^a	(OH) _{ν=0}	(OH) _{ν=1}	(OH) _{calcd} ^b	(H)	(H) _{calcd}
0.26	4.5	18.1	8.60	4.16	3.62	14.5	5.88	1.47	10.5		36
0.27	3.9	31.3		2.72	5.43	25.9	4.32	1.33	12.7	13	16
0.30	4.1	30.9	11.7	4.16	5.70	25.2	7.64	2.68	15.0	27	30

^a Estimated as (HBr)₀ - (Br). ^b The sum over all vibrational states.

quantities that vary with vibrational quantum number are g_{eff} , Z , and μ_{ij} . In going from OH($\nu = 0$) to OH($\nu = 1$) g_{eff} decreased by 0.3%,⁶ Z increases by 2.6%,⁶ and $|\mu_{ij}|^2$ also increases by approximately 2.6%.¹² Thus the intensity relationship is effectively unchanged. This result is quite general and can be applied to any vibrational state of a molecule. It arises because, to a first approximation, for a given electronic state, both Z and $|\mu_{ij}|^2$ depend mainly on the square of the equilibrium internuclear separation. Thus, increases in Z and in $|\mu_{ij}|^2$ tend to cancel each other. The concentrations of OH($\nu = 0$) and OH($\nu = 1$), as determined from their epr spectra, are separately listed in Table II. The ratio of OH($\nu = 1$) to OH($\nu = 0$) was measured as approximately 0.3 under the conditions of this study.

The reaction stoichiometry was determined for all mixtures by measuring the ratio of atomic bromine formed to atomic oxygen removed, between two points 3.3 and 25 cm downstream of the HBr inlet. The first point was chosen to be immediately downstream of the mixing zone and the other point represents the largest reaction time that can be measured in this apparatus. Approximately 70-80% of the total reaction occurred between these two points. Measurements were not made in the mixing zone because it is clear that the stoichiometry depends on the ratio (HBr)/(O) which varies greatly in the mixing region. Table I displays experimental measurements of the ratio of Br formed to O removed. For comparison, values of this ratio were computed from the mechanism by integrating the rate equations for reactions 1-4 using measured reactant concentrations and the rate constants given previously. These computed values are also included in Table I.

An unsuccessful search was made for the electronically excited bromine atom, Br(²P_{1/2}), which had previously been observed⁷ in small yield in the reaction of atomic hydrogen with HBr.

Discussion

In general all of the results obtained are consistent with a mechanism composed of reactions 1-4. In the presence of excess HBr, the results illustrated in Figure 1 are exactly predicted by the mechanism, and in leaner mixtures the values of k_1 estimated using the mechanism are independent of the initial (HBr)/(O) ratio. The measured ratio of Br formed to O removed is within 10% of that calculated from the mechanism for 9 of the 11 mixtures studied, and deviations of this magnitude are within the experimental error associated with this type of absolute concentration measurement.¹³ Finally, both intermediates predicted by the mechanism were observed at close to their expected concentrations.

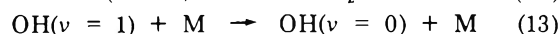
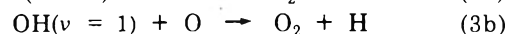
While reactions 1-4 reproduce the general features of the overall reaction, a more detailed inspection of the re-

sults reveals a small but consistent discrepancy between the predicted and measured concentrations of H and OH. Also, OH was detected in both its ground and first vibrationally excited states (a detail not contained in the above mechanism). Both of these features can be explained by considering the mechanism in more detail.

Reaction 1 can be broken down into three components



and while this division is somewhat arbitrary, it has some relevance in that vibrational relaxation and electronic quenching occur on a time scale that may be slow compared to that of this experiment. The OH($\nu = 1$) produced in reaction 1b can react in three possible ways



Several recent papers have shown that reactions are often promoted by vibrational excitation of the reactants,^{14,15} and thus it seems likely that $k_{2b} \geq k_2$ and that $k_{3b} \geq k_3$. Now, reaction 2 has an activation energy of 1.15 kcal/mol, and at room temperature its reaction rate is $\frac{1}{50}$ of the gas kinetic collision rate.¹ Therefore, it is probable that this reaction is more strongly promoted by vibrational excitation of OH than is reaction 3 which has zero activation energy and which proceeds at $\frac{1}{3}$ of its collision rate.⁸ Little is known about vibrational relaxation of OH (reaction 13), except that it occurs very slowly when M is an inert gas, and that it occurs efficiently at the walls.¹⁶ However in this experiment, in the presence of atomic oxygen, most OH radicals will react before they diffuse to the walls. Br(²P_{1/2}), the product of reaction 1c, is known to be efficiently quenched at the wall,¹⁷ and electronic quenching by O may also occur. No chemical reaction between it and other reaction products or reactants are likely since they are too endothermic to be of importance in this system.

The above discussion suggests that the observed OH($\nu = 1$) is produced by reaction 1b. The fact that the mea-

(12) See, for example, A. J. Herbert, F. J. Lovas, C. A. Melendres, C. D. Hollowell, T. L. Story, Jr., and K. Street, Jr., *J. Chem. Phys.*, **48**, 2824 (1968).

(13) (a) A. A. Westenberg and N. deHaas, *J. Chem. Phys.*, **40**, 3087 (1964); (b) A. A. Westenberg, *Progr. React. Kinet.*, in press.

(14) T. J. Odiorne, P. R. Brooks, and J. V. V. Kasper, *J. Chem. Phys.*, **55**, 1980 (1971).

(15) W. A. Chupka and M. E. Russell, *J. Chem. Phys.*, **49**, 5426 (1968).

(16) A. E. Potter, Jr., R. N. Colthorpe, and S. D. Worley, *J. Chem. Phys.*, **54**, 992 (1971).

(17) D. Husain and J. R. Wiensfeld, *Trans. Faraday Soc.*, **63**, 1349 (1967).

sured OH concentration is below that calculated can be adequately explained by assuming that $\text{OH}(\nu = 1)$ reacts more rapidly with HBr and O than does $\text{OH}(\nu = 0)$, and the discrepancy in the measured and calculated atomic hydrogen concentration can be explained by assuming that the rate of reaction 2 is more highly promoted by vibrational excitation of OH than is that of reaction 3. Unfortunately, quantitative estimates of the rates of reactions 2b and 3b cannot be made with any certainty at this time. At face value an increase in their rates, over those of reactions 2 and 3, by a factor of 3 is sufficient to reduce the $\text{OH}(\nu = 1)$ steady-state concentration from a value consistent with the calculation to the actual observed value, but the large uncertainty in the measurement (resulting from the poor S/N ratio of the signal), and a lack of knowledge concerning reaction 13, prevents this estimate from being more than mere speculation.

Since $\text{OH}(\nu = 1)$ is expected to be more reactive than $\text{OH}(\nu = 0)$, the ratio k_{1b}/k_{1a} should be greater than the measured ratio $(\text{OH}(\nu = 1))/(\text{OH}(\nu = 0))$. Thus a lower limit of 0.3 can be assigned to k_{1b}/k_{1a} . It is impossible to place an upper limit on this ratio because rate constants for reactions 2b, 3b, and 13 are not known. No estimate can be made of k_{1c}/k_{1a} because, in our system, any $\text{Br}(^2P_{1/2})$ formed by the initial reaction would be quenched at the wall before detection.¹⁷ However, it should be noted that the initial reaction is not sufficiently exothermic to produce $\text{OH}(\nu = 1)$ and $\text{Br}(^2P_{1/2})$ simultaneously, and this fact places an upper limit of 2.33 on the ratio k_{1c}/k_{1b} .

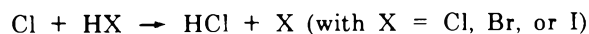
At 298 K, the overall rate constant for reaction 1 was measured as $4.4 \pm 1.0 \times 10^{-14} \text{ cm}^3 \text{ molecule}^{-1} \text{ sec}^{-1}$. This value is not consistent with the estimate given by Clark, *et al.*⁵ Using our room temperature rate constant, an activation energy of 5.2 kcal/mol was obtained by assuming the Arrhenius preexponential factor to be equal to the gas kinetic collision number. This maximum possible value was then used to calculate an upper limit for the rate constant at 773 K. The number obtained, $6 \times 10^{-12} \text{ cm}^3 \text{ molecule}^{-1} \text{ sec}^{-1}$, is almost an order of magnitude smaller than that used by Clark to fit his measured explosion limits. The reason for the discrepancy is not clear. However, it is stated by Clark that the fit is very insensitive to the actual value of k_1 used. Also it is possible that the set of rate constants and the mechanism used to fit his data is not unique.

A theoretical estimate of the rate constant for reaction 1 has been obtained by Mayer and Schieler⁴ using the BEBO method. Their value is three orders of magnitude greater than that measured in this study at 298 K. One possible reason for this difference could be the neglect, in the calculation, of the enhanced triplet repulsion caused by atomic oxygen. The origin of this repulsion can be seen by considering the model used for BEBO calculations. For the reaction $\text{A} + \text{HC} \rightarrow \text{AH} + \text{C}$, the atoms A, H, and C are maintained in a collinear configuration, and the energy of the system at any particular value of the reaction coordinate is calculated by supposing it to be decomposed into that due to two partial bonds (AH and HC) and one antibond (AC) as suggested by the spin orientation $\uparrow \text{A} \dots \downarrow \text{H} \dots \uparrow \text{C}$. The bonding is maximized by keeping $n_1 + n_2 = 1$, where n_1 is the Pauling bond order for AH, and n_2 is that for HC, and the antibonding is minimized by the collinear geometry. In terms of this model reactions of

triplet atomic oxygen must occur with enhanced anti-bonding as provided by the structure $\uparrow \uparrow \text{O} \dots \downarrow \text{H} \dots \uparrow \text{C}$.

Mayer and Schieler have suggested that reactions of triplet atoms can be adequately treated within the BEBO approximation by doubling the antibonding energy,⁴ which is normally calculated using a modified Sato triplet function.¹⁸ Therefore we have repeated part of the calculation for O + HBr using this suggested modification. The following results were obtained: (1) the potential energy of activation was increased by approximately 1 kcal/mol and (2) the nature of the transition state was not significantly modified, *i.e.*, it still occurred very much in the entrance valley of the potential energy surface with $n_1 > 0.9$. In spite of the increased triplet repulsion, the calculated and measured rates still differed by more than two orders of magnitude.

The failure of the BEBO method in predicting the rate of reaction 1 may be part of a more general failure. Mok and Polanyi¹⁹ have drawn attention to the fact that the measured change in activation energy throughout the series



is much greater than predicted by the BEBO method. They note that the experimental activation energy for $\text{Cl} + \text{HCl} \rightarrow \text{HCl} + \text{Cl}$ is $6.5 \pm 0.5 \text{ kcal/mol}$ whereas the predicted value is 0.6 kcal/mol. This situation is almost certainly mirrored in the series $\text{O} + \text{HX} \rightarrow \text{OH} + \text{X}$. BEBO calculations predict room temperature rate constants of 7.5×10^{-12} , 3.2×10^{-11} , and $5.1 \times 10^{-11} \text{ cm}^3 \text{ molecule}^{-1} \text{ sec}^{-1}$ for X = Cl, Br, and I, respectively.⁴ The measured values are $<10^{-16}$, 4.4×10^{-14} , and $\sim 2 \times 10^{-12} \text{ cm}^3 \text{ molecule}^{-1} \text{ sec}^{-1}$.²⁰ It is interesting to note that for both series the calculations predict transition states that lie early in the entrance valley of the potential energy surfaces, and surfaces that are very "attractive."²¹ However, for the reaction $\text{Cl} + \text{HI} \rightarrow \text{HCl} + \text{I}$, Polanyi and coworkers²² have reproduced the product energy distribution using classical trajectory studies on quite repulsive ($A = 24\%$, $R = 76\%$) London-Eyring-Polanyi-Sato surfaces.

Shortly after submission of this paper, a theoretical study of the O + HBr reaction appeared.²³ This study predicted a moderate preponderance of the $\nu = 1$ state over the $\nu = 0$ state of OH. Unfortunately the potential energy surface used in the calculation was modeled using certain parameters (activation energy, transition state) determined from the BEBO study, which we have shown to be inconsistent with experiment.

Acknowledgments. Acknowledgment is made to the Donors of the Petroleum Research Fund, administered by the American Chemical Society, for the support of this research. The authors would like to thank the Robert A. Welch Foundation of Houston, Texas, for the use of the epr spectrometer.

(18) The details of the BEBO calculation are described in detail by H. S. Johnston, "Gas Phase Reaction Rate Theory," Ronald Press, New York, N. Y., 1966, pp 80, 209, 339.

(19) M. H. Mok and J. C. Polanyi, *J. Chem. Phys.*, **51**, 1451 (1969).

(20) G. P. Glass, unpublished results.

(21) The usage is as defined in ref 19.

(22) K. G. Anlauf, J. C. Polanyi, W. H. Wong, and K. B. Woodall, *J. Chem. Phys.*, **49**, 5189 (1968).

(23) E. J. Shipsey, *J. Chem. Phys.*, **58**, 232 (1973).

Radiation Chemical Studies of the Oxidation and Reduction of Nitrofurans.

Oxidative Denitration by OH Radicals¹

C. L. Greenstock, I. Dunlop,

Medical Biophysics Branch, Whiteshell Nuclear Research Establishment, Atomic Energy of Canada Limited, Pinawa, Manitoba, Canada

and P. Neta*

Radiation Research Laboratories and Center for Special Studies, Mellon Institute of Science, Carnegie-Mellon University, Pittsburgh, Pennsylvania 15213 (Received January 22, 1973)

Publication costs assisted by Carnegie-Mellon University and the U. S. Atomic Energy Commission

Nanosecond pulse radiolysis has been used to determine the bimolecular rate constants for the reactions of OH and e_{aq}^- with simple nitrofurans derivatives. The transient optical absorption spectra of the radicals produced by these reactions have been characterized. Positive identification of the radicals has been achieved from the electron spin resonance spectra recorded with *in situ* irradiated solutions. The reactions of OH radicals with simple nitrofurans take place with very high rate constants, $\sim 5 \times 10^9 M^{-1} \text{sec}^{-1}$, and involve OH addition mainly to the 5 position. Addition of OH to this carbon which bears the nitro group is followed by rapid elimination of nitrous acid. Nitro anion radicals are formed by reaction of e_{aq}^- with the nitrofurans or by electron transfer from α -hydroxyisopropyl radicals. The rate constants for these reactions with 5-nitro-2-furoic acid are respectively 2.2×10^{10} and $1.5 \times 10^9 M^{-1} \text{sec}^{-1}$. The nitrofuran anion radicals protonate on the nitro group with $pK_a \approx 1$. In the case of the radical from 5-nitro-2-furoic acid the pK_a values for the nitro and the carboxyl groups were found to be 1.22 and 3.77, respectively.

Introduction

Nitroaromatic compounds have been shown to act as radiosensitizers, *i.e.*, they enhance the destruction of pyrimidine bases,² the release of inorganic phosphate from mononucleotides and phosphate esters,^{3,4} and the number of single strand breaks in DNA.⁵ In model systems of chemical radiosensitization, the nitrofurans have emerged as a class of excellent sensitizers, the degree of their effect being correlatable directly with their electron affinities.^{3,4,6} In order to understand the elementary processes involved in the radiosensitization this combined pulse radiolysis and esr study has been undertaken.

In a recent study of irradiated aqueous solutions of 5-nitouracil and its derivatives,⁷ the radicals produced by reaction of e_{aq}^- and OH have been characterized. The hydrated electron has been found to produce the nitro anion radical whereas the OH reaction results in oxidative denitration. Similar results have been found in the present study with the nitrofurans. Several pK values for the nitro anion radicals are also reported.

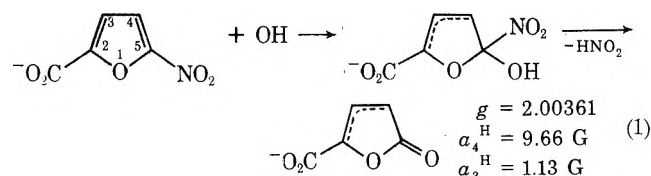
Experimental Section

The pulse radiolysis experiments were carried out at the Whiteshell Nuclear Research Establishment using nanosecond kinetic spectrophotometry. The radiation source was a 3.5-MeV Van de Graaff accelerator delivering 50-nsec pulses of electrons in the dose range 1-10 krad/pulse. The experimental details are similar to those reported earlier.⁸ The esr experiments were performed at Carnegie-Mellon University using a continuous 2.8-MeV electron beam from a Van de Graaff accelerator. All the experimental details of the preparation of solutions and their *in situ* irradiation while flowing through the esr cavity are

identical with those used in previous studies.⁹ The nitrofuran derivatives used were obtained from Aldrich Chemical Co., Pfaltz and Bauer, and Sigma Chemical Co. and were used without further purification.

Oxidative Denitration by OH Radicals

Radicals produced by reaction of OH with 5-nitro-2-furoic acid have been studied in N_2O saturated solutions. The esr spectrum observed with an irradiated solution at pH 9.1 consisted of four lines only. Two proton hyperfine constants of 9.66 and 1.13 G were calculated from the spectrum and no nitrogen splitting was present. This result indicates that the nitro group has been eliminated by a mechanism which involves initially the addition of OH



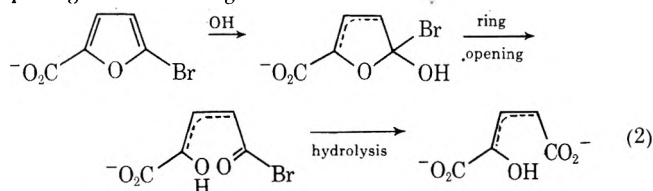
- (1) Supported in part by the U. S. Atomic Energy Commission and Atomic Energy of Canada Limited.
- (2) C. L. Greenstock, J. A. Raleigh, W. Kremers, and E. McDonald, *Int. J. Radiat. Biol.*, **22**, 401 (1972).
- (3) J. A. Raleigh, C. L. Greenstock, and W. Kremers, *Int. J. Radiat. Biol.*, in press.
- (4) C. L. Greenstock, J. A. Raleigh, R. Whitehouse, and E. McDonald, *Biochem. Biophys. Res. Commun.*, manuscript in preparation.
- (5) D. L. Dugle, J. D. Chapman, C. J. Gillespie, J. Borsa, R. G. Webb, B. E. Meeker, and A. P. Reuvers, *Int. J. Radiat. Biol.*, in press.
- (6) J. D. Chapman, C. L. Greenstock, A. P. Reuvers, E. McDonald, and I. Dunlop, *Radiat. Res.*, in press.
- (7) P. Neta and C. L. Greenstock, *Radiat. Res.*, in press.
- (8) J. W. Hunt, C. L. Greenstock, and M. J. Bronskill, *Int. J. Radiat. Phys. Chem.*, **4**, 87 (1972).
- (9) K. Eiben and R. W. Fessenden, *J. Phys. Chem.*, **75**, 1186 (1971).

to the carbon atom bearing the nitro group (eq 1). A similar denitration reaction was observed with 5-nitouracil and several of its derivatives and the identification of the radicals was confirmed by producing them *via* different reactions.⁷

In the case of furans it has already been found that OH radicals add preferentially to positions 2 and 5 rather than 3 and 4.¹⁰ The adducts undergo a rapid ring opening in alkaline solutions,^{10,11} but apparently elimination of HNO₂ in the case of nitrofurans is a faster process than the ring opening. The radicals resulting from ring opening have higher *g* factors and lower hyperfine constants than those observed in the present case. The parameters observed in the present study resemble those of the allylic type radicals produced from the furans in acid solutions,¹⁰ where the ring does not open, so that the assignment given here is very reasonable.

A further confirmation can be obtained by following the reaction of OH with 5-bromo-2-furoic acid. A similar mechanism involving elimination of HBr is expected to take place, as has been found with 5-halouracils,¹² to yield the same final radical. Indeed, the spectrum observed with an irradiated solution of 5-bromofuroic acid at pH 11.5 contained the same lines as those observed with 5-nitrofuroic acid, with the esr parameters $g = 2.00360$, $a_4^H = 9.68$ G, and $a_3^H = 1.15$ G. Obviously, the same radical is produced from the two compounds and the mechanism suggested is the only one that can explain these findings.

In the case of 5-nitrofuroic acid the same esr spectrum was observed at pH 9.1, 11.8, and 13.0. A few extra weak lines were present at the higher pH values but assignment could not be made. With 5-bromofuroic acid, on the other hand, a second radical was present at a steady-state concentration three times as high as that of the first radical and the esr parameters are $g = 2.00427$, $a^H = 6.56$ G, and $a^H = 0.21$ G. Tentatively these parameters can be assigned to an allylic type radical produced *via* a mechanism which involves ring opening (reaction 2) as a competing reaction along with the HBr elimination.



Attempts to identify the radical produced by reaction of OH with 5-nitro-2-furaldehyde and 5-nitro-2-furadoxime (nifuroxime) were not successful because the esr spectra had very low signal-to-noise ratios.

The transient optical absorption spectra observed with irradiated solutions of 5-nitrofuroic acid and 5-bromofuroic acid (5×10^{-4} M and saturated with N₂O at pH 7) are shown in Figure 1. The two spectra are evidently very similar and must be mainly the absorption of the radical produced by either denitration or debromination. Other radicals produced by addition of OH to positions 2, 3, and 4, apparently contribute very little to these observed spectra. The similarities in the absolute values of the absorbance per unit dose obtained with the two compounds indicates that the fractions of OH radicals which add to position 5 of the two compounds are very similar.

The rate constant for the reaction of OH with 5-nitro-2-furoic acid has been measured both from the rate of

buildup of absorption at 500 nm and from the rate of destruction of the parent compound absorption at 300 nm. Both rates are first order in 5-nitrofuroic acid concentration and give a rate constant of 5×10^9 M⁻¹ sec⁻¹. These results show that oxidative denitration occurs rapidly after OH addition and that the rate-limiting step, as measured in the above experiments, is the addition of OH to the nitrofurans.

Formation of Nitro Anion Radicals

The nitrofurans can be reduced either by reaction with e_{aq}⁻ or by a reducing organic radical such as (CH₃)₂COH. Experiments have been carried out with solutions of 5-nitro-2-furoic acid containing either *tert*-butyl alcohol, which scavenges OH to form an unreactive radical, or isopropyl alcohol, which reacts with OH to form a radical which reduces the nitro compound. In acid solutions e_{aq}⁻ reacts with H⁺ to form H, which is expected to add to the furan ring rather than reduce the nitro group. The nitro anion radical must, therefore, be produced in acid solution by reduction with the radical from isopropyl alcohol.

The esr spectra recorded with irradiated solutions of 5-nitro-2-furoic acid at all pH values show splittings by one nitrogen and two protons. The values of the esr parameters, however, change with pH. The changes in the nitrogen hyperfine constant and in the larger proton hyperfine constant are shown in Figure 2. It is reasonable to assume that these changes are the result of acid-base equilibria in the radical. In this case the splitting measured at any pH is the weighted average of the splittings of the acid and basic forms (if the exchange between these forms is rapid). When two proton dissociations are involved the relationship is

$$a = \frac{a_{AH_2} + a_{AH} \frac{K_1}{[H^+]} + a_{A^{2-}} \frac{K_1 K_2}{[H^+]^2}}{1 + \frac{K_1}{[H^+]} + \frac{K_1 K_2}{[H^+]^2}}$$

where a_{AH_2} , a_{AH} , and $a_{A^{2-}}$ are respectively the splittings for the nondissociated, singly, and doubly dissociated forms, and K_1 and K_2 are the first and second dissociation constants. Using this equation and the experimental $a_{A^{2-}}$, and varying the other parameters, the best fit to the experimental points as shown in Figure 2 has been obtained by using the splittings summarized in Table I with $pK_1 = 1.22$ and $pK_2 = 3.77$. The three forms of the radical shown in the table are expected to have second-order disappearance rates which decrease with the increase in charge because of electrostatic repulsion. The slower radical-radical reactions at the higher pH values can be manifested by the observed esr signal intensities. The ratio in intensities, at similar production rates, is 1:15:100 for the radicals at pH 0, 2.5, and 9–13, respectively.

The pK of 3.77 assigned to the carboxyl group of the radical is higher than $pK = 2.06$ for the parent compound and the difference can be explained by the effect of the additional charge, located partly on the ring, to enhance protonation. The lower pK of 1.22 is assigned to the nitro anion group. To support this assignment, and because no other protonated nitro anion radical has been previously

(10) R. H. Schuler, G. P. Laroff, and R. W. Fessenden, *J. Phys. Chem.*, **77**, 456 (1973).

(11) J. Lilie, *Z. Naturforsch.*, **B**, **26**, 197 (1971).

(12) P. Neta, *J. Phys. Chem.*, **76**, 2399 (1972).

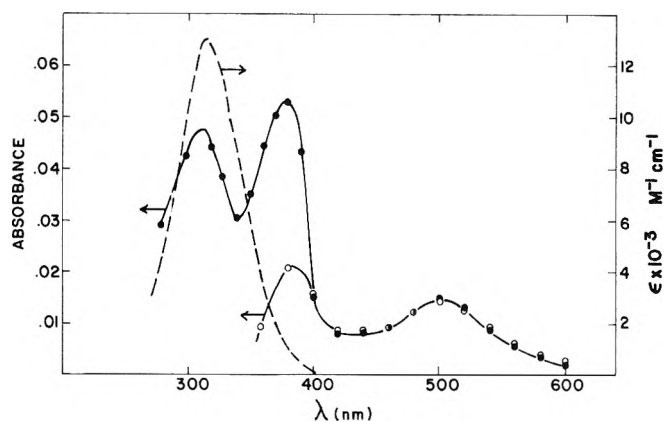


Figure 1. Transient optical absorption spectra observed in N_2O saturated $5 \times 10^{-4} M$ neutral solutions of 5-bromo-2-furoic acid (●) and 5-nitro-2-furoic acid (○). The dose per pulse was 6.2 krads and the spectra were recorded 1 μ sec after the pulse. The self-absorption of the 5-nitro-furoic acid (whose absorption spectrum, referred to the right-hand extinction coefficient scale, is shown by the dashed line) prevents its transient spectrum from being followed below 375 nm. The 5-bromofuroic acid does not have any absorption below 300 nm.

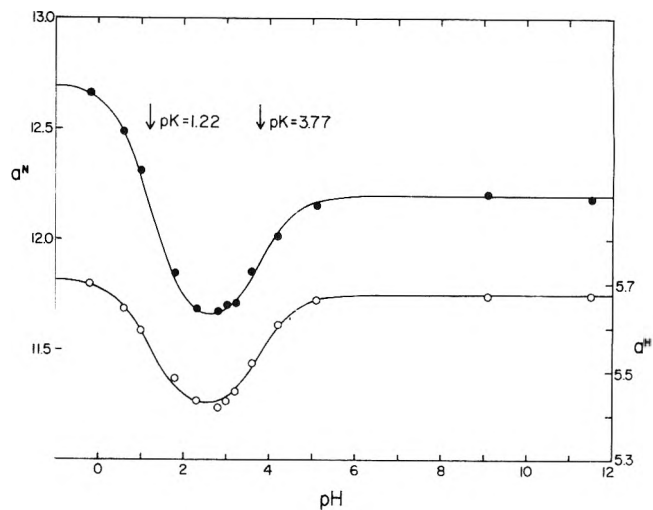
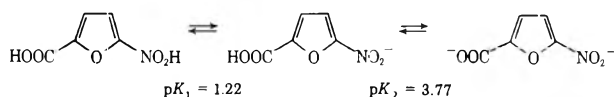


Figure 2. The effect of pH on the nitrogen (●) and proton (○) hyperfine constants of the radical anion formed in irradiated solutions of 5-nitro-furoic acid containing isopropyl alcohol. The pK values of 3.77 and 1.22 are assigned respectively to the carboxyl and nitro groups of the radical anion.

TABLE I: ESR Parameters for Radicals Formed by Reduction of 5-Nitro-2-furoic Acid^a

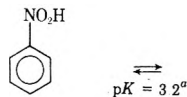
	pH < 0	pH 2.5	pH 9.1, 11.5, 13.0
a^N	12.70	11.58	12.20
a_4^H	5.71	5.40	5.67
a_3^H	1.38	1.33	1.28
g	2.00454	2.00471	2.00461



^a The g factors are measured relative to the peak from the silica cell and are accurate to ± 0.00005 . Hyperfine constants are given in Gauss and are accurate to $\pm 0.03 G$.

TABLE II: ESR Parameters for the Nitrobenzene Radical Anion and Its Protonated Form

	pH 0.1	pH 6, 12
a^N	15.81	14.20
a_o^H	3.36	3.38 (2)
a_p^H	3.36	3.65 (1)
a_m^H	1.11 (2)	1.15 (2)
g	2.00439	2.00448



^a W. Grunbein, A. Fojtik, and A. Henglein, *Z. Naturforsch. B.* **24**, 1336 (1969). This pK is higher by about two units than those for the nitrofurans derivatives (Tables I and III) in line with the comparison of benzoic acid ($pK = 4.2$) with 2-furoic acid ($pK = 3.2$). ^b The para and the two ortho protons have accidentally the same hyperfine constants.

observed, it was decided to prepare the nitrobenzene anion and examine the change in its hyperfine constants when the solution is acidified. Table II summarizes the esr parameters for the acid and basic forms of the nitrobenzene radical. Comparing the changes in the parameters for $C_6H_5NO_2H$ and $C_6H_5NO_2^-$ with the corresponding ones for 5-nitro-furoic acid (Table I) it is seen that, in both cases, dissociation causes an increase in the g factor

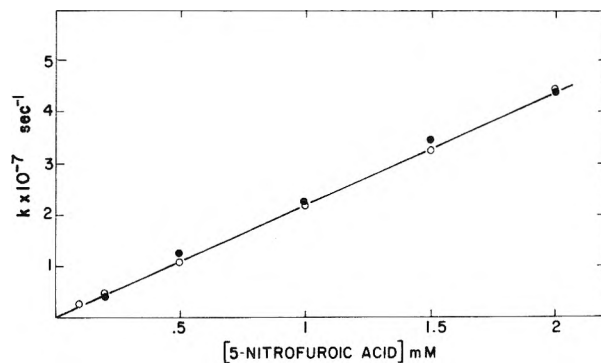


Figure 3. The effect of 5-nitro-furoic acid concentration on the rate of formation of the anion radical absorption at 375 nm (●), or the rate of decay of the e_{aq}^- absorption at 600 nm (○). The oxygen-free neutral solutions contain 0.5 M *tert*-butyl alcohol.

and about a 10% decrease in a^N . The dissociation of the carboxyl group in 5-nitro-furoic acid reverses this pattern as is clear from Figure 2.

To further support the assignment of the two pK values of the 5-nitro-furoic acid anion radical to the corresponding groups other nitro-furan derivatives have been studied. Table III shows the results for 5-nitro-2-furaldehyde and 5-nitro-2-furaldehyde diacetate. A $pK \sim 1$ is estimated for both nitro anions. The changes in a^N and in the g factor are similar to those in the previous compound. No change in esr parameters, *i.e.*, no pK, has been observed between pH 3.3 and 7.3 as expected.

The esr spectrum of the anion radical from 5-nitro-2-furaldoxime (nifuroxime) has been observed at pH 9.4 and the hyperfine constants of all the magnetic nuclei were analyzed (Table III). Because of the large number of lines (144) the spectrum in acid solution had a very low signal-to-noise ratio and could not be analyzed.

The rate constants for the reaction of e_{aq}^- with nitrofurans at neutral pH have been determined by following the rate of decay of the e_{aq}^- absorption at 600 nm at various nitro-furan concentrations. In all cases the absorption decayed exponentially and the rate of decay was first order in nitro-furan concentration. Figure 3 shows the plot for 5-nitro-2-furoic acid from which a rate constant of $2.2 \times$

COMMUNICATIONS TO THE EDITOR

Comparison of Micellar Effects on Singlet Excited States of Anthracene and Perylene¹

Publication costs assisted by Mellon Institute

Sir: Recent fluorescence depolarization studies by Shinitzky, *et al.*, made use of aromatic hydrocarbon fluorescent probes to measure the microviscosity in the interiors of certain cationic micellar systems.² Almgren has examined the sensitized fluorescence of naphthalene in sodium phenylundecanoate, an anionic surfactant, and determined that naphthalene lies at the micelle core in his system.³ We have begun to investigate the behavior of excited states of condensed aromatic hydrocarbons in micellar systems, and our preliminary findings indicate that the locations of these hydrocarbons depend both on the substrate and surfactant used. Further, it may be seen that in certain systems the excited substrate can provide useful data concerning the nature of the micellar surface.

In these experiments we have compared the influences of cationic hexadecyltrimethylammonium bromide (CTAB), $\text{CH}_3(\text{CH}_2)_{15}(\text{CH}_3)_3\text{N}^+\text{Br}^-$, and the corresponding chloride (CTACl), upon the fluorescence lifetimes (τ_f) of anthracene and perylene in aqueous systems. Fluorescence lifetime measurements were carried out by the conventional method of pulse fluorimetry utilizing a nanosecond spark, pulse sampling oscilloscope, and PDP-8 computer for data control and analysis.⁴ It was found that in water solutions perylene ($\sim 10^{-6} M$) has a very short lifetime ($\tau_f < 0.5$ nsec) and exhibits a very low intensity of emission. However, addition of either CTAB or CTACl at concentrations corresponding to the region of the micelle concentration (cmc) or above is accompanied by a sharp increase in τ_f and emission intensity. In CTAB solutions, the fluorescence lifetime plateaus just above the cmc ($9 \times 10^{-4} M$) at a value of 5.0 ± 0.2 nsec, in agreement with an earlier finding of Shinitzky, *et al.*, for solubilized perylene.² In direct contrast, however, similar addition of CTAB to an aqueous solution of anthracene ($\sim 3 \times 10^{-6} M$, $\tau_f = 2.3 \pm 0.2$ nsec) sharply quenches the anthracene fluorescence in the cmc region. These effects are illustrated in Figure 1. Substitution of CTACl for CATB produces very little decrease in the anthracene fluorescence lifetime compared to water solutions. Measurements of $\tau_{f \text{ anthracene}}$ were then carried out in systems of mixed CTAB and CTACl micelles maintaining the total surfactant concentration at 0.01 M. From a plot of τ_f vs. the concentration of CTAB, [CTAB], it is seen that τ_f may be related to [CTAB] by the pseudo-first-order quenching relationship given in Figure 2. This expression assumes no substantial changes in structure upon the formation of the mixed micelles which might effect the location of anthracene within the system. In aqueous solution Br^- has been found to be an inefficient quencher of these excited singlets, $k_q < 10^8 M^{-1} \text{sec}^{-1}$. Hence for τ_f to be affected to the extent observed by

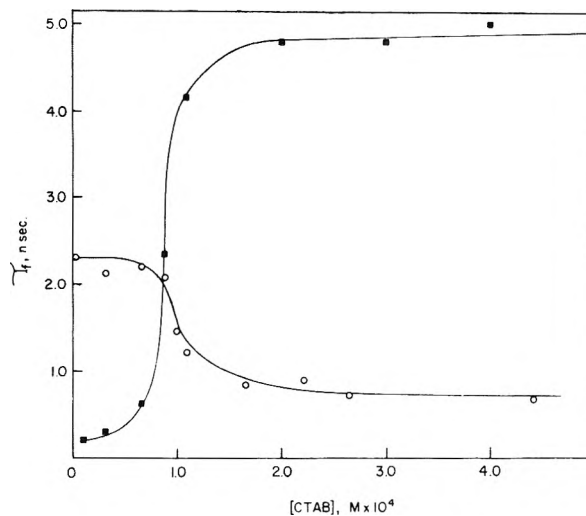


Figure 1. Effect of CTAB micelle formation on the fluorescence lifetimes of $\sim 1 \times 10^{-6} M$ perylene (■) and $\sim 3 \times 10^{-6} M$ anthracene (○) in aqueous solution.

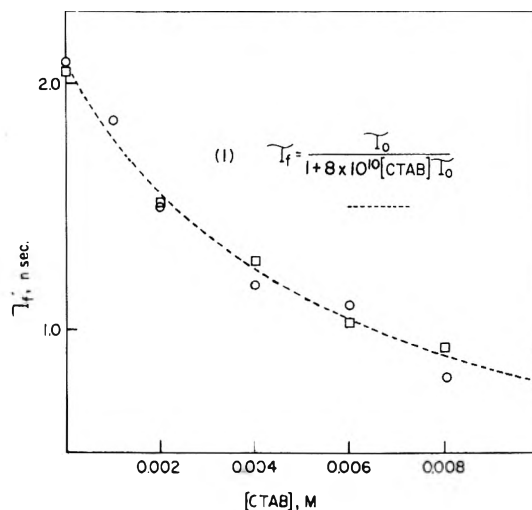


Figure 2. Fluorescence lifetime of $\sim 3 \times 10^{-6} M$ anthracene as a function of increasing CTAB concentration, [CTAB], in a CTACl-CTAB mixed micelle system. Total surfactant concentration is maintained at 0.01 M.

the presence of Br^- , the anthracene must be solubilized at the micelle surface, readily accessible to the high concentration of Br^- ions in the Stern layer. By contrast, the perylene must as previously suggested² reside in the interior of the micelle, well removed from the Br^- ions.

Given the high sensitivity of anthracene fluorescence to the surface environment, the singlet state should provide

- (1) Supported in part by the U.S. Atomic Energy Commission.
- (2) M. Shinitzky, A.-C. Dianoux, C. Gittler, and G. Weber, *Biochemistry*, **10**, 2106 (1971).
- (3) M. Almgren, *Photochem. Photobiol.*, **15**, 297 (1972).
- (4) L. K. Patterson, to be published.

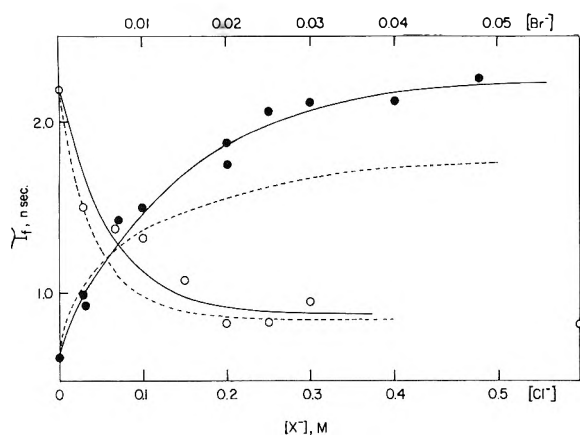


Figure 3. Effects of Br^- added to 0.01 M CTACl (O) and Cl^- added to 0.01 M CTAB (●) upon τ_f of solubilized anthracene. The upper horizontal scale applies to the CTACl- Br^- system while the lower is for the CTAB- Cl^- system. The curves represented by the dotted lines were calculated from eq 1 in Figure 2 and an equilibrium constant of 10 for eq 2.

a good probe for stability of counterion binding in the Stern layer when other competing ions are introduced into the system. Substitution of a nonquenching ion for Br^- at the surface should, then, be accompanied by increasing τ_f . Accordingly, τ_f anthracene was measured in 0.01 M CTAB solutions as a function of added NaCl. The results are given in Figure 3. It is apparent that Cl^- rather inefficiently replaces Br^- at the micelle surface. The inverse experiment, beginning with 0.01 M CTACl and determining τ_f anthracene with increasing KBr confirms that Br^- is much more strongly bonded at the positively charged surface or in the Stern layer (Figure 3). Assuming reversibility and an equilibrium constant of 10 for the system



one may calculate concentrations of [CTAB] produced either by the addition of Br^- to CTACl or Cl^- to CTAB. By substituting [CTAB] calculated in this way into eq 1

which was applied to the mixed micelle data, one may construct quenching curves for both sets of experimental data. The CTACl + Br^- case may be seen to give the better fit to the proposed equilibrium. It must be noted that the model reflected in eq 2 represents considerable simplification of the real system, ignoring as it does structural changes and substrate distribution changes that may occur in the micelle at high concentrations of added electrolyte.⁵ The large deviation in the CTAB + Cl^- case may be due to just such changes in micelle structure. Meguro and Kondo measured the rates of increase in specific conductance with concentration above the cmc in dodecylpyridinium halides and found the value for the chloride to be greater than that for the bromide by a factor of about 2 indicating for that case a relatively stronger binding of Br^- .⁶ In the pyridinium systems it has been shown that some portion of the binding is due to charge-transfer phenomena.⁷ With this taken into account the conductance studies do indicate trends in relative stability of halide binding qualitatively consistent with findings presented here.

It has been suggested that the binding of conjugated molecules at the CTAB micellar surface may be explained in terms of an interaction between the π system of the molecule and the positively charged surface.⁸ However, all the factors determining the selectivity by which some aromatic hydrocarbons are solubilized at the surface of CTAX while others are found in the interior are not fully understood and are the focus of further investigation.

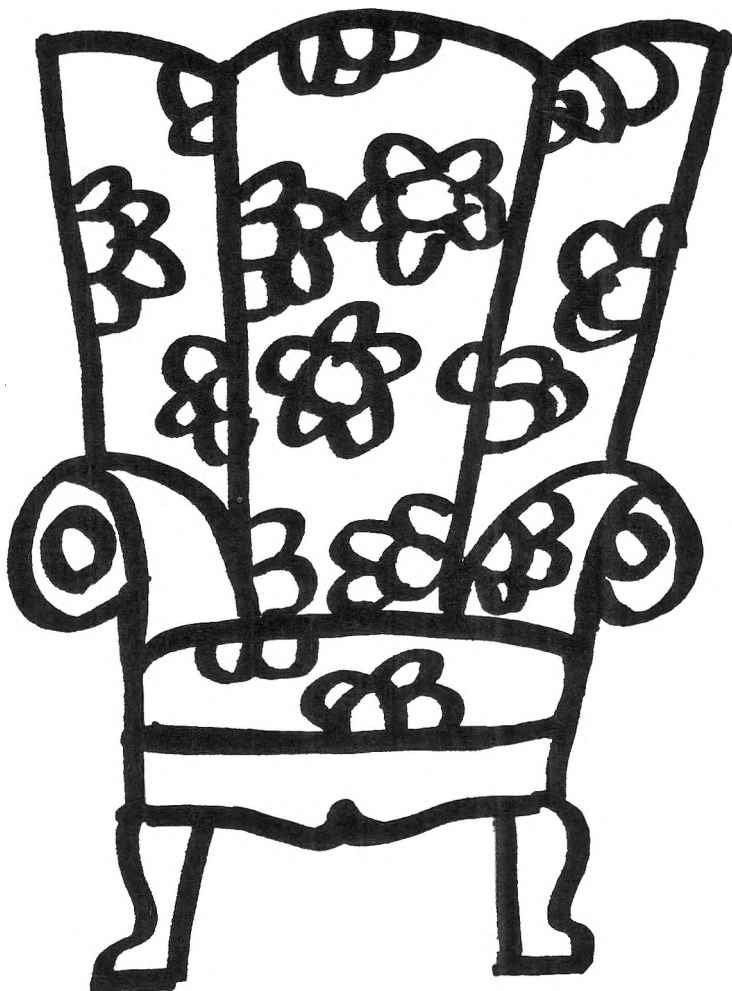
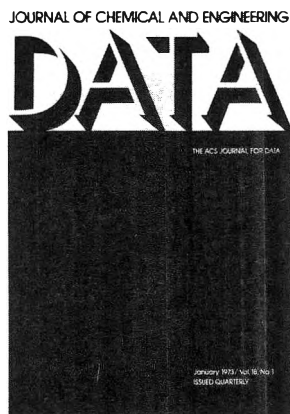
- (5) J. Cohen and T. Vassiliades, *J. Phys. Chem.*, **65**, 1774 (1961)
 (6) K. Meguro and T. Kondo, *Nippon Kagaku Zasshi*, **80**, 818 (1959).
 (7) P. Mukerjee and A. Ray, *J. Phys. Chem.*, **70**, 2150 (1966).
 (8) J. H. Fendler and L. K. Patterson, *J. Phys. Chem.*, **74**, 4608 (1970).

Radiation Research Laboratories
 and Center for Special Studies
 Mellon Institute of Science
 Carnegie-Mellon University
 Pittsburgh, Pennsylvania 15213

Larry K. Patterson*
 Eric Vieil

Received October 30, 1972

**You
don't have
to search
the archives
for data . . .**



. . . because THE JOURNAL OF CHEMICAL AND ENGINEERING DATA will bring precise, reliable, useful technical information right to your fingertips quarterly! With a year's subscription, you'll receive a total of over 500 pages of valuable science and engineering data that are especially relevant now in light of today's new instrumentation. The information in JCED includes:

- experimental data relating to pure compounds or mixtures covering a range of states;
- manuscripts based on published experimental information which make tangible contributions through their presentation or which set forth a sound method of prediction of properties as a function of state;

- experimental data which aid in identifying or utilizing new organic or inorganic compounds; and
- papers relating primarily to newly developed or novel synthesis of organic compounds and their properties.

Start to benefit now from this "arm-chair" source of pertinent technical data—with your own personal

subscription to JCED . . . just complete and return the form below . . . get your data without the dust.



. . . another ACS service

**Journal
of Chemical
& Engineering
Data**

**Journal of Chemical & Engineering Data
American Chemical Society**

1155 Sixteenth Street, N.W.
Washington, D.C. 20036

Yes, I would like to receive the JOURNAL OF CHEMICAL & ENGINEERING DATA at the one-year rate checked below:

ACS Member Personal-Use	U.S.	Canada	Latin America	Other Nations
One-Year Rate	<input type="checkbox"/> \$15.00	<input type="checkbox"/> \$18.00	<input type="checkbox"/> \$18.00	<input type="checkbox"/> \$18.50
Nonmember	<input type="checkbox"/> \$45.00	<input type="checkbox"/> \$48.00	<input type="checkbox"/> \$48.00	<input type="checkbox"/> \$48.50

Bill me Bill company Payment enclosed

Name _____

Street _____

Home

Business

City _____

State _____

Zip _____

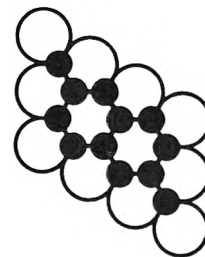
T-73

A new indispensable reference work
in Inorganic Chemistry

Contributors:—

E W Abel *PhD, DSc, FRIC*
C J Adams *MA, DPhil*
S Ahrland *PhD*
B J Aylett *MA, PhD*
K W Bagnall *DSc, FRIC*
A J Banister *PhD*
N Bartlett *DSc*
O F Beumel *Fr PhD*
D J M Bevan *PhD*
D C Bradley *PhD, DSc*
D Brown *PhD, DSc*
R J H Clark *PhD, DSc, FRIC*
A H Cockett *BSc*
J A Connor *PhD*
R Davis *BSc, PhD*
R M Dell *BSc, PhD*
M F A Dove *MA, PhD*
A J Downs, *MA, PhD*
S H Eberle *PhD*
E A V Ebsworth *DSc, FRIC*
D A Everest *PhD, FRIC, AMINN*
R D Goodenough *BSc*
J C Green *PhD*
M L H Green *BSc, PhD*
N N Greenwood *PhD, ScD, FRIC*
W P Griffith *PhD, DSc*
P Hagenmuller *DSc*
W A Hart *PhD*
A K Holiday *DSc, FRIC*
G Hughes *BSc, PhD*
B F G Johnson *BSc, PhD*
K Jones *PhD*
C Keller *PhD*
R D W Kemmitt *PhD*
D L Kepert *PhD*
J A Lee *BSc, PhD*
J O Liljenzin *tekn Dr*
S E Livingstone *DSc, FSTC*
K M MacKay *PhD*
P G Mardon *MA*
J A C Marples *MA*
A G Massey *DSc*
G W C Milner *DSc, FRIC, AInstP*
T Moeller *PhD*
D Nicholls *PhD, ARIC*
T A O'Donnell *PhD, DSc*
R D Peacock *PhD, DSc*
G Phillips *ARIC*
P E Potter *BSc, PhD*
P Powell *MA, DPhil, FRCO*
J E Prue *MA, DPhil*
E G Rochow *PhD*
C L Rollinson *BSc, PhD*
J Rydberg *DSc*
M Schmidt *PhD*
B L Shaw *BSc, PhD*
W Siebert *BSc, PhD*
F O Sladky *PhD*
K C Smith *BSc, FRIC*
J D Smith *MA, PhD*
V A Stenger *DSc*
N R Thompson *BSc, PhD*
P Thornton *BSc, PhD*
A D F Toy *PhD*
N I Tucker *BSc, PhD*
J J Turner *MA, PhD, FRIC*
R C Vickery *DSc*
K Vrieze *PhD*
K Wade *PhD, DSc*
S M Walker *BSc, PhD*
T P Whaley *PhD*

COMPREHENSIVE INORGANIC CHEMISTRY



Over 6000 pages in 5 volumes

- The most modern and authoritative standard work and literature guide to Inorganic Chemistry
Compiled under the editorial control of **JC Bailar Jr** **HJ Emeléus FRS**
† **Sir Ronald Nyholm FRS** **AF Trotman-Dickenson**
- Written by 71 of the world's most eminent research workers, industrial practitioners and teachers in chemistry
- Easy retrieval - each volume has an individual subject index and the fifth volume contains a master index to the entire work.

Pre-publication price to July 31, 1973

5-volume set only \$350.00
5-volume set with microform* \$386.00

August 1, 1973 and thereafter

5-volume set only \$386.00
5-volume with microform* \$476.00

* Microform available only when purchased in conjunction with hard copy set.

Please write for a full color twenty page descriptive brochure.

*Save
up to \$90.00
by ordering
Now*

COMPENDIUM PUBLISHERS

A Division of MICROFORMS INTERNATIONAL MARKETING CORPORATION
380 Saw Mill River Road, Elmsford, New York 10523

OUTSIDE THE WESTERN HEMISPHERE Pergamon Press Ltd, Headington Hill Hall, Oxford, OX3 0BW